Role of selenium in articular cartilage metabolism, growth and maturation

Caroline Bissardon

Communauté
UNIVERSITÉ Grenoble Alpes

Prifysgol Abertawe
Swansea University

THÈSE

Pour obtenir le grade de

DOCTEUR DE LA COMMUNAUTÉ UNIVERSITÉ GRENOBLE ALPES

préparée dans le cadre d'une cotutelle entre la *Communauté Université Grenoble Alpes* et Swansea Université

Spécialité: Sciences de la Terre, de l'Univers et de l'Environnement

Arrêté ministériel : 25 mai 2016

Présentée par

Caroline BISSARDON

Thèse dirigée par **Prof. Laurent CHARLET** et **ILYAS KHAN**
codirigée par **Sylvain BOHIC et Francis LEWIS**

préparée au sein des **Laboratoires : Institut des sciences de la Terre (ISTerre) et Centre for NanoHealth (CNH)**
dans **les Écoles Doctorales : Terre, Univers, Environnement (TUE) et College of Medicine**

Rôle du Sélénium dans le Métabolisme, la Croissance et la Maturation du Cartilage Articulaire

Thèse soutenue publiquement le **2 Décembre 2016,**
devant le jury composé de :

M. Steve, CONLAN
Professeur, Director of the Centre for NanoHealth, Président du Jury
M. Lutz, SCHOMBURG
Professeur, Charité - Universitätsmedizin Berlin, Rapporteur
M. Matthieu, REFREGIERS
Chercheur Synchrotron SOLEIL, HDR, Rapporteur
M. Dominique, HEYMANN
Professeur, The Medical School Beech Hill Road Sheffield, Examinateur
M. Laurent, CHARLET
Professeur, Université Grenoble-Alpes, Directeur de Thèse
M. Sylvain, BOHIC
Chargé de Recherche INSERM, EA 7442 RSRM - ID17 /ESRF, Université Grenoble-Alpes, Co-Directeur de Thèse
M. Ilyas, KHAN
Associate Professor, Swansea University, Co-Directeur de Thèse
M. Francis, LEWIS
Senior Lecturer, Swansea University, Co-Directeur de Thèse

Role of Selenium in Articular Cartilage Metabolism, Growth and Maturation

Caroline Bissardon

Cotutelle

Université Grenoble-Alpes, Institut des Sciences de la Terre (ISTerre), Equipe Géochimie 4D

Ecole doctorale: TUE (Terre, Univers, Environnement)

Swansea University, Centre for NanoHealth, Tissue Regenerative Medicine Research Unit

PhD School: College of Medicine

(First PhD Student in Cotutelle between these two universities)

Abstract

Role of Selenium in Articular Cartilage Metabolism, Growth and Maturation

In China, a severe musculoskeletal disease called Kashin-Beck disease (KBD) is largely endemic over a large geographical area. It has been reported that more than 2.5 million people in China suffer from KBD and about 30 million people are at risk. Geological and epidemiological investigations have shown that a strong correlation exists between the location of selenium (Se) deficient soils and the distribution of KBD in the population. The disease is manifested as degradation of the extracellular matrix, cell necrosis mainly in the articular and growth plate cartilage, which can result in growth retardation, secondary osteoarthrosis, and disability in daily life. The worst forms of this disease tend to start in childhood, which may lead to dwarfism.

Selenium is present everywhere in the environment (water, air, soils) and it is mainly incorporated into human organism through the daily diet (water, cereals). Although this trace nutriment element is essential for normal cellular function, most of the selenium-related -functions and pathways remain incompletely understood. Whilst vital for normal function, it is toxic at a concentration slightly higher than that required by the body. Consequently, it is present within the organism in parts per billion (microgram per liter) making it difficult to localize, and to analyse its role in metabolism. Despite being a trace element it is an essential component of antioxidant and anti-inflammatory-related proteins that protect cells against oxidative attack. Furthermore, several studies exposed the role selenium plays in tissue development such as in articular cartilage. This action seems to be mediated via selenoproteins that are indirectly involved in normal cartilage growth and homeostasis. In the USA, a clinical study has shown strong evidence that Se-deficiency influences cartilage metabolism, inducing a favorable environment for the onset and the progression of osteoarthritis. Even if the selenium is not the only factor in the development of degenerative joint disease, it is highly likely that its absence impacts its growth and development of articular cartilage. The main focus of this study was further to understand on the role of Se in the normal metabolic processes of articular cartilage. Cultures of articular cartilage explants were used on a previously validated *in vitro* model of tissue maturation to analyse the role of selenium in growth and development. Physical and chemical experiments were performed to understand how the presence of selenium affects tissue organisation. It has been possible to determine a fundamental recurrent pattern of Se-distribution in the tissue. Se appears to be localized at cell-matrix interfaces and it can be hypothesized that Se plays role in cell signaling or mechanotransduction. Biomechanical, structural and molecular analyses have been made to characterize the extracellular matrix of articular cartilage treated with different concentrations of Se. We discovered that Se-deficiency induces morphological changes in the cartilage matrix during the fast maturation-like process which could be related to degenerative-like morphology of the cartilage. This could potentially be associated with degenerative changes that occur in KBD patients during childhood. This project is a prospective work a potential for future enhancement of regenerative or preventive treatments for specific musculoskeletal diseases with a metabolic component.

Résumé

Le Rôle du Sélenium dans le Métabolisme, la Croissance et la Maturation du Cartilage Articulaire.

En Chine, une grave maladie musculo-squelettique appelée la maladie de Kashin-Beck (KBD) se retrouve distribué sur une large zone géographique. Cette maladie touche plus de deux millions d'individus, notamment dans le centre de la Chine, et il est admis que plus de 30 millions d'individus seraient à risque. Par ailleurs, des études géologiques et épidémiologiques ont montré une forte corrélation entre les zones de déficience en Se dans les sols la zone de KBD. La maladie de Kashin-Beck est une ostéoarthropathie, caractérisée par la destruction des chondrocytes du cartilage qui est très douloureuse au niveau des articulations et très invalidantes. Dans les régions hyperendémiques, elle peut entraîner dans les cas les plus graves un nanisme avec des déformations articulaires importantes à l'état adulte. Le sélénium est présent partout dans l'environnement (eau, air, sols) et nos besoins physiologiques en sélénium sont couverts par notre alimentation quotidienne (eau, céréales). Bien que cet élément trace soit un nutriment essentiel pour la fonction cellulaire normale, ses mécanismes d'action ainsi que les transformations métaboliques de ses composés dans le corps humain ne sont toujours pas bien déterminés. Toutefois, à une dose un peu supérieure à la dose recommandée, il peut, selon la forme chimique sous laquelle il est ingéré, devenir toxique. Par conséquent, on retrouve le sélénium en très faible quantité (quelques microgrammes par litre) dans l'organisme, ce qui rend difficile sa localisation et l'analyse de son rôle dans le métabolisme. Le sélénium fait partie de sites biologiquement actifs d'un nombre important de protéines, en particulier celles qui sont impliquées dans les mécanismes antioxydants de défense, le métabolisme hormonal de la thyroïde et le contrôle rédox des réactions intracellulaires. En outre, plusieurs études ont mis en évidence le rôle que joue de sélénium dans le développement des tissus tels que le cartilage articulaire. Cette action semble être médiée par l'intermédiaire de sélénoprotéines et seraient indirectement impliqués dans la croissance du cartilage normal et l'homéostasie. Aux Etats-Unis, une étude clinique a montré des preuves solides de l'influences d'un déficit en Se dans le métabolisme du cartilage conduisant un environnement favorable à l'apparition et la progression de l'arthrose. Même si le sélénium n'est pas le seul facteur dans le développement de maladies dégénératives du cartilage, il est fort probable que son absence impacte la croissance et le développement du cartilage articulaire. Des cultures d'explants de cartilage articulaire, modelé précédemment validé, ont été utilisées. Ce modèle *in vitro* de maturation accélérée du cartilage articulaire nous a permis d'analyser l'impact du sélénium dans la croissance et le développement de ce tissu. Des expériences biologiques, biophysiques et chimiques ont été réalisées pour comprendre comment la présence de sélénium affecte l'organisation des tissus. Il a été possible de déterminer un schéma récurrent de la distribution du Se dans le tissu. Il semble être localisé au niveau des interfaces cellule-matrice, orientant vers une hypothèse intéressante pour de futures études sur le rôle potentiel du Se dans la signalisation cellulaire ou transduction mécanique. Des analyses biomécaniques, structurelles et moléculaires ont été faites pour caractériser la matrice extracellulaire du cartilage articulaire traités avec différentes concentrations de Se. Il semble être localisé au niveau des interfaces cellule-matrice, ce qui suggère que le Se joue un rôle dans la signalisation cellulaire ou transduction mécanique. Des analyses biomécaniques, structurelles et moléculaires ont été faites pour caractériser la matrice extracellulaire du cartilage articulaire traités avec différentes concentrations de Se. Nous avons découvert qu'un déficit en Se peut induire à une morphologie proche de celle de l'arthrose (1er stade) lors de la transition d'un cartilage immature à cartilage ayant un phénotype mature. Cependant, le rôle exact de ce déficit en Se induisant ce type de phénotype reste inconnu. Ce projet est un travail prospectif qui contribue à une meilleure compréhension du Se dans le cartilage tout en montrant les difficultés d'étude du Se dans les milieux biologiques et les techniques permettant d'y répondre, mais aussi souligne l'importance de prendre en compte le sélénium comme éléments important de traitements régénérateurs ou préventifs pour ce types de maladies musculo-squelettiques.

Acknowledgments

Entrée par hasard dans ce domaine innovant et méconnu qu'est la géologie médicale, cette thèse fût plein de surprises, de challenges, de découvertes mais surtout de belles rencontres.

Au cours de ces trois années, j'ai évolué au sein de plusieurs équipes, toutes aux spécialités et personnalités très différentes mais aussi exceptionnelles: l'équipe de géochimie à Isterre avec des remerciements plus particuliers à Constance, Ana, Valérie et Sarah avec qui j'ai travaillé et partagé des moments mythiques aux laboratoires, en Suisse et aux synchrotrons, et l'équipe galloise, à Swansea, avec de grands mercis à Yadan, ma mentor - my "boss" qui m'a soutenue et beaucoup appris, et à Andrea que j'ai fait travailler de nombreux soirs et week-ends. Merci à Lenny et Elke qui m'ont permis de faire des analyses dans leur laboratoire à Zürich et de découvrir cette jolie ville avec une belle balade sur le lac.

Le synchrotron a été une expérience merveilleuse avec des résultats aussi surprenants que la réalisation de ces expériences où malheureusement quelques surnoms me poursuivront encore quelques années... un grand merci à Olivier, Jean-Louis, Christophe, Frédéric, Matthieu, Hiram, Emmanuel, Sébastien, Jean-François et Hélène et bien sûr Sylvain.

Cette thèse a été, pour moi, une véritable chance. Elle m'a poussé à aller au devant de moi-même et m'a appris que, malgré de nombreuses difficultés, toute expérience est enrichissante intellectuellement mais aussi humainement. Ce projet m'a aussi valu d'obtenir la bourse L'Oréal-UNESCO 2016 pour les femmes et la science (avec en prime le surnom de "Miss Lumière"), une véritable fierté mais également une reconnaissance de mon parcours peu ordinaire et du formidable travail d'équipe qui a été effectué durant ces trois ans.

Je tiens à remercier l'Université Grenoble-Alpes et le programme "Explora'doc" de m'avoir permi de réaliser ce projet, mes quatre directeurs de thèse qui m'ont soutenu tout au long de ce long périple: Laurent Charlet, Sylvain Bohic, Ilyas Khan et Lewis Francis, mais aussi les membres du jury: Steve Conlan, Lutz Schomburg, Matthieu Réfrégiers et Dominique Heymann.

Je n'aurais probablement pas fini cette thèse aussi bien sans mes collègues et amis grenoblois et gallois qui par leur gentillesse, leur humour et leur passion m'ont redonné le sourire, mes amis d'enfance et mes nombreux colocataires (15 et Tomy le chat en 3ans!) qui m'ont encouragée et soutenue.

Mais c'est le soutien inconditionnel de ma famille, mes parents, ma sœur, mes grands-parents et du chat Mallow qui m'ont donné la force de continuer dans les moments où je rêvais de m'écharper, et de me surpasser chaque jour pour donner le meilleur de moi-même.

Executive Abstract: Résumé de la thèse

Le Rôle du Sélenium dans le Métabolisme, la Croissance et la Maturation du Cartilage Articulaire

Introduction

Qu'est-ce que la géologie médicale? Ce terme semble très étrange et quelque peu surprenant. Comment deux domaines qu'apparemment tout oppose, se retrouvent ainsi joint? Peut-être une nouvelle fantaisie, un nouveau domaine émergeant? En réalité, ce domaine s'avère capital à notre époque où finalement les pollutions des sols et de l'air ne sont qu'omniprésentes. Effectivement, on s'aperçoit que notre « bonne santé » dépend fortement de la qualité du monde qui nous entoure et nous nourrit. Ces études complexes prennent plusieurs formes car les modifications de l'environnement peuvent être induites de façon naturelle ou forcées par l'homme, l'industrie ou la surpopulation entrainant la destruction des sols initiaux. Néanmoins, la géologie médicale s'intéresse également à des éléments dits « traces », peu ou mal connus, présents dans l'environnement et les sols en (très) faible quantité. Selon leur concentration, ces éléments ont un impact important voire capital sur la santé, étant incorporés par l'organisme par le biais de notre alimentation (céréales, eau, viande, poissons, légumes, fruits...) [a]. Généralement, grâce à une alimentation équilibrée et contrôlée, le corps prélève alors tous les éléments nécessaires à ses besoins en juste proportion. Ces éléments traces prennent alors place au sein de notre corps, et ce même jusqu'aux parties les plus fondamentales: nos cellules. Cependant, si un déséquilibre apparait, ces éléments jouant un rôle plus ou moins important ont des effets plus ou moins négatifs. En excès, ils peuvent, selon leur concentration et la forme chimique sous laquelle ils sont ingérés, être toxique et induire de sévères symptômes tels que perte de cheveux, dégradation des ongles, cécité, paralysies, ou des problèmes cardiovasculaire, hépatiques, et rénaux. En revanche, en déficit, certains éléments peuvent également générer des maladies. Pour paraphraser le grand médecin Paracelse:

«Toute substance peut être un poison. C'est simplement son juste dosage qui différencie un poison d'un remède».

C'est cet axe de la géologie médicale que ce projet explore. Ce travail consiste à comprendre comment un élément géologique peut influencer le fonctionnement de certains organismes, et donc être employé à titre de "remède".

L'élément, appelé sélénium, est un élément extrêmement intéressant, souvent décrié pour son ambivalence. Auparavant, il fût célèbre pour sa toxicité, comme cela fut démontré par Marco-Polo lors de son expédition en Chine, où ses chevaux ont sévèrement souffert, leurs sabots se dégradant à cause de l'herbe riche en sélénium qu'ils mangeaient. Récemment, sa célébrité subit un revirement. En effet, il devient l'élément à la mode pour son action antivieillissement. En vogue, il est souvent présent dans certains compléments alimentaires mais aussi dans des cosmétiques tels que les shampooings. Le sélénium est un élément trace essentiel. Il agit comme un cofacteur dans certaines enzymes et possède un rôle important dans la protection cellulaire par son caractère antioxydant et anti-inflammatoire [b]. En effet, un déficit en sélénium peut affecter la production de certaines protéines, les sélénoprotéines, capitales dans les mécanismes de réparation de l'ADN et de protection cellulaire contre le stress oxydant. Ces disfonctionnements affecteraient alors cette capacité de défense anti-oxydante et anti-inflammatoire et cela générerait une sensibilité accrue aux agressions extracellulaires telles que l'inflammation des tissus et une désorganisation de la structure tissulaire. Actuellement, environ un

milliard de personnes sur Terre souffriraient d'un déficit en sélénium, à des degrés différents avec des pathologies sous-jacentes diverses. Malgré de grandes avancées sur le sélénium, les connaissances restent limitées, notamment son rôle dans les tissus tels que le cartilage articulaire. L'intérêt premier de cette thèse sera donc d'établir une vue d'ensemble sur le rôle potentiel du sélénium, issu des sols, de l'eau et de la nourriture, dans le métabolisme, la croissance et la maturation des cartilages articulaires (Figure 1).

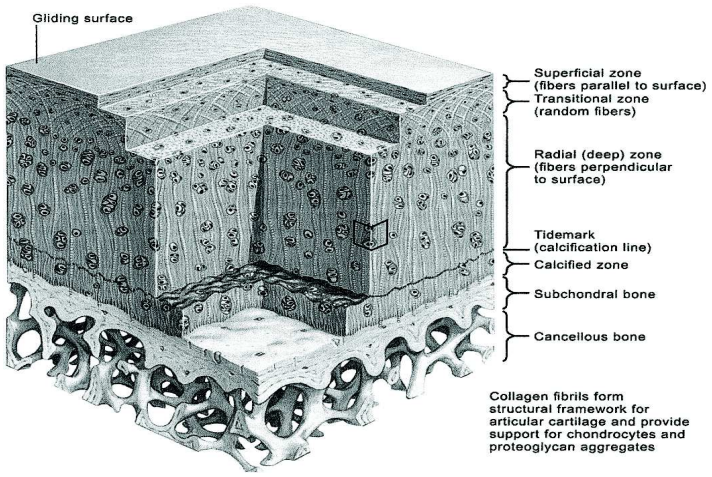

Figure 1: Articular Cartilage is divided into several zones (superficial, middle and deep zones, calcified cartilage). In each zone, the composition and the distribution of the diverse componennts of the extracelllular matrix vary [24-25].

Le cartilage articulaire est un tissu précieux, sollicités quotidiennement (en courant, en sautant, marchant ou simplement en restant en position statique). Il faut le préserver le plus possible afin de prolonger son intégrité et sa fonction, et donc assurer la longévité du corps en bon état. Les cartilages articulaires protègent notre squelette en assurant mobilité et flexibilité. Il joue notamment un rôle d'amortisseur de chocs, comme une éponge qui écrasée par compression, reprend sa forme une fois la pression appliquée évanouie, et permet de réguler la friction induite lors des diverses contraintes latérales appliquées aux articulations. Depuis, longtemps, la simple usure du cartilage due aux frictions de ces tissus, liée au vieillissement de l'articulation, a été défini comme la raison principale des maladies reliées à la dégradation voire dégénération de ces tissus. Néanmoins, dans la société actuelle, d'autres facteurs sont à prendre en compte dans le développement de ces maladies articulaires: des traumatismes répétés liés à un sport ou à une activité professionnelle répétitive, l'inactivité physique des jeunes. L'obésité, par exemple, est en augmentation dans nos sociétés. Face à ce nouveau phénomène, nos articulations sont soumises à un stress c'est-à-dire une augmentation des contraintes et des traumatismes, qui fragilise et rend plus vulnérable nos cartilages Actuellement, de nombreuses recherches (cellules souches, impression biologique 3D, greffes) tendent à développer des techniques de reconstruction du cartilage articulaire (CA) afin d'obtenir un ersatz compatible et bio-implantable. Cependant, cette substitution voire reconstitution n'est pas simple et les méthodes utilisées ne suffisent pas pour résoudre des pathologies affectant les articulations telles que l'arthrose, touchant des millions de personnes en France, ou la maladie de Kashin-Beck, touchant des millions de personnes en Chine. Ces maladies, correspondant à une dégénérescence des cartilages articulaires, sont douloureuses et souvent même handicapantes. Les causes de ces disfonctionnements ne sont pas uniquement mécaniques, dues à la vieillesse ou à des accidents, mais peuvent être également d'ordres biologiques et génétiques (terrain génétique). Des études sur l'impact de l'environnement sur la santé montrent que certains minéraux et éléments traces peuvent avoir un impact important

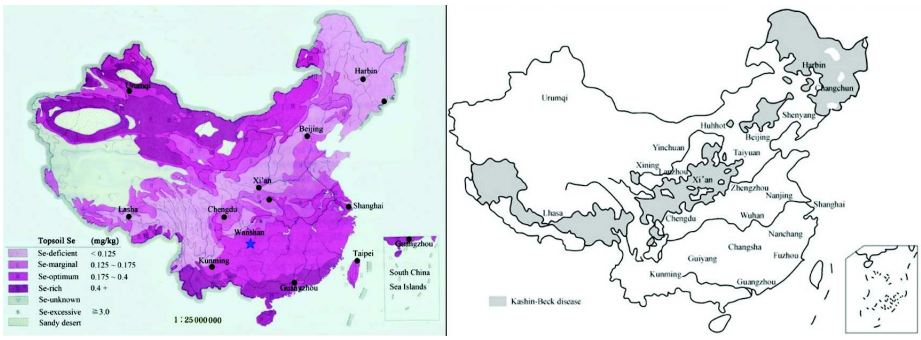

Figure 2: Geological and epidermiological correlations exposed a strong link between selenium deficient soil and the distribution of kashin-Beck disease in China. (Left) Map of the distribution of selenium in soils of China from the paper of Zhang et al 2014, the light purple area refers to the Se-deficient soil and (Right) Map of the Kashin-Beck Disease distribution (in grey) in China from the paper of Li et al. 2009.

sur la santé. Suite à la corrélation des données environnementales (des sols et de la géologie sous-jacente) et épidémiologiques en Chine, établie par Stone en 2009 [d], il est apparu un besoin pressant d'évaluer l'importance du sélénium (Se) et de préciser le rôle dans les maladies tels que la maladie de Kashin-Beck affectant le cartilage articulaire. En effet, un lien très fort a été établi entre un déficit en sélénium des sols et ces cas ostéochondrodysplasie permanente et invalidante (Figure 2).

Une étude récente, appelé "Johnston project" menée par Dr. J. Jordan, aux États-Unis, a montré un lien clinique entre une déficience en sélénium et l'arthrose du genou [e]. Le sélénium semble donc bien être un acteur clé dans le développement des chondrocytes, cellules spécifiques du cartilage, et de la matrice extracellulaire. L'objectif de la présente étude est de déterminer le rôle exact du sélénium dans le cartilage articulaire du point de vue biologique, biomécanique et dynamique. Et donc, parmi ses nombreuses fonctions, notre projet vise à comprendre son rôle dans le métabolisme des cartilages articulaires.

Cette thèse est basée sur l'hypothèse principale que le sélénium est un composant crucial dans le métabolisme et l'homéostasie du cartilage articulaire, comme notamment exprimé dans la maladie de Kashin-Beck et de l'arthrose. Afin de déterminer le rôle du sélénium dans le fonctionnement normal des chondrocytes (cellules spécifiques du cartilage), deux grands axes d'études ont été mis en place: (i) déterminer l'implication du sélénium dans l'organisation et les fonctions du tissu, au moyen d'une étude de spéciation et localisation de cet élément trace, et (ii) caractériser les variations apparaissant dans la matrice extracellulaire du cartilage articulaire lorsque le cartilage est traité avec différents concentrations de sélénium durant le processus de maturation. La caractérisation de la structure de la matrice extracellulaire organique du cartilage articulaire est le point central des travaux. Cette maturation induite correspond à la phase de croissance "post-natale". Il s'agit de mieux comprendre si le sélénium influe sur la différentiation d'un tissu immature possédant une part de cartilage de croissance en un tissu quasi mature. L'identification des différentes cibles biologiques critiques tels que les sélénoprotéines impliquées dans ce processus, et la distribution et la forme chimique du sélénium dans la matrice voire dans les cellules pourraient bien être une information clé pour évaluer le(s) mécanisme(s) potentiels sur lesquels il serait possible d'agir pour améliorer la régénération et la réparation du cartilage

L'étude d'éléments tels que le sélénium dans des milieux biologiques n'est pas aisée, étant présent en microquantité dans l'organisme. Grâce à des études ICP-MS (Inductively coupled plasma mass spectrometry), il a été possible d'évaluer cette concentration en sélénium au sein de ces tissus. Les concentrations en sélénium au sein du cartilage sont de l'ordre de quelques centaines de ppb (μg/kg)

(1 goutte sur 1 milliard de gouttes en somme) rendant les analyses très complexes, et nécessitant le développement de techniques de microspectroscopie particulières utilisant la lumière synchrotron. Grâce à une technologie optique de pointe, il nous permet d'aller au-delà des techniques de microscopie classique et de sonder la matière à très petite échelle (micro & nano-scopique). Jonglant alors entre la culture d'explants en laboratoire et mesures sur synchrotron, il a été possible d'évaluer des variations de compositions et de structure de la matrice organiques du cartilage, apparaissant pour différentes concentration en sélénium. Pour répondre à nos objectifs, plusieurs techniques spécifiques sont utilisées : la microscopie synchrotron à fluorescence X (ESRF-ID16B) pour la distribution subcellulaire du sélénium et la microspectroscopie infrarouge à transformée de Fourier (FTIRM) (ERSF-ID21, SOLEIL-SMIS) pour l'évaluation des variations biologiques et morphologiques de la matrice organiques du cartilage apparaissant en fonction de la concentration en Se et supposant que le Se agit par le biais de sélénoprotéines et de gènes. La microscopie synchrotron deep-UV (combiné avec la microscopie seconde harmonique, SOLEIL-DISCO) permet enfin l'étude de la matrice organique (principalement le collagène) du cartilage en phase de maturation et en présence ou absence de sélénium afin d'obtenir la distribution et les niveaux de tyrosine/tyrosinase, Tryptophan et collagène au sein de la matrice cartilagineuse.

Des analyses ont aussi été faites afin de comprendre les changements induits par la variabilité génétique. Plusieurs investigations biologiques telles que des analyses d'expression (PCR/qPCR, CNH-Swansea) et la localisations des protéines et des gènes (immunofluorescence, CNH-Swansea) ont été menées en parallèle. Afin d'interpréter les résultats synchrotron obtenus (caractérisations de structures et variations chimiques du tissu), des analyses histologiques, colorations, immunohistochimiques, biochimiques, et AFM (CNH-Swansea) ont été réalisées afin de corréler nos analyses microspectroscopiques aux variations de composition biologique du tissu telles que les variations de la prolifération cellulaire, de concentration des protéoglycannes et du collagène. La localisation de la présence du Se dans les tissus a été possible grâce à des techniques synchrotrons de pointe (microspectroscopie synchrotron à fluorescence X (ESRF-ID16B)). Un résultat surprenant montre un motif récurrent de distribution du sélénium. La spéciation (HERFD-XAS) (ESRF-BM30B, CRG FAME) et le dosage ICP-MS (ISTerre-Grenoble, EAWAG-ETH-Zürich) de la concentration dans les tissus ont été réalisés. L'identification de l'espèce chimique est importante car elle permettra de comprendre à quel niveau le sélénium entre en jeu. Le sélénium dans le cartilage articulaire est donc un élément ultra-dilué qui rend son analyse extrêmement difficile. Une véritable performance technologique a été effectuée permettant de réaliser cet exploit grâce à la puissance de flux et à une technique adaptée. Pour la première fois nous avons donc pu déterminer la localisation du sélénium et la spéciation pour cette échelle de concentration. Cette première est le résultat de développement de la nanoanalyse X et d'une nouvelle méthode de spectroscopie XANES haute résolution qui fait l'objet d'un article soumis à publication. La dynamique du collagène a été suivie de près afin de comprendre les variations biomécaniques résultant des changements biologiques et chimiques observées en fonction des traitements en sélénium des différents explants de cartilages. Des analyses sur l'expression des gènes et de protéines (qPCR, Western Blot, protéomique) devront être poursuivies dans un futur proche dans le but d'identifier les cibles (exactes) induisant des changements dans le développement du cartilage articulaire mais également du cartilage épiphysaire et du cartilage de croissance. Tout a été effectué dans le but de vérifier qu'un déficit ou une supplémentation en sélénium pendant la phase critique de croissance au développement du cartilage coïncide avec l'apparition de symptômes identiques à ceux de la maladie de Kashin-Beck et à l'arthrose entre autres. Notre second axe d'étude est donc plus ciblé sur l'implication du sélénium dans l'organisation et le fonctionnement du tissu.

Matériels & Methodes:

Modèle Biologique: Le cartilage articulaire immature est une base idéale (modèle) et malléable pour le conception d'un nouveau tissu et pour l'évaluation de l'évolution de ce tissu lors de la maturation. La croissance et la maturation post-natale du cartilage articulaire peut durer jusqu'à 12 ans dans des conditions *in vivo*. L'équipe de Charles Archer and Ilyas khan (Cardiff, Wales) a développé un modèle biologique induisant une maturation accélérée d'explants de cartilage articulaire, ne demandant alors que quelques semaines. Cette « maturation accélérée » est basée sur une mise en culture *in vitro* statique d'explants durant 21 jours traités avec un cocktail de facteurs de croissance [f,g].

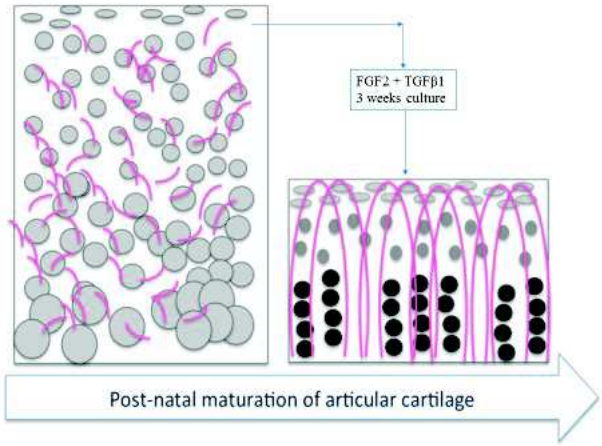

Figure 3: Effet des fecteurs de croissance sur les explants lors du traitement de maturation. *Ben Morgan*

Basé sur ce modèle, nous avons essayé de vérifier si le manque ou la supplémentation en sélénium pendant cette phase critique de développement, coïncidant avec l'apparition de la maladie de Kashin-Beck (et l'arthrose), révèlent quelques pertinences biologiques. La condition "déficit en sélénium" est notre condition d'étude et correspond à un retrait de tout sélénium pouvant se trouver dans le milieu de culture utilisé dans notre modèle de départ . Ce modèle a été développé pour décrire la croissance et le métabolisme du cartilage articulaire durant la phase de maturation. Ceci donne une excellente base pour le développement d'un modèle *in vitro* afin de comprendre l'impact du sélénium sur la maturation du cartilage et comment prévenir sa dégradation et potentiellement trouver un traitement régénératif innovant.

Pour ce nouveau modèle, des explants de 4-mm de diamètre ont été excisés, sous conditions stériles, de la partie latérale du condyle médian de l'articulation métacarpophanlangeale de jeunes bovins agés de sept jours et ont été cultivés *in vitro*. Ces explants présentent une fine couche d'os sous-chondral à leur base. Afin d'induire la maturation des ces explants de cartilages, ceux-ci sont placés dans un mileu sans sérum ("serum-free medium" - Dulbecco's modified Eagles medium). De l'insulin-transferrin-selenium (ITS), un tampon HEPES (buffer - 1M), des antibiotiques (gentamicin, 50 mg/mL) et des anti-mycotiques sont supplémentés avec un cocktail de facteurs de croissance composé de 100 ng/mL fibroblast growth factor 2 (FGF-2) et 10 ng/mL transforming growth factor β1 (TGF-β1) (19). Cette combinaison spéciale de facteurs de croissance entraîne des profonds changements morphologiques dans le cartilage articulaire immature (19). Cette stimulation semble aboutir à l'apoptose et la résorption de la zone basale c'est-à-dire dans la zone de proche de l'os et de la prolifération cellulaire des chondrocytes en surface (15). Cette maturation induite est déjà fondée sur une supplémentation en sélénium (dû à la présence d'ITS), cependant son importance n'a pas été évaluée. Ainsi, différents sets d'explants ont été cultivés en présence de différentes concentrations en sélénium. Trois groupes majeurs d'échantillons

ont été cultivés dans trois types de milieux de cultures: (a) sans trace de Se, nommé "No Se" (au lieu d'utiliser de l'ITS, de la transferrine humaine et de l'insuline bovine ont été employées dans des quantités prodiguant la même concentration en insuline et transferrine que l'ITS), (b) avec de l'ITS, nommé "ITS" (protocole classique développé où 5 ng/mL de sélénite de sodium est présent dans la solution), et (c) avec une supplémentation en sélénium donnant une solution finale d'une concentration totale de 50 ng/mL de sélénite de sodium solution, nommée "Se-supplemented". Pour chaque groupe, les explants sont placés en deux sous-groupes: les explants contrôles et les explants "FT-treated" correspond aux explants traités avec des facteurs de croissance. Chaque pool provient du même pied afin d'avoir une parfaite corrélation entre contrôles et traités. Ce large panel est donc utilisé afin d'évaluer l'impact du sélénium sur la croissance, la maturation mais aussi le métabolisme.

Préparation des échantillons:

Après les trois semaines de cultures, les explants sont donc fixés et préservés et ceci par deux méthodes différentes selon le besoin des analyses.

Enrobés en paraffine après déhydratation, pour les analysis histologiques, des coupes de 7 μm sont préparées et ensuite teintes à la Safranine-O et à l'Hematoxicin & Eosin. Les coupes sont ensuite analysées au microscope pour déterminer de façon qualitative les changements morphologiques (taille, formes et distribution des cellules) et la distribution globale de tous les protéoglycannes. Pour les analyses PCR classiques et quantitatives, les explants (de différentes conditions) ont été cryo-broyés par un "dismembrator" en une poudre ultrafine. L'ARN de ces échantillons est alors extrait et isolé à l'aide du kit RNeasy Mini Kit de QIAGEN. L'ARN est converti en ADNc. Des analyses PCR et qPCR (transcription des sélénoprotéines) permettent alors d'évaluer la modulation de l'expression génétiqueen fonction des traitements en sélénium.

Pour les analyses ICPMS (Inductively coupled plasma atomic emission spectroscopy) et XANES (X-ray Absorption Near Edge Structure Spectroscopy), les explants de différentes conditions sont également cryo-broyés par un "dismembrator" en une poudre ultrafine, cette poudre est alors lyophilisée à -40°C sous vide 0.150 mbar pour 12 heures et sont conservées à 4°C dans une boîte scellée sous un environnement anoxique pour éviter tout modification (états d'oxydation) des espèces séléniées au sein du cartilage. Pour les échantillons analysés par l'ICPMS, diverses attaques acides sont faites successivement afin de digérer au mieux la matrice extracellulaire organique très dense présente dans la poudre. Premièrement, 3mL de 14 M HNO_3 (double distillé) est ajouté aux échantillons et laissés à 100 °C pour 24h , puis 1 mL de H_2O_2 ultrapure est ajouté à la solution et laissé à température ambiante pendant 12 h avant d'être re-chauffé à 100 °C pour 72h. Une évaporation finale se fait à 100 °C pendant 6h. Les différents résidus solides sont alors dissous dans 5 mL d'un solution de 1L HNO_3 1%) et chauffés à 100 °C pour 10 min et sont ensuite placés au bain d'ultrasons pendant 5 min afin de resuspendre totalement le résidu avant analyse. Cette analyse permet l'évaluation de la concentration intrinsèque en sélénium des explants placés dans différentes conditions de cultures pour les études XANES. Les échantillons sont préparés sous condition anoxique. Les poudres étant mises sous presse afin de former des pastilles adaptés au porte échantillons du set-up expérimental. Cette analyse microscopique permet d'étudier la spéciation des échantillons en sélénium afin de déterminer l'état d'oxydation. Ceci permettrait d'entrevoir les processus biochimiques agissant sur le tissu en cas déficit ou de supplémentation en sélénium.

Pour les analyses par microspectroscopies de fluorescence X (XRF) et Deep-UV (DUV) induites par rayonnement synchrotron, des coupes très fines de 20 μm sont montées sur des feuilles d'ultralene spécifique pour XRF de 4 μm d'épaisseur et sur des lames de quartz de 0.16 mm d'épaisseur, respectivement. Pour la microspectroscopie XRF, l'échantillon a été légèrement défocalisé de façon à pouvoir

faire une carte multi-élémentaire par fluorescence X à différentes échelles: pour sonder des aires de 200 μm, on utilise un faisceau de 1 μm et un faisceau de 0.1 μm pour les chondrocytes (10-40 μm). Cette technique est nécessaire pour déterminer la localisation du sélénium dans le cartilage, identifier sa position cellulaire, extracellulaire, ou les deux. Des analyses semi-quantitatives ont été faites par le logiciel PyMca pour la fluorescence X. Les analyses en DUV permettent de visualiser la distribution les principaux fluorophores endogènes au sein de coupes histologiques des différents explants de cartilage articulaire de bovins. Ces fluorophores, tels NAD(P)H, tyrosine et Tryptophane, ayant une localisation tissulaire et des fonctions biologiques différentes, la microspectroscopie deep UV est plus particulièrement sensible aux variations du métabolisme cellulaire et ; à l'organisation structurelle du tissu à travers l'émission du collagène (autofluorescence résultat du cross-link) . Cette technique est exploratoire, inspirée d'une étude menée sur les os [h], et très complémentaire des résultats obtenus en microspectroscopie infrarouge.

Les analyses en microspectroscopie infrarouge à transformée de Fourier ont été effectuées sur des cryo-coupes de (10 μm) déposées sur des fenêtres IR de BaF_2. La taille de l'ouverture est de 10x10 μm^2 et la résolution spectrale est de 6 cm^{-1} permettant d'obtenir des spectres d'absorption de haute qualité avec seulement 16 scans par pixel. Cette technologie permet d'apporter une information semi-quantitative de l'influence du sélénium dans la composition biologique de différents explants: distribution et concentration des bandes d'absorption telles que celle des bandes amide I, Amide II, et la bande des sucres "sugar-rings". La collection de spectres est réalisée sous la forme de cartographie spectrale point par point sur une bande allant de la zone surfacique du cartilage jusqu'à l'os sous-chrondral.

Résultats & Discussion:

Notre hypothèse générale est reliée au fait que le manque de sélénium dans le milieu de culture des explants de cartilage articulaire peut induire une dégénérescence du tissu aux propriétés biomécaniques proches de celles observées dans les cartilages touchés par l'arthrose. L'action du sélénium se fait essentiellement par l'intermédiaire de sélénoprotéines. La fonction principale du sélénium serait alors fortement reliée à ses actions anti-oxydantes et anti-inflammatoires utiles pour la protection cellulaire. Partant d'un modèle déjà validé dans la littérature, nous l'avons modifié pour évaluer l'influence du sélénium sur la maturation post-natale du cartilage articulaire (immature) et comprendre l'impact de cet élément sur la phase critique de croissance qui coïncide avec l'âge où la maladie de KBD se développe. Les différentes expériences entreprises dans ce projet vont tenter de répondre à plusieurs questions telles que : quelle est la distribution du sélénium dans le tissu ? Sous quelle forme (spéciation)? Quel impact éventuel a-t-il au niveau cellulaire et de la matrice extracellulaire? Quel est son impact sur les propriétés nanomécaniques du cartilage ? Comprendre l'intérêt du sélénium dans le métabolisme et la croissance du cartilage articulaire est fondamental pour d'établir des solutions préventives adéquates à la dégradation des cartilages mais également améliorer les différents traitements à visée régénérative en cours de développement.

Comme décrit précédemment, la détermination de la concentration du sélénium dans les explants est difficile. Etant donné que le sélénium est un élément trace, il est présent dans le corps en microquantité, et réparti de façon inégale, selon son utilisation dans les différentes parties du corps et les cellules. Des analyses ICPMS (Inductively coupled plasma atomic emission spectroscopy) ont permises d'évaluer la concentration intrinsèque des explants traités. Il y a trois groupes d'échantillons et deux de références provenant de conditions natives/originales sans mises en culture. Pour les conditions natives et les échantillons provenant d'une culture sans sélénium, la présence de Se a été évaluée à

environ une centaine de ppb (μg/kg). Les échantillons traités avec de l'ITS ou avec du sélénite de sodium ont quant à eux une concentration intrinsèque d'environ 450 ppb et 2500 ppb, respectivement (Table 1). Il n'y a apparemment pas de différences significatives entre les échantillons contrôles et ceux traités avec le cocktail de facteurs de croissance; les facteurs de croissance permettant la maturation accélérée du tissu n'influencent pas l'incorporation du sélénium ni sa production. Néanmoins, cette expérience nous donne une information importante: la supplémentation en sélénium présente dans les milieux de cultures se retrouve dans les échantillons. Cette augmentation de teneur en Se est quasi proportionnelle à la concentration présente dans le milieu de culture.

Echantillons	Moyenne Totale (ppb)	Ecart type σ (ppb)
Immature	176 μg/kg	49 μg/kg
No Se Control	193 μg/kg	76 μg/kg
No Se FT-treated	188 μg/kg	54 μg/kg
ITS Control	401 μg/kg	56 μg/kg
ITS FT-treated	519 μg/kg	160 μg/kg
Se-Supplemented Control	2172 μg/kg	540 μg/kg
Se-Supplemented FT-treated	2979 μg/kg	739 μg/kg
Mature	159 μg/kg	83 μg/kg

Table 1: Les concentrations totales en sélénium (Se_{tot}) des explants des cartilages articulaires bovins en µg/kg (ppb) sont mesurées par analyse ICP-QQQ après une procédure de digestion acide. Les échantillons ont été exposés à différents traitements: conditions standards sans sélénium dans le milieu de culture en présence (No Se FT-treated) ou absence (No Se Control) de facteur de croissances, insulin-transferrin-selenium (ITS) en présence (ITS FT-treated) ou absence (ITS-Control) de facteurs de croissances, ou avec une supplémentation additionnelle de 50 µg/L de sodium selenite, (N$\geq$4) pour chaque condition (intitulées "Se-supplemented control" et "Se-supplemented FT-treated"). Des explants de cartilage articulaire immature et mature (natifs, sans avoir été placé en culture ou traités) ont été analysés. Ce tableau correspond à la moyenne des explants traités et analysés dans les mêmes conditions. L'écart-type représente la variation des réplicas et est relié à la variation biologique provenant du modèle de culture. La limite de quantification est de 0.020 µg/L et la limite de détection des échantillons est fixée à 0.09 µg/L correspondant à environ 70 ppb µg/kg (poids sec) en Se dans les échantillons.

Au vu de ces concentrations extrêmement basses, l'analyse du sélénium s'avère très complexe. Des techniques de pointes ont dû être utilisées pour poursuivre cette étude en ayant recours à la lumière synchrotron. Afin de comprendre le rôle du Se, une analyse de sa distribution et de sa spéciation au sein du tissu furent menées par le biais de diverses études spectroscopiques sur synchrotron. L'étude a été faite sur toute la hauteur du cartilage articulaire de la surface à la zone profonde. Une étude préliminaire de microscopie en fluorescence X a révélé un schéma de distribution très intéressant du sélénium dans le cartilage articulaire, fortement corrélé à une zone ponctuelle en bordure/limite des chondrocytes, et cela quel que soit la zone. Ce positionnement particulier du sélénium pourrait être relié à un organite spécifique. Ce schéma de distribution semble indépendant du type de l'échantillon (contrôle ou traité par des facteurs de croissance) comme cela est montré 4. Au vu de ce positionnement, à l'interface cellule/matrice extracellulaire, le sélenium pourrait être un médiateur entre cellules et matrice et donc jouer un rôle dans l'organisation et la structuration du tissu. En observant la Figure 4, un seul pixel (vert, Se) est visualisé par cellule. Dans la littérature [l],il a été montré qu'un organite, appelé cil primaire, unique, est présent sur quasiment toutes les cellules. Cette organelle est un élément moteur et essentiel dans le processus de transduction mécanique, permettant le maintien de l'intégrité du tissu. Ainsi, une hypothèse peut être avancée: le sélénium pourrait jouer un rôle important dans le métabolisme des chondrocytes, et avoir une fonction rétroactive sur la structuration de la matrice, et notamment dans la transduction mécanique, par exemple. Nous pouvons rappeler que par exemple la capsule mitochondriale du spermatozoïde contient trois sélénocystéines et que le

sélénium joue vraisemblablement un rôle structural en permettant la formation de la gaine hélicoïdale mitochondriale autour du flagelle du spermatozoïde. Faire ce type de parallèle avec les chondrocytes reste encore purement spéculatif compte tenu de nos résultats mais il serait très intéressant de pouvoir prouver cette hypothèse.

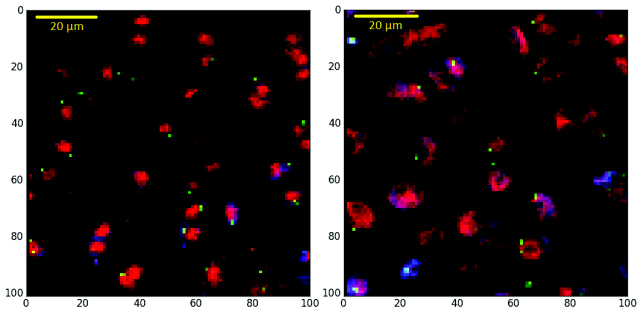

Figure 4: Localisation du Sélénium dans le cartilage articulaire obtenue par synchrotron (XRF) microspectroscopie de fluorescence X. Zn est representé par la distribution de points rouges réfèrant aux cellules, Fe par les points bleus (cytoplasme) et Se par les points verts. La figure de gauche correspond à l'échantillon "ITS-Control" et celle de droite à l'échantillon "ITS-FT-treated". Les deux figures montrent la même distribution en Se. Cartographies de Cartographies de 100x100 μm^2.

Après avoir détecté la distribution sub-cellulaire du sélénium, des analyses en "high energy resolution fluorescence detected X-ray absorption spectroscopy" (HERFD-XAS) couplées à un ensemble de cristaux analyseurs ont permis d'identifier la spéciation du sélénium dans les explants traités. Cette technique apporte un bien meilleur rapport signal sur bruit que les techniques XAS classique, ce qui permet d'obtenir des spectres d'éléments en concentration extrêmement faible. Cela nous a permis d'identifier sans ambiguïté les espèces séléniés dans le cartilage du modèle de maturation à l'aide d'une librairie de spectres de référence des composés séléniés organiques et inorganiques. La forme sélénocystéine apparait comme l'un des composants principaux du Se dans le cartilage (Figure 5). Ceci n'est pas surprenant. L'activité du sélénium biologique correspond à sa présence et son incorporation dans des sélénoprotéines telles que la gluthatione peroxidase, l'iodothyronine deiodinases ou la thioredoxin reductase, qui possèdent au sein de leur site actif du sélénium sous forme de l'acide aminé sélénocystéine (Sec) [l]. Il est important de remarquer que le polymorphisme génétique du gène gluthatione peroxidase 1 a souvent été décrit comme étant associé à des risques accrus de développer la maladie de Kashin-Beck [m]. D'autres contributions sont présentes comme des composants thiosélèniure, tels que la sélénodiglutathione (GSSeSG). La GSSeSG est le principal métabolite du gluthation réduit (GSH) présent dans les tissus mammaliens [n] avec des sels inorganiques de sélénium, comme le sélénite de sodium utilisé dans ce travail et qui est un nutrient essentiel [l]. Sélénite et GSH réagissent spontanément pour former de la GSSeSG [o]. La concentration de glutathion réduit est très élevée dans presque tous les tissus. Nous retrouvons environs $\frac{3}{4}$ de HSSeSG et $\frac{1}{4}$ de sélénite de sodium pour les échantillons dont le milieu de culture a été supplémenté en sélénium (sélénite de sodium) pendant trois semaines. Quantifié par ICP-MS, la concentration intrinsèque en sélénium croit de 5,5 fois dans les cartilages cultivés avec une supplémentation en sodium de sélénite (50 μg/L soit 7,5 fois plus de sélénium) par rapport aux échantillons cultivés avec seulement de l'insuline-transferrine sélénium. Ceci corrèle avec l'augmentation du nombre de coups (~5 fois plus grand) de la raie Se-K α du spectre de fluorescence des rayons X obtenu lors des mesures en HERFD-XAS. Cette observation reste valable pour les échantillons traités ou non avec des facteurs de croissance. Cela suggère que lors d'une supplémentation avec du sélénite de sodium, l'incorporation du sélénium dans les cartilages articulaires reste limitée et ce indépendamment du traitement avec des facteurs de croissance connu pour réguler le métabolisme des chondrocytes [p]. La sélénodiglutathion est une espèce intermédiaire

chimique produite par une réaction non-enzymatique entre le sélénite et la glutathione [l], et peut-être ensuite métabolisée en "hydrogen selenite" (HSe^-) via la formation de selenopersulfide (GSSeSH) par les glutarédoxines en présence d'un excès de GSH qui mène à une oxydation spontanée de HSe^- en Se^0 (sélénium élémentaire). Se^0n'est pas détecté dans nos échantillons ce qui suggère que la GSSeSG est préférentiellement incorporée dans notre modèle de maturation du cartilage articulaire exposée à des concentrations élevées sélénite de sodium. Il serait intéressant de pouvoir résoudre spatialement la distribution de ces espèces et d'explorer la nature du sélénium lié aux chondrocytes ou dans des fractions de protéines présentes dans la matrice du cartilage articulaire. Cette expérience montre que la technique de " HERFD-XAS " peut être appliquée a des études sur des espèces élémentaires extrêmement diluées dans des matrices biologiques très complexes tout en permettant d'obtenir une bonne signature, quel que soit l'élément. Cela montre également qu'à présent, les portes sont ouvertes sur la spéciation d'éléments ultra-dilués dans des échantillons biologiques et notre étude permet de lever une limitation importante de la spéciation par spectroscopie d'absorption par rayons X qui restait jusqu'à maintenant possible pour des concentrations en élément de quelques dizaine de ppm (mg/kg) et ainsi de gagner presque un ordre de grandeur pour la spéciation.

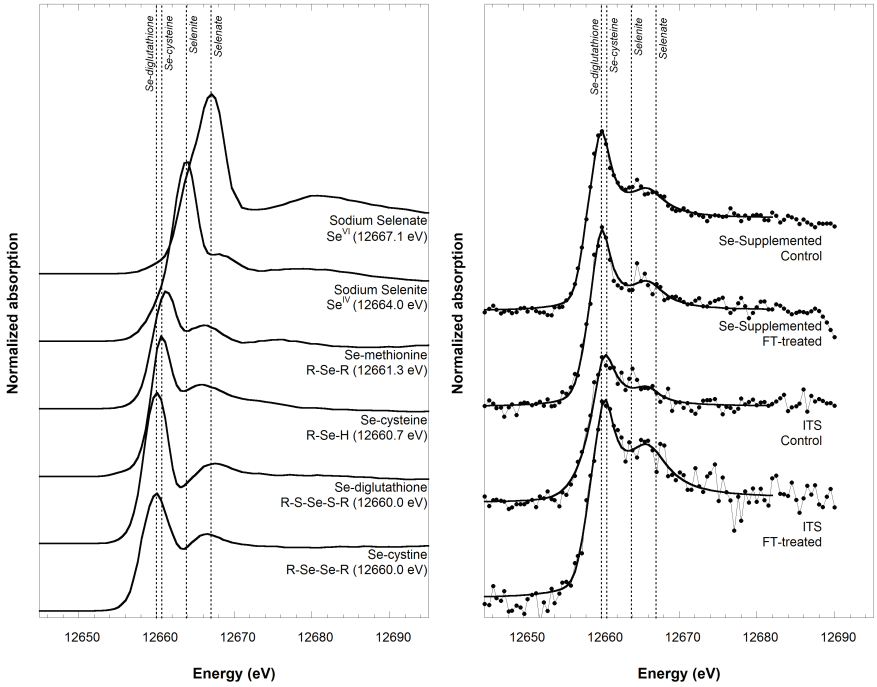

Figure 5: *Gauche:* Spectres de "High energy resolution fluorescence detected x-ray absorption" du "K-edge" du sélénium de plusieurs composantes en sélénium (analysés en solution sauf la sélénocysteine analysées à l'état solide) utilisant un fit de combinaison linéaire combination fitting pour chaque spectre expériemental. La position du maximum de la raie blanche est indiquée entre paranthèses. *Right:* Spectres du sélénium pour les différents explants de cartilage articulaire cultivés en présence d'insuline-transferrine sélénium (ITS) seul (spectres du haut) et en présence d'ITS et de sélénite de sodium "Se-supplemented" (spectres du bas). Les contrôles sont présentés pour chaque groupe ("ITS" et "Se-supplemented") et ils correspondent à des explants cultivés sans aucun facteur de croissance et donc n'ayant pas subit le traitement de maturation accélérée.

Afin de caractériser l'impact du sélénium sur la structure et la morphologie du cartilage, des coupes histologiques des différents tissus traités avec différentes concentrations en sélénium ont été colorées avec de la safranine-O afin de mettre en évidence la distribution des protéoglycannes dans ces tissus. Les explants traités avec du sélénium, et de l'ITS, sont la reproduction du modèle développé par Khan et al. 2011 [f], et donnent les même résultats au niveau de la morphologie et de la densité cellulaire

(figures 6C&D), par exemple[i]. Une singularité intéressante apparait dans les cultures sans aucun apport en sélénium et ayant subi un développement de maturation accélérée (Figure 52B). A leur surface, des variations caractéristiques apparaissent: la formation d'un cluster où les chondrocytes se regroupent sous forme d'unité indépendante, morphologie de surface similaire à celle de l'arthrose de stade précoce [j]. Cependant, un environnement sans sélénium semble procurer un environnement favorable au développement de caractéristiques cellulaires assimilables dans une certaine mesure à ce que l'on peut retrouver dans l'arthrose. L'effet de cluster, caractéristique de l'arthrose, apparait faiblement dans certains des échantillons cultivés mais est nettement moins important dans les tissus natifs. Ceci peut être expliqué car le tissu, encore jeune et placé dans un environnement sans contraintes bio-mécaniques essentielles pour la formation d'un cartilage mature fonctionnel. Ces résultats restent prometteurs sur la création d'un modèle déficient en sélénium qui pourrait être intéressant pour l'étude de certains aspects de l'arthrose. Il reste, néanmoins, beaucoup d'analyses complémentaires à effectuer afin de valider officiellement ce modèle et conclure sur les origines et les effets de ces clusters observés dans notre modèle.

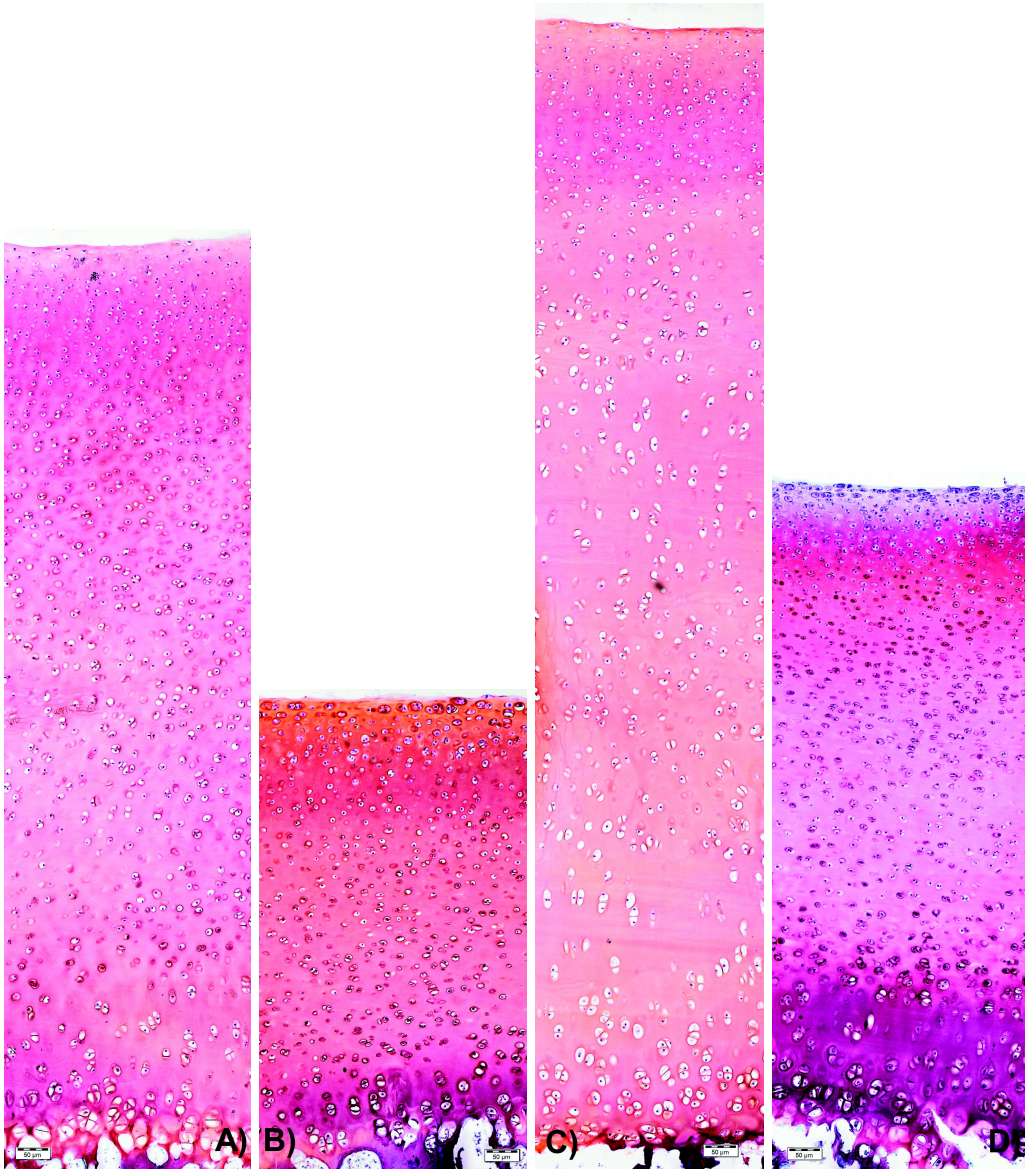

Figure 6: Maturation post-natale du cartilage articulaire pour des explants cultivés dans différents milieux de culture. Les explants proviennent de l'articulation metacarpophalangeale d'un veau mâle. Les coupes font 7 μm d'épaisseur et ont été teintées avec de la Safranine O pour souligner la composition en protéoglycanes présente dans les tissus soumis aux différents traitements: A) No Selenium Control, B) No Selenium FT-treated, C) ITS Control, and D) ITS FT-treated.

Afin de préciser et de potentiellement quantifier les changements apparaissant dans la matrice, des analyses de microscopies infrarouges à transformée de Fourier (FTIRM) ont été réalisées. Complémentaires de l'histologie et des études d'immunofluorescence, la FTIRM nous a permis d'évaluer les variations de la biochimie et de la morphologies des cartilages en présence ou non de sélénium dans le milieu de cultures. En effet, plusieurs index de la littérature ont été sélectionnés afin de visualiser les principales composantes moléculaires constituant le cartilage articulaire c'est à dire des fréquences caractéristiques d'absorption en IR des groupes fonctionnels relatifs au collagène et aux protéoglycannes. La bande des amides I est souvent rattachée à la bande du collagène, composante élémentaire et majoritaire du cartilage. Cependant cette bande, souvent utilisée dans la littérature pour les quantifier le collagène dans les cartilages matures n'est pas idéale dans notre modèle de maturation accélérée dû à des bandes d'autres composantes contribuant dans cette région spectrale. Afin d'affiner et de caractériser ces composantes au plus juste, deux autres bandes ont été choisies: la bande

1062 cm^{-1} [r] pour les protéoglycannes et la bande à ~1338 cm^{-1}pour la signature du collagène [q]. Dans les échantillons traités avec du sélénium et des facteurs de croissances (ITS FT-treated), une matrice dense et homogène en protéoglycannes ainsi qu'une répartition uniforme du collagène a été révélée (Figure 7 B&C). Pour les contrôles (ITS Control), c'est-à-dire les explants cultivés avec du sélénium mais sans facteur de croissance, il est possible d'observer des variations locales de la composition en protéoglycannes qui restent toutefois relativement homogène et légèrement moins dense que dans les ITS FT-treated et présentent une réduction du signal du collagène surtout dans la zone profonde (Figure 7 B&C).Pour les explants de cartilage articulaire traités dans un milieu déplété en sélénium (No Se Control), une altération de la distribution du collagène dans les zones médiane et profonde comparé à celle présent dans les tissus immatures natifs (Figure 7C). Cette forte altération pourrait être directement reliée à l'absence de sélénium dans le milieu de culture. La distribution des protéoglycannes quant à elle est complexe et anarchique présentant une forte concentration qui semble corréler à la position des chondrocytes dans la zone profonde (Figure 7B). En revanche, la distribution en collagène est relativement homogène dans ces zones plus profondes et possèdent en zone superficielle, une décroissance de cette distribution. Ces observations corrèlent fortement avec ce qui a été observée sur les coupes histologiques (figure 6D). Combinant ces informations sur le collagène et les protéoglycannes, le traitement par des facteurs de croissance semble donc plus que jamais essentiel dans le processus de maturation des cartilages articulaires, dans ce modèle *in vitro*. La composition en collagène augmente donc et est bien homogène dans l'ensemble pour les matrices des tissus maturés. Cependant, le milieu déplété en sélénium a un impact certain sur cette distribution. La combinaison "facteur de croissance et déficit en sélénium" semble induire une balance dans cette distribution, les facteurs de croissance pourraient compenser partiellement le manque en sélénium, mais aucune information n'est apportée quant à la qualité de la matrice extracellulaire. Les échantillons "ITS FT-treated" présentent des distributions en protéoglycannes et en collagène en accord avec celles attendues pour une maturation accélérée de cartilage articulaire [f] contrairement aux explants "No Se FT-treated" montrant seulement une intense croissance de la composition en protéoglycannes dans cette matrice extracellulaire. Ces informations infrarouges ne donnent qu'une vue qualitative des variations biochimique de la matrice cartilagineuse, sans indication formelle de sa qualité. D'autres expériences sur les propriétés biomécaniques du cartilage doivent être explorées pour ce modèle *in vitro*.

Des tests en microscopie à force atomique ont été effectués pour établir des cartes topographiques et pour évaluer les altérations nanomécaniques, potentiellement induites par le manque de sélénium dans les milieux de culture, apparaissant à la surface des matrices de ces cartilages traités. La zone superficielle est une région très active dans le métabolisme du cartilage où se déroulent le renouvellement et la ré-organisation de la matrice. Reproduisant des tests sur des échantillons déjà publiés (groupe d'échantillons ITS), les résultats montrent une concordance avec ceux publiés par Khan *et al.* 2013 [g]. Ainsi, comme présenté sur la Figure 90, il est possible de voir que l'absence en sélénium dans les milieux de culture influence donc bien la nano-mécanique du tissu cultivé, ces échantillons ayant alors un module de Young inférieur à ceux traités avec du sélénium (ITS), induisant alors une réduction de la rigidité du tissu et augmentant sa capacité de déformation.

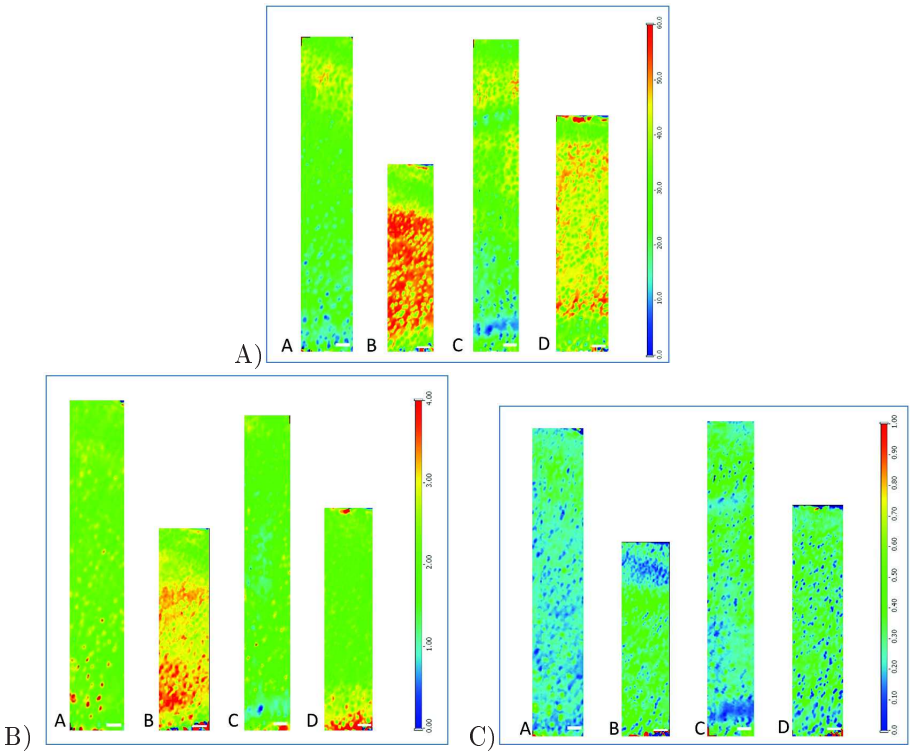

Figure 7: Cartes FTIR correspondent aux bandes d'absorption (A) Amide I (collagène), (B) 1062 cm^{-1} (protéoglycannes) and (C) 1338 cm^{-1} (collagène) des quatre explants cultivés avec une résolution spatiale de 10μm x 10μm et une résolution spectrale de 6 cm^{-1}: A) No Selenium treated explant - No Se control, B) No Selenium and growth factors treated explant -No Se FT-treated, C) Selenium treated explant - ITS control and D) Selenium and growth factor treated explant - ITS FT-treated. La ligne blanche est donnée à l'échelle (100 μm).

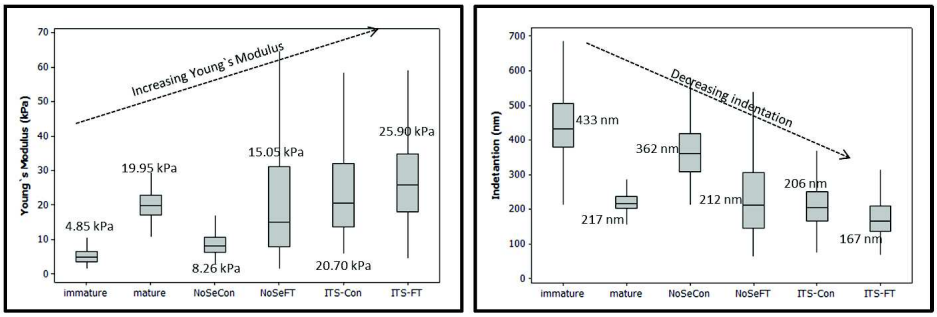

Figure 8: Modulus de Young et Indentation des références de cartilage articulaires immature and mature natifs et des quatre types d'explants cultivés (No Selenium treated explant - No Se control, No Selenium and growth factors treated explant -No Se FT-treated, Selenium treated explant - ITS control and Selenium and growth factor treated explant)

Des analyses sur l'étude de l'expression de certains gènes codant pour des sélénoprotéines présents dans le cartilage ont été effectuées et des résultats intéressants ont émergés. Une augmentation de l'expression du gène Iodothyronine deiodinase type II (DIO2) est observée dans les explants traités avec du sélénium contrairement à ceux traité sans sélénium. Cela peut suggérer que le sélénium a une importance dans l'activation de ce gène durant la phase de maturation de cartilage. Comme montré dans le papier de Cheng *et al.* 2012 [s], la suppression de DIO2 induit de forts effets pro-inflammatoires. Le manque de sélénium dans le milieu de culture de ces explants conduit à une réduction de l'expression de ce gène par rapport à notre condition de référence "ITS Control" (sélénium

basal dans le milieu de culture et sans facteur de croissance), le sélénium peut donc induire de changements relativement importants dans la transcription génétique. Il est possible qu'un environnement pauvre en sélénium soit favorable au développement d'un terrain pro-inflammatoire et par voie de conséquence, la production de stress oxydant. Pour le gène de la glutathion péroxidase 1 (GPX1), une augmentation de l'expression de ce gène apparait entre les échantillons contrôles et les échantillons maturés (FT-treated). Là aussi, le déficit en sélénium dans le milieu de culture des explants semble avoir un impact sur l'expression de ce gène durant cette phase de maturation. L'expression du gène GPX1 croit lors de la maturation (FT-treated) en présence d'un milieu supplémenté en sélénium (ITS) comme attendu selon les résultats obtenus par Yan *et al.* 2013 [t]. Ces résultats montrent des évidences concernant le manque de sélénium causant des changements relativement importants dans la transcription dû probablement à l'augmentation de la production de dérivés réactifs de l'oxygène (ROS) et/ou d'autres raisons qui restent à mettre en évidence. Certes d'autres expérience de qPCR sont nécessaires pour confirmer ces résultats cependant nous prévoyons des analyses protéomiques et d'expression des sélénoprotéines afin de préciser les résultats de qPCR.

A) 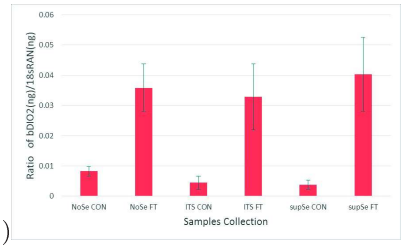

B) 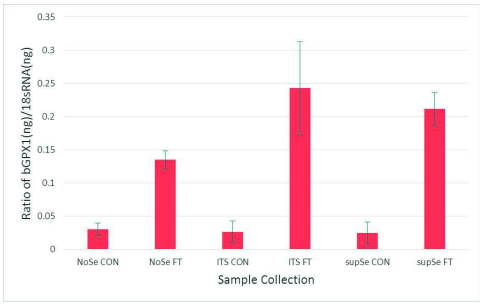

Figure 9: Expression des gènes transcripts (A) DIO2 and (B) GPX1 des différents explants traités en présence (FT) ou absence (Control) de facteurs de croissance et avec différentes concentrations en Se (NoSe, medium depleted in Se, milieu de culture usuel ITS (and SupSe avec addition de sodium selenite dans le milieu de culture usuel ITS). (A) Tous les groupes sont significativement différent ($P < 0.01$) sauf les couples NoSe Control vs ITS Control, NoSe Control vs SupSe Control, No Se FT vs ITS FT, NO Se FT vs Sup Se FT, ITS Control vs SupSe Control and ITS FT vs SupSe FT. (B) Tous les groupes sont significativement différent($P < 0.05$) sauf les couples NoSe control vs ITS Control, No Se Control vs SupSe Control, ITS Control SupSe Control and ITS FT vs SupSe FT.

Dans l'ensemble, même si les mécanismes exacts non pas été identifiés et caractérisés, ces résultats tendent à confirmer que le déficit en sélénium joue un rôle non négligeable dans le métabolisme et la structuration du tissu. Ce travail prospectif a permis d'établir des méthodes et des techniques pour l'étude complexe du sélénium par rapport à sa très faible concentration et ce pour la première fois au sein du cartilage articulaire.

Conclusion & Perspectives

Cette thèse pluridisplinaire avait pour but d'explorer les techniques possibles permettant l'étude fine de l'impact du sélénium dans le cartilage articulaire en maturation. Elle tend également à montrer que le lien entre environnement et santé est ténu mais extrêmement précieux. Basé sur ce cas d'étude très particulier, mêlant géologie, biologie et physique, ce travail donne des méthodologies et propose des techniques, la plupart ne pouvant pas être réalisées en laboratoire, mais qui permettent d'analyser l'importance et les effets sur les tissus biologiques, comme ici sur le cartilage, de déficience ou de supplémentation en sélénium.

Comprendre l'intérêt du sélénium dans le métabolisme et la croissance du cartilage articulaire

est fondamental pour établir des solutions préventives adéquates à la dégradation du cartilage mais également améliorer les différents traitements en cours de développement pour régénérer ces tissus complexe. Les résultats présentés précédemment tendent à confirmer une similarité avec les observations pathologiques des maladies telles que l'arthrose mais plus encore la maladie de Kashin-Beck. En effet, la maladie de Kashin-Beck se développe dès l'adolescence lors de la croissance et de la formation de l'articulation finale. Ainsi, les analyses de maturation des cartilages partant de ces tissus immatures simulent cette étape critique de la croissance. Cependant, le modèle développé et utilisé dans ce travail, présente quelques limites. En effet, il est une base d'étude très intéressante mais les conditions de culture statique entrainent des limitations dans le développement du tissu, notamment au niveau de sa structuration. Nos conditions de cultures ne soumettent pas les explants à des contraintes mécaniques, ce qui dans la nature est indispensable. Ainsi, afin de confirmer et valider ces expériences d'autres expériences avec des cultures et des mises sous contraintes idéalement de façon dynamiques devraient être effectuées.

Le cartilage est un tissu extrêmement difficile à régénérer dû à son renouvellement très lent. Ainsi le sélénium pourrait être un élément essentiel à prendre en compte dans les techniques actuelles de régénération du cartilage articulaire (cellules souches, greffes,...). Il pourrait être l'un des facteurs additionnels jouant un rôle essentiel dans la biocompatibilité (et l'intégration) du nouveau tissu crée ou greffé. Ce projet permettrait ainsi de proposer et d'améliorer ou booster les nouvelles stratégies de traitements mais aussi celles de régénération tissulaire, potentiellement applicable à d'autres tissus. Cependant le sélénium semble avoir également un rôle dans d'autres maladies telles que le cancer, le diabète et peut-être même la maladie d'Alzheimer [k]. Ainsi, cette recherche prospective et exploratoire peut également apporter des connaissances plus générales sur le sélénium, des techniques et des méthodologies d'analyses pouvant donner des pistes et être transposée à des études plus ciblées telles que le cancer, par exemple. La majorité des résultats ne proviennent que de coupes très fines et donc peuvent ne pas être totalement représentatives d'un métabolisme plus large. La tomographie se développe, que ce soit en utilisant la lumière infrarouge ou de rayons X. Une visualisation plus complète pourra ainsi avoir lieu dans un proche avenir. La tomographie infrarouge indiquerait où les variations moléculaires apparaissant localement au sein d'un tissu permettant de voir en 3-dimensions l'impact des traitements et des contraintes appliqués. Une tomographie par rayons X en contraste de phase combinée à des presses de compression et/ou une dynamique de rupture pourrait conduire à l'étude des points de ruptures du cartilage. Ces techniques, combinés à des tests de tribologie et de cultures mises sous contraintes mécaniques, permettraient d'évaluer les points faibles du tissu et les éléments les plus sensibles et susceptibles de se rompre sous l'effet de fortes contraintes mécaniques. Ceci servirait notamment à établir des corrélations entre l'absence ou la supplémentation en sélénium et la résistance biomécanique du cartilage. Grâce à nos analyses en micro-tomographie en contraste de phase, une meilleure compréhension de la croissance et maturation du cartilage dans les conditions natives deviennent possible et ce directement en 3D. La représentation de la structure 3D du cartilage permet la visualisation des canaux des cartilages essentiels pour l'approvisionnement du cartilage en éléments nutritifs et facteurs de croissance. Ces canaux auraient alors le rôle d'alimenter la matrice en éléments nécessaires pour la calcification du cartilage de croissance. L'interconnexion avec l'os sous-chondral serait un élément d'étude très intéressant La visualisation 3D des changements de répartition cellulaire et de densité de la matrice permettrait alors de voir l'impact de différents traitements (néfaste dans le cas d'un déficit en sélénium ou bénéfique quand il est utilisé comme un traitement) sur cette croissance et maturation. L'ensemble de ce travail et des expériences que suscitent nos résultats, basé sur une culture de tissus immatures comme présenté tout au long de cette thèse, devrait permettre une meilleure compréhension du développement de pathologies sévères telles la Maladie de Kashin-Beck ou l'Arthrose.

References

[a] Fordyce, F. in Essentials of Medical Geology. (ed. Selinus, Olle.) Chapter 16, 375–416 (Springer Netherlands (2013)

[b]S.J. Fairweather-Tait, Y. Bao, MR. Broadley, R. Collings, D. Ford, JE. Hesketh, R. Hurst. Selenium in Human Health and Disease. Antioxid. Redox Signal. 14, 1337-1383 (2011).

[c] A. Benninghoff (1925). Form un Bau der Gelenkknorpel in ihren Beziehungen zur Funktion. II. Der Aufbau des Gelenkknorpels in seinen Bezeihungen zur Funktion. Zeit Zellforsch und Mikroskop Anat 2 : 783-862.

[d] R. Stone A Medical Mystery in Middle China 2009 Vol. 324, Issue 5933, pp. 1378-1381

[e] JM. Jordan. Low selenium levels associated with knee OA risk, severity. Orthopedics today 2005

[f] IM. Khan, SL. Evans, RD. Young, EJ. Blain, AJ. Quantock, N. Avery. FGF2 and TGFβ1 induce precocious maturation of articular cartilage. Arthritis Rheum 2011;63(11):3417e27.

[g] I. M. Khan, L. Francis, P. S. Theobald, S. Perni, R. D. Young, P. Prokopovich, R. S. Conlan, C. W. Archer, *In vitro* growth factor-induced bio engineering of mature articular cartilage. Biomaterials 34, 1478-1487 (2013).

[h] S. Pallu, GY. Rochefort, C. Jaffre, M. Refregiers, DB. Maurel, D. Benaitreau, E. Lespessailles, F. Jamme, C. Chappard, CL Benhamou. Synchrotron Ultraviolet Microspectroscopy on Rat Cortical Bone: Involvement of Tyrosine and Tryptophan in the Osteocyte and Its Environment. August 2012, Volume 7, Issue 8, e43930- PLOSONE

[i] EB Hunziker, E Kapfinger, J Geiss. The structural architecture of adult mammalian articular cartilage evolves by a synchronized process of tissue resorption and neoformation during postnatal development. Osteoarthritis Cartilage. 2007 Apr;15(4):403-13.

[j] MK. Lotz, S. Otsuki, SP. Grogan, R. Sah, R. Terkeltaub, D. D'Lima. Cartilage Cell Clusters. Arthritis Rheum. 2010 Aug; 62(8): 2206–2218.

[k] DL. Hatfield, MJ. Berry, VN. Gladyshev, Eds., Selenium: its Molecular Biology and Role in Human Health (Springer, ed. 3, 2012)

[l] SR. McGlashan, CG. Jensen, CA. Poole. Localization of Extracellular Matrix Receptors on the Chondrocyte Primary Cilium. J Histochem Cytochem September 2006 vol. 54 no. 9 1005-1014

[m] YM. Xiong, XY. Mo, XZ. Zou, RX. Song, W.Y. Sun, W. Lu, Q. Chen, Y.X. Yu, W. J. Zang, Association study between polymorphisms in selenoprotein genes and susceptibility to Kashin-Beck disease. Osteoarthritis Cartilage 18, 817-824 (2010).

[n] T.C. Stadtman, Selenocysteine. Annu Rev Biochem. 65, 83-100 (1996). doi:10.1146/ annurev.bi.65.070196.000503

[o] 19. Lu, Shelly C. "Glutathione synthesis." Biochimica et Biophysica Acta (BBA)-General Subjects 1830.5 (2013): 3143-3153. doi: 10.1016/j.bbagen.2012.09.008. 20. Ballatori, N., Krance, S.M., Notenboom, S., Shi, S., Tieu, K. and Hammond, C.L., 2009. Glutathione dysregulation and the etiology and progression of human diseases. Biological chemistry, 390, 191-214.

[p] Fortier, L.A., Barker, J.U., Strauss, E.J., McCarrel, T.M. and Cole, B.J., The role of growth factors in cartilage repair. Clinical Orthopaedics and Related Research®, 469, pp.2706-2715. (2011)

[q] J.Yin, Y. Xia. Macromolecular Concentrations in Bovine Nasal Cartilage by Fourier Transform Infrared Imaging and Principal Component Regression. Appl Spectrosc November 2010 vol. 64 no. 11 1199-1208

[r] L. Rieppo, J. Rieppo, JS. Jurvelin, S. Saarakkala. Fourier transform infrared spectroscopic imaging and multivariate regression for prediction of proteoglycan content of articular cartilage. PLoS One. 2012;7(2):e32344.

[s] AWM. Cheng, M. Bolognesi, V. Byers Kraus. DIO2 Modifies Inflammatory Responses in Chondrocytes. Osteoarthritis Cartilage. 2012 May;20(5):440-5.

[t] J. Yan, Y. Zheng, Z. Min, Q. Ning, S. Lu. Selenium effect on selenoprotein transcriptome in chondrocytes, Biometals (2013) 26:285–296

[u] M. Roman, P. Jitarub and C. Barbante. Selenium biochemistry and its role for human health. Metallomics. 2014 Jan;6(1):25-54

Contents

Part I
General Introduction

"Solely the dose determines that a thing is not a poison."

Paracelse

Medical geology is an emerging field establishing relationships between human health and environment. Nowadays, this field is important to a society where soil and air pollution are omnipresent. Human health is dependent on the quality of the environment and the food that is available. Medical geology studies help to make sense of how man-made environmental variations such as industrial pollution, agriculture and urban development or natural variations of climate and bedrocks affect populations. Medical geology thus aims to identify the cause of health issues induced by environmental factors (such as minerals and metals) which daily affect large portions of the world population. Mineral trace elements are the focus of this study. These trace elements, present in the environment (soil, aquifers and surface waters) in low concentration, are essential to human health. They are incorporated into organisms through the diet in cereals, water and fish. A normal, balanced diet provides the body with all the trace elements needed for organisms well-being. Nevertheless, disequilibrium in this balance of trace elements can have serious short and long-term health effects. Solely, the dose determines that an element is not a poison, but a deficiency may be just as harmful as a poison. In this thesis, the objective is to understand how a geological trace element, selenium, can influence an organism, with particular emphasis on articular cartilage.

Selenium (Se) is an essential trace metalloid for normal growth and development of human beings. Historically, it was first well-known for its toxicity. Nowadays, it is a highly prized element for its anti-aging effect. Sharing several physical properties with the metal and non-metal groups, it can establish interesting interactions and relationships with other elements in order to provide necessary cellular protective functions. Selenium is vital at low concentration but also toxic at slightly higher concentrations. Selenium deficiency can affect protein production required to DNA repair. This deficiency can also affect cellular defense, through reduction of expression and function of antioxidant enzymes. About one billion people in the world potentially could be suffering from a selenium deficiency, expressed in different pathologies. This "double-edge sword element" is present within the organism in minute quantity. Consequently, all these parameters (toxicity, necessity, micro-amount) contain the ability to study the biological role of selenium. It is also very difficult to detect and analyze its partition within a tissue and to define specific correlations with organelles in order to understand its functions. The different functions of selenium and processes influence within living organisms are not fully understood. Nevertheless, several studies attest to the fact that selenium plays an extremely important role in cellular and tissue development of the brain, heart, bone and articular cartilage.

Articular cartilage (AC) is a soft tissue that lines the ends of bones and functions mainly to enable smooth articulation of joints. This precious tissue is highly solicited by physical activities such as walking, running, standing up. It is then vital to preserve and maintain AC function and integrity. Cartilages in joints allow a frictionless and painless motion of skeletal elements and acting a shock absorber [1] (like a sponge) to transmit forces through the skeleton. For a long time, cartilage wear and friction were thought to be the principal causes of tissue degradation. In our current society, physical inactivity induces new metabolic causes of cartilage stress such as obesity where our joints support an additional weight, which in combination with other factors such as poor posture weakens cartilage tissues. In order to repair defects in cartilage research has focused on using stem cells transplantation and techniques such as 3D bioprinting to try and develop reconstructive strategies to obtain a biocompatible replacement tissue. However, this substitution and/or reconstruction is

not simple and current methods are not sufficiently advanced to resolve the underlying pathology in osteoarthritis (millions people affected in France) or Kashin-Beck disease (hundreds thousand people affected in China up to the 70's). Degenerative joint diseases refer to articular cartilage degeneration which is painful and disabling. The causes of disease are multiple, not only biomechanical, but also linked to aging and accidents, and to biological and genetical disorders. In order to preserve the homeostatic metabolism of cartilage many factors are needed to maintain normal function, many factors which can include the trace elements such as Se. Selenium is a co-factor in many enzymes that play a critical role in anti-oxidant and anti-inflammatory protection of cells and tissues.

In China, a severe joint disease, called Kashin-Beck disease (KBD), is endemic and widespread in the so-called diagonal belt ranging the northeast to southwest of the country where the soil selenium content is extremely low. Kashin-Beck Disease is a chronic, osteochondropathy which is mainly found in China and mainly affects small children and young adults. Nowadays, approximately one million adults have been affected or potentially at high risk developing it. Correlations between geological and epidemiological studies established a strong link between selenium depletion in soils and Kashin-Beck disease (KBD) distribution [2-4]. KBD is characterized by significative alteration in chondrocyte phenotype, necrosis/apoptosis and abnormal terminal chondrocyte differentiation [5]. Chondrocyte cell death is the basic pathological feature of diseased cartilage and results in growth retardation (in severe cases, dwarfism) and secondary osteoarthritis. Therefore, normal cartilage growth and development in patients suffering of KBD is compromised and this induces a partially or complete loss of their mobility, self-sufficiency and working capabilities. This has a severe impact on patient life-quality and also increases the medical burden on society [6]. Se-supplementation has been used to prevent KBD disease and its use appears to reduce disease incidence [7]. But, because the function of Se and its role in metabolism are still unknown, more research is needed so that long-term as well as short-term effects of selenium deficiency on cartilage health are understood. KBD appears to be a multifactorial disease stemming from a combination of selenium and iodine deficiencies, the presence of humic acid in water and a cereal contamination by mycotoxins [8]. Nevertheless, as it has also been described in the literature that some potential risk factors can interact with genetic susceptibility, so care must be taken in interpreting these data. Furthermore, another clinical study called the Johnston Country Osteoarthritis Project performed by Prof. Jordan in North Carolina has exposed evidence of Se in knee-osteoarthritis development [9]. It has been demonstrated that a strong correlation exists between the Se-level and the severity of the disease, which is significatively amplified with age, gender and race. Understanding these Se-action mechanisms may shine a light on diseases and repair mechanisms that occur much later in life in population where there is little or no selenium deficiency. Homeostatic cartilage metabolism preservation relies on many factors required to maintain normal function, including trace elements such as Se [8,10,11]. Selenium is a co-factor in many enzymes that play critical roles in anti-oxidant and anti-inflammatory protection of cells and tissues [12]. Selenium seems to be a key player in chondrocyte development and the matrix structuralisation. The objective of this study is to increase our understanding of selenium's implication in the diverse articular cartilage (biological, biochemical, biomechanical and dynamical) properties.

Joint diseases are generally related to a dysregulation of homeostatic processes of the diverse components of the extracellular matrix. Consequently, over time, the cartilage matrix progressively degrades, increasing the biomechanical stress on chondrocytes [13,14]. Chondrocytes usually function to produce and maintain the extracellular matrix (ECM) components of cartilage. During degradation, catabolism of cartilage extracellular matrix outcompetes anabolic repair mechanisms, and the collagen network frays, fibrils break down under mechanical stress and collagen degrades. Chondrocytes undergo apoptosis and the remaining cartilage undergoes a slow progressive degeneration [15]. Indeed, unlike bone, cartilage has a low regenerative capacity. It lacks a vascular network and has

a dense extracellular matrix including a low cell to matrix ratio. It is thus currently challenging to restore full tissue function in damaged or diseased articular cartilage. To investigate the potential of selenium supplementation potential in the prevention of disease and regenerative treatments, robust and well-defined models have to be selected for study.

Currently, knowledge about the specific biological implications of selenium in normal cartilage metabolism is poor; selenium remains an elusive element to study, and so many of its biological functions remain elusive. As mentioned previously, deficiencies in oligo-elements often lead to inflammatory disease. To address the lack of information, a precise and robust base-model is needed to study selenium. Animals, as an *in vivo* model, cannot be used in this context due to their high biological variability and the potential of unpredictable effect of the selenium-concentration variations in the entire organism. Therefore, I used a biological model developed by Charles Archer and Ilyas khan (Cardiff University, Wales) which produces an "accelerated maturation of the bovine immature articular cartilage" in static *in-vitro* conditions. This model has been developed to describe the growth and metabolism of articular cartilage during the maturation stage. Usually, growth and post-natal maturation of articular cartilage can take up to 12 years to occur *in vivo*, however using fibroblast growth factor-2 and transforming growth factor β1 immature cartilage explants can reach this developmental milestone within 21 days [16-17]. This model, published and validated, is an excellent model to start an exploration of the Se-implication on articular cartilage development, particularly as this is the timeframe within which KBD exerts its most severe effects, especially on the growth of the skeleton. Consequently, experiments were conducted under Se-depletion, through its absence in culture medium, and Se-supplementation to determine how it affects tissue development during this critical window of growth which coincides with age-related incidence of KBD.

This thesis is based on the hypothesis that selenium plays a crucial role in articular cartilage metabolism and homeostasis. This seems to be confirmed by the association between the pathological development of Kashin-Beck and osteoarthritis diseases and geological and dietary selenium deficiency. Our general hypothesis is that a selenium depletion in explant culture medium and consequently in the surrounding nutritional environment, induces a degenerative tissue with biomechanical properties close to those of osteoarthritis. It is suggested that the selenium action is mediated by selenoproteins and some specific gene [11]. The main function of selenium is often assumed to be its anti-oxidant and anti-inflammatory cellular protection. Nevertheless, if selenium plays an important role at the level of chondrocyte metabolism, it can be proposed that it has a retroactive function on the organisation and the structuralisation of the extracellular matrix (ECM) with a potential impact in the mechanotransduction for example. Therefore, the objective of this work is also to characterize the impact of Se on structure, metabolism and properties of articular cartilage. This can provide further complementary or novel hypotheses on its role and functions in the articular cartilage development.

The main objectives are: (a) to determine the involvement of selenium in tissue organization and function i.e its localisation and speciation in tissue, (b) the characterization of the ECM of articular cartilage under Se supplementation or depletion, specifically the effect on maturation processes. The characterisation of organic matrix and structure of articular cartilage during maturation and growth and the determination how selenium contributes to cartilage growth and differentiation are our principal questions. The identification of critical selenoproteins involved in this process and the determination of structural and biological positions of the selenium within cells/tissue could be key information to assess and identify the potential agent/mechanism of cartilage repair and regeneration. In order to determine this relative importance of the selenium in normal chondrocyte function, X-ray fluorescence microscopy (XRFM) has been used to detect the sub-cellular distribution of the selenium. This was followed by analyses on high energy resolution fluorescence detected X-ray absorption spectroscopy (HERFD-XAS) coupled to an array of crystal analysers which provide demonstration of

selenium speciation within a model of maturation of the articular cartilage at unprecedented low concentration of hundreds of ppb. This concentration range was determined using the inductively coupled plasma mass spectrometry (ICP-MS). Fourier transform infra-red microspectroscopy (FTIRM) was used to evaluate the biological and morphological (complete with histology) constitutional variation appearing for different selenium concentrations. Complementary histological, genetic (PCR-qPCR) and protein (immunofluorescence) analyses have been performed in parallel to validate this out-coming information. Furthermore, biomechanical properties of the articular surface treated or not with selenium have been investigated to present some preliminary insights of the selenium retroactive action on the AC structuring.

This project would give new strategies to increase the resistance of cartilage to degradative processes, to develop an extracellular matrix having adequate components to generate a functional articular cartilage. Articular cartilage is extremely difficult to regenerate due to the lack of vascularity. Selenium could be an additional factor playing an essential role in the biocompatibility and incorporation of newly created (*in situ* or not) or transplanted tissue . It could be interesting to use selenium to enhance and boost actual regenerative techniques. The comprehension of the fundamental mechanisms and the methodology given can give interesting study directions for other diseases where selenium has potentially a role such as cancer, diabetes and Alzheimer [18]. This can open up new strategies to study the present model when exposed to mechanical load or to upcoming engineered cartilage systems and to develop an ECM with adequate components to generate a functional articular cartilage tissue "fingerprint".

Part II

Articular Cartilage

Two bones involved in a synovial joint (diarthrosis) are covered by a smooth and slippery surface called articular cartilage [19]. This contact interface is contained in a closed and sterile cavity (synovial cavity) limited by a synovial membrane, the whole stabilised by ligaments and tendons (Figure 10). In the synovial cavity, a lubricating fluid produced by the synovial membrane, called synovial fluid is present to facilitate motions and allow cartilage nutrition [19]. Articular cartilage functions are to absorb and to distribute shocks and loads, and to reduce friction during movement in order to preserve bones [19].

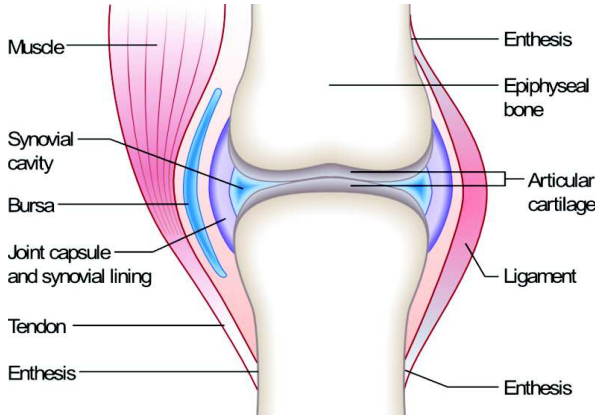

Figure 10: Diarthrosis structure

Hyaline articular cartilage (AC) is an extremely important tissue in health allowing smooth and painless motion. Macroscopically, the articular cartilage is a smooth shinny translucent white surface with articular cartilage thickness of few mm[1]. This connective tissue[2] can be defined using several specific characteristics such as being avascular, aneutral, hypocellular, no lymphatic, and no basement membrane [20] . Consequently, nutriments are provided via the synovial fluid and the subchondral bone delivering specific molecules that diffuse through and penetrate the cartilage extracellular matrix (ECM). Articular cartilage is generally described by a large and complex extracellular matrix meshwork in which cells, called chondrocytes, are entrapped, the whole immersed in fluid (mainly composed of water). Physiologically, this tissue is highly quiescent with a cellular division extremely limited. These chondrocytes are responsible of the production and the maintenance of this highly organized ECM. The turnover of collagen fibers is very low such as for some essential polypeptides such as aggrecan. In concordance with the avascular and non-innervative tissue characteristics, the restricted turnover of the diverse components of the cartilage matrix explains the low regeneration of cartilage after injuries and damage.

Articular cartilage is vital in the weight-bearing force transmission between long bones and the biomechanics of the diarthrodial joint articulation. Essential functions such as the minimization of contact stresses resulting from the joint loading and the lubrication of the joint are provided by the intrinsic AC composition. Its specific hydrated and macromolecular ECM structure allows an

[1]The thickness of the AC varies also according to the maturation stage. A mature tissue is thinner that a immature tissue.

[2] A connective tissue can be defined as a tissue with a complex and dense extracellular matrix (ECM) used to well separate the cells from each others.

absorption stress regulation under mechanical loads and a fine control to distribute stresses along the joint [20]. Articular cartilage is subjected to diverse kinds of loadings mainly compression, torsion and shear. The hydrated load-bearing surface generates a low friction coefficient, useful during sliding movements. Mechanico-electrochemical properties provide particular strength and wear-resistance capacity to bear and distribute the diverse loads. Articular cartilage can be considered as a sponge, absorbing diverse shocks due to its high water concentration and to reduce maximally the friction during any type of motions.

This part will provide general information about articular cartilage: its main characteristics and properties. The biological composition and structure will be reviewed. This will provide an understanding on the disease related to joint degradation.

1 Biological Composition

Even if a low replenishment of AC components tends to attest that mature articular cartilage is a relatively inert tissue, it is under constant tension from the diverse stresses applied on it; it has to balance the huge quantity of stress forces continuously applied on the joint. It can be considered a sponge, acting like a buffer which has to absorb all loading deformations (diverse shocks and compressions). This anisotropic and heterogeneous tissue can be stretched out on composite stratified structure organized in a sophisticated organic solid matrix saturated with water and mobile ions. The water fluid and positive cations are concentrated by the action of proteoglycans and of collagen Type II. AC is composed of specific cells embedded in a multi-component extracellular matrix, mainly supported by an important collagen meskwork. Zones appear in this complex organisation where the components are differently distributed within the tissue height.

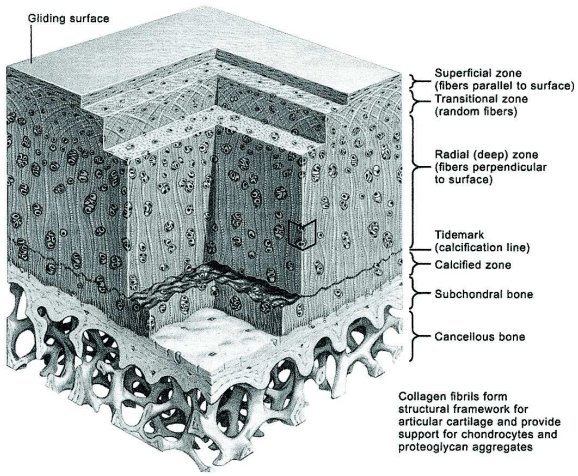

Figure 11: Articular Cartilage is divided into several zones (superficial, middle and deep zones, calcified cartilage). In each zone, the composition and the distribution of the diverse components of the extracellular matrix vary [24-25].

1.1 Chondrocytes

Unique and specific cells of AC, chondrocytes represents 10% of the AC volume corresponding to∼1-2% of the dry weight of the healthy human AC [21-22]. They have a mean size of 13 μm, ranging between 10 and 40 μm [23] . Chondrocytes evolve in an anaerobic environment where the

hypoxic gradient varies with the depth - the oxygen concentration is higher in the superficial zone than in the radial zone. The nutriment essential for the cell subsistence is provided by the synovial fluid. These nutriments have to pass through a restrictive double barrier (synovial membrane and matrix) that allow just the smallest molecules to penetrate in the synovial cavity. Chondrocytes are principally fed by fluid diffusion during pumping action generated by motion (compression or flexion).

These chondrocytes are encapsulated in a viscoelastic extracellular matrix (ECM). This limits cell-to-cell contacts [21]. This ECM is located far from the cells and consists in a large meshwork of type II-collagen (COLII) fibers. Cells are preserved in a cavity-like space, the periplasmic space. Cell mobility is extremely limited and chondrocytes have a low rate of cell division. Normal mature chondrocytes are quasi-inactive and can be characterized by their spheroidal-shaped cells, the abundant presence of type II collagen, large proteoglycan aggregates, and several non-collagenous proteins.

As illustrated Figure 11, variations in cell morphology and ECM structuration appear in mature articular cartilage. This is representative of the cellular metabolism and organisation to support dynamical loading and sheer stress. Mechanical properties of the AC depend not only on matrix components (types and concentrations of the diverse macromolecules, water concentration) but also mainly on their high organized framework mediated by chondrocytes. To preserve the integrity of the synovial joint maintenance of the articular cartilage surface is required. This is related to a turnover of the macromolecules and an alteration/remodeling of the cartilage matrix composition/structure in response to diverse stimuli (electrochemical signals - growth factors and cytokines concentration variations) expressing the joint mechanical stress action. Chondrocytes are the key players of the matrix maintenance allowing a functional recovery of the articular cartilage properties [21]. They are regulators of the renewal and the degradation of the matrix material. To enable this function, as for other cells, chondrocytes possess several organelles (endoplasmic reticulum-Golgi membranes) necessary for the matrix synthesis [21]. These cells synthesize but also degrade the diverse macromolecule components of the ECM in appropriate amounts in order to mediate the maintenance of cartilage function, such as the Co-II, Co-IX, Co-XI and (negatively charged) glycosaminoglycans (GAGs) and other (non-collagenous) structural proteins. Hence, they also regulate the ECM homeostasis[3] by a perpetual balance between these enzymatic degradation and secretion of the diverse components of the extracellular matrix [20].

1.2 Rich and Complex Extracellular Matrix

The extracellular matrix represents the major part of the articular cartilage[4] composed of water ($\sim$ 70% wet weight (WW) of the AC) and structural macromolecules (30% WW) (Figure 12). The structural macromolecules of the matrix can be separated in three groups: proteoglycans ($\sim$ 30% of dry weight DW), collagens ($\sim$ 60% DW), non-collagenous proteins and glycoproteins ($\sim$ 10% DW) [20,22]. Collagen is relatively uniformly distributed within the AC providing tensile property. The rest of the proteins are bound and trapped within this collagen meshwork, the whole immerged in the water medium. Glycoproteins and non-collagenous proteins are proteins with few attached polysaccharides or oligosaccharides. The role of the glycoproteins and non-collagenous proteins, potential structural agents, is not yet well-understood. It is assumed that they have to stabilize the ECM, helping in the architectural organization and facilitating the binding of cells to this matrix and between the diverse components of the matrix themselves. The ECM can be visualized as a viscoelastic biphasic material with a tissue fluid and macromolecular structural framework providing the form/structure and the

[3] Homeostasis: property of a system in which variables are regulated in order to maintain the internal conditions stable and relatively constant.

[4] organic matrix composed of three major components: water at $\sim$ 70%, collagen fibers at $\sim$ 20% and proteoglycans (PGs) at $\sim$ 7%

stability of the tissue. The matrix also contributes in cell protection, adhesion and regulation. The interaction between these two phases of the matrix confers the mechanical properties (stiffness and resilience) to the articular cartilage [21]. Interstitial water fluid plays an important role in the control of several physical properties such as the swelling pressure regulation. The collagen molecules and the negatively charged proteoglycans are the structural components involved in the load-carrying process. ECM is cations-rich (electrolytes, assimilating to electrostatic charges) to balance the negative charges of PGs [22]. The integrity of the extracellular matrix is preserved by continuous interactions between the different matrix protein molecules (e.g. PGs, collagen). This integrity is directly linked to the material properties of the articular cartilage which are determined by several parameters such as the size and the degree of cross-linking of the different matrix components, the collagen fibril orientation.

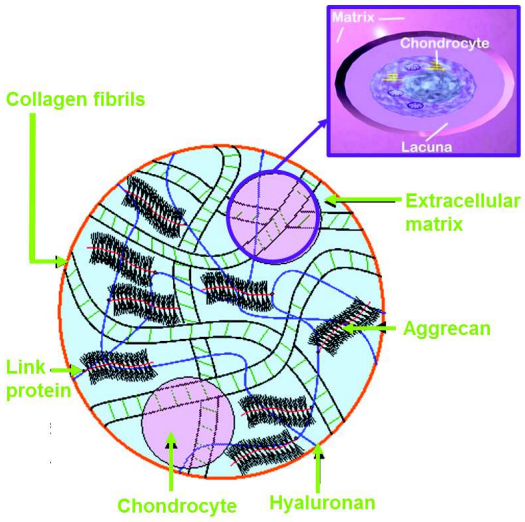

Figure 12: Global view of articular cartilage composed of a rich and complex extracellular matrix and chondrocytes. Chondrocytes expose a lacuna in their surrounding and the whole is entrapped in the large collagen meshwork interacting with proteoglycans and glycosaminoglycans.

1.3 Interstitial Tissue Fluid: Water

Water is the most abundant component of the articular cartilage. It represents approximately 70-80% of the total wet weight of the normal articular cartilage tissue (80% near the surface) [21] . The concentration of water vary according to the zone of the AC (section 2.1) because the interstitial water is non uniformly distributed from the surface to the depth. Several elements are incorporated with this water fluid: gases, small proteins, metabolites and also a high concentration of mobile cations necessary to compensate the negative charge beared by proteoglycans in order to preserve the electroneutrality of the system [22]. These cations will have an influence on the mechanical and the physicochemical behavior of the articular cartilage. This interstitial fluid is essential because it allows the transport of nutrients in the AC but it also allows gaze circulation liberated by the cell activity and the evacuation of the waste [20].

In the synovial cavity, water fluid can circulate partially freely. This fluid can move in or out of the tissue in tissue and cavity to release the tissue pressure during stress actions. Most of the interstitial fluid characteristics (volume/concentration - behavior) strongly depend on its interaction with all the structural macromolecules, mainly large proteoglycan aggregates. Hence, these aggregates have the property to contain the fluid within the tissue preserving the fluid electrolyte concentrations. Since all of these proteoglycan macromolecules are negatively charged they attract positively charged ions increasing the positive ion concentration (sodium Na^+, potassium K^+) and decreasing the negative ions

one (chlorine Cl^-) [1,21]. Consequently, the global increase in inorganic ion concentration generates a drop of the tissue osmolarity inducing a Donnan effect [1, 21]. The collagen fibrillar meskwork is organized in order to resist to this Donnan osmotic pressure caused by the combination of the inorganic ions and the proteoglycans [1]. Thus, water is directly associated with collagen fibrils to support the ECM structure by filling the interfibrillar spaces. It is a major actor in the joint lubrification and has a control on the dynamical behavior of the AC.

1.4 Collagen Fiber Types and Fibrillar Meshwork

1.4.1 Articular Cartilage Collagen Composition:

Cartilage collagens are formed by a heterotypic fibril system. To provide tensile force-resisting properties to AC, a specific configuration of all the collagen macromolecules is required. The complex collagen configuration is composed of different collagen types dividing into two classes. These two classes are based on the primary structure and the supermolecular arrangement. First, an assembly of tropocollagen[5] II units into fibers and fibrils forms the base of the cartilage collagen. The type II collagen is a fibril-forming collagen characterized by its long length, its central asperity, its triple-helix domain without any interruptions in glycine repetition [20]. This assembly of the heteropolymer type II collagens is controlled by other types of minor collagen molecules, mainly the type XI collagen is located in core of fibers in order to maintain the different part of the type II collagen bind together. The type XI collagen is composed of a single globular domain located at one end of the triple-helix. Type XI molecules act as a filamentous template at the core of the fiber. The type IX collagen is covalently bound at the surface of the type II collagen [20]. Type IX collagen can also bind to itself. It possesses a side-arm which allows it to interact with further type II molecules present in its vicinity. It provides an interfibrillar linkage between type II collagen fibrils which may improve the mechanical stability of the fibrillar meshwork. The type IX collagen presents triple helical segments connected by flexible kinks (interrupted triple-helix) and an N-terminal globular domain. This N-terminal domain serve as anchor for the type II collagen to other components of the extracellular matrix. The type IX collagen molecules can be seen as a proteoglycans due to the presence of four globular domain within its triple helix structure. The type IX and XI collagen is defined as a non-fibril-forming collagen. They are characterized by the size which can fluctuate and they have imperfections in the glycine X-Y sequence. Nevertheless, these two types of collagen constitute a sub-class of the non-fibrillar collagen called Fibril-Associated Collagens with Interrupted Triple helices (FACIT) [20]. The triple helices rupture allow their association with other collagen such as the type II and also can be bound with other matrix components. The most important role of the FACIT is to stabilize the meshwork in order to balance the swelling pressure action generated by the hydrated proteoglycan aggregates.

1.4.2 Collagen Fiber Meshwork:

Collagen fibrillar meshwork is a fundamental element of the cartilage organization. The collagen fibers contained within the AC is a structured mixture of mainly four different types of collagen. The type II collagen is the dominant type of fibers representing within the articular cartilage at $\sim 94\%$. Then, three other collagen types appear: VI ($\sim 1\%$), IX ($\sim 2\%$) and XI ($\sim 3\%$) [20]. Collagen types II, IX and XI are complementary. They form cross-banded fibrils generating an important collagen

[5] Tropocollagen: Fundamental unit of the collagen. It represents a asymetrical molecule of approximatively 280 nm long and 1.5 nm diameter. It corresponds to a kind of glycoprotein formied by the winding of the three $\alpha-$ left-handed helices bearing some glucids overwinding in right-handed helix. The winding of the α-chainis made via the contribution of tropocollagen molecules where the cohesion is supported by hydrogen bindings between glycine and hydroxyproline.
Each collagen molecule is composed by a combination of three α-chains generally characterized by a repetition of a sequence of Gly-Pro-Hyp. Every α-chain must possess a Gly (glycine) at every 1/3 residue because it is the only amino acid (AA) small enough to fit into the triple-helix center. A left-handed helix formation structure takes place but the conjugation of the three α-helix generates a right-handed structure formation.

framework.

The type II collagen is the primary element of this composite network [20] . Type II collagen provides tensile strength. Type IX collagen molecules are bound covalently to superficial layers of type II collagen fibers in order to develop an interconnected fibrils meshwork (interactions with other type IX collagen molecules of other fibers) and interactions with the other components of the ECM [21]. It appears to help in the resistance against shear force and obviously contribute to the support of the tensile strength. Type XI collagen molecules are also covalently bound to type II collagen fibers [21]. It is supposed that they play a role in the internal organization structure of type II collagen fibers such as fibril nucleation. It contribute to resist to the tensile force properties via the supportive structure combination (II and XI) [20]. The exact roles of type IX and XI collagen molecules remains not well-defined [21]. They are probably stabilizers of the ECM by connecting the different elements all together.

The type VI collagen is highly present in the surrounding neighborhood matrix of chondrocytes (pericellular matrix) and has a function in the chondrocyte adhesion to the ECM [20,21, 26]. The type VI collagen corresponds to short helix with a globular domain on each end of the helix. This appears to be a help in the cell adhesion to the ECM. It also seems to facilitate the formation of fibrillar meshwork around cells to protect them (non-covalent bindings with hyaluronan and fibronectin). The last point also results from the basket-formation around chondrocytes called chondrons which is an agglomeration of thin fibrils of collagen (types II, VI and IX) in order to create a bubble around the chondrocyte. The type VI collagen play a role in the chondron integrity.

Type X collagen is only present in the calcified zone and the hypertrophic zone of the growth plate and has a potential role in the matrix mineralization/calcification [21].

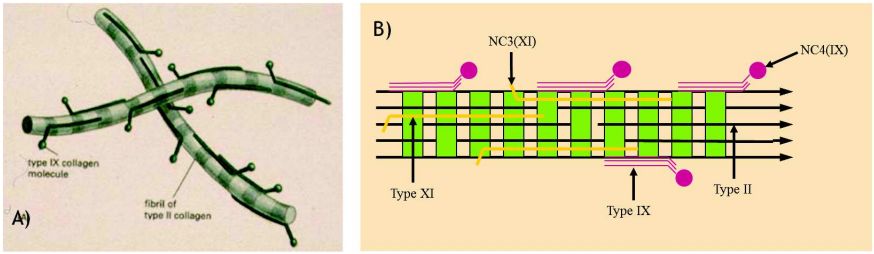

Figure 13: Schematic view of the collagen fiber structure in articular cartilage. Collagen Type II is the main component of the AC and other collagen type support and complete the fiber structure of the tissue (Collagen type IX and XI)

1.4.3 Collagen Fibril-Associated Proteins

At the surface of the type II collagen fibers/fibrils, several proteins are attached such as fibromodulin, lumican, decorin, chondroadherin, biglycan. These glycoproteins can be seen as new actors developing a secondary meshwork. It is composed of cartilage matrix proteins CMP or matrilins and cartilage digomeric matrix protein (COMP) [21].

1.4.4 Collagen Cross-Linking

The collagen cross-linking functions to stabilize collagen fibres after their spontaneous assembly into the quarter-stagger arrays. This generates filaments, fibrils and also fibers. The cross-linking of different types of collagen results also in inter- and intra-molecular crosslinks in order to provide a tensile resisting structure and to stabilize the matrix [27]. The cross-linking begins in the pericellular region of the chondrocytes, immediately after fibrillogenesis. The intermolecular cross-links stabilize the molecular arrangement within the collagen fibrils [27]. They confer their physical and mechanical

properties to diverse connective tissues, especially to articular cartilage. These cross-links are vital to provide to the fibrils the necessary tensile strength to perform their structural role. The collagen cross-links have a structural role as described previously but they also play a role in metabolism functions. The maturation of the cross-linking system induces the formation of multi-functional and stable cross-linkage which participate in the aging process.

1.5 Proteoglycans

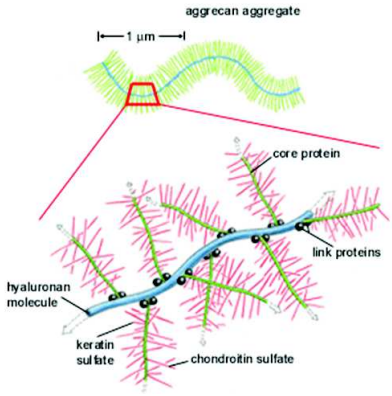

Figure 14: Composition of Aggrecan of AC with diverse GAGs (keratin sulfate and chondroitin sulfate) related to hyaluronan by core proteins.

Proteoglycans are essential in articular cartilage function and represent 5-10% of the tissue wet weight [20]. With composite properties, they trap water to confine it within AC to contribute to AC mechanical properties. They play a role in molecular signaling in regard to different stress signals transmitted through the matrix. They also play the role of regulator, a pump for high osmotic pressurized cartilage system by attracting cations and water molecules. Proteoglycans are hydrophilic and (more precisely aggrecans) contribute to the stability of the extracellular matrix, providing a kind of rigidity that is necessary to resist to applied stresses. The turgid nature of the AC is provided by osmotic properties that are necessary to support compression loading. Aggrecans form a hydrated gel-like structure by their interactions with hyaluronan and link protein that endows cartilage with load bearing properties.

Proteoglycans are a combination of a backbone core protein and glycosaminoglycan (GAGs) chains [20,21]. Glycosaminoglycans are "long unbranched polysaccharide chains consisting of repeating disaccharides that contain an amino sugar" as defined by Buckwalker [21]. Each dissaccharide unit has at least one negative charged carboxylate or sulfate group in order to generate long negatively charged chains by repetition of one or several negative groups in order to attract diverse cations present in the interstitial medium [21]. These carboxyl and sulfate groups have a strong binding affinity to water molecules. In articular cartilage, some GAGs are predominant such as hyaluronic acid (HA, also called hyaluronan), chondroitin suftate (CS) and keratan sulfate (KS) [20,21]. The core protein contains several domains that are involved in protein-protein, protein-carbohydrate and protein-cell interactions.

Proteoglycans are present within AC in two groups: large aggregating molecules (macromolecules) and small leucine-rich (molar mass) repeat proteoglycans (SLRPs) [20]. These small proteoglycans are non-aggregated proteoglycans and they characterized by multiple adjacent domains bearing a common leucine-rich motif. They consist of mainly decorin, biglycan and fibromodulin [20]. These small PGs have essential functional roles such as metabolism modulations or integrity maintenance. They approximately represent 5% of the proteoglycan of articular cartilage. Decorin and fibromodulin

are mostly located in the superficial zones of articular cartilage in association with collagen fibers. Smaller amounts of decorin are also found in deeper cartilage layers. Biglycan and decorin are both found in the pericellular lacunar regions of chondrocytes. Decorin is bound to type II collagen fibrils and some growth factors. Biglycan is also bound to other types of growth factors present near to the cell surface receptors in the pericellular region and may interacts with type VI collagen fibrils[20]. Fibromodulin is bound to type II collagen fibril surfaces in order to regulate the fibrillogenesis (fibril diameter and fibril-fibril interactions) [20]. More precisely, decorin is able to inhibit type I and II collagen formation. The fibromodulin can inhibit collagen genesis. Both biglycan and decorin possess properties of competitive binding with transforming growth factor (TGF)-β which can have an important impact on the role of this growth factor in repair processes in cartilage due to its possible inhibition, since (TGF)-β has great significance in the control of repair processes [21]. Both decorin and biglycan also bind with other adhesion proteins such as fibronectin and type VI collagen [20]. Each of these so-called adhesion proteins have the RGD amino acid sequences as playing key roles in cell adhesion. The presence of the decorin or the biglycan on the adhesion proteins induces an inhibition of the cellular attachment of fibroblasts, another key step in the control of connective tissue healing. They act in the binding to collagen, serve as bridges between cells and matrix and between themselves and in the binding of diverse polypeptides to hyaluronan.

Large aggregated[6] proteoglycans are mainly aggrecans [20]. Aggrecans are major proteoglycans of the articular cartilage. The proteoglycan aggregation is an essential process. Small PGs cannot be trapped within the collagen meshwork. The aggregation allows the formation of large PGs (one core protein with at max. 100 GAGs). The link proteins are an essential element in the aggregation. They also retain the small GAGs, limiting the escape of these GAGs into the tissue. In this way, large PGs can be entrapped. Generally, it is described as a conjugation of 30-50 monomers, 30-50 link proteins and one hyaluronic acid [20]. A simple aggrecan monomer has a molecular mass of 25000 kDa[7]. Aggrecans possess multiple functional domains. They are composed by a core protein covalently bound to several sulfated GAGs, mainly chondroitin sulfate (CS) and keratan sulfate (KS). The location of the KS side arms is preferentially found close to the linkage region to the hyaluronan (HA). KS has a lower molecular mass than the CS chains. These aggregated core proteins are then non-covalently bound to a hyaluronic acid protein (non sulfated GAG) via some link proteins. All the aggrecans are entrapped within the collagen cross-banded fibril meshwork via adhesine (glycoproteins).

1.6 Interactions between Chondrocytes and Matrix

Chondrocytes and extracellular matrix are highly interdependent because chondrocytes generate the extracellular matrix components. Extracellular matrix modulates stresses applied on chondrocytes and protects them to prevent damages [21]. The interstitial fluid is essential in the cartilage well-being; it is the transporter of nutrition, synthetized and degraded matrix molecules, metabolic waste products, cytokines and growth factors (cell function regulating help). This fluid carries them on or out of the cartilage tissue by its flow through the synovial cavity [21]. The control of the synthesis or degradation is mediated by cytokines having catabolic or anabolic effects. Under stress conditions, chondrocytes receive diverse stimuli which could stimulate the production of cytokines. These cytokines are released and trapped within the matrix and tend to link to cell receptor in order to induce anabolic actions to response to structural needs of the matrix. Opposite reactions of catabolism (generation of diverse proteins: activators or inhibitors) will appear to regulate the overproduction of diverse components and maintains cartilage equilibrium [21]. The interaction between proteoglycans

[6] Aggregate: ability of the PG molecule to form aggregates of great molecular size in order to amplify its physiological functioning properties as the "pump" of the articular cartilage. This allows a better integration of the PGs within the collagenic framework interstices and consequently perserves the osmotic swelling pressure.

[7] Dalton is a mass unit of proteins: $1\,\text{kDa} = 1.6601 \times 10^{-21}\text{g}$. Here, $25000\,\text{kDa} = 25000\,\text{g/mol}$

and collagens (molecules, fibers) forms a porous composite fiber-reinforced organic solid matrix (see 3.1) interacting with the interstitial fluid [28]. This porous solid matrix combined with water fluid protect the cartilage against high levels of stress and strain generated within the extracellular matrix during external loadings. This interaction serves of basis for the further interactions between the cells and their local environment. These complex interactions contribute to a high ordered assembly of the diverse components of the articular cartilage [28].

2 Articular Cartilage Structure

The AC is organized in different zones towards tissue depth. Chondrocytes manufacture collagens, proteoglycans, non-collagenous proteins and glycoproteins (main of the extracellular matrix components) in order to form the highly ordered structure of the articular cartilage. The cell morphology change with the zone appearing from the articular surface to the subchondral bone. Every zone has specific biochemical and mechanical properties corresponding to an organization and composition. The organisation of matrix changes in function of the zone where all component contents vary but also an ECM local organisation close to cells. This is the articular cartilage anisotropy which provides its fiber-reinforced material characteristics.

2.1 Articular Cartilage Zones: Benninhoff Arcades and Collagen Ultrastructure

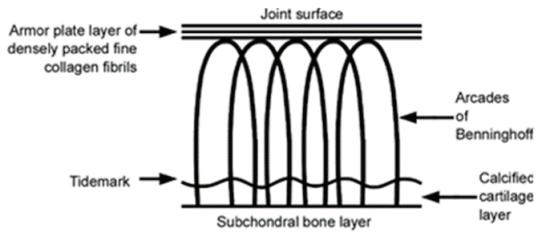

Figure 15: Arcade Collagen Structure: a schematic description of the collagen fiber orientation in articular cartilage

Articular cartilage is divided in four different morphological zones: superficial, transitional/middle, radial/deep and calcified zones [20,21]. The collagen pattern from the surface to deeper layers of the cartilage is architecturally quite different. In 1925, Benninghoff described an arcade-like macroarchitecture of the articular cartilage collagen (Figure 15) [29]. This arcade pattern is responsible for the zonal appearance of the AC, explaining how to reflect a folding over of radial fiber bundles to lie in the plane of the surface in a series of layers or leaflets that makes up the tangential zone. This concept is partially correct, but it is useful to visualize and understand cartilage biomechanics. In fact, it is also possible to consider that as a juxtaposition on collagen leaves in an arcadian way. The surface fibrillar pattern expresses a strong divergence from those of fibers in deeper layers. Surface fibrils are thinner and closely packed compared to those of middle and deeper layers [20,21]. The surface pattern of the collagen framework can be qualified by the term “armor plate” layer, referring to the tough, resilient, skin-like cartilage surface [29]. The highest collagen concentration appears at the surface where the small fibrils are compacted tangentially. This arrangement creates a small pore size. Small ions, glucose and other essential nutriment proteins can easily traverse these pores. For example, the hemaglobin is the largest molecule which can traverse these pores. Nevertheless larger molecules (hyaluronic acid) cannot penetrate within the cartilage in significative amounts under normal conditions.

Literature of the subsection: [20-22, 30-33]

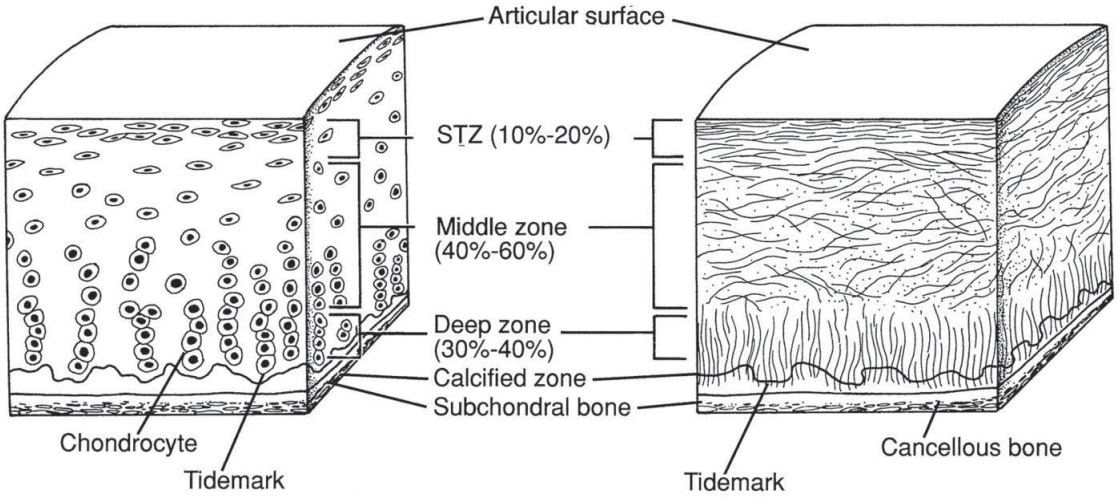

Figure 16: Cellular distribution and Collagen fiber orientation of the different zone of AC. Superficial Zone has small flat cells entrapped in a thin fiber collagen meshwork oriented parallel to the surface. In the deep zone, exhibit spheroidal-shaped chondrocytes disposed in column along a large and thick collagen fiber meshwork, perpendicular to the articular surface [30].

2.1.1 Superficial Zone:

The superficial, tangential or gliding zone is the thinnest zone of the AC (10-20% of articular cartilage - immature $\sim 200\,\mu$m, mature $\sim 40\,\mu$m) [22] (Figures 11&16). This zone can be divided in two parts. First, at the surface, a so-called "lamina splenda" is an extremely thin acellular layer. This zone can be seen as an interface allowing the molecular adhesion of macromolecules (e.g. hyaluronic acid) present in the synovial fluid necessary for the chondrocyte nutrition. This constitutes a protective layer of cartilage against some harmful molecules such as free-radicals. This region is rich in fibronectine and in water. corresponding to fine polysaccharide fibrils. Under this thin layer, the supercificial zone presents flattered chondrocytes well organized along of the collagen fibers. These cells have an ellipsoidal shape. Chondrocytes are arranged parallel to the surface within a dense collagen meshwork composed of tightly compacted thin fibrils (about 20 nm diameter [22]). They synthesize diverse matrix components in different proportions (always relative to other zones). A high synthesis of collagen molecules (fibrils) contrary to the PGs synthesis which weak [22]. The water content is the highest in this zone composed to the rest of the tissue. The structure and the composition of the zonal ECM provide specific mechanical and biological properties to the AC. The collagen mat mainly provide tensile stiffness and strength, resistance to shear forces occurring during the motion. Actually, the compact parallel fibrils allow the distribution of the loadings across to the surface. This zone is used as a buffer creating an impermeable (isolator) barrier against injuries and a protection against an extreme loading generating compression of the molecular matrix.

2.1.2 Transition Zone:

The middle or transitional zone is an intermediate zone between the superficial and the deep zones (Figures 11&16). It represents a relatively large part on the height of the AC (40-60% of AC, mature $500\,\mu$m) [20, 33]. There, chrondrocytes are larger and spherical-round appearing in a random-like distribution due to the apparent randomness of the structural-supportive collagen fibers [22] . The cellular density is lower than in the superficial zone [20]. The collagen fibers become larger than the fibrils in the superficial zone and are organised into radial bundles or layers [20]. The concentration in proteoglycans increases and concentration in water and collagen decrease. All the synthesizer organisms, such as endoplasmic reticulums and golgi membranes, are present in a higher

proportion.

2.1.3 Deep Zone:

In the deep or radial zone (30% of AC, mature $< 500\,\mu$m) spheroidal-shaped chondrocytes tend to follow a column disposition along a large and thick collagen fiber meshwork, perpendicular to the articular surface [20]. The cellular density decreases compared to the transition zone and the collagen content is relatively variable [22]. The collagen fiber diameter increase progressively from the surface to the deep zone until reaching a size of 70-120 nm [20]. This zone possesses the highest concentration in proteoglycans but also the lowest concentration of water [22]. The collagen fibers of this region pass into the tidemark, a thin basophilic line corresponding to the boundary between calcified and non-calcified articular cartilage, in order to continue the collagen fiber orientation (within is different from this of the bone). A delimitation between the deep zone and calcified zone exists and is called "tidemark" [33]. This boundary is a kind of barrier which prohibits the vessel penetration within the subchondral bone. The tidemark can be seen as a reminiscent "high water mark" for calcification with fine fibril band.

2.1.4 Calcified Zone:

The calcified zone is the region in contact with the subchondral bone (Figures 11&16). It serves to a delimitation between the radial zone and the subchondral bone. Cells are spherical and smaller than the cells of the other zones. Cell population is extremely scarce [20]. They are like trapped within a calcified cartilage. They are usually in a hypertrophic phenotypes [22]. PG and water contents are both very low. This zone is important in articular cartilage safeguarding. Qualified as semipermeable, this zone represents a physical barrier for vascular invasion and mediates the passage of small molecules, essential for the tissue activities, from the subchondral bone to the articular cartilage [34]. The tidemark defined the separation between cartilage and bone but seem also to anchor the hyaline cartilage to the subchondral bone as collagen fibrils from the deep zone penetrate into the calcified cartilage [20].

2.2 Cellular Regions in Extracellular Matrix

In all articular cartilage zones, ECM variations are observed and ECM can be divided into three regions corresponding to different organisation and composition of this matrix. The different regions are defined relatively with the separating distance from the chondrocyte. The two first regions, pericellular and territorial, are identified to serve to the sustain of chondrocytes. It means that these two regions support the cell function, contributing to transfer of mechanical signals from matrix to chondrocytes and binding matrix macromolecules to chondrocyte membranes which also provide a cell protection against the diverse loading or deformations injuries. The main function of the interterritorial matrix is to provide mechanical properties to the AC.

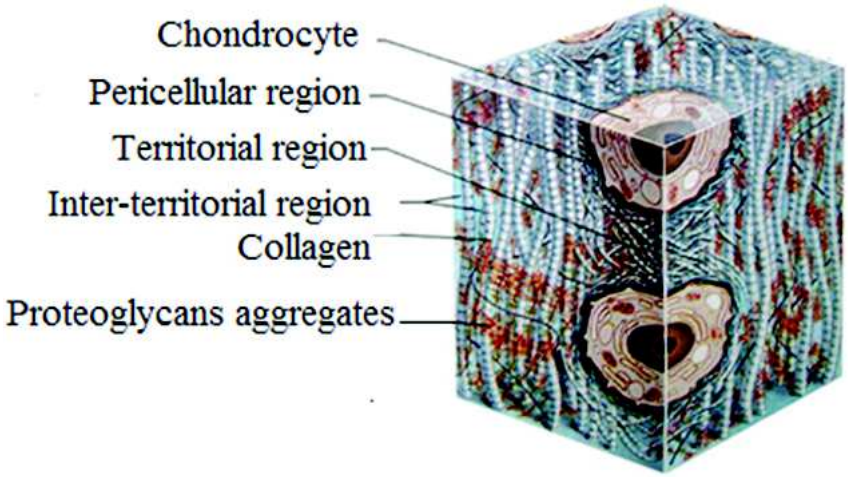

Figure 17: ECM regions of the AC. Chondrocytes are surrounded by a lacuna. The whole is encapsuled in the first thin region called pericellular region . The second regioon is the territorial region. The whole is finally entrapped in the large interterritorial region [24,25].

2.2.1 Pericellular Matrix:

Pericellular matrix ($\leq 2\,\mu$m large) is the region of contact between cell surfaces and ECM [26] and surrounds chondrocytes (Figure 17). This area is made of a thin layer of nonfibrillar material (proteoglycans and glycoprotein), related to the cellular synthetic products [20]. The direct surrounding matrix is rich in proteoglycans and other non collagenous proteins. It appears that the cell membrane associated molecule anchorin CII and non-fibrillar type VI collagen [21] are two important components of this region [26]. The fibrils within the newly synthesized extracellular matrix are enrolled in the network of interconnected fibrils within the surrounding pericelullar matrix. It is a starting point for initiation of stable collagen fiber production [26]. It was observed that in this region, nigh of the cell the fibrillar structure are orientated radially to the cellular surface. It is strongly assumed that the hyaluronan can play a role in the small fibril dimension. The hyaluronic acid (HA) could be an essential component of this region during the collagen fibrils synthesis which could influence the structural assembly.

2.2.2 Territorial Matrix:

This region ($\leq 9\,\mu$m large) envelops the pericellular matrix of individual chondrocytes or a cluster of pericellular regions of pairs of chondrocytes [21] (Figure 17). All the thin collagen fibrils at the "interface" with the pericellular region seem to be adhered to those of the pericellular matrix. At the interface between these two regions, thin collagen fibrils seem to be anchored to pericellular matrix. The collagen meshwork is dense with a large number of decussated fibrils [20]. Different packets intersect to each other in diverse angles in order to form a mechanical protective "layer" against potential loadings and deformation damages [21]. The boundary between this region and the interterritorial matrix is not well defined because it is difficult to observe the passage to the different collagen fibril orientation connections between these two regions. A sudden increase of collagen fibril size happens with a differentiation in these fibril orientations: the arrangement passes to a basket-like structure to a parallel structure [21].

2.2.3 Interterritorial Matrix:

In mature AC, this region represents the largest part of the matrix volume (Figure 17). The meshwork is composed of large collagen fibrils which areperpendicularly oriented to the joint surface [21]. The fibril diameter vary depending on the zone (superficial, middle or deep). As it is noted

previously (2.1) the fibril diameter is very thin in the superficial zone and arranged parallel to the joint surface, in the transitional zone, fibrils are larger and oriented according diverse angles, oblique relatively to the articular surface and in the deep zone, they are larger than all the other fibrils and perpendicularly oriented relatively to the joint surface [21].

3 Multiphasic Theory: Biological, Biomechanical, Chemical and Physical Properties

In articular cartilage, numerous interactions occur between diverse components of the ECM (water fluid, PGs, electrostatic charges...). Electrostatic attractions take place between the positive charges along collagen molecules and the negative charges generated by the diverse functional groups of GAGs. During articular cartilage loading, deformation and hydrostatic forces are generated. Interstitial water tends to propagate through the cartilage and to escape from the tissue. Negatively charged proteoglycans placed under stressed and compressed conditions have properties to resist the water flow. The combination of these interactions provides the mechanical properties of the material. Articular cartilage has a composite structure conferring its anisotropic properties. Articular cartilage can be seen as a viscoelastic material. The porosity of cartilage allows the interstitial fluid circulation. As a sponge, when a compressive loading is applied, the fluid is squeezed out of the cartilage tissue but once the stress is removed, the water fluid flows in back to the tissue. It is important to remark that the mechanical properties are different as a function of the position within the cartilage and the pathology.

Properties	Involved Components
Stiffness	Collagen Fiber Network
Elasticity	Hydrophilic Proteoglycans allowing water motion
Slithering/Shear	Water - Extremely Low Friction Coefficient

Table 2: Sum-up of the different mechanical properties of the articular cartilage in regard to its compositional material. The articular cartilage is an elastic material able to support deformation and to resist under compressive actions. It acts as a pressure absorber.

3.1 Multiphasic Theory

In order to combine the different components required in mechanical response of articular cartilage to deformation stresses, a multiphasic theory has been developed. This model highlights the interdependence of electrochemicostatic and hydrostatic mechanics, the temporal relationship between water flow and mechanical deformations. Cartilage can be stretched as a sponge-like (porous) mixture of different phases with fluid and solid components [1, 35].

The biphasic model of cartilage refers to two phases: one liquid corresponding to the free mobile interstitial water and the other to the solid substance of AC composed of densely woven, strong, collagen fibrillar network enmeshed with proteoglycan macromolecules and other proteins. The solid phase is defined as incompressible elastic material and the fluid phase as incompressible, invisced and non-viscous. The idea is that two phases exist but they can be visualized as one and unique phase under instantaneous and brief loading deformations. In this moment, the phase can be defined as an incompressive and elastic solid because during instantaneous loads water does not have time to react and to be evacuated out of the cartilage (because it is the solid elements which generate a fluid displacement by perturbations). The biphasic model is based on diverse viscoelastic models used to describe diverse applied forces such as creep, stress relaxation and oscillating shear [1].

All the biomechanical properties appearing in the articular cartilage can also be related to the triphasic model. Articular cartilage is a porous and viscoelastic tissue composed of three principal phases [1]:

(a) Solid phase: composed of densely woven, strong, collagen fibrillar network enmeshed with proteoglycan macromolecules

(b)Fluid phase: composed of water which is squeezed out under compressive loading,

(c) Ion phase: composed of ionic species of dissolved electrolytes with positive and negative charges.

It is the common and simultaneous action of these 3 phases which generate the enormous compressive load capacity and the resistance against shear forces [1].

3.2 Articular Cartilage Biomechanics

AC mechanical properties strongly depend on the ECM quality and complexity related to the large framework of the diverse macromolecules and the component concentration [21]. Articular cartilage continuously supports several static and dynamic mechanical loads with different intensities. Normal cartilage can present a peak stress about $15-20\,\mathrm{MPa}$ when an instantaneous [21] mechanical stress is applied. For this dynamical stress, the compressive strain is weak (1-3%) [21]. For static loadings, the time of the applied stress is longer ($5-30\mathrm{min}$) and the compressive strain is consequently larger (35-45%). The extracellular matrix allows the repartition of all exerted forces (compressive, tensile, shear) within the cartilage. Its structural integrity and molecular composition are the most important parameters. To preserve essential properties of precise ECM control of this matrix is required. The control of the ECM is mediated by chondrocytes, they maintain the ECM via diverse pathways (synthesis, assembly, degradation) for most matrix components (PGs, diverse other proteins and molecules). Previous experiments have been performed to characterise the biomechanical properties of AC based on applied forces, their effects, and their related matrix structure or component actors. Dense collagen fibrils appear to be the element essential to resist to tensile and shear deformation forces. Compressive forces and fluid flow are mediated and controlled by the aggrecan PGs since highly charged GAGs act as regulator of fluid trap. These GAGs constituting aggrecans also generated electrostatic repulsion and osmotic swelling between their anionic parts (sulfated-carboxylate group) and cations present within the interstitial fluid. Diverse regulation processes are required in the maintenance of ECM. In the physiological intensity range, static compression can induce a reversible inhibition in the synthesis of some essential matrix components, e.g. the downregulation production of type II collagen, aggrecan, core and link proteins and also some gene expressions. Hydrostatic/Hydraulic pressures and compressive strain can stimulate the catabolism of several type of proteins. Mechanical forces present in the microenvironment of chondrocytes could influence molecular matrix catabolic/anabolic activities. Resistance of AC is related to viscoelastic properties in compression which are induced to frictional dissipation and resistance produced by the passage of the fluid though porous solid matrix [1,27].The perfect balance in the deformation-dependence permeability seems to be required to regulate and dissipate load repartition between the different phases. Resistance of AC is related to viscoelastic properties in compression which are induced to frictional dissipation and resistance produced by the passage of the fluid though porous solid matrix [1,19, 27, 35]. However, all of these response mechanisms are still not well-understood [21].

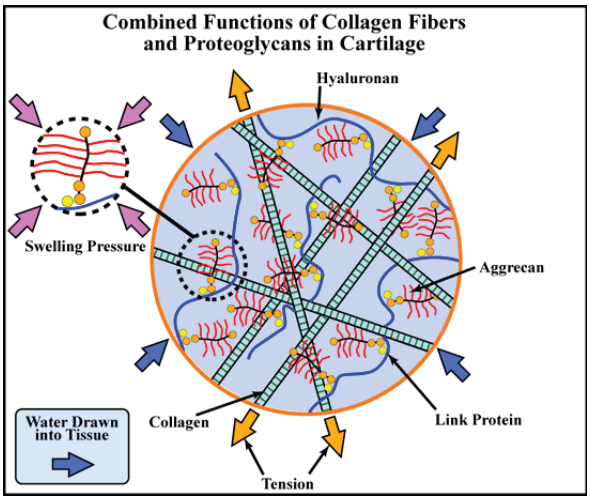

Figure 18: Aggrecan function in articular cartilage. The load-bearing properties of cartilage are provided by the tensile properties of the collagen fiber network and the osmotic swelling pressure of the high concentration of aggrecan. The aggrecan is immobilized within the matrix by forming supramolecular aggregates with hyaluronan and link protein. Source: http://glycoforum.gr.jp/science/hyaluronan/HA05/HA05E.html

Proteoglycans can be considered as polyanionic components of the ECM because their molecules are negatively charged due to the presence of sulfated or carboxyl groups [21]. This cartilage swelling is related to the important concentration of PG molecules, interacting electrostatically between each others. This swelling can be controlled because the PGs are entangling in the dense fibrillar collagen meshwork restraining their expansion [27]. This mechanical response is supported by electrostatic and electrochemical phenomena and is related to the Donnan osmotic pressure principle [36]. Under compression, cartilagenous extracellular matrix is contracted. The negatively charged sites of large aggregated proteoglycans are pushed closer together. Mutual repulsive forces generated by the vicinity of the same charge molecules resist compression. This provides compressive stiffness in the ECM of AC. Nevertheless this compressive stiffness is also supported by the collagen fibrillar meshwork. Damage or injury of collagen structure is related to a PGs concentration decrease and an increase hydratation. If negatively charged proteoglycans are placed within water without any restrictive collagen meshwork, they will find a configuration with a maximal expansion. Consequently, the trap of the PG aggregates provokes a pressure against the collagen fibrillar meshwork. When the compressive loads are applied, water is forced out of the tissue, forcing the proteoglycans to be concentrated in restricted zone into an unfavorable thermodynamic state. This generates again a higher pressure within the articular cartilage providing a stronger resistance to the applied stress. Then, as soon as the load is removed, the water is allowed to flow back into the tissue in order to restore the cartilage shape [36]. When proteoglycan content and equilibrium stiffness decrease, the fluid can take more place within the tissue increasing the permeability and the rate deformations [19].

Mechanical responses also take into account another important parameter: the interstitial fluid flow through the articular cartilage. This mechanism linked to elastohydrodynamic physics contribute to the joint lubrication. Water fluid is trapped between two articulating surface within synovial joint. Studies assumed that the fluid could form a wedge to counterbalance the overpressure and help the charge repartition on the articular surface (hydrodynamic mechanism). Another assumption is also made concerning a potential hydrostatic reaction. Under loading deformations, a compression is applied on a solid element which pushes the liquid to move. A pressure difference appears then and fluid is obliged to flow through the cartilage and is pushed out of it (via the articular surface) into the synovial cavity. These restrictions allow maintenance of the cartilage density integrity. They also

contribute to the low friction coefficient characteristic of the AC. This coefficient is also defined by another mechanism called boundary effect. The boundary lubrication effect is simply the fact that the lubricant is absorbed onto the rough surfaces [37].

In AC, dynamic compressions can generate matrix (and cells) deformations, hydrostatic pressurization of the interstitial fluid [38,39]. This fluid induces pressure gradient, streaming potentials and currents. A prolonged compression such as static condition can cause local variations of the ECM physiological properties. Local variations can alter water content, fixed charge density, mobile ion concentration and osmotic pressure. All these mechanical, chemical or electrical changes in the cell environment could affect cellular metabolism. They are part of physical stimuli acting in parallel with biologic factors (cytokines, growth factors) to regulate chondrocyte homeostasis within AC tissues. All of these phenomena (mechanical, physicochemical and electromechanical) are well described by diverse theoretical models such as the multiphasic theory[28, 35,36, 38, 39, 40-43].

4 Articular Cartilage Maturation, Degeneration and Diseases

Here, the study will be focused on the two most important diseases related to the articular cartilage degeneration.

4.1 Cartilage Development: Growth and Maturation

The mature articular cartilage is a highly structured tissue in contrast to the fetal articular cartilage, qualified as immature. The native articular cartilage matures to develop an adequate structure providing the completely functionality of the tissue. This tissue will be able to support all the different applied stress loads. Immature cartilage is a thick tissue rich in all the extracellular matrix components, especially PGs [22]. Cell number and the water concentration are higher than in more mature articular cartilage. During the long maturation phase, several structural and compositional alteration appears [44-46] with increases in collagen content [44-46] and in proteoglycan concentration [45]. A reorganisation of the diverse zones of the collagen network takes places [47-48] with the changes in fiber characteristics, for example. The fine fibrils of young growth cartilages is composed by $\geq$ 10% collagen IX, $\geq$ 10% collagen XI, $\leq$ 80% collagen II) compared to the thicker and more varied fibril diameters of mature articular cartilage composed of 1% collagen IX, 3% collagen XI, $\geq$ 90% collagen II. Tissue thickness decreases with the extensive modifications of collagen structure . These modifications occurring during the maturation stage are probably induced by the altered loading conditions of the joints, referring to the necessary functional adaptation of articular cartilage [22, 49]. Postnatal AC maturation is a critical developmental step in shaping the function of this tissue. Regarding the lack of information about biochemical stimulators, it is important to understand how is initiated this maturation to latter control processes and to enhance intrinsic repair *in vivo* and grow high quality cartilage *in vitro* [16–17].

The immature articular cartilage undergoes diverse differentiation. One part of this tissue called epiphyseal or conjugation cartilage will become bone by endochondral ossification and the other part will mature into permanent articular cartilage. In the embryonal stage, the cartilage appears through a process of condensation. It will progress in order to establish a template for the future bony scaffold. In the long bone growth, the cartilage will undergo several processes such as proliferation, calcification and ossification. A differentiation of the fetal cartilage occurs, this cartilage present in shaft of these bones will be ossified except at their ends where the tissue remains permanently cartilaginous [34]. At birth, the heads of long bones, the epiphyses, will undergo a second ossification. In this epiphyseal

cartilage, chondrocytes perform an active and complex cellular maturation that ends in endochondral ossification. Two structures will appear: the growth plate cartilage and the articular cartilage. At the surface, which is also a growth plate, of the bony ends, the chondrocytes undergo mitosis cell division. Chondrocytes undergo intense activity during the development process in order to create and generate the extracellular matrix composing the articular cartilage [34]. Endochondral ossification progresses the deep to articular surfaces to develop epiphyseal growth plate [33]. The growth plate and future articular cartilage are indistinguishable in the first stage of postnatal development [33]. The formation of articular cartilage is complex and required several chondrogenic factors such as articular chondrocyte differentiation. During post-natal development and homeostasis in the mature joint, mechanical stresses are also necessary to form the normal zonal organization of cartilage [33]. Two types of growth exists: the interstitial growth and the apposition growth [34]. During the interstitial growth, chondrocytes undergo several division in their lacunae. The daughter cells are then momentarily in the same lacunae. After matrix production they will occupy their own separated lacunae. Several division cycles appear in the last growth stage and isogenic groups are formed. In the appositional growth, perichondral cells produce type I collagen. However some cells of the deep zone undergo a transformation to chondroblastes which start to secrete type II collagen. Chondronblastes are transformed to chondrocytes to support the full production and maintenance of the cartilage matrix [50]. In mature conditions, chondrocytes maintain joint function throughout life. They safeguard a stable and permanent phenotype maintaining the constant production of the diverse components (aggrecan and collagen II) allowing functional resilience of the AC tissue and to prevent hypertrophy and hence loss of cell and tissue function. In contrast, transient chondrocytes present a intense dynamic phenotype of a limited life span and are extremely proliferative with progressive modifications of the growth plate during maturation (cellular hypertrophy and apoptosis). This process remains unclear. During this endochondral ossification phase, part of this tissue can be replaced by bone cells [51]. Epiphyseal chondrocytes, or transient chondrocytes, form a template for long bone growth. They do this by undergoing rapid proliferation, they mature by a process called hypertrophy. The calcified matrix is then invaded by osteoclasts and osteoblasts which remodel the matrix into bone. Due to this particular growth process, the interface between the two different tissues (cartilage and calcified cartilage) is distinguished by the so-called tidemark. The subchondral bone growth front is stabilized by the equilibrium local balance between intermittent shear stresses and hydrostatic pressures in the deep zone of the articular cartilage during loadings. In the advanced fetal stage, two types of zones can be seen: one at the surface of the immature cartilage with flattened cells and the remaining epiphysis in which spherical cells are spread in a homogeneous extracellular matrix. After the birth, the pressure related to motions induces the apparition of a tissue stratification. Once this stratification is established, the different zones of the articular cartilage will develop their own biological structure in order to provide their specific mechanical functions. First loaded under hydrostatic pressure, the transitional and radial chondrocytes (from the deeper zones of the articular cartilage) will synthesize and maintain a high amounts of glycosaminoglycans and type II collagens [34]. For the superficial oblong chondrocytes which undergo fluid flow and matrix consolidation in addition of the hydrostatic pressure.

4.2 Articular Cartilage Aging and Diseases

4.2.1 Aging

Aging profoundly alters chondrocyte function with a reduction of the cellular ability to synthesize some types of proteoglycans [21]. Their proliferative capacity and their response to anabolic stimuli including growth factor decrease. These changes may have an impact on the maintenance and the preservation of the tissue, and this can contribute to the development and progression of AC degeneration. With aging, a possible diminution of the articular cartilage thickness can appear [16]. AC surface can become softer due to degradation inducing a loss of matrix mechanical properties (tensile strength and stiffness) [52]. During aging, the proteoglycan turnover decreases (synthesis) and consequently proteoglycan quantities decrease. Nevertheless in opposition to this decrease phenomenon, an increase in shorter-length hyaluronic acid (HA) concentration occurs [21].All of these proteins and glycosaminoglycans changes have fundamental consequences on the organization of cartilage. Chondrocytes are surrounded by non-appropriate proteoglycans, impairing their signaling from matrix to cell, which then affect cell phenotype. Furthermore, the diversity of aggrecan species within the extracellular matrix will confer onto the proteoglycans other properties (loss of hydrophilicity) and make cartilage less resistant to diverse mechanical stimuli, proteoglycans being the key of the resistive force. This will also have a direct impact on the viscoelastic properties of the cartilage. A re-organization of the collagen meshwork could also be important in the degeneration of cartilage. Aging is associated with cartilage hydration decrease and a significant decline of chondrocyte cell number. The synthesis of some matrix component is insufficient to compensate for tissue catabolism. Age also affects the cell replicative senescence generating a state of irreversible cell cycle arrest [52] with a deterioration of the cellular function. This cell senescence can have a major role in the development and progression of osteoarthitis.

To summarise, natural aging present progressive loss of extracellular matrix and resilience in articular cartilage, resulting in stiffness and reduced biomechanical properties. Age related changes in the molecular composition and structure of AC matrix include an increase of collagen cross-linking and decreased water, carbohydrate/protein ratio and CS concentrations with an increase of KS occur [52]. Osteoarthritis, rheumatoid arthritis and other joint degradation diseases affect billions of patients worldwide [51].

4.2.2 Joint Degeneration, Diseases and Osteoarthritis

Articular cartilage degeneration start with a disruption or alteration of molecular structure and composition of the matrix. When tissue damages appear, chondrocytic synthetic and proliferative responses are activated in order to maintain or even restore the articular cartilage. During joint degeneration, the stiffness of articular cartilage declines and its permeability increases [52]. Joint degeneration concerns all the tissues participating in the functioning of the synovial joint: articular cartilage, bone (subchondral and metaphyseal), synovium, ligaments, tendons, joint capsules and muscles. Degeneration refers to modifications in the structural and functional organization of the synovial joint: loss and possible calcification of articular cartilage, subchondral bone remodeling. Generally, the first visible microscopic modifications are a fibrillation and disruption of the superficial zone of the AC. This surface becomes roughened and irregular. With time, this fibrillation is extended to the transitional zone and the rest of the AC. This fibrillation can lead to ruptures generating fissures with the entire depth of the AC until it reaches the bone. This weakening of the AC structure can induce this degradation process. Furthermore, fibrillation has a direct impact on the biological components of the AC. Degradation of collagen fibrils and proteoglycans occurs. Proteoglycan content loss is an

important factor in the progression of the degeneration because it provides the biomechanical support to loading stresses through their retention of large quantities of water. Simultaneously, several other enzymatic degradation pathways occur within the matrix contributing to the volume contraction and remodeling of AC. During all these processes (fibrillation, ruptures...) small fragments of cartilage and bones are released into the synovial cavity. Moreover, the bony remodeling contributes to a violation of the tidemark by blood vessels. The articular cartilage cannot play the role of sponge and bearing tissue. The stiffening of the subchondral bone is postulated as another reason of the AC degeneration progression.

Osteoarthritis (OA) is an important clinical challenge because it is one of the most prevalent joint diseases in the entire world, touching almost ten millions people in France (INSERM). OA impacts the life quality of aged-people and is a major economical problem causing a major burden on health and social care [53]. OA presents a degradation and loss of AC with subchondral bone remodeling. An inflammation of the synovial membrane impacts on cartilage matrix homeostasis by altering chondrocyte metabolism to enhance catabolism and reduce anabolism [20] inducing biochemical and structural alterations in the extracellular matrix macromolecules [20]. Osteoarthritis is a degenerative joint disease characterized by progressive degradation of the articular cartilage and a loss of its biomechanical properties. Nowadays, no optimal cure for OA exists and current diagnostic techniques are not efficient enough to detect early signs of OA.

The loss of cartilage properties is expressed by structural and functional dysfunction. Degeneration correlates with an attempt to repair the AC inducing remodeling and sclerosis of the subchondral bone. OA can be defined as an unbalanced state between diverse catabolism processes and attempts of repair by the chondrocytes. The degradation of extracellular matrix components is mediated by several chemical substances that stimulate in matrix turnover). Repair is mediated mainly by the secretion of growth factors and anti-inflammatory cytokines. OA is in part a disease of mechanical overloading, consequently the most affected joint regions are knees, foot, hip, spine, hands. It is correlated with the age of patients, contributing to the reduction of reactive response under mechanical stresses. Genetic factors could also have an impact on the cartilage degradation providing some predispositions for osteoarthritis [21].

OA is a degenerative disease with a gradual loss of ECM [54]. Fibrillation starts because of chondrocyte number decrease. Their production is disorganized and becomes more random in the tissue [21]. The chondrocyte state undergoes changes, they appear to become more undifferentiation with several types of chondrocyte phenotype: dedifferentiated with a morphology resembling fibroblasts, and hyperdifferentiated down the epiphyseal lineage which can lead to cellular apoptosis. Hypertrophic chondrocytes appear in OA-affected articular cartilage [55]. At the cellular level, the degeneration of AC is related to transdifferentiation of chondrocytes which may lead to the formation of osteocytes similar to a thickening/condensation of the underlying subchondral bone. Articular cartilage starts to become thinner. This modification of the AC architecture is associated with several clinical symptoms: joint pain, difficulty and restriction of motion appear due to mechanical instability and deformation [21]. Biologically, the water concentration decreases which consequently causes a decrease of the biomechanical properties of the cartilage. The “sponginess” role is lost. The dysfunction of the chondrocytes alters the collagen content, type I and III collagen become more abundant within the extracellular matrix. These two types of collagen are not expressed within the normal articular cartilage, generating a re-organization of the collagen meshwork. A degradation of the type II collagen in the pericellular matrix and then in the interterritorial matrix is observed [20,26]. Reaching a certain stage in the evolution of OA, chondrocytes cannot fully compensate for the proteoglycan loss, even in the presence of increased synthesis, resulting in a net loss of matrix. New aggrecan synthesis does occur in OA cartilage, presumably in an attempt by the chondrocytes to initiate repair [20]. Early

stages of OA are characterized by a decrease of PGs, especially in the superficial zone in early OA [288,289] and a orientation changes of the superficial collagen fibril network [56-58]. Because of these compositional and structural changes cartilage tissue starts to swell. AC mechanical integrity starts to be deteriorated inducing a progressive reduction of the dynamic stiffness of the tissue[59]. The pericellular matrix is also enlarged around many chondrons in osteoarthritic cartilage as determined by examination of cartilage sections [26]The ECM molecules synthesized and assembled are smaller and cannot compensate the function of the previously larger molecules in matrix stabilisation. All of these factors lead inevitably to a reduction of articular cartilage properties to resist to diverse applied forces. The cartilage does not support the diverse biomechanical forces and an refinement occurs until the cartilage degrades generating pain when the subchondral bone is exposed. The osteocondensation begins with an increase in cartilage calcification and mineralization and contributes to the stiffness of the joint [21]. Apparition of osteophytes and propagation of some bony crystallite formation within the deep zone of AC occurs. Osteophytes are bone spurs or parrot beak and they are bony projections/excrescence that form along joint margins and which hinder joint movement. Osteophytes are assumed to be an attempt to repair caused by an overexpression of growth factors locally present within the extracellular matrix [21]. It is interesting to establish the possible tight link between cartilage senescence and osteoarthritis development, cartilage aging can lead to a predisposition to OA.

Part III
Selenium, Geological Element and Interest in Biology

This part will provide general information about selenium in the environment and in biology. Selenium source, human exposure and Se-pathway, from environment to our metabolism, will be described. An overview of selenium implication in disease will be presented to introduce its potential role in articular cartilage metabolism.

5 Selenium Characteristics : Physico-chemistry, Benefits and Toxicity

Discovered by the chemist Jöns Jacob Berzelius in 1817, selenium is below sulfur in the periodic table of elements [4]. Biological research related to Se began one hundred years later, demonstrating for instance its anti-oxidative effect. Selenium is characterized by an atomic mass of 78.96 g.mol^{-1} and an atomic number of 34. Selenium belongs to the group VI like sulfur and oxygen, next to arsenic and the phosphorus (group V in the periodic table). From this position and consequently from its electronic configuration, it is classified as a metalloid. It is thus different from metallic and non-metallic elements but shares some fundamental physical properties with metals and non-metals. Selenium occurs in nature as six stable isotopes (Table 3).

Element	Selenium	Sulfur
Atomic number Z	34	16
Chemical Symbol	Se	S
Density	4.79 g/mol	2 g/mol
Atomic mass	78.96 g/mol	32.065 g/mol
Electronic Configuration	[Ar]3d^{10}4p^{4}4s^2	[Ne]$3s^2 3p^4$
Electrons pro energy level	2,8,16,6	2,8,6
Stable Isotopes and Isomers	^{74}Se,^{76}Se, ^{77}Se,^{78}Se,^{80}Se	^{32}S, ^{33}S, ^{34}S, ^{35}S, ^{36}S
Ionic Radius	190 pm	180 pm
1st Ionization Potential	9.752 eV	10.36 eV
Oxidation States	6, 5, 4, 3, 2, 1, −1, −2	6, 5, 4, 3, 2, 1, −1, −2

Table 3: Selenium and Sulfur Properties [4]

Selenium (Se) is an element from the chalcogen family. It is the only non-metallic (semi-metallic) element which is not present in organic matter as a macroelement as C, N, O, S, P. Selenium has many chemical similarities with the sulfur S, e.g. ionic radius, length and binding energy and ionization energy/potential. Selenium can occur in different oxidation states: -2, 0, 4+, and 6+ (Table 4). In regard to these similarities, S-substitution by Se could happen naturally. This is the reason why some organic molecules (proteins, amino acids) are found containing Se instead of S. Methionine or cysteine have therefore selenomethionine (SeMet) and selenocysteine (SeCys) analogues. Selenium can then be found in a variety of natural materials such as rocks, soils, waters, air, and plant, animal and human tissues [4]. As example, in French “eaux seleniteuses” refers to waters-rich sulfur.

Oxydative State	Chemical Forms
Se^{2-}	Selenide (Se^{2-}, HSe^{-},$H_2Se_3(aq)$)
Se^{0}	Elemental Se
Se^{4+}	Selenite (SeO_3^{2-}, $HSeO_3^{-}$,$H_2SeO_3(aq)$)
Se^{6+}	Selenate (SeO_4^{2-},$HSeO_4^{2-}$,$H_2SeO_4(aq)$)
Organics	Selenocysteine, Selenomethionine

Table 4: Selenium Natural Forms in Environments [4]

Selenium is an essential oligo-element useful for very important organ (e.g brain and thyroid) function. This "double-edge sword" element is essential for human organism in a restricted range of concentration. Actually, at a dose slightly superior to the vital dose, the selenium becomes toxic or even highly toxic. At too high or too low selenium concentration, it can contribute to some disease developments. The clinical symptoms of toxicity due to an over-intake of Se are nausea, nail degeneration, hair loss, skin lesions and neurologic deficiencies. Selenium toxicity depends on several factors such as Se chemical form and concentration, number of compounding factors and its synergy with other molecules [4, 60]. Usually, it is set that Se intake must be limited to $[40 - 400]\,\mu$g pro day [61].

Selenium is a very interesting element, widely distributed in human organism. Selenium toxicity was first described during a Marco Polo expedition in China (1295). Horses became sick with a hoof degradation due to the consumption of high Se-rich plants [4]. It is in the 20^{th}century that selenium was officially described as toxic and dangerous for human health.

Sulfate concentration, hardness, heavy metal concentration, pH, temperature influence Se toxicity and bio-accumulation [62]. From its particular electronic configuration, Se can combine to a large variety of natural elements. For example, it can be bound to heavy metal present in toxic amount in the cellular environment, restricting this toxicity by complexation and/or precipitation. Selenium further acts on the toxicity of several inorganic and organic substances (arsenic, cadmium, copper, mercury, silver). Selenium is also a powerful anti-oxidative and anti-inflammatory agent, critical in the protection of cells and organism well-function, as it will be discussed latter.

6 Environment Selenium

Selenium can be abundant in the Earth surface environment. It comes from diverse natural processes such as rock weathering, volcanic activities and phytoplankton emissions but also from diverse human activities (Figure 19). It is present in different forms within soil, air and water. Its migrative path and its incorporation within diverse organisms are mediated by several bio-geological processes. The distribution and the mobility of the environmental Se is important to know because it provide information on its bioavailability. Living organisms ingest selenium by means of their diets (seeds, fishes, vegetables and drinks). For humans, diet is the main source of selenium. In regard to the different forms of this element, selenate (+IV) absorption is superior to that of selenite (+VI). Selenium is present within organisms mostly as selenoproteins. Metabolism and catabolism helps to produce these organic forms of Se. For example selenate and also selenite are reduced by the glutathione enzyme in order to produce selenoaminoacids. This complex pathway from its environmental context to its biological expression has to be perfectly defined to properly evaluate selenium-related health risks.

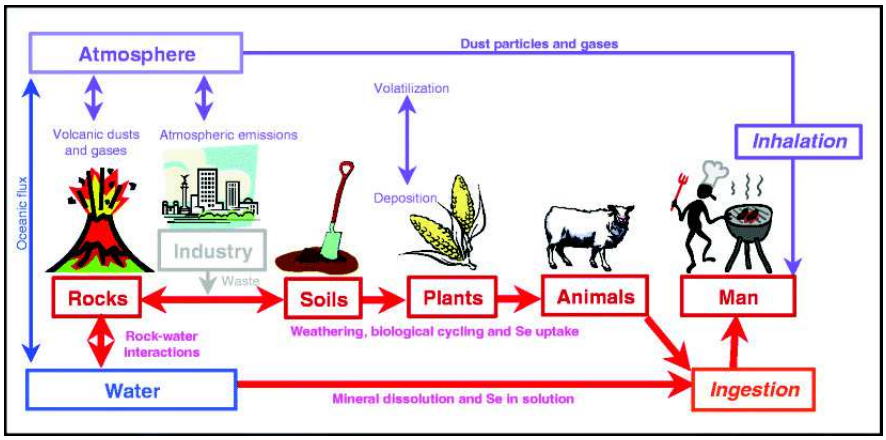

Figure 19: Cycling of selenium from environment to men with the main geochemistry and health pathways, from Fordyce [4] . Se is derived from both natural and man-made sources

6.1 Selenium: Source & Bioavailability

Selenium physico-chemical interactions within the environment are critical for the correct function of living organisms. Several ongoing studies on the identification of bioavailable Se-species in the environment attempt to define the most appropriate and favorable conditions for human health. Se cycling is mediated by diverse processes: redox reactions, diffusion, adsorption, precipitation or interactions with organic matter [62]. Selenium speciation and mobility in the environment have been identified as the two most important parameters to assess the selenium bioavailability in cultivated soils. Plants and bacteria intake Se as inorganic Se and metabolize selenium into bio-forms that can be incorporated and useful their organism. In humans and animals, Se is reduced and converted into Se(-II) as selenocysteine or selenomethionine.

Diverse processes such as atmospheric, marine, and terrestrial flux perpetually recycle the Se-content in the environment, as described Figures 20 & 21. These selenium fluxes are not equally involved in the Se-cycle: anthropogenic activity is a major source of selenium release, whereas the marine/oceanic system constitutes the main natural pathway. The atmosphere selenium cycling pathway is significant due to the rapidity of aerian transport. However, the terrestrial system remains the most important pathway for animal and human health. All foodstuff production is related to agricultural activities made on soils. Natural selenium is dispersed from rock weathering through the food chain by the mediation of several complex biogeochemical processes. This complex and multifactorial cycle induces a heterogeneous selenium distribution in the soils with a potential for severe concentration variations depending on local conditions [4]. For instance in Europe, several Scandinavian countries are critically deficient in Se, due to lack of Se in rocks constitutive of the Baltic shield.

Selenium is found in the Earth's crust as the 70^{th} most abundant element. This trace element is not equally distributed on the Earth crust surface. Se compounds are widespread over the diverse Earth compartments: atmospheric (air), marine (waters) and obviously terrestrial (rocks, volcanic, and soils). Depending on regions, the selenium concentration in soils and water vary. The selenium concentration is generally low in crystalline rocks ($50 - 200\,\text{g/kg}$). Rocks are the Earth compartments containing the largest amount of selenium. However, selenium is often found in some minerals (e.g. in shales) because of its substitution to sulfur in metallic sulfides and organic matter. Selenium concentration of soil depends on that in the "parent" materials. The world mean soil selenium content

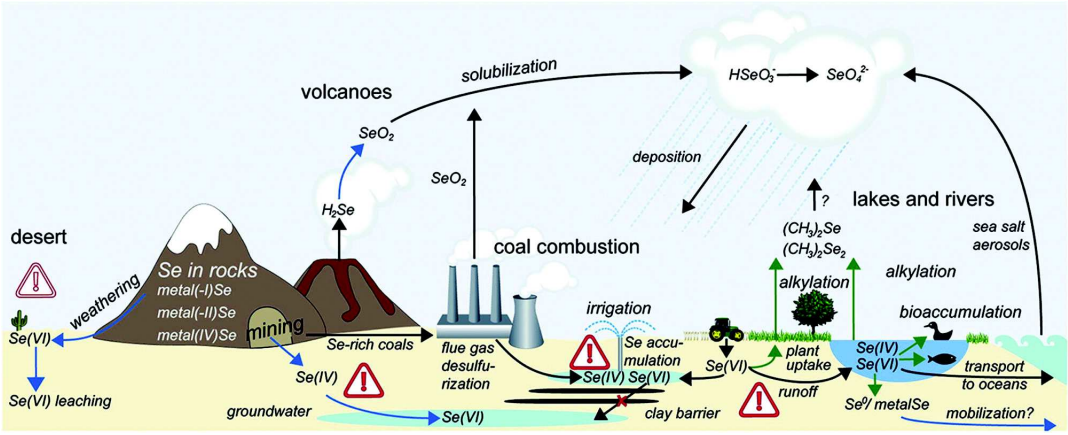

Figure 20: Schematic global cycle of Se with main focus on the terrestrial environment where the blue arrows indicate processes that involve oxidation of Se species and green arrows indicate processes that involve reduction of Se species. Warning symbols indicate specific environmental settings that are at risk of either developing Se deficiency (open warning symbol) or Se excess (shaded warning symbol) from [61]

is about 0.4 mg/kg [4]. Se-repartition in so-called seleniferous soils is correlated to variations of geochemical processes such as leaching or erosion [62] in different parts of the world. Consequently, the Earth is a heterogeneous place where areas presenting toxic, adequate and deficient selenium levels exist side by side [62] e.g. in China [63], India [64], Ireland [65] and USA [66].

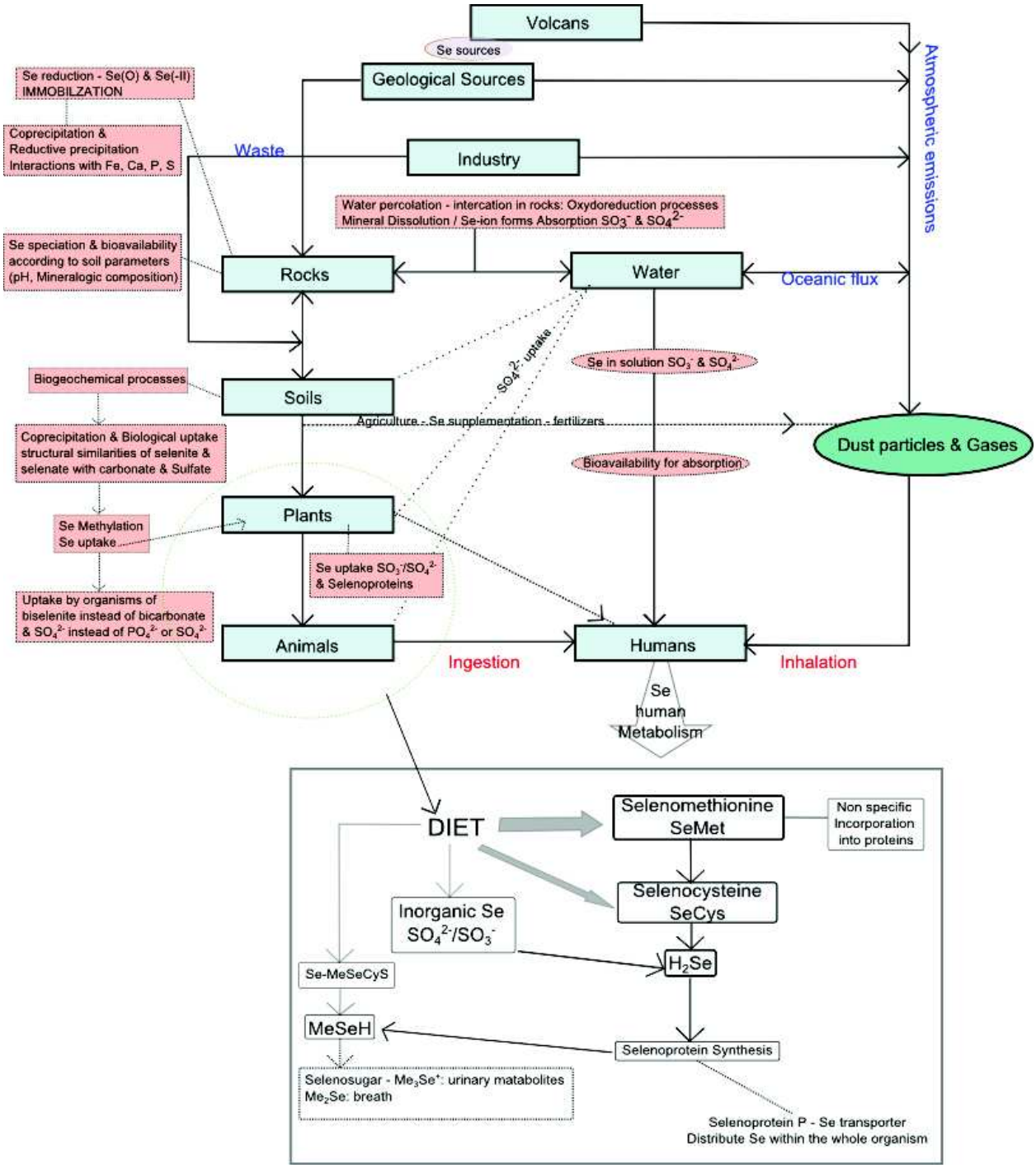

Figure 21: Selenium Cycling pathway from environment to human organism (Fordyce 2007 & Winkey 2013)

Several natural factors influence selenium distribution and bioavailability [61]. Bioavailability and bioaccumulation are two different terms used in bio-geological concepts, both related to bio-storage. Bioavailability establishes the relationship between the concentration and chemical form of an element and its availability to organisms. Bioavailability controls selenium uptake by plants and animals and influence the biochemical functions of selenium within organisms. Contrary to bioavailability, "bioaccessibility expresses the fraction of a substance that becomes soluble within the gut (intestine) or lungs and stay available for absorption through a membrane" [62]. The bioaccessibility of a trace element is related to the factors that make it available to an organism, that is, in a form that can be transported across the organism's biological membrane. However, this concept is not very precise, as a substance can be adsorbed on a colloidal particle small enough to pass through the membrane [67]. Se-bioavailability depends not only on absorption by the intestine but also on conversion to a biologically active form [67].

Both concepts are influenced by diverse physico-chemical factors such as speciation, ionic strength, pH, redox potential, adsorption properties of soils, sediments and aquifer substrates, guts solid materials, and mobility of different species and solubility with respect to membrane [62]. For example, selenite and selenate are selenium soluble inorganic species found in respectively anaerobic and aerobic waters. Selenite is more bioavailable but is 5 to 10 times more toxic than selenate [62].

It is important to understand the mechanisms related to Se-bioavailibility to preserve human health. Selenium balance is organism is fragile, and a perpetual adequate selenium supply is required to efficiently maintain the organism well-function.

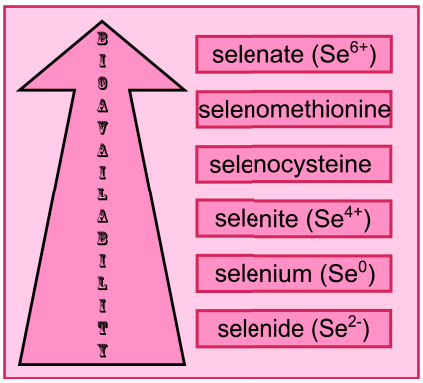

Figure 22: Bioavailability of the diverse selenium forms present in soils

Selenium deficiency (in soils) can result from non-availability of selenium which is bound to soil particles. These soils are usually rich in organic matter. The organic matter contributes to the accumulation of the selenium within the soil but they also generate a selenium immobilization through several diverse processes such as direct adsorption or through redox processes. The most probant example is the reduction of selenate to selenite that would favor the adsorption of the latter onto iron and aluminium oxyhydroxides [62].

6.2 Selenium Forms in Environment and Uptake

Selenium is present in the natural environment in different forms related to different oxidative states: selenate Se(IV), selenite Se(IV), selenium element Se(0), selenide Se(-II) (Table 4). Selenides are involved in the organoselenium composition. The Se-accumulation within soils depends on the climate and soil characteristics. In pore soil or drainage water, selenium concentrations and chemical forms are

controlled by physico-chemical factors. Oxidation states, adsorbing surface, mineralogical composition and pH are the most relevant factors governing the selenium form diversity, allowing the weathering of elemental selenium and/or Se-bearing metals (such as $FeSe_2$) [62]. The conversion of Se oxidation state highly depends of the type of soils: the higher the aridity, the higher is the selenium concentration, and at contrario, hydromorphic soils have very aqueous selenium concentration. Indeed, selenium solubility is largely dependent of its oxidation state. In acidic soils, Se(-II) Se-form (selenide) oxidizes into selenite (form Se(IV)) in presence of an adequate amount of water. This induces a high quantity of selenite SeO_3^{2-} available to plant uptake. However, in alkaline (and dry) soils, Se(-II) is oxidized into selenate. Selenate is the most soluble and mobile form of Se in water and soils, and readily available for plant uptake. Selenite possesses a higher affinity for adsorption to soil particle surface than selenate, but the form is less soluble. This strong affinity to soil particles decreasing their mobilities and consequently reduce their bioavailability. Both Se-species are specific to surface waters but selenate appears to be the most bioavailable form of the dissolved inorganic selenium. Consequently, selenate is generally actively incorporated by plants at a higher rates than selenite which appears to be passively absorbed and has been used, e.g in Finland, as fertilizer. Actually, selenate is less toxic than the selenite [62].

In aqueous phase, selenium is mainly present as SeO_3^-, SeO_4^{2-}, $Se_2O_5^{2-}$ oxianion species. Their formations are controlled by pH and oxidoreduction conditions. In sediments, selenium is present in strongly bond reductive forms. In soils, selenium behavior is influenced by redox conditions, pH, presence of oxides, clays and organic matters, and competitive anions. Selenides of heavy metals and selenium disulfide solids are insoluble, and predominantly present in acid soils or soils rich in organic matter. Sodium and potassium selenites are soluble and selenite ion strongly absorbs on soil minerals and organic matter and is thus present in mineral soils neutral pH and adequate drainage. Selenate ions are mobile since they are highly soluble in water and are weakly absorbed by sediment and alkaline and oxidic soils. The Se-mobility in soil is thus controlled by several processes known as "sorption" of Se to mineral material. Organic matter influences the complexation and the precipitation of selenium, together with other chemicals which also govern Se-mobility. Nevertheless, Se mobility, Se speciation and Se-bioavailability are highly affected by local environments, and more precisely the microorganisms present within soils, rocks, and pore waters. Selenium is often associated with aquatic or terrestrial organic matter (OM). These OM present a large diversity, and this heterogeneity lead to specific and complex properties, such as formation processes. They appear to have an important impact in regards to the bio-geochemical variables defining soils. For example, insoluble selenides and elemental selenium are generally present in organic-rich soils with poor drainage conditions. The bio-geochemical variables influence the mobility of the trace element according to diverse complexation processes. Two processes can induce the selenium incorporation within OM: cation bridging selenium complexation to organic matter and the biotic transformations, see reviews by Fernandez *et al.* 2009 and Fordyce 2005 [4,62]. Organic selenium mainly contain the selenide Se(-II). Selenium can be hosted by some minerals as Se(-II) solid components. Se is also incorporated within solid host structures e.g. gypsum or calcite by isomorphic substitutions.

Selenium is taken up by plants as phosphate substitutes by an enzyme called adenosine triphosphate sulfurylase. This enzyme plays a role in the selenate conversion into a non-toxic form of selenium. Selenium is present in different forms (inorganic/organic), in foods, in organisms and in plants [61-62]. For example, the selenium incorporation in plants follows a substitution process. The most relevant process is substitution of sulfur S by Se which occurs mainly in biological processes [69]. Plants absorb some inorganic selenium from soil. Then, it metabolizes selenium instead of sulfur in order to form the Se amino acid forms. Sulfur and selenium have many physico-chemical similarities. Because of a high stability of selenium within some S-rich biological molecular structures, substitution can

take place, and the sulfur atom is replaced by the selenium atom generating selenomethionine SeMet, selenocysteine SeCys [70-72]. These selenoamino acids undergo the same reactions as those of their sulfur analogues which allow a perfect functionality of the generated polypeptide. Then, this amino acid is incorporated in to the protein instead of the usual S-rich methionine or cysteine, in order to form selenoproteins [4].

7 Biological Expression of Selenium and its Functions

7.1 Selenium Metabolism

Biochemical interconversions involved in the Se-absorption and metabolism of the different Se-species in mammals have been defined but their complete understanding remains not fully understood [69]. Two principal Se-compound groups are present in the body: (i) unregulated selenomethionines and (ii) well-regulated selenocysteines and/or inorganic selenium. This variety of Se-compounds suggests complex underlying metabolism and Se-storage related to the selenium nutritional intake concentration. Each tissue has its own selenium content with regard to Se needs in the tissue function. Selenoproteins contain selenium in the form of the 21st amino acid, selenocysteine (Sec) [79], which is an analog of cysteine with the sulfur-containing side chain replaced by a Se-containing side chain. The regulation of these selenoproteins participates to selenium homeostasis [69].

Pathways of the Se-absorption include: pulmonary, cutaneous, digestive uptakes. The later is the major pathway directly related to food ingestion.

During intracellular metabolism of selenium, oxidation, reduction, methylation, and selenoprotein synthesis processes are involved [73]. Indeed, as selenium (Se) is a nonmetal, it is transformed into Se-containing compounds having carbon–Se covalent bond(s), i.e., selenometabolites, in the metabolic pathway. Especially common are selenides (R_2Se, analogues of thioethers), diselenides (R_2Se_2, analogues of disulfides), and selenols (RSeH, analogues of thiols).

Inorganic forms of Se like selenite exists in drinking water for example. Selenite is metabolized through non-enzymatic reactions that involve glutathione (GSH) or glutathione reductase generating, hydrogen selenide (H_2Se) via selenodiglutathione (GS-Se-SG) and glutathionylselenol intermediates [12,18,74] (Figure 23c). Of note, selenodiglutathione is a substrate more reactive to the thioredoxin system

(Figure 23a).

$$2H^+ + 4GSH + {SeO_3}^{2-} \rightarrow GSSG + GS - Se - SG + 3H_2O$$

This selenodiglutathione acts in the redox cycling as potential antioxidant in the presence of oxygen. Nevertheless, its life-time is very short due to its interaction with glutathione reductase which converted selenodigluthatione back into selenide (organic form) [12, 69, 74](Figure 23b):

$$GS - Se - SG + NADPH \rightarrow GS - Se^- + GSH + NADP*$$

$$GS - Se^- + H_2O \rightarrow Se0 + GSH + OH^-$$

$$GS - Se^- + NADPH + H_2O \rightarrow HSe^- + GSH + NADP^+ + OH^-$$

$$GS - Se^- + GSH \rightarrow HSe^- + GSSG$$

$$HSe^-(O) \rightarrow Se^0 + OH^-$$

$$HSe^- + (O) + 2GSH \rightarrow HSe^- + GSSG + H_2O$$

This reductive reaction mainly occurs in intestinal cells (Figure 23i) or in red blood cells. At this stage, it appears that first selenomethionine and selenate are better absorbed than selenite or selenocysteine, but all these interaction and metabolism pathways remain yet misunderstood [12,69]. Unlike other essential trace elements, such as copper, iron or zinc, selenium is introduced into selenoproteins directly at the stage of polypeptide chain biosynthesis and not after the protein is already built. To incorporate the selenium during the protein synthesis, each selenoprotein mRNA must contain two specific mRNA elements: a UGA codon and a unique SECIS (SElenoCysteine Insertion Structure) element [12,73]. This selenium can also then be reduced non-enzymatically to selenide by glutathione or other thiols. Synthesis of selenocysteines can be initiated from selenide with the formation of selenophosphate ($HSePO_3^{2-}$). active Se-compound used in the synthesis of selenoproteins [12,73]. This reaction is catalyzed by selenophosphate synthetase using ATP (Adenosine TriPhosphate). As intracellular Se-metabolism is correlated to its affinity with other mineral nutriments by inducing covalent bonds carbon-selenium [12,69], amino acid serine is used as carbon skeleton for selenocysteine synthesis. Serine is then esterified to the 3´ terminal adenosine of $\mathrm{tRNA}^{Sec}_{UCA}$ to form $\mathrm{tRNA}^{[Ser]Sec}_{UCA}$ catalyzed by seryl-tRNA synthases [12,73] replaces the serine-OH with -SeH from selenophosphate to form selenocysteine-$\mathrm{tRNA}^{Sec}_{UCA}$ [12,73].The selenocysteine synthase (SeCysS) exchanges the phophate group with activated SePhp (Figure 23k) to selenocysteyl-$\mathrm{tRNA}^{[Ser]Sec}$. The $\mathrm{tRNA}^{[Ser]Sec}$ reads the UGA codon, needed for synthesis is generally encoded in the ribosome-mediated system and is used for the integration of selenocysteine (SeCys) into the amino acidic sequence to form selenoproteins (Figure 23l). Selenate is also absorbed by passive diffusional process[12,75] and is reduced to selenite (Figure 23d) via nondefined process similar to ATP-sulfurylase (Se-PAPS, Se-isologue of 3-phosphoadenosine 5-phosphosulfate). The Se-amino acids selenomethionine (SeMet) and selenocysteine (SeCys) are absorbed. Selenomethionine can be incorporated non-specifically into proteins (Figure 23e) or it can be also transformed into selenocysteine (Figure 23f) possibility to be reconverted into selenide (Figure 23g) [12,74]. Finally, several specific selenoproteins are involved in selenum transport and their antioxidant action such as the plasmatic selenoprotein P (SeP-P) (Figure 23) [12, 69].

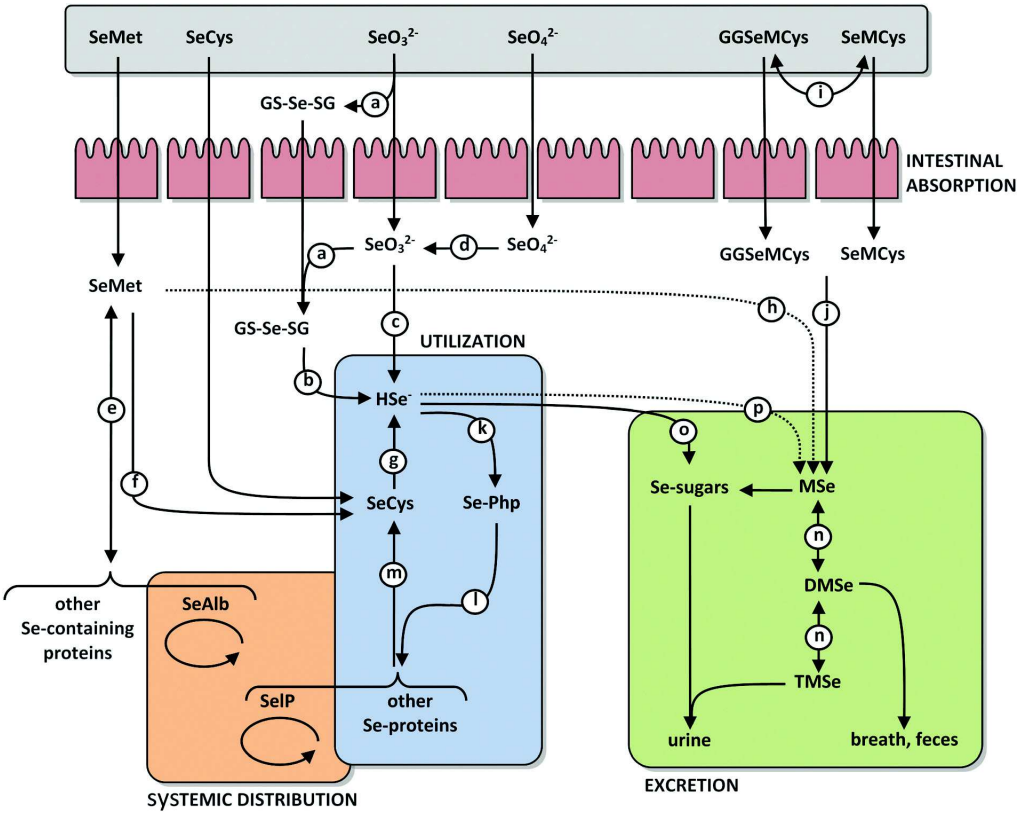

Figure 23: General overview of Se-metabolic pathways, figure extracted from the paper of Roman *et al.* 2014 [12]

7.2 Selenoprotein Functions: Antioxydant & Anti-inflammatory Actions

Selenium is an essential trace element, acting in biology, present in humans, animals and some micro-organisms [76-77] under the form of selenoproteins. This element confers unique activities to selenoenzymes [78]. Its beneficial role in human health is mainly related to antioxidant and anti-inflammatory actions. Selenocysteine (Sec or SeCys) is the 21^{st} amino acid used for protein synthesis in human organism. The residual SeCys contained in the active site of the protein polypeptide chain provides biochemical properties of selenoproteins, increasing their catalytic efficiency. Two groups of selenoproteins can be distinguished: a first group with a selenocysteine SeCys in the C-terminal, called thioredoxin reductases and a second one where the SeCys is located in the N-terminal of the protein. Contrary to the other 20 amino acids present in proteins, Sec is used only when it is required for a special protein function, mainly redox catalysis. Nowadays, twenty-five selenoproteins have been discovered in the human proteome. Some biological functions and utilities of these selenoproteins have been identified but a major part of their biochemical functions remains unclear or even unknown. Selenoproteins present some specificity providing biomarkers for disease detection such as diabetes or cancer and maybe cartilage degradation (osteoarthritis). Se (especially selenoproteins) appears to be also involved in the biosynthesis of diverse components which are required to cell functions such as deoxyrobonucleoside triphosphates (dNTPs) for DNA, in the reduction of some oxidized proteins and/or membranes and also in diverse regulation mechanisms (redox, apoptosis, immunomodulation, thyroid hormones...). They also take place in every day maintenance of the cellular life by storing the selenium and control the protein folding [12]. The selenoproteins are very sensitive to the overall intake of selenium received by the organisms. Each tissue takes its own part of Se, in a Se-needs

hierarchy in which some of them have the priority. The hierarchy is established according to the selenium necessity for biological functions.

Selenium major task is to contribute to the complex immune system defense in order to prevent and defend the organism against diverse injuries. Reactive Oxygen Species (ROS) generation is one of these [12]. The ROS are chemical reactive molecules containing oxygen and are generally produced as byproducts of the normal metabolism of oxygen. They contribute to the cell signaling and regulation of redox homeostasis[8]. Nevertheless, these free radicals are highly chemically reactive because of their unpaired valence electrons. They are overproduced in stress periods which can induce cellular structural damages through diverse interactions. They can take the place of other molecules generating a dysfunction or block the anchoring/receptional site of some proteins. Combination of C- and E-vitamins, β-caroten to selenoproteins allows an enhanced control of these ROS and a protection of the cell function via the glutathione peroxidase (GPx) activity. The metalloenzyme GPx as the superoxide dismutase plays a role in the regulation of ROS production. GPx catalyzes the hydrogen peroxide (H_2O_2) reduction by two molecules of glutathione. The iodothyronine deiodinases (DIOs) actively participate to the thyroid hormone metabolism and selenophosphate synthetases 2 (SPS2) contribute to the selenoprotein biosynthesis.

Every Se concentration variation within the body influences the Se-protein activity. Organisms are very sensitive to the overall selenium intake: every tissue needs a specific Se-concentration to support its biological function. For example selenium is particularly well maintained in brain even upon prolonged dietary selenium deficiency. Furthermore, selenium can play a role of protector against toxic heavy metals and metalloids by the way of interactions: direct sequestration of toxicant or migration via metal-induced oxidative stress. Small Se-proteins can bind to the metal and the selenium action could decrease the bioaccumulation of some metals. Damages are limited by selenium antioxidant action on the cells. Selenium is also involved in radioprotection effect [80].

7.2.1 Thioredoxin Reductase

Thioredoxin reductases TrxRs contain selenocysteine enzyme and possess three isoforms: a cytosolic TrxR1, a mitochondrial TrxR2 and a thioredoxin glutathione reductase TGR-TrxR3. These TrxRs are involved in the reduction of oxidized thioredoxins Trxs helping to bind some redoxactive peptides in DNA. They are able to catalyze NADPH and then contribute to the regulation and metabolic activities. Mammalian thioredoxin Trxs acts as cell growth factors and help in the apoptosis inhibition. They appear to have an essential role for maintenance of ascorbate levels, preventing oxidative aggressions. TrxRs present a large variety of essential biological functions. TrxR1 and TrxR2 are known to be involved in embryogenesis. TrxR2 function is linked to the protection from mitochondrial-mediated oxidative stress and apoptosis during embryogenesis. TrxR3 is a testis-specific glutathione/thioredoxin reductase that is expressed in maturing spermatids and implicated in the disulfide bonds formation during sperm maturation. TrxR proteins seems to help in cellular proliferation [4, 12, 73, 79] and it have demonstrated TRXR to be a potential novel molecular target for anticancer therapy, indeed, the chemical or genetic inhibition of thioredoxin results in cell cycle arrest [287]

7.2.2 Glutathione Peroxidase

"GPx gene is one of the first and the most important antioxidant enzymes in human, and the few proteins known in higher vertebrates to contain selenocysteine" [81].

Glutathione peroxidase (GPx) family includes a group of enzymes involved in organism protection against oxidative damage by reducing lipo hydroperoxides and hydrogen peroxide [82-83]. GPxs family

[8]Homeostasis: abitily for any system to preserve its stability in regard to the divers external forces applied on it.

is composed of eight isoforms, all having antioxidant functions. Hydrogen peroxide (H_2O_2) and lipid hydroperoxides belongs to the ROS (Reactive Oxygen Species) which induce chemical reactions that results in alteration of the matrix protein components. GPx1 is found in diverse chondrocyte compartments (cytosol and mitochondria), and are used to remove intracellular H_2O_2 from many tissues and cells to prevent oxidative damage, and the formation of other deleterious reactive oxygen species such as hydroxyl radical [84].This enzyme also participates to cellular processes (cytokine signaling and apoptosis) modulated by hydroperoxides. It is highly sensitive to Se-status changes and oxidative stress conditions while the demand for global protein synthesis decreases under the aforementioned conditions. GPx3 is the only extracellular enzyme of this family. Found in heart and thyroid gland, these enzymes act as a local source of extracellular antioxidant capacity. Nevertheless, several other chemical components such as thiols and more precisely thioredoxin can be taken as electron donor (oxidant) in order to support and pursue also the antioxidant action. GPx4 is an intracellular enzyme present in the cell cytosol, nucleus, and in mitochondrial. It also plays a major role of antioxidant defense during cellular differentiation in embryonic development and protects photoreceptor cells against oxidative stress. The four other GPx possess specific function which remain unknown [4, 12, 73, 79].

7.2.3 Selenoprotein P

Selenoprotein P (SeP-P) is the only known eukaryotic selenoprotein that contains multiple selenocysteine (Sec) residues. It is a secreted glycoprotein, often found in the plasma. Its major biochemical activity functions remain still unclear. It has been reported that it acts as an antioxidant to protect cellular membranes, involved in Se-transport within the whole body via the plasma circulation. It is also expressed in several tissues, associated with cell membrane. SeP-P may be a mediator of Se distribution regulation within the whole body. SeP-P regulates selenium homeostasis and oxidant defense against injuries, acting in concert with the gluthatione peroxidases which are less performant [4, 12, 73, 79]. Furthermore, SePP is also involved in the constant and hierarchical Se-supply of essential tissue like brain or endocrine organs to preserve the safeguarding vital Se-dependent processes during Se-deficiency conditions for example [85].

7.2.4 Iodothyronine Deiodionases (DIOs)

Iodothyronine deiodionases family is composed of three integral membrane proteins. DIO1, DIO2 and DIO3 have different locations. DIO1 and DIO3 are found in the plasma membranes contrary to DIO2 where it is mainly located in the ER (Endoplasmic Reticulum) membranes. They are all three oxido-reductases with the SeCys residue present in their active sites in order to contribute in the thyroid hormone metabolism. The DIO1 and DIO2 will activate diverse thyroid hormones such as tetraiodothyroxine called T4, triiodothyronine T3 and reverse-triiodothyronine rT3. These hormones regulate thermogenesis, homeostasis-related processes allowing the development of diverse organs such as brain. Precise and complete functions of these three isoforms are not yet really established and not well-understood. Actually, studies have reported that (i) DIO1 is more expressed in the liver, kidney, thyroid and pituitary gland, (ii) DIO2 is mainly located in the thyroid, the central nervous system and pituitary gland and the skeleton muscles, (iii) DIO3 can be considered as particular because it is mostly present in the embryonic and neonatal tissues [4, 12, 73, 79]. DIO2 appears to be involved in the Se-deficient-related diseases.

8 Possible Impact and Influence of the Selenium on Articular Cartilage Integrity

8.1 Geological Environment and Health: Selenium Deficiency Soils

Selenium spatial distribution in the terrestrial environment remains globally mis-understood at large geographical scales because no fixed pattern is observed in a systematic study. However, to explain why some soils are Se-deficient, major geological processes such as loess and bedrocks are hypothesized as the main reasons.

Food is the most important source of Se to humans [4]. The largely heterogeneous distribution of the selenium content in the diverse soils (terrestrial environment or agriculture) induces a highly variable Se intake worldwide [86-90]. It has been evaluated that 0.5 and 1 billion people can be affected by low Se intake [61]. This promotes then the Se deficiency as one of the major health problem in our society [91]. This can perfectly be illustrated by the China example. Actually, a Se-poor region, also called the Se-deficient crescent belt, in Central China is an area with an extremely low soil-Se concentrations. This has been correlated to the low Se intake generating a high prevalence to specific diseases such as Kashin–Beck disease, a chronic bone and cartilage disease, and Keshan Disease, a chronic heart disease, both of which primarily affect young children and women of child-bearing age [2, 93, 94].

As everywhere in the world, the primary source of Se in soils are generally provided by the underlying bedrock geology has traditionally been viewed as the primary source of Se in soils [95]. However, in China, this factor alone cannot explain the diverse and heterogeneous large-scale distribution of Se with localized areas of high soil-Se concentrations, where weathering of carbonaceous black shales has led to very high soil-Se. Se-depleted environments underlying processes remains elusive. Actually, several studies [96] refer to the action of the climatic factors in the Se distribution in loess–paleosol sequences in the Chinese Loess Plateau (CLP), correlating with a severely Se-depleted region. Blazina *et al.* [97] have suggest that atmospheric Se inputs via precipitation could also play an important role in regions worldwide, e.g. East Asian monsoon-derived precipitation in China. However, the Se-soil deficiency and the bioavailability remains to be clarified, the accumulation of Se in edible part of plants being highly dependent on Se level in soils [91, 98]. Sun *et al.* [91] declare that Se spatial distribution in continental soils understanding is required to better define its biogeochemical cycling and improve Se transfer into diets. It has been hypothesized that both deposition and volatilization mediated by microorganisms of Se could play a key role in Se balance in other terrestrial environments worldwide, remaining to be correlated to the climatical precipitation factor. Nevertheless, in China, the Se-deficient soil explanation is not obvious and further studies have to been performed to completely characterize this phenomenon.

8.2 Selenium Implication in Diseases

Selenium has a very subtle balance where excess or deficiency can lead to diseases. In a Se-excess state, the body is not able to eliminate it and according to the exposure types (inhalation, oral) diverse intoxications, irritations and chronic poisoning fatal effects can occur. All the organs can be affected (nose, lungs, trachae, stomach...). Several symptoms are known: stomach pain, headaches, pulmonary problems (irritation, edema, spams, asphyxia), nausea, vomiting, diarrhea, tachycardia and irritability. Physical changes appear as hair and nail loss, skin and teeth degradation, nervous system degeneration [4].

However, Se- deficiency has an impact on the risk of developing diseases such as cancers, dia-

betes, cardiovascular and immune system disorders [4, 12, 67, 69, 99, 101]. This impact seems to be mainly mediated by selenoproteins. Indeed, the biological effects of Se are mainly exerted through its incorporation into selenoproteins, and selenoproteins are involved in the activation, proliferation, and differentiation of cells. For example, it is known that serum-free media, especially for immune cells and neurons, contain insulin, transferrin, and sodium selenite. Without selenium, these cells can neither proliferate nor survive. Se deficiency has been shown to increase oxidative stress [113]. Two endemic diseases are related to a severe selenium deficiency. They are diffused in Se-poor soil regions in China and Russia. They are called Keshan and Kashin-Beck diseases [4]. In KBD, it has been often assumed to be linked to a possible selenoprotein gene polymorphism but no definitive evidence has been presented. At present, it is mostly suggested that Se-deficiency possibly combined with other deficiencies and environmental factors such as toxins, fungi, and contribute to the development of disease such as KBD. The KBD is related to OA and in both diseases chondrocytes produce lower type II collagen levels. Chondrocytes in diseased tissue also show an unbalance in the production of type I collagen which is usually produced by dedifferentiated cells (discussed latter). Keshan disease is a congestive cardiomyopathy (muscular disorder) caused by a combination of dietary deficiency (including selenium) and by the presence of a mutated form of coxsackievirus. It is considered to be fatal. This disease is mainly localized in China, in the Keshan region, where the soil is very poor in selenium. Approximately 10 millions of people are suffering from these 2 diseases, the majority being children (2-10 years-old) and women [4]. This strong association between low Se in soil and disease was observed. It was found that food supplements containing sodium selenite or selenomethionine could inhibit disease manifestation or reduce symptoms caused by the disease [100]. Selenium supplements can be used to balance deficiency in order to restore the antioxidant activity of selenoproteins and consequently, its protective effects on health and wellbeing. Selenium is recently assumed to be an active preventive agent against several cancer types, using its antioxidant action. Se present a strong ability to reduce carcinogen induced and spontaneous cancer incidence. Oxidative stress appears to be actively involved in carcinogenesis. Reactive oxygen species can induce DNA damage leading to potential genes dysfunctions involved in the genesis of cancer, by generating and maintaining the oncogenic phenotypes [4]. Selenoproteins can be a further cure mediator using their genetic polymorphisms, regulating the loss of antioxidant enzyme functions. GPxs has for example a huge potential in the study of cancer therapy [101].

8.3 Selenium Implication in Bone Health

The selenium present in the bone is exclusively correlated to the organic matrix and not the mineral part [85]. An interesting relationship between bone and selenium has been established in the literature. Certain selenoproteins such as GPx1, TrxR1, DIO2 [102] and SePP [85] appear to be essential to maintain bone health principally to regulate bone homeostasis and protect from bone degradation [103]. They would support an antioxidative and anti-inflammatory functions to maintain and regulate cell redox balance, proliferation and differentiation in the bone microenvironment [104] and remodeling [105]. Using an animal models (rat and mice), it was observed that Se deficiency contributes to induce a growth retardation [106,107] and bone metabolism variations [107-108] such as a low bone mineral density which can negatively disturb the bone microstructure [108]. An *in vitro* experiment confirms that selenium has an influence on osteoblast differentiation related to the tissue resorption by regulating the oxidative stress appearing in the bone [108-109]. All the underlying molecular process on bone metabolism remains misunderstood. Actually, another study presents that subtle Se-status variation can affect bone mineral density (BMD) [110]. The transport of the selenium to bone is

mediated by the plasma selenoprotein P (SePP) [103,111] and appears to be also related to BMD and bone homeostasis [111] influencing osteoblasts and osteoclast metabolisms [103]. SePP acts as a receptor-mediated uptake and permits to safeguard the adequate required bone Se supply [85].

Selenium also acts in diseases such as Kashin-Beck disease (KBD) which is an endemic Se-dependent severe osteoarthritis related to joint development. In KBD, Se-deficiency induces changes in bone physiology [85]. Animal studies placed in similar conditions that KBD patient expressed growth defects and impaired mineralization [106-112]. Actually, KBD disease is a joint disease, consequently the cartilage is also affected, and it has been reported that in mature chondrocytes of the growth plate and articular cartilage, chondronecrosis appears resulting in impaired endochondral ossification and skeletal development. Endochondral bone formation is responsible for most longitudinal bone growth and during this process, chondrocytes in the growth plate undergo a process of maturation and terminal differentiation precisely regulated by signaling molecules. Any disturbances in this complicated regulation system could lead to shortened, or even deformed bones. Studies, investigated on the KBD pathology, established that a strong correlation exists between low selenium and low iodine status. DIO2, related to thyroid hormone linked to iodine expression, appears as a potential mediator which can influence cartilage lesions [102], affect mineralization and bone quality [114] and can be indirectly related to growth retardation and delayed bone maturation in children [103]. Further studies have also demonstrated that a suppression of the Trsp gene encoding tRN $A_{UCA}^{[Ser]Sec}$, required for Sec-incorporation into selenoproteins, from skeletal progenitor cells modify skeletal development [115].

Most of the selenoproteins are expressed in bone. This highlight the importance of the preservation of selenoproteins in bone which is required to protect and promote a normal skeletal development [103]. Se-cellular activities appear to be vital for bone (and cartilage) development. A potential nutritional Se-supplementation could be an interesting solution to prevent and preserve bones and cartilages to several joint diseases [104].

8.4 Selenium Implication in Joint Diseases

8.4.1 Kashin-Beck Disease - Big Joint Disease

Kashin-Beck disease (KBD) is one of the disabling polyarticular degenerative joint disease largely endemic in some remote regions of the world. The disease is prevalent in a crescent shaped region that extends through Tibet, northern China, Mongolia, Siberia, and North Korea. In China, hundreds of millions people live in the oblique median geographic area running from the northeast to the southwest of China where there are Se-deficient soils, and at least 645,000 people seemed to be affected according to the Statistical Center of Ministry of Health (P.R. China 2012) [116]. The aetiology of KBD remains controversial. Several dominant hypotheses postulated a combination of diverse environmental factors leading to a predisposition for this disease. In Chinese soils, a temperate and humid environment has been associated with low Se levels, resulting in a specific area of reduced levels occurring from north-east to south-west. A geographical correlation between areas of low Se status and the occurrence of endemic areas (KBD) was first noticed in the 1970s, and recently several studies have established precise maps to better exposed this strong link (Figure 24). In addition, no reports of the disease have been recorded in areas of Se rich soils [117] . The hypothesis relying to this correlation comes from low Se soil levels results in reduced Se concentrations present in food grains, vegetables and drinking water, therefore causing a Se deficient diet [93]. This is directly in correlation to the Se content found in the hair and blood of individuals suffering from KBD around the endemic areas [118]. It has been calculated that the average Se intake in the affected areas was around 3-5μg/day compared to

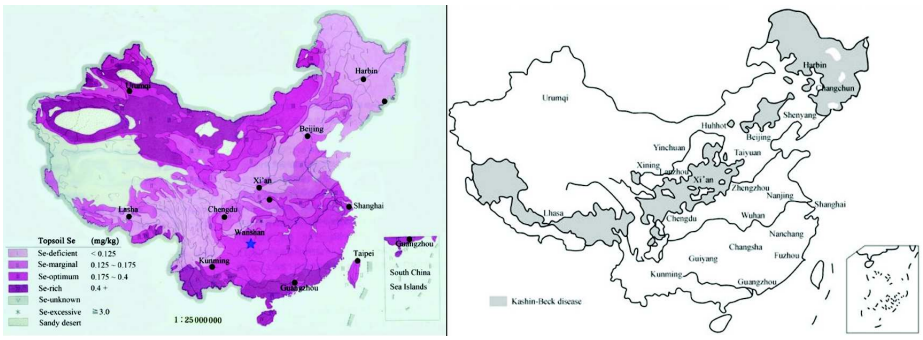

Figure 24: Geological and epidermiological correlations exposed a strong link between selenium deficient soil and the distribution of kashin-Beck disease in China. (Left) Map of the distribution of selenium in soils of China from the paper of Zhang *et al.* 2014 [291], the light purple area refers to the Se-deficient soil and (Right) Map of the Kashin-Beck Disease distribution (in grey) in China from the paper of Li *et al.* 2009 [292].

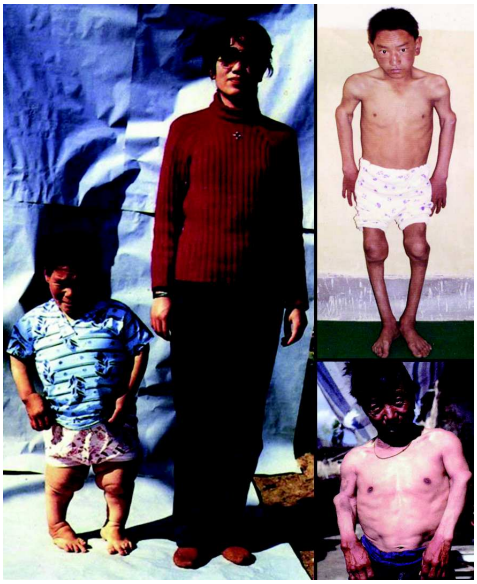

Figure 25: Kashin-Beck Disease patients suffering from the most severe pathologies: deformities, dwarfism - source-tan2004-Stone2009

approximately 10-11μg/day in non-affected regions [96] . Selenium and iodine deficiencies, a cereal fungal contamination of barley (the staple grain) and high organic matter (humic and fulvic acid) levels in drinking water are often presented as the combined factors inducting the Kashin-Beck disease. These multifactors create an environment in which mycotoxins can easily enter the rural food supply from the contaminated storage grains, and favour the disease development. The precise proportion and the importance of each factor remain still subject to debate. Nevertheless, it is important to note that some unaffected individuals are living within endemic areas and are also exposed to a Se deficient diet [119]. Consequently, additional aetiological factors are important in the onset and pathological development of KBD such as genetical factors. Several studies showed that a Se-feed supplementation seems to attenuate the symptoms of the disease, although no long-term studies present an obvious cure and/or preventive treatments.

This disease affects particularly the children and adolescents because it affects bone growth and joint cartilage during the growth and maturation phases. For these patients, the breakdown of the articular cartilage starts in an early phase development, around 2-3 years old. The clinical symptoms are mainly diarthrodal joint deformation leading to joint stiffness and consequently a limited and

painful motion. Dwarfism and deformities can be considered as symptoms because they are found in the worst forms of KBD(Figure 25). KBD is a constant progressive disease occurring in stages starting with stiffness and swelling of finger and wrist joints in young persons, later inducing an osteoarthritis affecting all the joint globally with a prevalence for the elbows, knees and ankles [120]. The KBD can be qualified as chronic endemic osteoarthropathy, and often associated with an extremely severe degenerative secondary form of OA. Recent studies have shown the similarities as well as the differences of KBD in regard to OA and other degenerative joint diseases using tissue and serum from children and adults suffering from KBD [121]. Histological staining on articular cartilage sections obtained from KBD patients showed cellular necrosis, decreased proteoglycan content and surface fibrillation similar to different stages seen in many degenerative joint disease conditions [122]. Cellular necrosis in many degenerative joint diseases (mainly OA) occur in patches above the subchondral bone with a progressive degeneration from the surface to the deeper zones. In contrast, in KBD patient articular cartilage sections necrotic cells are present throughout all morphological cartilage zones [123]. The alteration (up-regulation) in CD44 (related to cell-matrix interaction and proteoglycan retention around chondrocytes) expression is observed in KBD and OA, and could be hypothesised to an indication of increased matrix metabolism in the joint diseases [124]. Many proteolytic enzymes (aggrecanases) appear to be involved in cartilage extracellular matrix degradation, and aggrecanase-mediated aggrecan degeneration occur during osteoarthritis as well as in KBD [122,125, 280]. KBD exposes lesions in osteochondral tissue in the epiphysis and articular cartilage at the ends of long bones [126]. During normal endochondral ossification, the growth plate is the center of bone development and growth where the ECM synthesis, hypertrophy, matrix mineralization and vascular invasion leading to apoptosis. Thus, when the growth plate is active, there is progressive replacement of chondrocytes with bone cells (osteocytes, osteoblasts and osteoclasts) [127] . Therefore, KBD is hypothesized to be linked to impairments of growth processes that result in articular and epiphyseal cartilage atrophy and chondronecrosis [126], leading to the degeneration of growth plate and articular cartilage, mainly in the deeper zones. Compared to normal healthy tissue, necrotic lesions are observed in KBD affected individuals and are predominantly located in the deep zones of articular cartilage close to the subchrondral bone and bone marrow. At these locations, chondrocytes start dying and undergo degenerative changes directly impacting all the tissue organisation. First, there is a loss of membrane organelles, swelling of mitochondria and endoplasmic reticulum that leads to the generation of nuclear deterioration with the remaining cells called cell ghosts. Secondly, amongst these necrotic regions, a loss of collagen fibrils and proteoglycans within the ECM appears. The surviving chondrocytes adjacent to the necrotic regions pursue their proliferation and form cell clusters with a high content of GAG in the ECM surrounding these clusters [128]. However, this induces a global deregulation and degradation of the extracellular matrix leading to a PG metabolism disruption, PG content loss and an activation of the matrix metalloproteinases (MMPs) in the whole tissue. The mis-functioning of the chondrocytes also provokes a cartilage surface fibrillation. Furthermore, another cause has been suggested: the vascular penetration reduction. Actually, diverse related processes start to propagate within the cartilaginous tissue such as tissue resorption, remodeling, dystrophic calcification and ossification. Epiphyseal impairment can generate developmental disturbance causing limb reductions and dwarfism. Pathological disturbance in AC may progresses slowly with severe secondary OA with osteophyte formation. Several histological studies have investigated the hands of young KBD patients where it have been shown a deficit of blood vessel penetration into the epiphyseal end plates. Vascularisation is an extremely important step in normal endochondral ossification and this apparent lack of vascularisation can been hypothesized as an initiator of KBD in some patients. This deficiency in vascularization can be related to a blood vessel vasoconstriction in peripheral joints [128] and this can be induced by poor thyroid response to the cold and linked to an iodine and selenium deficiency

Mycotoxins can also have an impact on vasoconstriction and on epiphyseal ossification [129].

It is thought that the effect of selenium deficiency (linked to a iodine deficiency) has several consequences in the biological initiation and progression of KB disease [130-132]. Some studies have found that genetic factors can be involved in the development and the progression of KBD disease. The gluthatione peroxidase 1 (GPX1) seems particularly relevant to be a potential genetic factor. This gene produces a protein that provides protection against oxidising agents, and different versions of this gene can have an impact on the usual metabolism of the iodine and the selenium. Other genes seem also important such as the thioredoxin redactase 1 (TRX1) and the type II iodothyronine deiodinase (DIO2) through their role as selenoproteins. Selenium is also incorporated into other proteins, such as phospholipid hydroperoxide, selenoprotein P (SePP), which all have important human health functions [93] such as in bones [85]. The gluthatione peroxidase 1 acts mainly as an antioxidant. It is possible that Se-deficiency can generate a reduction in the enzyme levels resulting in increased oxidative damage (lipid peroxidation/DNA damage) within chondrocytes. Indeed, the selenium deficiency predisposes the chondrocytes to an excess of oxidative stress generated by ROS (reactive oxygen species). Combined with toxins, these deficiencies can cause an excessive source of oxidative stress which could potentially mediate the articular cartilage destruction. Selenium supplementation appears to reduce the symptoms of KBD but this is still a matter of debate. Indeed, the role of selenium in articular cartilage metabolism is still poorly understood [132]. Furthermore, biological studies have been performed on the effect of mycotoxins found in soil fungi and in cereals in KBD prevalent-areas. An analysis of cultured rabbit chondrocytes in the presence or absence of selenium, have shown that a dependence exists between selenium levels and mycotoxin effects. The nivalenol (mycotoxins) reduce the production of proteins such as proteoglycans and induce impaired DNA synthesis. The presence of selenium positively influenced protein content and improved proteoglycan metabolism in cartilage [133]. Further studies have also shown that Se deficient rats have a delay in bone growth and a reduction in bone calcification that directly correlates to abnormal biomechanical properties of the developing bone: lack of strength and higher elasticity [107].

8.4.2 Osteoarthritis

Preliminary studies performed on animals with selenium deficiency have shown that they have irregular bone formation, decreased bone strength, and abnormalities in types I and II collagen in cartilage [134]. As already mentioned above, and low selenium content, amongst other risk factors, is associated with Kashin-Beck Disease which cause joint problems relatively early in life. Based on these observations, a hypothesis has been made on the potential selenium influence to prevent osteoarthritis. In the southeastern United States, low Se-levels have been identified. The Pr. Jordan at North Carolina university developed the Johnston County Osteoarthritis Project in order to investigate the role of selenium in osteoarthritis. The study has been done on the knees of 940 participants suffering of osteoarthritis over 15 years. Preliminary data showed that a selenium deficiency influences the articular cartilage metabolism, particularly when low selenium levels are observed in patients, they were more likely to have knee osteoarthritis [135]. This result also present significative difference according to the gender, the race and the age. It have been found that for every additional tenth of a part per million of selenium in volunteers' bodies, there was between 15 and 20 percent decrease in their risk of knee osteoarthritis. Individuals who had less selenium than normal and healthy standard in their organism faced higher risks of degeneration of cartilage of the knee . It appeared that the lower the Se-level is, the most severe the arthritis was. Consequently, these results are supporting the idea that it may be possible to prevent or delay osteoarthritis of the knees and other joints in some people having selenium deficiency. Selenium may be then suggested as a modifiable environmental factor that could influence

the onset and progression of osteoarthritis . As it was also described in literature of the KDB, some additional potential factors can be involved such as genetic and environmental factors. This part still need to be investigated as said by the Prof. Jordan: *"The next step will be in the laboratory to see how selenium affects cartilage. It might act as a protective antioxidant. Later, we'll want to expand the study with larger samples and see whether selenium supplementation reduces pain or other symptoms."* It is exactly the interest of this project: understand how Se impacts the articular cartilage metabolism, growth and maturation [136-137]. Several studies have reported that deiodinase iodothyronine type 2 (DIO2) gene, encoding for selenoprotein iodothyronine-deiodinase enzyme type 2 (D2), is associated with OA [138]. Actually, D2 promote the local bioactive thyroid hormone T3 necessary to growth plate development [139-140]. It has been observed that the upregulation of this selenoprotein is related to inflammation. Suppression of the selenoprotein DIO2 resulted in strong pro-inflammatory effects with increased expression of inflammatory mediators, IL-1b and COX2, and decreased expression of LXRa suggesting that this may be the upstream target through which the anti-inflammatory effects of DIO2 are mediated. DIO2 is hypothetized to be involved in the modulation of the inflammatory response in chondrocytes due to the observation of the proinflammatory effects (downregulation of LXRa, and upregulation of both IL-1b and COX2 gene expression) in primary human chondrocytes related to the suppression of DIO2 by siRNA knockdown. DIO2 can then exert a protective anti-inflammatory effect in chondrocytes [141]. Deficiency in D2 can be a regulator of the endochondral ossification process [142] and may predispose to the incidence of OA [138]. It has been shown that there is an extensive up-regulation of DIO2 expression in OA cartilage as compared with non-OA cartilage [138]. The DIO2 knock down in *in vitro* chondrocyte culture permits to visualize that a significant up-regulation in the gene expression during chondrogenic differentiation [144] suggested a key role in endochondral ossification [143], having a functional effect on chondrogenesis [144]. In the study of Nagase *et al.* on transgenic rats, selenoprotein DIO2 overexpression tend to increase the risk of articular cartilage destruction [145]. High upregulation of DIO2 expression in osteoarthritic cartilage present changes in the ECM when chondrocytes differentiate, become hypertrophic, tending to OA pathophysiology [55]. DIO2 polymorphism can provoke a DIO2 deficiency and can induces variations of cartilage matrix integrity, chondrocyte viability, and degradation and mineralization of the cartilage matrix, and bone formation [146] with osteophyte formation.

Part IV
Biological Model & Rationale of this PhD Work

This part presents the goal of this study and the rationale to use the selenium enhanced "fast maturation-like" articular cartilage model. All tissue culture protocols will be detailed. The rationale and hypotheses of this project will be defined.

9 Reasons of this Investigation

Up to now, knowledge related to selenium implication in biological processes remains very poor. The main problem lies in the fact that selenium remains an elusive element to study. Many of its biological functions are unclear and misunderstood. An association between selenium and Kashin-Beck disease has been demonstrated and preliminary data shows that articular cartilage metabolism is affected. To further understand the role of selenium in articular cartilage a robust model for cartilage growth and development was required. Observations show that the skeletal defects in Kashin-Beck disease occur peri-pubertally, implicating perturbation of skeletal maturational processes. **The Se-concentration in organisms is extremely restricted, and a validated in vitro cartilage model of maturation and development was used giving us more control over the experimental variables like for example maturation stage of the cartilage or the Se level that effectively reach the AC.** Immature articular cartilage is an interesting template upon which biomechanical and biochemical cues act in adapting the tissue to joint-specific functions through induction of morphological, structural and biomolecular heterogeneity [148]. By using immature articular cartilage from the metacarpophalangeal joint of bovine steers, Khan *et al.* (2011) [16] have used fibroblast growth factor-2 and transforming growth factor β1 to induce precocious (early) maturation of this cartilage [16-17]. Growth factor-induced *in vitro* maturation occurs within 21 days in culture and does not require any biomechanical input. **This *in vitro* maturation model of articular cartilage is useful for two main reasons: first, Kashin-Beck disease often occurs in children that often have severe joints' deformities during development, secondly, and most critically, the accelerated growth in this model allows us to observe changes in days that would take many months in *in vivo* models.** This *in vitro* model of "accelerated maturation" has some limitations, while the matured cartilage possesses the biochemical and biomechanical properties of adult cartilage our model does not possesses fully the mechanical properties of mature cartilage. A potential explanation might be that this model grow in an environment that lacks mechanical stimuli to which cartilage are exposed *in vivo*. Indeed, this is a very important parameter to be investigated when AC are exposed to a selenium deficient environment. However, the *in vitro* growth factor model of maturation provides a useful starting point for the study on the growth and metabolism of articular cartilage during the maturation stage in presence or absence of selenium. It provides an ideal basis to develop osteoarthritic-like model or to study how degenerative processes are induced. This provide a potential tool to study strategies to prevent AC degradation and potentially to find a novel regenerative cure.

Currently, it is not known how to provide therapeutic relief for sufferers of osteoarthritis or even cure this disease or some other related cartilage degenerative disorders such as Kashin-Beck disease. As described previously, Se is a trace element strongly related to the development of the disease. In this maturational model, selenium was present in the serum-free culture medium in the form of sodium

selenite, a component of insulin-transferrin-selenium (ITS; additive reagent in the culture medium). Selenium at quite high concentrations is toxic for cells in culture but selenium supplementation is required primarily for its antioxidant effect. To our knowledge, there is no literature that report the influence of Se on such *in vitro* model of maturation of articular cartilage. However, experiments have been performed on chondrocyte cultures showing that selenium has an impact on cellular metabolism [11]. **Indeed, selenium supplementation is often required in certain cell culture protocols of mammalian cell lines.** In this study, we hypothesised that selenium plays an essential role in articular cartilage metabolism through maintaining proper growth and development, in particular during maturation. We tested this hypothesis by inducing maturation in immature articular cartilage in the absence of selenium in the culture medium. We predicted that articular cartilage explants should show aberrant growth or organisational properties. We analysed cartilage explants in various stages of growth and development using histological, biophysical and biochemical (gene expression) analyses to determine if the proposed hypothesis was true or false.

10 Biological Model Development

10.1 Biological explant Culture

An *in vitro* culture of 4 (or 6)-mm explants excised under sterile conditions from the lateral aspect of the medial condyle of the metacarpophalangeal joints of immature male (7 days-old) bovine calves is used. A thin layer of the subchondral bone is present on the basal aspect of each explant. To induce maturation in cartilage explants, cartilage is grown in serum-free medium (Dulbecco's modified Eagles medium. Insulin-transferrin-selenium (ITS), HEPES buffer, and antibiotic and antimycotics) are supplemented with 100 ng/mL fibroblast growth factor 2 (FGF-2) and 10 ng/mL transforming growth factor β1 (TGFβ1) [16]. The combination of growth factors induces profound morphologic changes in immature articular cartilage, consistent with a highly accelerated maturational response occurring within 21 days. Growth factor stimulation induced apoptosis and resorption from the basal aspect and cellular proliferation in surface chondrocytes [17].

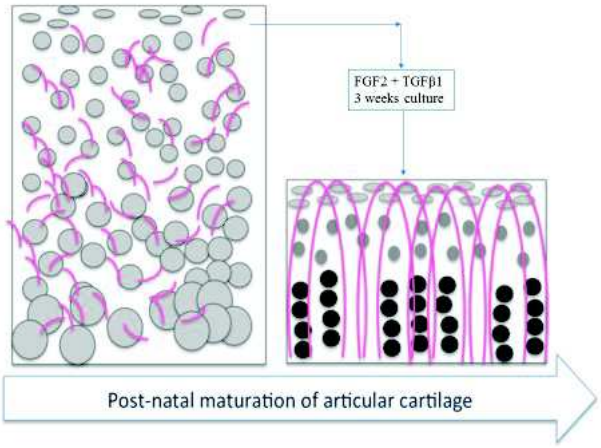

Figure 26: Scheme of Growth Factors Effects on Explants using the Maturation Treatment. *Inspired by my colleague's presentation Ben Morgan*

This maturation-like procedure has been expanded to include the selenium parameter, where selenium importance had not been previously verified. A transposition of the model has been made and the explants were then also treated according to a gradient of Se-concentration in culture medium.

The major sample groups are: (i) culture medium totally depleted in Se (instead of ITS, human transferrin and bovine insulin are used in quantity providing the same concentration of insulin and transferrin that the ITS) called "NoSe" culture, (ii) medium with ITS (usual protocol described in the patent where 6.7 ng/ml of sodium selenite are present the solution) called "ITS", and (iii) medium with a Se-supplementation provided by a 50 ng/ml sodium selenite solution added to the usual procedure and called "Se-Supplemented" culture. For each group, explants are then placed in two sets: one control and another called "FT-treated" where explants are treated with the growth factors cocktail given previously (Table 5). All the conditions provide a pool of 6 sample types. Each pool is provided by the same foot in order to have a perfect comparison among samples. This sample panel will allow to evaluate impact of selenium during growth, maturation processes and consequently it could allow us to assess Se-influence on the cellular metabolism.

"Se-supplemented" groups did not present significant differences with the "ITS" groups. Consequently, the following part will be mainly focused on the comparison observed between the "NoSe" group and the "ITS" group.

Of note the "fast-maturation" occurs within 21 days culture period only. For longer culture period, explant plugs start to degrade with change in cellular metabolism and cartilage ECM components (i.e. collagens and proteoglycans) contents [149]. Still, in the limit of 21 days, the tissue is stable and the complex remodeling dynamics of the model can be assessed.

10.2 Explants Culture Treatments

In the present investigation of the role of selenium in the metabolism and structuration of immature articular cartilage, a static "accelerated" model has been used for three major AC sample groups with their control and their FT-treated sub-groups. Table 5 provides details on the different treatments. The ITS-group will be our general control group. The treatment has been characterised and published [16-17]. It has been confirmed that this "static accelerated" model presents high similarities with mature articular cartilage. The NoSe-group will be used to determine the Se-depletion effect on the AC matrix.

Samples	Transferrin	Insulin	ITS	Sodium Selenite	TGFB1	FGF2
No Selenium Control	yes	yes	no	no	no	no
No Selenium FT-treated	yes	yes	no	no	yes	yes
ITS Control	no	no	yes	no	no	no
ITS FT-treated	no	no	yes	no	yes	yes
Se-Supplemented Control	no	no	yes	yes	no	no
Se-Supplemented FT-treated	no	no	yes	yes	yes	yes

Table 5: Treatment applied on articular cartilage explants

10.3 Reagents Importance

The DMEM-F12 with L- glutamine is an artificial medium which, once combined with insulin, transferrin (or Insulin-Transferrin-Selenium), ascorbic acid, gentamicin, and HEPES provides a complete medium supplementation and all physiological growth requirements specific to different cell lines and explants cultures. The DMEM-F12 is composed of several diverse inorganic salts (ie.

NaCl, KCl, $CaCl_2$, $MgCl_2$, NaH_2PO_4), glucose, amino acids (nitrogen sources), vitamins, cofactors and water. These are necessary to provide adequate energetic imputs and to sustain a cellular survival and well-function in culture. The mineral ions contribute to maintain the osmolarity close to natural physiological environment. As checked by colored indicators (here, phenol red) and CO_2/HCO_3^- buffer combined with phosphates, the pH is maintained constant at a value close to 7.4.

HEPES is used as buffer due to its similarities with water to better preserve enzymatic structure under temperation variations. It also presents an ability to maintain physiological pH in culture conditions. Actually, the cellular activity (mainly respiration) produces carbon dioxide which can lead to cellular asphyxia. The gentamicin is an antibiotic required to better protect and prevent the cells or explants from any external contamination (microbiological organisms, bacteria). Ascorbic acid is used as medium complement for its important water soluble anti-oxidant action[9]. It appears that ascorbic acid can help the articular cartilage explant metabolism at transcriptional level and post-transcriptional level by enhancing the synthesis of collagen and it could be a controlling factor of the matrix gene activity. The transferrin is used as extracellular antioxidant (toxicity and ROS reductions) [150]. It is also applied on culture medium for its ability to provide and facilitate extracellular iron storage and transport in cell culture. Transferrin binds iron so tightly under physiological conditions that virtually no free iron exists to catalyze the production of free radicals[10]. The insulin hormone is used to help the absorption of several elements such as glucose, amino acids. It is also involved in several processes such as intracelluar transport, lipogenesis, protein and nucleic acid syntheses. It can be visualised as an additional growth factor due to the growth-promoting effect mediation by insulin receptor and can also be interesting for anabolic metabolism balance during cell growth and tissue formation boosting the secondary mitogene effect. Selenium is present additionally in the composite solution "insulin-transferrin-selenium" - ITS - under the sodium selenite form. It is mainly used as a cofactor for (seleno-)proteins such gluthatione peroxidase (GPX), as supplementary antioxydant agent in the culture. In *in vitro* auricular chondrocytes, ITS seems to enhance cellular proliferation and phenotype preservation by inhibiting the gene related to cellular dedifferentiation and hypertrophic differentiation. [151]. Growth factors (fibroblast growth factor 2 (FGF-2) and transforming growth factorβ1 TGFβ1) are added to fresh medium . They are used as booster and regulator in cell differentiation, proliferation, growth, healing, and development [16-17]. FGF2 and TGFβ1combination promotes the cell number in the chemically stimulated cultured tissue [152].

10.4 Explant Cultures and Treatments Protocols

10.4.1 Selenium Culture Media

- DMEM/F-12 (1:1) (1X) + GlutaMAXTM-I – Dulbecco's Modified Eagle Medium F-12 Nutriment Mixture (Ham) 500mL – Gibco by life technologiesTM, Ref 31331-028, (LOT 1426996)
- L-Ascorbic Acid-2-Phosphate, sesquimagnesium salf hydrate $\geq$ 95% - Sigma, Ref A8960-5G
- Gentamicin Reagent Solution, 50 mg/mL, Gibco by life technologies, Cat. No 15750-060
- HEPES, Sigma H-3375, special preparation, 1M, pH 7.5 filtered
- ITS, Insulin-Transferrin-Selenium, Gibco by life technologies, Cat No. 51500-056

[9] http://www.sigmaaldrich.com/life-science/cell-culture/learning-center/media-expert/ascorbate.html
[10] http://www.sigmaaldrich.com/life-science/cell-culture/learning-center/media-expert/transferrin.html

Reagents	Quantities
DMEM F12	500 mL
Ascorbate	50 mg
Gentamicin	500 μL
HEPES	5 mL
ITS	5 mL

Table 6: Selenium Medium Reagents [16-17]

- DMEM/F-12 (1:1) (1X) + GlutaMAXTM-I – Dulbecco's Modified Eagle Medium F-12 Nutriment Mixture (Ham) 500mL – Gibco by life technologiesTM, Ref 31331-028, (LOT 1426996)
- L-Ascorbic Acid-2-Phosphate, sesquimagnesium salf hydrate $\geq$ 95% - Sigma, Ref A8960-5G
- Gentamicin Reagent Solution, 50 mg/mL, Gibco by life technologies, Cat. No 15750-060
- HEPES, Sigma H-3375, special preparation, 1M, pH 7.5 filtered
- Insulin Solution, from Bovine Pancreas, 10 mg/mL – 25 mM – HEPES, pH 8.2, Sigma, ID516-5ML, SLBD6620
- Transferrin, human, 100mg, Sigma, T 2036

Reagents	Quantities
DMEM F12	500 mL
Ascorbate	50 mg
Gentamicin	500 μL
HEPES	5 mL
Human Transferrin	5 mL
Insulin	500 μL

Table 7: No Selenium Medium Reagents

- DMEM/F-12 (1:1) (1X) + GlutaMAXTM-I – Dulbecco's Modified Eagle Medium F-12 Nutriment Mixture (Ham) 500mL – Gibco by life technologiesTM, Ref 31331-028, (LOT 1426996)
- L-Ascorbic Acid-2-Phosphate, sesquimagnesium salf hydrate $\geq$ 95% - Sigma, Ref A8960-5G
- Gentamicin Reagent Solution, 50 mg/mL, Gibco by life technologies, Cat. No 15750-060
- HEPES, Sigma H-3375, special preparation, 1M, pH 7.5 filtered • ITS, Insulin-Transferrin-Selenium, Gibco by life technologies, Cat No. 51500-056
- Sodium Selenite (powder), stock 10g, Sigma, S5261 - Solution of Sodium Selenite: powder diluted with ddH2O 100 μg of sodium selenite powder for 100mL of ddH2O. Use of Sodium Selenite (5μL/mL or 5ng/μL stock used solution) put 9μL of sodium selenite per mL of medium.

Reagents	Quantities
DMEM F12	500 mL
Ascorbate	50 mg
Gentamicin	500 μL
HEPES	5 mL
ITS	5 mL
Sodium Selenium	9μL/medium mL

Table 8: Supplemented Selenium Medium Reagents

Previous studies of Khan *et al.* 2011&2013 [16-17] have shown that the static *in vitro* culture of immature articular cartilage in the presence of the combination of two specific growth factors (FGF2 and TGFβ1) induces morphological changes related to the "normal" postnatal developmental transition to tissue maturation [16-47]. These changes present a reduction in cartilage height of 50% through resorption of the deep zone and the related epiphyseal-derived zone [16]. The height reduction and the loss of hypertrophic chondrocytes show similar features than observed in postnatal maturation in patellofemoral joints of mice and rabbits, as investigated by Hunziker *et al.* and Slotz *et al.* [47, 153]. The large resorption in the deep zone of growth factor-treated explants was defined to be balanced by growth from the surface zone driven by chondroprogenitor stem cells. Consequently, using this specific growth factor cocktail, it has been shown that *in vitro* growth factor-induced differentiation of immature articular cartilage model (described above) results in biophysical and biochemical properties that are highly similar to those of native mature cartilage. Following the model developed by Khan *et al.* 2011 [16], the explants which will undergo the maturation (growth-factors) treatment will be cultured with TGFβ1 at a concentration of 10 ng/μL and FGF2 at 100 ng/μL concentration : 1 μL of each growth factor will be used per 1 ml of medium.

10.4.2 Materials

1. Lamina Flux Hood
2. Incubator 37°C – 5% Co2
3. Vacuum pump
4. Accurpette VWR
5. Finnpipette (1000-200-20-2 ul)
6. Corning 250ml filter system, non-pyrogenic, sterile
7. Tips (1ml, 200ul, 20ul, 2ul), Starlab, TipOne (sterile), free of detectable RNase, DNase, DNA& Pyrogens 20ul Bevelled Graduated, filter tip – Cat No. S1120-1810 200ul Bevelled Graduated, filter tip – Cat No. S1110-1810 1000ul Bevelled Graduated, filter tip – Cat No. S1122-1830
8. Pipettes (25-10-5 ml) cellstar, greiner bio one
9. Racks
10. Centrifuge tubes (50ml-25ml)
11. Eppendorf tubes
12. Universal tubes

13. 12 & 24 well plates
14. Scalpel
15. 4 & 6 mm biopsy punch, MILTEX by KAI, ref 33-36
16. Absordent Protector – Benchkote, Polysterene Backed, 460cm*50m, Cat No. 2300731, WhatmanTM
17. Autoclavable Disposal Bag, For disposal of contamined plastic laboratory ware neck should be left open to allow penetration of steam, Hazardous Waste, STERILIN (white bag)
18. Clinical waste for alternative treatment Medium Duty, (UN-approved weight 5kg, Un-closure methods, UN- SH4/Y5/S/II/GB/4/06 (orange bag)
19. Ethanol 70%

10.4.3 Protocol – Preparation of the explants Calves legs scalp

1. Prepare absorbent protector (spread of alcohol), scalpel
2. Clean the leg with soap and scrub with a brush
3. Clean the earth of the leg
4. When well clean, spread with 70% ethanol
5. Put the leg on absorbent paper
6. With scalpel, cut around the feet
7. Trace a delicate line along of the leg
8. BE CAREFUL NEAR THE JOINT
9. Skin out the skin of the leg slowly, carefully along the line
10. Put the skin, used tissue, paper and gloves in a double clinical bags
11. When skin out, clean/brush with soap and ethanol again
12. Place the leg in Al-foil and then all in the hazardous bag then in the clinical waste
13. Put in the fringe at 4°C
14. Throw away the clinical bags in adequate place

10.4.4 Preparation of explant extraction & Explant Culture

The explants have to be obtain from the internal part of the joint (see figure 27). In order to be in comparable conditions, four (or six) explants have to be punched from the same zone in order to apply the four (ou six) different treatments on samples possessing almost the same shape and characteristics.

1. Open the lamina flux hood 25min before use, clean with alcohol 70%
2. Warm media
3. Prepare (24-)well plate with 1.5ml of basic medium in each well – Put 30min in Incubator
4. Prepare the material in a rack: one universal tube with 70% ethanol & one universal tube with wash medium (basic one)

Figure 27: Bovine Articular Cartilage (bAC) from the metacarpophanlageal joint. *Left and middle pictures:* Opened joint under sterile conditions of immature bAC (7-days old). *Right picture:* Biopsies - Immature explants

5. Prepare a scalpel and a 4 or 6 mm biopsy bunch (placed in the alcohol tube)
6. Put an absorbent protector, spread of alcohol
7. Prepare some tissues spread with 70% ethanol (One per leg)
8. Dissection plate, cover with Al-foil
9. Take foots out of the fringe (4°C), spread them with ethanol
10. Dispose hazardous and clinical bags near the hood to autoclave the waste
11. Use two layers of gloves
12. Take the alcohol spread feet
13. Move the joint to find where the incision should be made
14. Cut in the opposite direction to you allowing the joint, cut really carefully
15. Cut without touching the cartilage of the feet
16. When the joint if open, cut carefully the ligament
17. Throw away the lower part of the feet in autoclave bags
18. Expose at maximum the cartilage
19. Be careful to not touch anything with the feet
20. Place the biopsy punch in alcohol then medium
21. Along the internal faces of the bones, make some circles with this punch (4-5 per face)
22. Place punch in alcohol when finish
23. Take scalpel put in alcohol then in medium
24. Cut (trace a line) between each circle and along the central line of the bone
25. To take the cartilage explant, cut vertically on one of the border of the circle biopsy, then cut horizontally on the subchondral bone very carefully
26. Remark: Explant should have as mush as possible an uniform thickness
27. Place the explant in the well plate in the well labelled location
28. Remark: always do a control and a treatement with the same leg, ideally with explant coming from the same location in the joint.
29. Check that the explant is well positioned (surface of the explant at the top and subchonbral part in the explant at the bottom of the well)
30. Close the well plate after each cartilage deposition

31. Remove the washing medium (wash medium = DMEM-F12)
32. Wash again with wash medium
33. Apply the treatments: Put 1.5ml of the adequate medium (Se-CONT, Se FT-treated, Without Se-CONT, Without Se FT-treated)
34. Be careful: don't touch anything with the pipette.
35. Check that explants are still in the right position (bone facing the bottom part of the well-plate)
36. Clean everything and throw away the clinical waste in adequate place.

Once placed in culture, the explant media have to be changed every two days with warm fresh media in order to susbtain to the diverse needs of the cells/tissue.

11 Hypotheses & Objectives

This thesis is based on the hypothesis that the selenium plays a crucial role in the articular cartilage metabolism and homeostasis. This seems to be confirmed by the pathological observation of Kashin-Beck and osteoarthritis diseases. **Our general hypothesis is that a selenium depletion in the surrounding nutritional environment, could contribute to articular cartilage tissue degeneration altered biomechanical properties, with some similarities with those present in osteoarthritic cartilage.** The biological activity of Se is related to its incorporation in the form of amino acid selenocysteine (Sec) into selenoproteins such as gluthatione peroxidase, iodothyronine deiodinases or thioredoxin reductase [69]. Indeed, most Se-proteins participate in antioxidant defence and redox state regulation, particularly the families of glutathione peroxidases and thioredoxin reductases. Some Se-proteins play more specific essential roles, such as iodothyronine deiodinases involved in thyroid hormones metabolism, GPx4 which is essential for spermatogenesis, and selenophosphate synthetases 2 participating in Se-proteins biosynthesis. In addition, it has been well recognized that Se plays a key role in cell cycle and apoptosis but mechanisms for Se action are not fully understood.

To our opinion, if the selenium plays an important role at the level of the chondrocyte metabolism, it can be proposed that it has a retroactive function on the organisation and the structuration of the extracellular matrix with potentially a role in the mechanotransduction for example. Growth and post-natal maturation of the AC can occur *in vivo* over a period of up to 12 years, however a group from Swansea, directed by Prof. Archer and Dr. Khan, has developed techniques to rapidly induce explant maturation in this tissue in a matter of weeks. This explant culture model has been modified in order to take into account the selenium variable. Consequently, tests have been performed under Se depletion, through its absence in culture medium, and Se-supplementation to determine how selenium affect the articular cartilage tissue development during this critical window of growth which coincides with age-related incidence of KBD. This project aims to characterize the Selenium implication in the articular cartilage development in a biological, biochemical and biophysical points of view. The main objectives are: (a) to determine the selenium involvement into tissue organization and function which means its localisation and its speciation in the tissue, (b) the characterization of the ECM of AC in presence or absence of Se during the maturation processes using microspectrochemical techniques and molecular biology tools. The characterisation of organic matrix structure through nanobiomechanics of the AC surface using atomic force microscopy (AFM). The identification of critical selenoproteins involved in this process and the determination of the distribution of selenium within cells/tissue could be key information towards the identification of the potential mechanism to improve cartilage repair and regeneration. In order to determine this relative importance of the selenium in AC maturation, X-ray fluorescence microscopy (XRFM) have been used to detect the sub-cellular

distribution of the selenium. This was followed by analyses on high-energy resolution fluorescence detected X-ray absorption spectroscopy(HERFD-XAS) coupled to an array of crystal analysers which provide demonstration of selenium speciation within our model of maturation of the articular cartilage at unprecedented low concentration of few hundreds of ppb range. This concentration range was determined using state-of-the-art inductively coupled plasma mass spectrometry (ICP-MS). Synchrotron Fourier transform infrared microspectroscopy (FTIRM) was used to evaluate the biological and morphological (in parallel to histology) constitutional variation appearing in presence of different selenium concentrations in presence or absence of growth factors. Complementary to these studies, histological, genetic (PCR-qPCR) and collagen (immunofluorescence) analyses have been performed. Furthermore, nanobiomechanical properties of the articular surface treated or not with selenium have been investigated to present some preliminary insights of the selenium retroactive action on the AC surface structuration.

Part V
Characterisation of Selenium in Articular Cartilage Tissue

This part will be focused on the intrinsic characteristics of the selenium in articular cartilage. As no documentation has been reported in literature, a quantification of the selenium concentration was investigated. Localisation of the selenium within the tissue were performed to hypothesize Se-involvement in cells, extracellular matrix or diverse organelles. Due to the extremely low concentration of the selenium in organism, synchrotron light and technology have to be used to explore the matter at sub-cellular levels. Selenium speciation studies were made to provide insights on its potential function.

This part refers to a paper that has been submitted.

12 Selenium Concentration Assessment in Articular Cartilage Treated-Explants

12.1 Induced Coupled Plasma Mass Spectroscopy ICPMS

This technique is able to carry out rapid multielement characteristic determinations with accurate detection limits and isotopic distinguish capabilities. This technique is highly used for geochemical analysis. To briefly described the principle, the ICP-MS instrument is a combination of a high-temperature Inductively Coupled Plasma (ICP) source and a Mass Spectrometer (MS). The first section of the instrument, the ICP source will convert the atoms of the elements of the samples to ions. These produced ions are then separated and detected by the second section, the mass spectrometer.

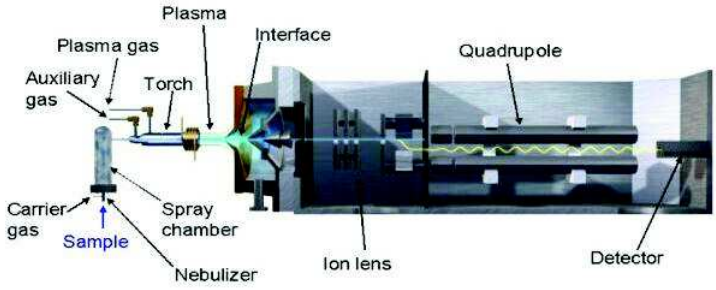

Figure 28: ICP-MS basic principle source agilent

The sample preparation is really important because the ionization depends on the matrix environment. Biological samples have to be transformed into a liquid form. Actually, the biological samples should be cleaned of their organic matrix in order to preserve the elementary element. Diverse acid attacks have to be performed in order to dissolve this organic matrix. After the organic removal, the sample solid residues are usually displayed in a liquid (composed of low concentrered acid). Using the first section of the ICP-MS, the high temperature plasma is discharged to generate positively charged ions. The sample solution is then pumped into the sample introduction system. The sample arrives in a chamber and with the help of the nebulizer the liquid is sprayed into tiny drops as an aerosol into the plasma torch (Figure 28). The argon gaz is perpetually injected in the system to maintain the plasma and cool down the torch. The final temperature of this plasma reached approximately 6000K. With the temperature variations present within the plasma torch, the sample will undergo several

transformations: it will be dried out and vaporized, then atomized to finally be ionized. At the end of the plasma section, the sample is then present under the form of excited atoms and ions (usually positively charged) representing the elemental composition of the sample. After the interface section called cones (Figure 28), a succession of lens focalizes and filters the ion beam. All the following part of the ICP-MS will be proceeded under vacuum. The selected ions are then positively charged. Nevertheless, some polyatomic ions remain present in this beam. The ion beam is then transported into the collision cell where a gas (H_2) will erase the polyatomic interferences using the collision effect between two atoms of different size. The combination of the H_2 molecule with large polyatomic ions producing a complex. This induces a kinetical energy lost of this complex which remains in this collision cell. This is the principle of the energy discrimination. Just as a remark, the H_2-mode reaction is usually used to analyse the selenium trace because it allows to reach detection limits close to the ppt (ng/L). After this monoatomic ion selection (with different mass), the total monoatomic ion beam is directed into a quadrupole mass filter (Figure 28). A mass/charge ratio is used to successively select the element of interest. The remaining ion beam arrives on an electron multiplier detector (Figure 28) where the number of ion of this element of interest is finally collected. This signal is proportional to the concentration of the initial solution. This is how the element quantification is then performed.

References: SPECTROSCOPY tutorial - A Beginner's Guide to ICP-MS Part I ROBERT THOMAS & Agilent technologies technical overviews.

12.2 Methods & Materials

ICP-MS References:

a) Single Cell Proteins (BCR 274): certified Se-concentration of 1.3 ± 0.05 μg/g, from LGC Standards

b) Bovine Liver (SMR 1577b): certified Se-concentration of 0.73 ± 0.06 μg/g, from LGC Standards

c) Human Hair (BCR 397): certified Se-concentration of 2.0 ± 0.08 μg/g, from LGC Standards

d) NIST-Reference National Institute of Standards and Technology: Standard Reference Material (SRM) 1643f, NIST Office of Reference Materials, Gaithersburg, MD 20899, 18.08.2015

e) Single-element ICP-Standard solution Se 1000 mg/L ± 0.2%, ROTH, ROTI®-STAR

ICP-MS: Chemicals used for digestions:

a) Hydrogen peroxide (H2O2) 30% suprapur - MERCK

b) Nitric Acid (HNO3) JT Baker 65% "Baker Analysed"; double distilled with picotrace system

***In vitro* model of articular cartilage maturation Preparation:** An *in vitro* culture of 4-mm explants excised under sterile conditions from the lateral aspect of the medial condyle of the metacarpophalangeal joints of immature male (7 days-old) bovine calves were used (Figure 27). A thin layer of the subchondral bone is present on the basal aspect of each explant. To induce maturation in cartilage explants, cartilage in serum-free medium (Dulbecco's modified Eagles medium, Insulin-transferrin-selenium (ITS), HEPES buffer (1M), and antibiotic (gentamicin, 50 μg/ml) and antimycotics were supplemented with 100 ng/mL fibroblast growth factor 2 (FGF-2) and 10 ng/mL transforming growth factor β1 (TGFβ1) [16]. The combination of growth factors induces profound morphological changes in immature articular cartilage consistent with a highly accelerated maturational response within 21 days [16]. Growth factor stimulation induced apoptosis and resorption from the basal aspect and cellular proliferation in surface chondrocytes [17]. This fast maturation-like

model patent has been modified developed to include the Se concentration parameter. Explants were then also cultured according to a gradient of Se-concentration in culture medium. Three major groups appear: (a) medium with ITS (usual protocol described in the patent where 6.7 ng/ml of sodium selenite are present the solution called ITS, (b) medium with a Se-supplementation provided by a total concentration of 50 ng/mL in sodium selenite solution added about ten times superior to the usual protocol and which are is called "Se-supplemented", and (c) medium totally depleted of selenium, called "No Se". For each group, explants are then placed in two sets: one control and another called "FT-treated" where explants are treated with the growth factors cocktail given described above. All the conditions provide a pool of six samples types. Each pool is provided by explant from the same animal in order to perform comparison. There was a minimum sample number of 4, and cartilage explants in each group were taken from separate joints. After 3 weeks in culture, explants were cryo-milled and the resultant powder were freeze-dried at -40 °C under vacuum (0.150 mbar) during 12 hours and stored at 4°C in a sealed box.

Samples Preparation: To determine total selenium concentrations (Se_{tot}) in the tissues, digests of the pre-processed material were performed. After 3-weeks of *in vitro* culture of cartilage explants, the samples were snap-frozen in precooled hexane and underwent an ultra-thin cryo-milling in order to obtain a highly homogeneous fine powder. The powdered samples and the reference materials (between 10 to 30 mg) were weighted into acid washed (HNO3 and HCl) Teflon beakers (Savillex). Digestion Protocol was realized based on the literature review [157-159]. The ultra-fine powder allows the diverse acid attacks to better dissolve the dense organic extracellular matrix. The digestion was performed in 3 mL of 14 M HNO_3 (double distilled) at 100 °C for 24 h followed by the addition of 1 mL of ultrapure H_2O_2 . It is used after a primary digestion due to its high oxidizing power and strong reactivity towards the biological samples (27). After H_2O_2 attack during 12 h at room temperature, the solutions were heated at 100 °C for 72 h to accelerate decomposition of the organic matrix. After evaporation at 100 °C for 6 h, residues were dissolved in 5 mL of 1% HNO_3 solution, heated at 100 °C for 10 min and further sonicated (ultra sonic cleaner Branson200) for 5 min to guarantee complete dissolution. Finally, these homogenized samples were used for analyses.

QQQ-ICP-MS Instrument and Operation Conditions: Total Se-concentration within these tissues were evaluated by Triple Quadrupole Inductively Coupled Plasma Mass Spectrometry (QQQ-ICP-MS, Agilent 8800, Figure 29). Hydrogen (H2, 5.0, PanGas) was used as reaction cell gas to avoid interference on m/z 78. The detection was performed in MS/MS mode (m/z 78/78). For total Se analyses in low concentrated matrices, the experience was operated in ^{78}Se-(H_2-mode) in collision cell in order to avoid as much as possible interferences. Due to the MS/MS mode the first quadrupole mass filter is set to the target mass 78. Interference reduction in the ORS3 (collision reaction cell = 3rd generation octopole reaction system) with H2 is thus specifically applied on Se and the respective interferences with m/z 78. The controlled interference removal process profits from simpler reactions specifically on the target m/z. Sample dependent interferences with other elements, newly created interferences and m/z overlaps are avoided resulting in improved signal to noise ratios and allowing matrix independent low level Se detection. Here, the possible interferences of the ^{78}Se were with ^{38}Ar^{40}Ar and ^{38}Ar^{40}Ca. These interferences are relatively easily suppressed using the H_2-gas of the collision cell. The ^{77}Se and ^{80}Se were not selected because of the strong polyatomic interference with the argon which are difficult to avoid. Indium (In) was used as internal standard (In, 5 ppb). Further experimental details on the conditions of the Agilent 8800 are given in Table 9.

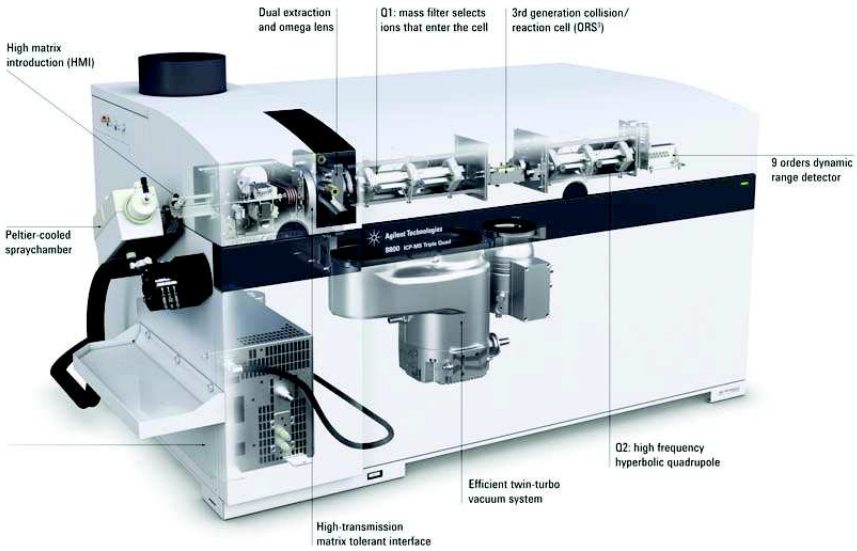

Figure 29: QQQ-ICP-MS Agilent 8800
(Source: ICP-MS Agilent 8800 website)

Parameters	Details
Plasma Conditions	General Purpose
Scan Type	MS/MS
ISTD In (5ppb)	115->115 In [H_2]
CRC Conditions	H_2 gas flow rate , 7 mL/min
Acquisition Mode	Spectrum
Q2 Peak Pattern	1 point
Replicates	3
Stabilisation Time	10 s
Acquisition Time	0.8 min
Integration Time	0.3 s (Se and In)
Pump Speed	2.50 RPS

Table 9: Agilent 8800 experimental set-up for articular cartilage explants in 1% HNO_3 solutions: acquisition method and parameters.

Instrument Calibration: For this ICP-MS experiment,the calibration was made using a mono-elementary Se-solution in the range of [0.005 – 5 ppb] with the specific concentrations of 0.005 ppb - 0.01 ppb - 0.05ppb - 0.1 ppb - 1 ppb - 5 ppb - 50 ppb in solution. Nevertheless, regarding to the range of the sample concentration in solution, a better calibration has been performed between 0.1 - 1- 5 ppb. The matrix based (1% HNO_3) calibration (Figure 30) was performed in a calibration range of 0.005– 50 μg/L (1 μg/L = 1 ppb). The detection limit (DL) calculated by MassHunter (based on the background signal for Se and according to definition 3 * BEC) equals to 0.007 μg/L (Figure 30). This DL was calculated using 10 blank solutions at 1% HNO_3. Five digestion blanks were analyzed and the obtained value for these blanks was 0.020 μg/L. According to these values, the quantification limit of the samples was 0.09 μg/L corresponding to 70 ppbμg/kg dry weight of the Se in samples. Each sample is analysed three times by the machine. The machine standard deviation is the standard deviation of these three measured values.(Machine Standard Deviation – RSD: (Variance/Average)*100)

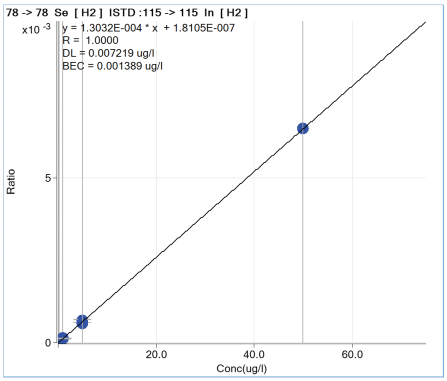

Figure 30: Calibration used for Se total analyses in a range of 0.005-50 μg/L (ppb) in a 1% HNO_3-matrix. The X-axis represents the standard concentration (μg/L). The Y-axis represents the ratio of the standard's counts per second (CPS) at the respective level divided by the ratio of counts per concentration of the internal standard at the respective level (Agilent Technologies, Inc. (2015): MassHunter 4.2 Workstation Software for 8800 ICP-QQQ, G7201C, Manual).Standard solutions present a concentration of 0.005, 0.01, 0.05, 0.1, 1, 5 and 50 μg/L (ppb).

Quality control of the digestions was done by co-digesting certified organic reference materials (Single Cell Proteins (BCR 274), Se_{tot} 1.3±0.05 μg/g, Bovine Liver (SMR 1577b) about Se_{tot} 0.73±0.06 μg/g and Human Hair (BCR 397) about Se_{tot} 2.0±0.08 μg/g) (Table 10) and yielded recoveries for Se of 97%, 89%, and 74%, respectively. An additional reference (NIST 1643f, Se_{tot} 11.7±0.08 μg/L) was run as a routine instrument performance test (Table 10) with a recovery of 102%.

As all samples had concentrations exceeding at least 10 times the quantification limit, the results of all samples can be taken into account. It appears that the Se is present within the articular cartilage tissue (independently of the applied treatment) at concentrations in a range of few hundreds ppb (Tables 11&12).

Information: The Machine standard deviation is based on the ICP-spectrum replicates. Biological replicate (duplicate or triplicate) of a digested sample solutions have been gone through the same complete digestion, preparation, and analyses. The biological variability of these samples is consequently using a usual standard deviation (STDEV).

12.3 Results & Interpretation

No studies have been performed to assess selenium within the articular cartilage. The ICPMS analyses were performed to assess the selenium concentration within this specific tissue which is the articular cartilage. Such study was an important starting in order to evaluate Se levels and plan the further possible experiments. Standard references from LGC standard References have been analysed to test the sample preparation protocol. The results reveal that the protocol and the instruments are able to obtain the tabulated Se-concentration values with a good accuracy and reproducibility: single cells proteins (σ^2<0.006), bovine liver (σ^2<0.001) and human hair (σ^2<0.02) (see Table 10). It appears that the Se is present within the articular cartilage tissue (independently of the applied treatment) at a concentration of few hundreds ppb (see Tables 11&12). Of note, following measurements of the Se-monoelementary standard solution for the calibration curve, the machine detection limit has been fixed to about 0.020 μg/L and the machine standard deviation about 15%. As an indication for this experiment, it has been considered that the limit of detection was fixed at three times the blank signal

and the limit of quantification at ten times the blank signal. Using five blank "samples", a blank quantification is about $<0.03\,\mu$g/L in solution. Consequently, the detection limit is about 0.09 μg/L for the samples, so about 70 ppb μg/kg dry weight of the Se in samples according to our dilution factor (1:5). As all samples had concentrations exceeding at least 10 times the quantification limit, the results of all samples can be taken into account.

Standard References (N replicates)	Reference Values ± SD (μg/g)/*(μg/L)	Measured concentration (μg/g)/*(μg/L)	Standard deviation (%)	Recovery (%)	Average ± SD (μg/g)/*(μg/L)
BCR274 - Single Cell Proteins (N=3)	1.03 ±0.05	0.95 0.91 1.08	11 6 8	97 93 100	0.98± 0.09
BCR397 - Human Hair (N=2)	2.0 ± 0.08	1.28 1.54	11 –	67 80	1.41 ± 0.18
SRM 1577b - Bovine Liver (N=2)	0.73 ± 0.06	0.56 0.62	13 9	84 93	0.59 ± 0.04
NIST-1643f (liquid)	11.7 ± 0.08 *	11.91∗	-	102	

Table 10: Quality control measurements for total Se analyses (Se_{tot}) of the digested reference materials (BCR 274, SMR 1577b, BCR 397 from LGC Standards) and the NIST reference material in a 1% HNO_3 matrix. The table represents the analyzed Se contents, the SD of duplicate and /or triplicate measurements and their recoveries. * value expressed in μg/L

Looking at Table 11, native tissues (immature and mature samples) and the No-Selenium group (Controls and FT-treated samples) present an average concentration in the range of 100-200 μg/L. It seems normal that the No-Selenium group presents a Se-concentration close to the one of native tissue. Of importance, insulin and transferrin were still added to medium, only Se was discarded. This shows that the NoSe-explant whatever treatment applied (growth factors or not) keep same level of Se as the native immature explants despite the 3-weeks of culture. As expected, the selenium provided through sodium selenite supplementation (either physiologically through ITS supplementation or exogenous sodium selenite) in the culture media influence the Se-concentration within the AC explants. The samples treated with ITS reach a Se 2.2 to 2.9-fold (whether treated or not with growth factor respectively) increase in Se concentration when compared to Se concentration within the native immature AC explants before *in vitro* culture. For those exposed to exogenous sodium selenite supplementation, Se concentration increase by 12 and ~17-fold (whether treated or not with growth factor respectively) when compared to Se concentration within the native immature AC explants before *in vitro* culture. This still a ~5.5 fold increase in Se concentration when compared to the ITS treated explants.

Samples	Total Average (ppb, μg/kg)	Standard deviation σ (ppb, μg/kg)
Native Immature (N=5)	176	49
No Se Control (N=7)	193	76
No Se FT-treated (N=8)	188	54
ITS Control (N=6)	401	56
ITS FT-treated (N=7)	519	160
Se-Supplemented Control (N=4)	2172	540
Se-Supplemented FT-treated (N=4)	2979	739
Native Mature (N=10)	159	83

Table 11: Total Se concentrations (Se_{tot}) of bovine articular cartilage explants in μg/kg (ppb) measured by ICP-QQQ analysis after an acid digestion procedure. The samples underwent different treatments: cultured in standard conditions with no selenium in culture medium in presence (No Se FT-treated) or in absence(No Se Control) of growth factors, insulin-transferrin-selenium (ITS) in presence (ITS FT-treated) or absence (ITS-Control) of growth factors, or further supplemented with 50 μg/L sodium selenite, (N$\geq$4) for each conditions (i.e., supplemented Se control and supplemented Se FT-treated). The native immature and matures explants were analysed without any further culturing or treatments. This table corresponds to the average values of explants treated and analysed under the same conditions. The standard deviation represents the replicate variation corresponding to the biological variation appearing in this culture model. The limit of quantification is 0.020 μg/L (sample solution diluted in 1% HNO_3) and and the sample detection limit is 0.09 μg/L which corresponds to about 70 ppb μg/kg dry weight of the Se in samples. The machine standard deviation is about 15%.

12.4 Conclusion

Three pools can be distinguished: one of the native and No-Se samples about 150 ppb, the second one of "ITS" samples close to 450 ppb and the third one of the " supplemented Se" about 2500 ppb. It is interesting to notice that the maturation treatment applied on the samples do not properly impact

the Se-concentration within the tissue. This means that this "fast maturation-like" treatment do not influence the selenium incorporation with the tissue.

Nevertheless, the experiment was just a starting point to determine which techniques will be the more appropriate to fulfil the objectives of this project. In which regions of the AC the selenium is distributed? Is it located in the cell nucleus, in the cells and/or in the extracellular matrix? Do the Se-supplementation or the Se-depletion induce some regions with higher Se concentration.? What are the Se-species present within the explant tissue? Do these species are specific depending the immature or maturated states of the tissue? Does Se influence extracellular matrix organisation and structure of the AC? These are key questions that can provide insights about the main question of this project: what is the impact of Se on the AC tissue and its maturation.

Samples	ppb (μg/L)	ppm (μg/g)	Standard Deviation (%)
Immature A	266.55	0.27	3
Immature B	177.9	0.18	11
Immature C	167.49	0.17	5
Immature D	125	0.13	-
Immature E	144	0.14	-
No Selenium Control A	169.66	0.17	5
No Selenium Control B	142.57	0.14	11
No Selenium Control C	313.28	0.31	20
No Selenium Control D	84.78	0.08	55
No Selenium Control E	85.2	0.09	18
No Selenium Control F	221	0.22	-
No Selenium Control G	116	0.12	-
No Selenium FT-treated A	151.48	0.15	17
No Selenium FT-treated B	146.63	0.15	6
No Selenium FT-treated C	274.74	0.27	13
No Selenium FT-treated D	170.43	0.17	22
No Selenium FT-treated E	75.63	0.08	6
No Selenium FT-treated F	79.13	0.08	1
No Selenium FT-treated G	190	0.19	-
No Selenium FT-treated H	192	0.19	-
ITS Control A	341.8	0.34	-
ITS Control B	355.9	0.36	10
ITS Control C	500.09	0.5	9
ITS Control D	428.4	0.43	1
ITS Control E	354	0.35	-
ITS Control F	427	0.43	-
ITS FT-treated A	401.94	0.4	1
ITS FT-treated B	475.04	0.48	12
ITS FT-treated C	691.02	0.69	11
ITS FT-treated D	403.5	0.4	7
ITS FT-treated E	828.75	0.83	10
ITS FT-treated F	457	0.46	-
ITS FT-treated G	377	0.38	-
Supplemented Se Control A	1432.36	1.43	16
Supplemented Se Control B	1903.61	1.9	8
Supplemented Se Control C	2812	2.81	-
Supplemented Se Control D	2541	2.54	-
Supplemented Se FT-treated A	3017.1	3.02	3
Supplemented Se FT-treated B	1781.2	1.78	13
Supplemented Se FT-treated C	3758	3.76	-
Supplemented Se FT-treated D	3358	3.36	-
Mature A	128	0.13	16
Mature B	126.46	0.13	9
Mature C	124.15	0.12	3
Mature D	117.32	0.12	41
Mature E	129.23	0.13	15
Mature F	118.99	0.12	22
Mature G	163.03	0.16	9
Mature H	230.18	0.23	7
Mature I	382.21	0.38	-
Mature J	75.24	0.08	29

Table 12: List of all analyzed samples with their respective intrinsic Se-concentrations including certified references materials (BRC 274, BCR 397, SMR1577b) and cartilage samples.

13 Selenium Localisation within Cartilage Tissue

13.1 Synchrotron Technology and Radiation

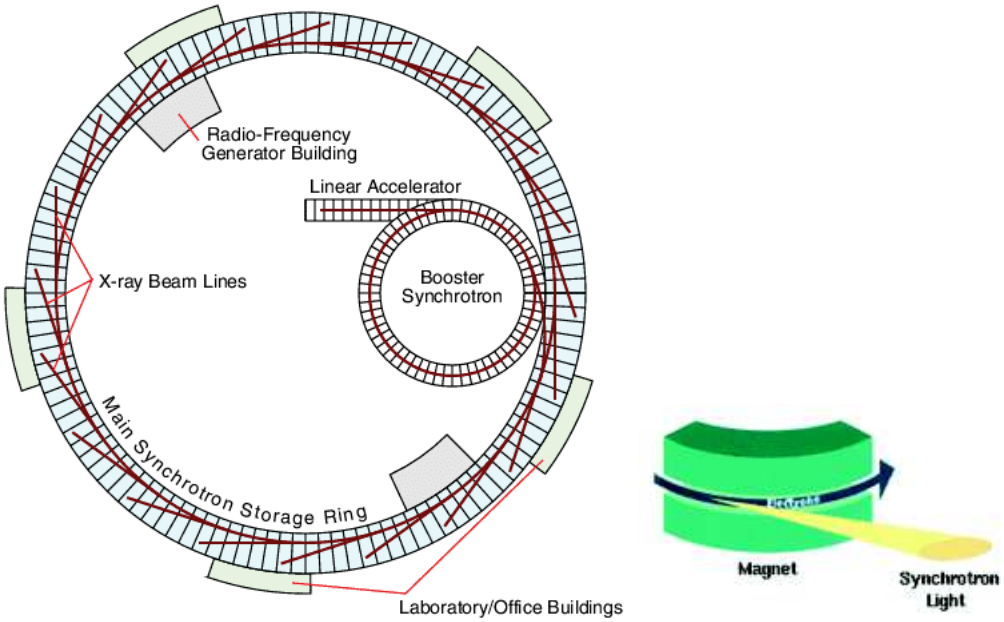

Figure 31: Schematic picture of the Synchrotron, Particle Accerelator. (Left) Electrons are first accelerated in the linear accelerator (linac) and in a booster synchrotron, then they are injected into a storage ring. Once in this ring, the electron beam is contained and collimated using magnets. The brown lines denote the paths of the synchrotron radiation emitted as the bunches of electrons pass through the dipole magnets (undulators/wigglers). (Right) Synchrotron radiation emission when the electron bunches are passing though the bending magnet.

When electrons or positrons are moving at relativistic speed, i.e., close to the velocity of light, they are subjected to a magnetic field, the trajectory follows a circular orbit and synchrotron radiation (SR) is emitted in the tangential direction. The radiated energy is proportional to the fourth power of the particle speed and inversely proportional to the square of the radius of the path. The beam is concentrated into a forward narrow cone with half angle of typically 0.1 to 1 mrad. Synchrotron radiation facilities typically consist of an injection system, a storage ring and beamlines. In the injection system, electrons are generated, pre-accelerated, and sometimes a second accelerator further accelerates these electrons to few GeV before injection into the storage ring. At ESRF, the electrons are accelerated to a nominal energy of 6 G eV. In the ring, bunches of electrons periodically circulate at relativistic speed for periods of up to many hours. The storage ring consists of radio-frequency (RF) cavities, bending magnets, other magnets, insertion devices and different control systems mainly to control the orbit of the electrons (Figure 31). The RF cavity system restores energy, which the electrons lose because of the emission of SR, and stabilizes the bunch of electrons. The high energy electrons are maintained in a planar orbit by using bending magnet. Synchrotron radiation is emitted when an electron received centripetal force in the magnetic field of the bending magnets. Synchrotron radiation emitted from an electron traveling at almost the speed of light is highly collimated by relativity effect. Higher brightness synchrotron radiation is produced by insertion devices, such as undulators in the straight sections of the storage ring [160]. They have the common feature of producing synchrotron radiation by passing relativistic electron bunches through periodic magnetic structures. The most powerful generators of synchrotron radiation at most modern storage rings are undulators. The

magnetic structure of today's most common (planar) undulator is an array of closely spaced vertically oriented dipole magnets of alter nating polarity. As the electron beam passes through the array, its trajectory oscillates in the horizontal plane. Owing to the relatively weak field, the radiation cones emitted at each bend in the trajectory overlap, giving rise to a constructive interference effect that results in one or a few narrow peaks (a fundamental and harmonics) in the energy spectrum of a beam that is highly collimated in both the horizontal and vertical directions. Tuning the wavelengths of the harmonics is done by mechanically adjusting the vertical spacing (gap) between the pole tips.

Synchrotron radiation possesses several major characteristics and properties produced by synchrotron light sources:

(a) High brightness (emitted flux per solid angle per unit source area) and High brilliance (brightness per unit source area):

It means that the beam size and its divergence are as small as possible while the photon flux remains as large as possible. The brightness, also called brillance, is defined as the phase-space density of the photon flux [163]. It is evaluated in the forward direction and at the origin of the phase space.

Mathematically, the brillance B (brightness per unit source area) is defined by the following equation:

$$B[\frac{photons}{(sec)(mm^2)(mrad^2)(0.1\%BW)}] = \frac{d^4F}{d\theta d\psi dxdy} \tag{1}$$

where F is the spectral flux, θ and ψ are the horizontal and vertical angles and x, y are the horizontal and vertical coordinates respectively, BW is the bandwidth described as $\delta\lambda/\lambda$.

(b) High intensity or flux (photons per second) over a large wavelength range:

The spatial or angular density of flux can be respectively obtained by integrating the phase space density over the angles or the position coordinates:

$$\frac{d^2F}{dxdy} = \int \frac{d^4F}{d\theta d\psi dxdy} d\theta d\psi \tag{2}$$

$$\frac{d^2F}{d\theta d\psi} = \int \frac{d^4F}{d\theta d\psi dxdy} dxdy \tag{3}$$

Then, the spectral flux is provided by the following integration:

$$F[\frac{photons}{(sec)(0.1\%BW)}] = \int \frac{d^2F}{dxdy} dxdy = \int \frac{d^2F}{d\theta d\psi} d\theta d\psi \tag{4}$$

(c) High level of polarization, relevant to the anisotropy of the source

(d) High collimation, refering to the small angular divergence of the beam

(e) Low emittance which refers to the product of beam size and divergence

(f) High coherence of the photon beam. The coherence can be defined by what makes a wave capable to produce observable interferences (patterns) and diffractions effects [161]. Two types of coherence [162] are observed: transverse and longitudinal. The transverse coherence refers to the coherence of electromagnetic disturbances at two points perpendicular to the propagation direction, and is related to the source size and the distance source-experiment. Longitudinal coherence refers to the case of two points along the propagation direction and is related to the monochromaticity of the beam. The transverse coherent flux is given by [163]

$$F_{coh,T} = B(\frac{\lambda}{2})^2 \tag{5}$$

where λ is the wavelength. The transverse coherence is characterized by the transverse coherence length l_{TC} by the formula:

$$l_{TC} = \frac{\lambda}{2\alpha} = \frac{\lambda s}{2L} \tag{6}$$

where α is the angular source size, L the distance to the source and s source size. The longitudinal coherence is characterized by the longitudinal coherence length l_{LC} by the formula:

$$l_{LC} = \frac{\lambda^2}{\delta\lambda} \tag{7}$$

where $\delta\lambda/\lambda$ refers to the bandwidth, as previously mentioned.

13.2 Synchrotron-based X-ray Fluorescence Microspectroscopy

When a sample is irradiated with X-rays, the X-rays may undergo either scattering or absorption by the atoms of the sample. This later process is known as the photoelectric effect. When an atom absorbs the source X-rays, the incident radiation dislodges electrons from the innermost shells of the atom, creating vacancies. The electron vacancies are filled by electrons cascading in from outer electron shells. Electrons in outer shells have higher energy states than inner shell electrons, and the outer shell electrons give off energy as they cascade down into the inner shell vacancies. This rearrangement of electrons results in emission of X-rays characteristic of t he given atom or so called Auger electrons [164]. The emission of X-rays, in this manner, is termed X-ray fluorescence and emitted isotropically. In addition, each characteristic X-ray line is defined with the letter K, L, or M, which signifies which shell h ad the original vacancy and by a subscript alpha (α) or beta (β), which indicates the higher shell from which electrons fell to fill the vacancy and produce the X-ray. For example, a K α line is produced by a vacancy in the K shell filled by an L shell electron. The K lines for a given element are the most energetic lines and are the preferred lines for analysis. For a given atom, the X-rays emitted from L transitions are always less energetic than those emitted from K transitions. Synchrotron x-ray fluorescence (SRXRF) imaging is a powerful technique which exploits the spectrally pure and finely focused X-ray beam from a synchrotron. It has opened up new application modes such as trace element analysis, sur face analysis, chemical state analysis and microanalysis [165]. Digital images of microscopic or nanoscopic samples are built, pixel by pixel, by scanning the sample through the beam. The resulting X-ray fluorescence radiation is characteristic of the chemical elements at that pixel. Mathematical deconvolution of the fluorescence spectrum reveals the chemical composition, from which quantitative elemental images of the sample are assembled. They are often displayed as false-colour maps. The combination of high flux and low emittance provided by synchrotron sources has proved to be crucial for the enormous success of experiments in the field of synchrotron-based X-ray fluorescence. It can be applied to solid and liquid samples. Its application to biomedical research can provide robust qualitative data about the behaviour and effect of metals and metalloids. The mapping capability essentially provides a picture of the elemental distribution within the material, which very easily provides a tremendous amount of information. In biological applications the maps may give a direct and clear observation of multiple element occurrences in different regions of the sample. Elemental maps depicting the subcellular distribution and concentration of a certain element have great potential in biomedical research, thanks to a low detection limit and the high spatial resolution of synchrotron X-ray fluorescence microscopy.

One approach to get a more comprehensive view of the role of elements like Se in the tissular and cellular physiopathology is to study their heterogeneous distribution quantitatively and their chemical local environment. This knowledge, however, is largely “static” as we still do not have appropriate sensitive approaches to follow fluctuations in normal metal homeostasis that accompany processes

of development, differentiation, senescence and stress responses, etc. The present study was undertaken to find out Se distribution within articular cartilage at the tissular and cellular level as we were expected to get some useful information to guide further experiments (RT-qPCR, immunohistochemistry, selenium speciation...). To the best of our knowledge this is the first report in the literature of spatially resolved imaging of Se distribution within articular cartilage tissue sections. According to ICPMS results, bulk Se concentration is extremely low (few hundred ppb in average) while detection limits for Se at the nano-analysis ESRF beamline ID16B is ~ 600-700 ppb level for 100 ms acquisition time and down to ppb for 500 s acquisition time with ~ 50 nm focused X-ray beam [166]. Despite the high flux of the synchrotron X-ray nanobeam, imaging Se in cartilage remain an extremely challenging task.

13.3 Methods and Materials

13.3.1 Samples Preparation

The samples, described section 10, were processed after three weeks cultures. The explants were first snap-frozen in precooled hexane and cryoembedded into cryomatrix prior to be sectioned using a cryostat. This procedure allows to preserve as much as possible the structural ans the chemistry of the tissues. The cryo-section of 20 μm thickness were used for X-ray fluorescence (XRF) microscopy and deposited on ultralene XRF 4-μm foil covered PEEK slides. The slides were stored at -80C and were slowly brought to room temperature in an isobox in presence of desiccant. Cryosections have been used to avoid as much as possible the potential residual trace coming from other diverse long embedding processes (paraffin or resin embedding).

13.3.2 Set-up & Parameters

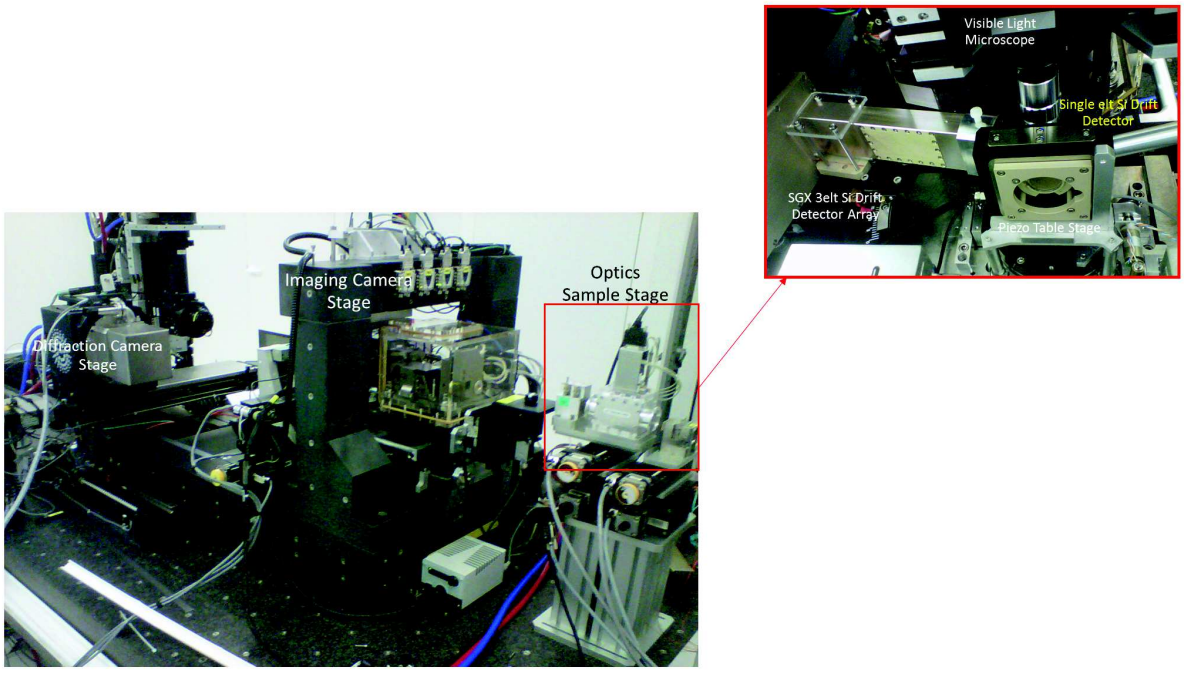

Figure 32: Current ID16B set-up with an SGX 3elt Si Drift Detector Array

The ESRF ID16B-NA beamline was used to image, at room temperature, the elemental distributions in the cartilage tissue cryosections prepared as describe above. The long distance between the experimental station and the X-ray source at this beamline, combined with a high demagnification Kirkpatrick-Baez (KB) focusing mirror system, yields a spot size focused down to 50 by 50 nm. In the present work, a 0.2 μm X-ray step size was used for highest resolution maps of single chondrocytes. The size of the illuminated area on the sample can be varied by slightly defocusing the sample (~ 1mm along the beam axis) resulting in our case in a 1 μm X-ray beam. This procedure was used to perform coarse mapping over a 100 μm x 100 μm region of interest of the cartilage sections. The energy of the incident X-ray photons is 17.5 keV ($\pm$1%) with a photon flux of approximately 2×1011 ph/s. A pierced mirror microscope is used to monitor online the sample positioning and to define the scan areas. The incident X-ray beam is oriented perpendicularly to the scanning plane defined by the sample positioning system, requiring the large solid angle 3-element SDD detectors to be positioned slightly off the ideal angle of 90° to the primary beam (13° deviation). The effect of this offset is limited, since the centers of the multi-element detectors are still placed in the plane of polarization; the outer detectors have a deviation of 26°. The dwell time was optimized to achieve an optimal tradeoff between short measurement time and adequate statistics and was put at 0.1 s/point.

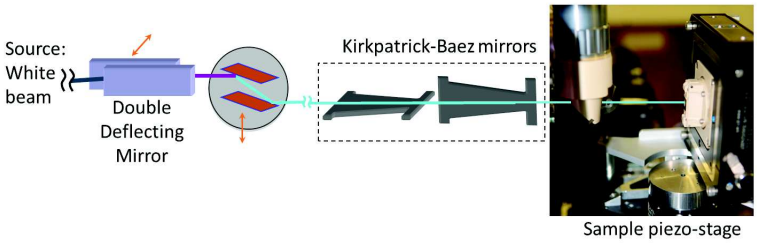

Figure 33: Optical path of X-ray beam.

13.3.3 Data Analysis

Interpretation of fluorescence data was conducted using PyMca, an ESRF code [167], based on a nonlinear least-squares fitting procedure which optimizes zero, gain, noise, and Fano factors for the entire fitting region and for all XRF peaks simultaneously. This allowed the background contribution to be removed, facilitated analysis of overlapping peaks, and accounted for the eventual escape or sum peaks. The background was estimated with the strip background model. Computed X-ray line intensities were normalised to the value of the incident photon flux.

13.4 Results

To the best of our knowledge, there are no studies that report the spatial distribution of Se in a cryosection of articular cartilage. The same conclusion can be drawn with regards to our study of Se bulk analysis of articular cartilage. Indeed, as shown in section 12, Se within the whole cartilage explants is of the order of few hundred ppb (μg/kg). In order to perform a X-ray fluorescence imaging and nanoanalysis, as for any experiment on Synchrotron, we submitted a project for peer-review at Diamond Light Source, the ESRF; we could not apply at the nanoprobe beamline Nanoscopium at Soleil in Paris because it was not open at that period. We had been granted three days of beamtime at the ESRF on the nano-analysis beamline ID16B. Using the X-ray fluorescence nanoprobe, it has been possible to observe the localisation of Se through mapping of 20 μm-thick cryosections. Eight samples have been analysed (ITS Control and ITS FT-treated). The technique requires long data acquisition

times despite improvement in scheme of data collection (continuous scan analysis) and in detection capabilities (the use of multielement energy dispersive detector provide larger solid angle and achieve high count-rate capability). This results in detection limits at ID16B of 6.28 ppm (i.e. μg/g) for Ca and 0.75 ppm for Zn and ~600-700 ppb for Se for 100 ms acquisition time in a pixel of 50 nm x 50 nm on a biological sample as determined by Laforce *et al.* on a thin standard reference material NIST bovine liver 1577C [290]. Still, a compromise between acquisition time (determined by the XRF signal intensity), the size of the representative area to be scanned and the spatial resolution has to be chosen. This led us to scan representative area of the articular cartilage as a mosaic of 4 areas (100 x 100 μm^2, the maximum scanning range of the piezo-stage) with a spatial resolution of 1um for a total acquisition time of ~6-8 h. Similar elemental distribution is observed in all maps we acquired and a single representative area of 100 x 100 μm^2 is shown in Figure 34 and Figure 36. This preliminary study allows us to distinguish an interesting recurrent pattern of the selenium distribution within the tissue. This was observed for all maps and specifically located at chondrocytes site. This suggests that it cannot account for a contaminant. The fraction of Se that could be detected by the method appears to have a punctual distribution and possibly at pericellular location. The spectrum derived from these "Se-rich" regions indeed display a clear X-ray fluorescence emission Se peak relative to the Kα X-ray emission line as shown in Figure 38. This is further confirmed with higher resolution scan of single chondrocytes (0.2 μm spatial resolution and 1s integration time/s) where the same punctual Se location is detected as shown in Figures 35 and 36. For other elements specific patterns are observed. Phosphorus and zinc distribution in cells are reported to be representative of the cell nucleus location; indeed they are mainly detected in part of chondrocytes that we can assume to be the nuclear location (Figure 37). Phosphorus distribution can be assigned to the nucleic acid content in the nucleus and as such can be used to identify the location of the nucleus. As expected sulphur (S) distribution depict well the surrounding ECM and only a very weak S contribution is observe within the chondrocytes lacunae (Figure 37). Interestingly, we show that Ca (the technique can only account for total Ca and in the case of such tissue preparation it is mainly Ca intracellularly bound) seems to correlate to the chondrocytes nuclear location while iron (Fe) appears to be more cytosolic (Figure 37). The presence of Fe in a non-negligible concentration is quite unusual and deserves further studies.

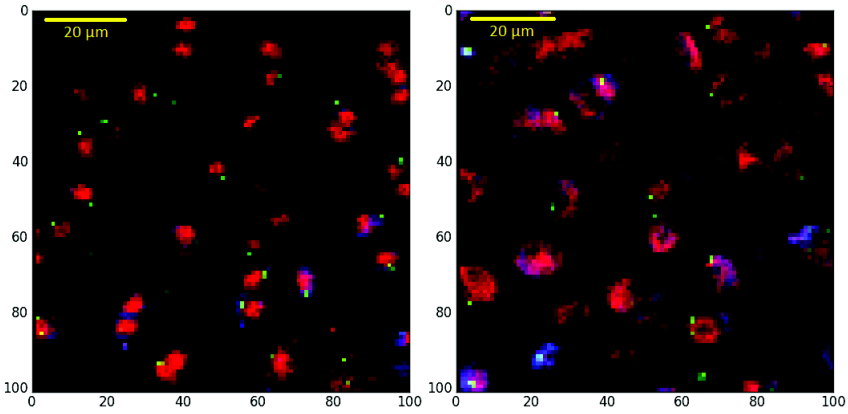

Figure 34: Selenium Localisation within the articular cartilage tissue using micro-XRFS. The Zn is represented by the red distribution, the Fe by the blue one and the selenium by the green one. The left figure corresponds to the ITS-Control sample and the right one to the ITS-FT-treated sample. Both exposed the same Se-distribution pattern. Map zones 100x100 $\mu m^2$with 1s per pixel for acquisition time.

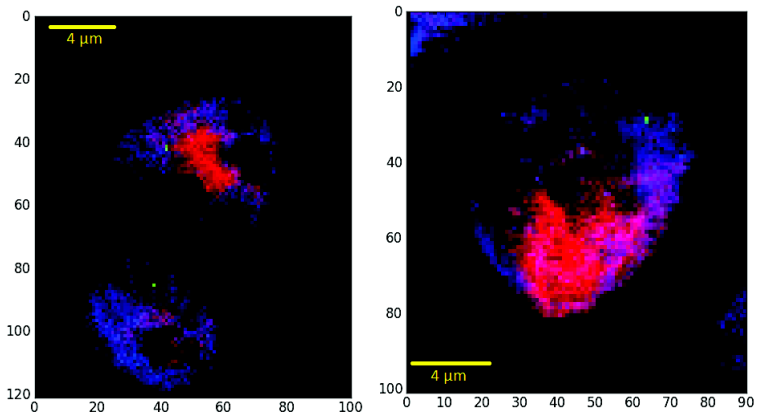

Figure 35: Selenium Localisation within the articular cartilage tissue using micro-XRFS. The Zn is represented by the red distribution, the Fe by the blue one and the selenium by the green one. The figures correspond to cells of the ITS FT-treated sample (right zone: 24x20 μm^2 and acquisition time of 500ms per pixel; left zone: 20x18 μm^2 with acquisition time of 700ms). A precise and unique location of the selenium location on a cell is observed for almost all cells.

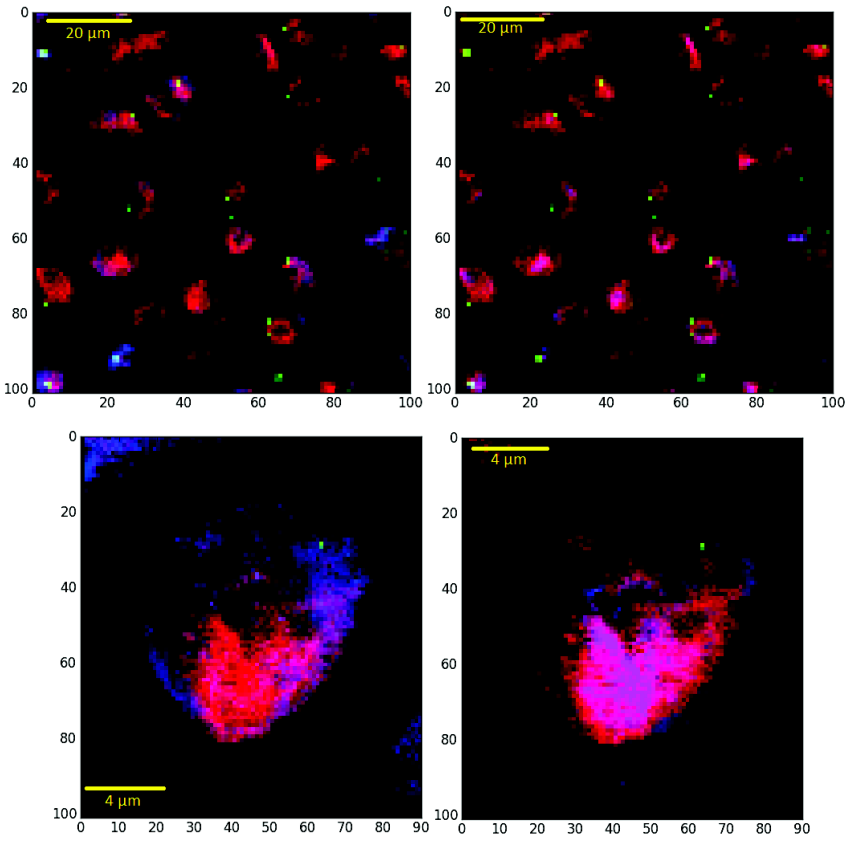

Figure 36: Selenium Localisation within the articular cartilage tissue using micro-XRFS. The Zn is represented by the red distribution, the Fe or Ca by the blue one and the selenium by the green one. The figures correspond to the ITS FT-treated sample. The left figures exposed the Fe location and on the right the calcium location in blue. In the upper figures, a zone of 100x100 μm^2 with an acquisition time of 1s to have a global overview of the distribution. In the bottom figures, a zone of 20x18 μm^2 with an acquisition time of 700 ms, centred on a cell.

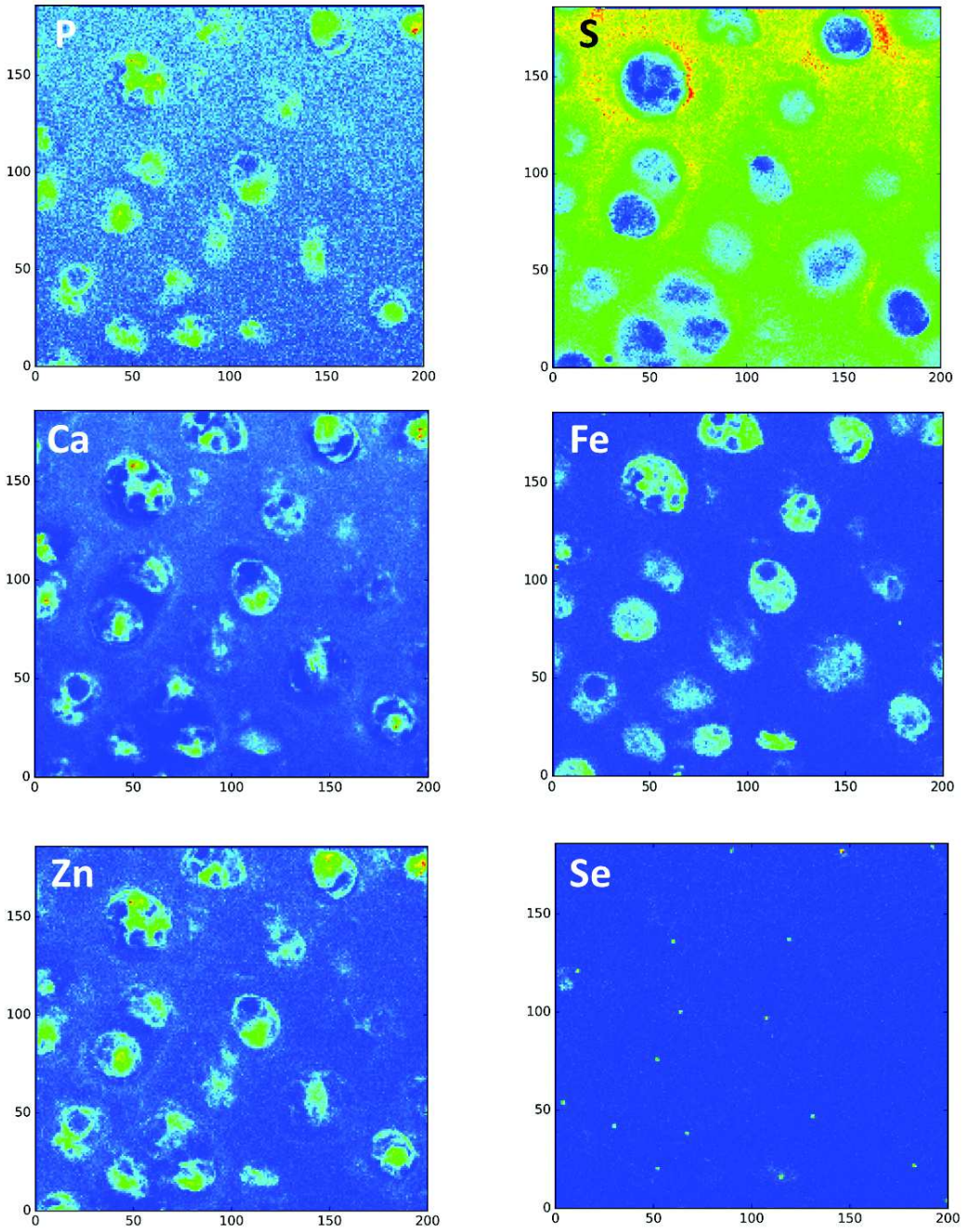

Figure 37: Distributions of different elements within articular cartilage tissue using micro-XRFS. The figures correspond to ITS FT-treated sample. From the upper left to the bottom right: distributions of Phosphorus (P), Sulphur (S), Calcium (Ca), Iron (Fe), Zinc (Zn) and Selenium (Se). These maps have a size of 100x100 μm^2 and have been made with an acquisition time of 1s and step size of 0.5 μm.

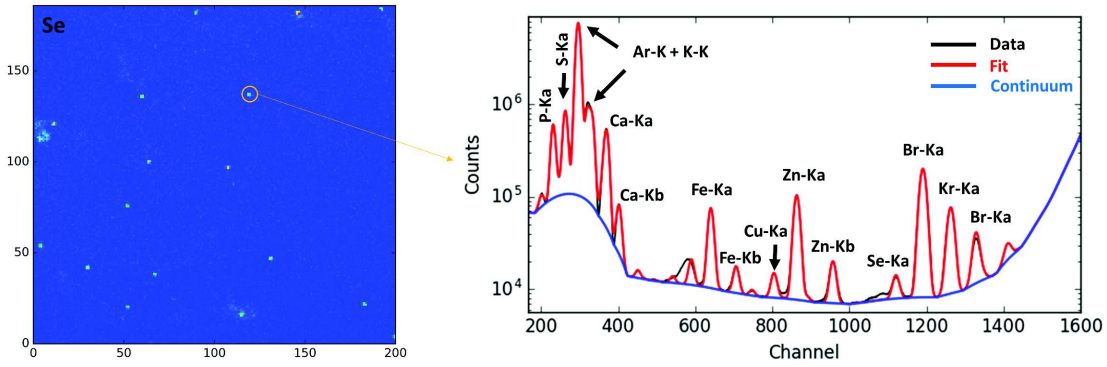

Figure 38: Selenium Distribution in ITS FT-treated sample and the corresponding spectrum refering to the global selenium expression in this samples. These maps have a size of 100x100 μm^2 and have been recorded with an acquisition time of 1s and step size of 0.5 μm.

14 Selenium Speciation with High Energy Resolution Fluorescence Detected X-ray Absorption Spectroscopy

The speciation of highly-diluted elements by X-ray absorption spectroscopy in a diverse range of materials is extremely challenging, especially in biological matrices such as cartilage. Here we present an innovative synchrotron spectroscopy analysis, namely high energy resolution fluorescence detected X-ray absorption spectroscopy (HERFD-XAS) coupled to an array of crystal analyzers, which provides, for the first time, a clear demonstration of selenium speciation at concentrations of few hundreds of ppb (μg/kg) within articular cartilage. This is a major advance in the speciation of highly-diluted elements through X-ray absorption spectroscopy and opens new possibilities to study the metabolic role of selenium and other elements in mammalian cells and tissues.

14.1 Background

Selenium (Se) is a dietary oligo-element essential for human health, with biological activities and toxic effects that are dependent on the total Se concentration and also on its chemical form [60]. Distinct chemical forms can be studied through X-ray absorption spectroscopy (XAS), an in-situ speciation method that can define elemental species according to their redox state and through metal-ligand information. Through XAS, the presence of elements such as Se in tissue can be fingerprinted in various organic or inorganic forms [168]. Importantly, the sample preparation for XAS is minimal, with samples being kept in a frozen hydrated state in an anoxic environment prior to analysis at cryogenic temperature allowing preservation of elemental species integrity, which is critical for redox sensitive elements such as Se. Samples can be investigated close to their natural, hydrated state with such cryogenic approaches that also contribute to reducing radiation damage. In this regard, XAS contrasts with hyphenated methods such as chromatography-mass spectrometry that are prone to speciation changes during multi-step sample preparation and analysis.

XAS sensitivity is however a problem as practical detection limits are only in the order of a few parts per million (mg/kg dry weight) compared to hyphenated techniques, for example high performance liquid chromatography-mass spectrometry, that have at least one order of magnitude lower detection limits, and allow detection of specific molecules [169-171]. Therefore, lowering the detection limits of XAS for elemental species to concentrations in the range of μg/kg or part per billion (ppb) is a major goal and challenge in analytical chemistry. Successful development would have direct implications in various fields such as biology, as toxic elements including arsenic, cadmium, lead or mercury as well

as elements of physiological importance such as manganese, copper or Se typically occur in cell and tissues in the low ppb concentration range.

Thus far, direct speciation and concentration of Se in cartilage have never been reported most probably due to a lack of in-situ methods with the required sensitivity. Our interest in analysing Se stems from its role in articular cartilage physiology, and in particular, the relationship between osteoarthritis and Se deficiency [9]. Kashin-Beck disease (KBD) is a multifactorial endemic osteochondropathy leading to short stature and cartilage degeneration, and coincides with a diagonal land belt crossing northeast and southwest China exhibiting low Se levels [2,115]. Selenium is incorporated in proteins through the amino acids selenocysteine, selenomethionine and methylselenocysteine. Selenocysteine has been shown to act as a co-factor in the reduction of antioxidant enzymes such as glutathione peroxidase and the redox-sensitive functions of selenoproteins during growth and differentiation [115]. The low bioavailability of Se is thought to be an important contributor to the etiology of KBD [5], as demonstrated through the deletion of the Trsp gene encoding selenocysteine tRNA in mice, which results in musculoskeletal abnormalities that closely resemble KBD [115]. The latter work, and observations of KBD pathology in humans show that many of the manifestations of disease appear during the process of postnatal skeletal maturation. We have developed a High Energy Resolution Fluorescence Detected X-ray Absorption Spectroscopy (HERFD-XAS) technique and used it to investigate an *in vitro* model of articular cartilage postnatal maturation in order to understand the role of selenium during this critical phase of cartilage development and relate these findings to pathological conditions such as KBD or osteoarthritis.

14.2 Methods & Materials

14.2.1 Sample Preparation

We used a model of maturation of the articular cartilage based on 3-weeks *in vitro* culture of cartilage explants obtained from the metacarpophalangeal joint of 7 days-old bovine (cf section 10). The samples were snap-frozen in precooled hexane and underwent an ultra-thin cryo-milling (during 2 min at 2500 RPM) in order to obtain a highly homogeneous fine powder easily transferred as a pellet to the sample holder of the He-cryostat for HERFD-XAS.

14.2.2 References Preparation

All the samples have been prepared in order to contain 1% Se in the solid or liquid references. The complete list of the references (solids and liquids) are presented in Table 48. Samples have been analysed in fluorescence mode for the analysis of ultra-diluted matrix. The solid powder was mixed with boron nitride (BN) powder and the liquid references have prepared with an ultra-pure water.

Selenium Reference Compounds:

a) Se^{VI} (Sodium) selenate, from Sigma-Aldrich (Sodium selenate, ref. S8295-10G)

b) Se^{IV} (Sodium) selenite, from Sigma-Aldrich (Sodium selenite, ref. S5261-10G)

c) Se^{-II} (Sodium) selenide from Sigma-Aldrich (Sodium selenide, ref. 796948-100MG)

d) Se-glutathione peroxydase, from Sigma-Aldrich (Glutathione peroxidase from bovine erythrocytes, ref. G6137-100U)

e) Se-methionine, from Sigma-Aldrich (Seleno-DL-methionine, ref. S3875-25MG)

f) Se-cysteine, from Sigma-Aldrich (Se-(Methyl)selenocysteine (hydrochloride), ref. M6680-100MG)

g) Selenodiglutathione – synthesis from L-glutathione and Sodium selenite (see receipt below)

h) Se-cystine, from Sigma-Aldrich (Seleno-DL-cystine, ref. S1650-25MG)

i) Se-cystamine dihydrochloride, from Sigma-Aldrich (Selenocystamine dihydrochloride S0520-25MG)

j) Se-urea, from Sigma-Aldrich (Selenourea, ref. 230499-1G)

k) (Elemental) Se^0 red from bacterial production, kindly provided by Geraldine Sarret

l) L-glutathione reduced, from Sigma-Aldrich (ref. G6013-5MG)

Selenodiglutathione Synthesis has been performed as described in the paper of Sarret et.al 2015 by mixing sodium selenite (compound b) and glutathione (compound l) with a molar ratio of 1:4 in a dilute 1M HCl solution for a final pH of 1.3.

14.2.3 X-ray Absorption Near Edge Spectroscopy

The X-ray absorption spectroscopy, also called Near edge X-ray Absorption Fine Structure (NEXAFS), is based on the light-matter interaction. XANES is an element-spectifc and local bonding-sensitive spectroscopic analysis. It allows the determination of the partial density of the empty states of a molecule which indicates its speciation. Actually, X-rays are ionizing electromagnetic radiation that have sufficient energy to excite a core electron of an atom to an empty below the ionization threshold called an excitonic state, or to the continuum which is above the ionization threshold. As described in the atom theory, each core electrons possesses a distinct binding energy. Consequently each element possesses a significative "signature" of this absorbance [175].

When an X-ray photon is absorbed from a core electron (X-ray absorption see Figure 39), this electron is ejected and generates a hole in this core shell. This core hole of the internal atomic shell is extremely energetic, and its state is highly unstable. The technique is firstly based on the scattering of photoelectron ejected from the absorbing atom by the photo-electric effect as described by the Einstein's equation:

$$E = h\nu = \frac{hc}{\lambda} \text{ with } h = 6.62606957.10^{-34}\,\mathrm{m^2.kg.s^{-1}} \tag{8}$$

where E is the energy of the (incident) photon energy, h is the Plank's constant, c the speed of light $c = 3.10^8\,\mathrm{m.s^{-1}}$, $\nu = \frac{1}{\lambda}$ the frequency of the electromagnetic wave associated to the photon. A core holes can also be created when a core electron only absorbs a part of an X-ray photon's kinetic energy, which is related to the X-ray Raman scattering. This unstability has to be balanced and consequently, an electronical cascade takes place to fill this hole. This decay/relax process of a highly excited core hole can be visualised through two ways: Auger electron emission or X-ray fluorescence (see Figure40). For higher-energy excitation (e.g., for the K edges of elements with atomic numbers greater than 40 such as Selenium), X-ray fluorescence is the primary relaxation process.

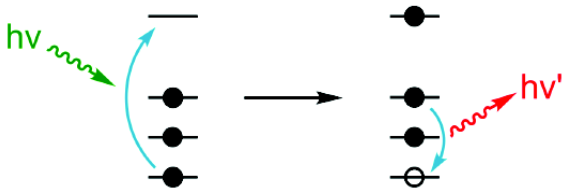

Figure 39: X-ray fluorescence process

The X-ray fluorescence intensity A is described by the following equation:

$$A = (\frac{I_F}{I_I}) \tag{9}$$

where $I_I$is intensity of the incoming photon and the I_F is the intensity of the outgoing photon. The intensity of X-ray fluorescence is directly proportional to the X-ray absorption cross-section of the sample. It is important to remind that other multiple (sample) scattering (such as compton scattering) can contribute generating other X-ray fluorescence signals and have to be taken into account to justify some uncertainties. In order to improve the sensitivity, energy-resolving solid-state fluorescence detectors or analyser crystals (as in the following case due to the highly diluted Se concentration in the matrix) are used to selectively distinguish background radiation from signal of interests [176].

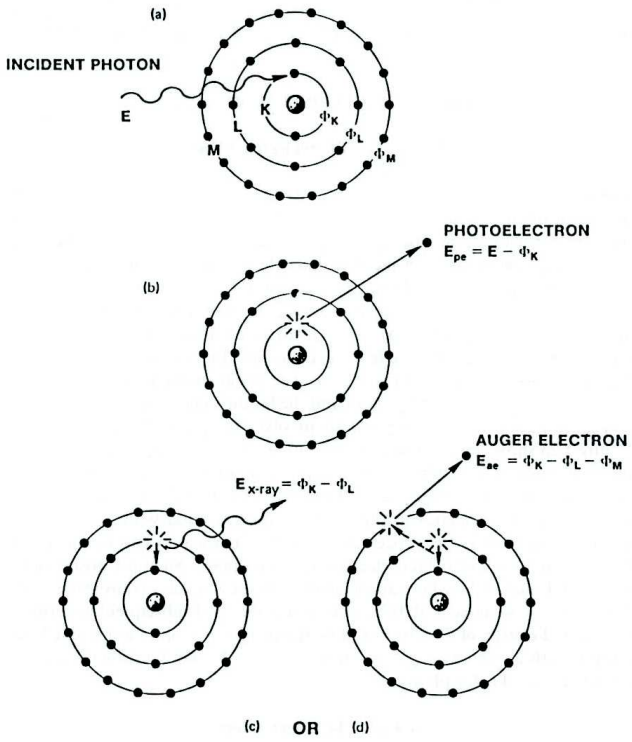

Figure 40: Photoelectric effect and Auger relaxation. From [James R. Connolly. Introduction to x-ray powder diffraction [283]. Legends: (a) incoming photon with a specific energy, (b) photoelectron extraction, (c) relaxation process by means of "secondary x-ray production", (d) relaxation process by means of Auger electron emission.

This technique is also related to another phenomenon: the absorption edge. A sudden increase of absorption appears as soon as the energy of X-ray radiation is scanning through the binding energy regime of a core shell. This corresponds to absorption of the X-ray photon by a specific type of core electrons and this "jump" is called absorption edge in the XAS spectrum due to its vertical appearance. These absorption edges energies in X-ray absorption spectra informs about the specific identity of corresponding absorbing elements. The X-ray absorption spectrum is highly complex (see Figure 41). Actually, there are some weak transitions below the absorption edge, on the so-called pre-edge structures. Some specific significative absorption features also frenquently appear in the closest neighborhood of the absorption edge. The structure found in the immediate neighborhood of the absorption edge, is referred to as X-ray Absorption Near Edge Structure (XANES). Beyond XANES, the oscillatory structure cause by the interference between the outgoing and the back-scattered photoelectron

waves is identifed as Extended X-ray absorption Fine Structure (EXAFS) [177].

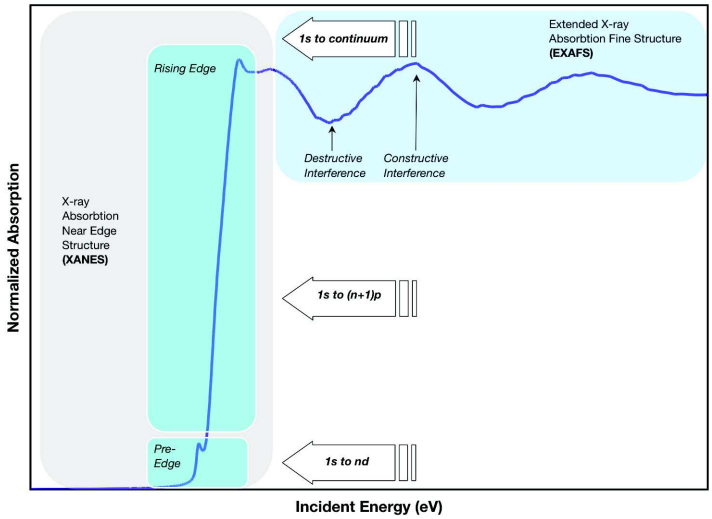

Figure 41: XAS example spectra with a pre-edge, rising edge, XANES ans EXAFS regions

These (structural) transitions respond to specific conditions called the dipole selection rule. XANES technique is interested by the angular momentum of the unoccupied electronic states which can be bound states or unbound states (continuum), discrete or broad, atomic or molecular. The dipole selection rule for determination of allowed transition is provided by $\Delta l = \pm 1, \Delta j = \pm 1, \Delta s = 0$ (see Figure 42). Just as a remark, regarding to the element (Se) concentration within the biomatrix (highly diluted matrix) of interest, the following experiment will be focused on the XANES part of X-ray absorption spectrum. In the XANES spectra, the absorption edge can lead to a sharp intense peak called "white line". The position of this "white line" will allow to identify the major Se-specie present within the samples.

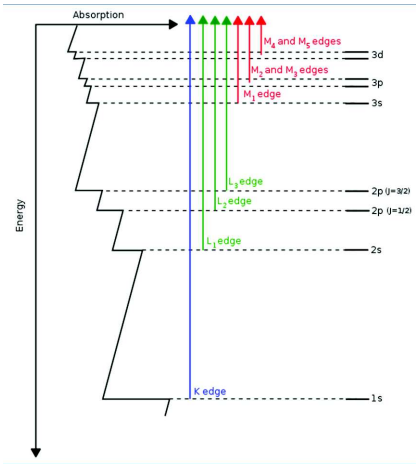

Figure 42: Illustration of possible electronical transition in metal atom. The major transitions are notified by the k,L and M edge and for L and M-edges additional transitions are present corresponding to the fine structures of the atom.

XANES data can provide two types of complementary information: the oxidation state sensitivity and the bound state transition. As notified in the electrostatic model, when an atom has a higher oxidation state, it will require more energetic X-ray to excite its core electron because the nucleus is less-shielded and carries a higher effective charge. This simply means that when the absoprtion

site possesses an increasing oxidation-state, the absorption edge energy also increases. However, this principe is not the only parameter to interprete the edge energies. Actually, the edge features can be visualized as continuum resonance which correspond to a short lived of the excitation process. The core electron has been excited into a higher energy state that is usually above this continuum. Consequently, it is possible to state that XANES region is oxidation sensitive. The XANES region is quite sensitive to small structural variations. This is related to the important multiple scatterings appearing in the XANES region because geometrical differences between sites alter the multiple scattering pathways and exacerbate the detailed structure in the immediate vicinity of the absorption edge.

Furthermore, weak pre-edge structures usually result from bound state transitions. Usually, the pre-edge structures prior to K edges of first row transition metals arise from 1s to 3d transition when the 3d orbital is not fully occupied. Even if the dipole selection rule excludes the 1s to 3d transition, it is possible to observe it due to the 3d to 4p orbital mixing induces a direct quadrupolar coupling. When the 3d to 4f mixing improves, the 1s to 3d transition increases which induces a another goemetric type of the absorption site, distorting away from a centrosymmetric geometry. Consequently, the 1s to 3d transition can be utilized as a tool to probe the molecular geometric properties of the absorption sites.

14.2.4 Set-up & Parameters

BM30B beamline developed High Energy Resolution Fluorescence Detected X-ray Absorption Spectroscopy (HERFD-XAS). This method is based on an array of crystal analyzers as a new highly sensitive in-situ XAS method for sub-ppm speciation, breaking the ppm concentration barrier for speciation while keeping the sample close to its natural, hydrated state. A schematic of the experimental setup of the CRG-FAME beamline (BM30B) at the European Synchrotron Radiation Facility (ESRF, France) is shown in the upper part of the figure 43.

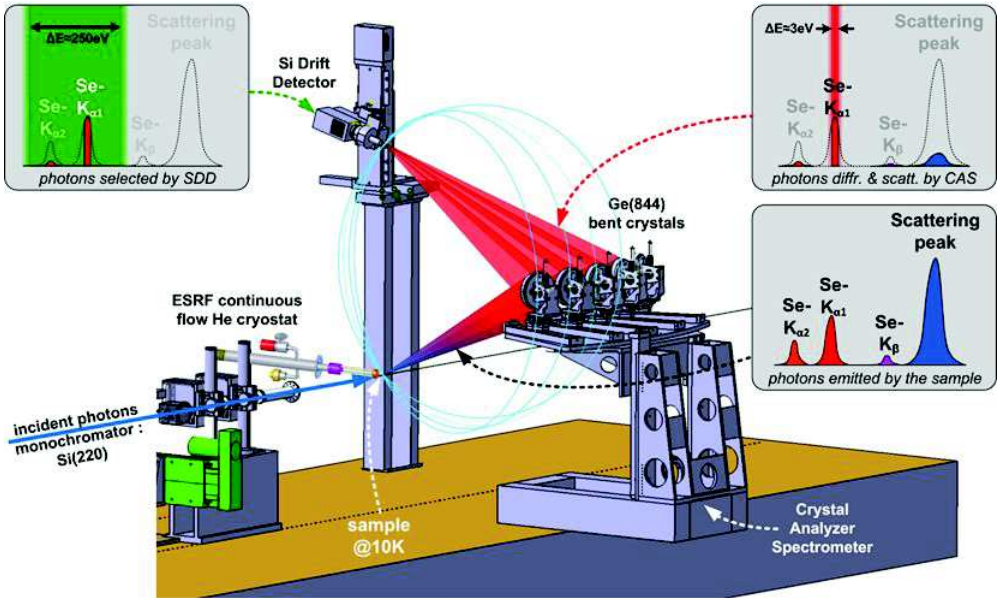

Figure 43: Schematic of the HERFD-XAS experimental set-up on CRG-FAME beamline (BM30b, ESRF, Grenoble, France) by Olivier Proux. A miniature small continuous flow helium cryostat from ESRF Sample Environment Support Service was used to cool down the samples and to protect them from radiation damages and potent photoreduction effects [180].

The X-ray produced by the 6 GeV ESRF storage ring operated with a maximum current of 200

mA, are tuned through a double crystal monochromator surrounded by 2 mirrors [178]. The size of the monochromatic beam on the sample was around 300x100 μm^2 (Full Width Half Maximum - FWHM, Hor. x Vert. (HxV)). The first crystal of the monochromator is liquid nitrogen cooled in order to optimize both the flux and the energy resolution of the incident beam [179]. Energy resolution is then close to the intrinsic resolution of the Si(220) reflection, i.e. around 0.65eV at the Se K-edge. The two mirrors at 3mrad (Si mirrors covered by an Rh layer) allow to suppress higher harmonics. The incident and transmitted beam intensities were measured with Si diodes. A continuous flow helium cryostat [180] was used to cool down the samples at 10K to further reduce potent X-ray radiation damage and photo-reduction. No beam effects were observed on selenium compounds measured previously at 300K on the same beamline, i.e. with the same photons flux on the sample [168], and therefore, that the spectra we obtained at 10K are free from any radiation damages.

HERFD fluorescence signals were measured using a crystal analyzer spectrometer (CAS) in the Johann geometry [171,182]. The set of crystals were provided by XRS TECH LLC Company (Freehold, NJ, USA) and Saint-Gobain Crystals (Nemours, France). The spectrometer was equipped with 4 spherically bent Ge(844) crystals in a Rowland geometry (Llorens 2012). Crystals had a 1m radius of curvature. The spectrometer was aligned at the maximum of the Se-$K_{\alpha 1}$ fluorescence line (11.222 keV, Bragg angle: 73.09°). A helium bag was used to limit the absorption of the fluorescence signal on the path sample - crystals - detector (~2m length). Photons diffracted by the spectrometer are focused on a Silicon Drift Detector (energy resolution: 250 eV). The narrow energy bandwidth of the CAS allows to filter out all unwanted X-ray events (mainly scattering processes) from the Se fluorescence signal (diffracted by the crystals), improving the signal-to-background ratio. The total energy resolution of the setup including both the spectrometer, for the emission photons, and the monochromator, for the incident photons, was 3.0 eV as measured from the pseudo-elastic peak (Figure 44). A comparison between conventional XAS measurement (obtained in the transmission mode) and HERFD XAS (obtained by measuring a fraction of the Se-$K_{\alpha 1}$ fluorescence line with a 3.0 eV energy resolution) is given on Figure 44.

The first observation is that the resolution of the HERFD-XAS spectra is better than that observed with conventional-XAS, as can be seen by comparing the characteristic widths of the energy levels involved. This is an effect that has been extensively explained previously [183-184]. In conventional-XAS, the final state has a 1s core–hole with an energy width of 2.33 eV [185]. In HERFD-XAS, the Kα1 fluorescence line corresponds to $2p_{3/2}$ to 1s transition (to fill the 1s core–hole created during the absorption process). In this case, the final core–hole is $2p_{3/2}$, the characteristic width is then 1.0 eV [185]. The improvement in the spectral resolution is (i) a direct consequence of the difference between the final state widths and (ii) an effect of the energy resolution of the CAS which allows to select between all the final state interactions. The second observation is that the pre-edge of the raw HERFD-XAS spectra is close to zero (insert on Figure 44). The narrow energy resolution of the CAS allows selection of only the photons with the appropriate energy, with almost no background. Even if the signal of interest is very small, which is the case when the probed element is highly diluted, the very limited background allows spectra with a good signal-to-background ratio to be obtained (Figure 45 and Table 46). The shape of the edge is sharper in HERFD-XAS mode than in classic CAS mode (Figure 44) which allows better extraction of the signal of interest from the pre-edge in the first mode.

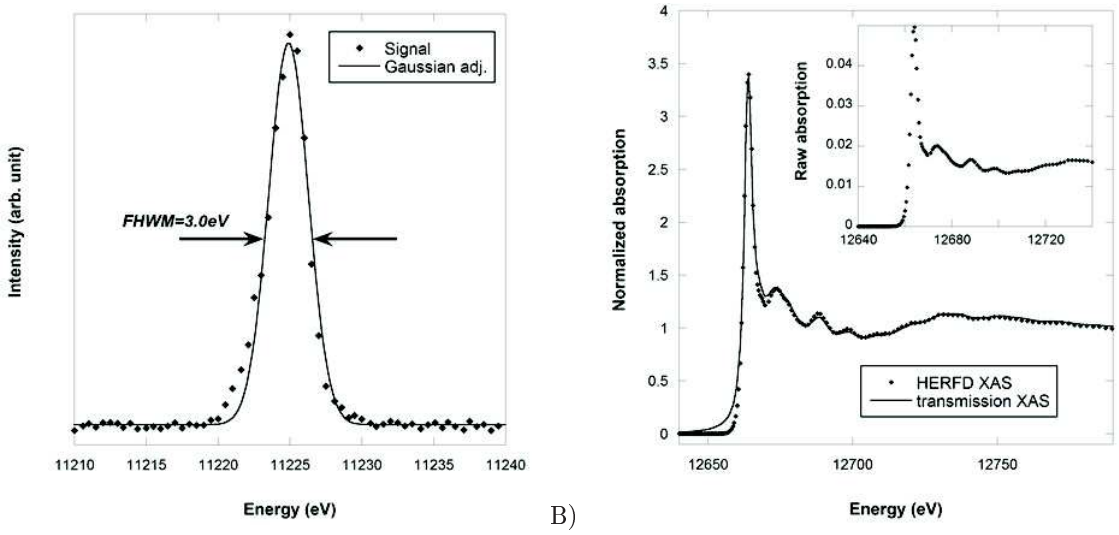

Figure 44: *A)* pseudo-elastic peak used to measure the energy resolution of the CAS. *B)* selenite spectra obtained in HERFD (dots) and transmission (line) modes. *Insert on the right figure*: raw spectrum obtained in HERFD mode.

At such concentration XAS techniques are not effective while we demonstrated good signal-to-noise ratio spectra with the present HERDF-XAS techniques. This allow to unambiguously identify major Se species present in cartilage in this model of maturation using a library of organic and inorganic Selenium-based reference compounds.

14.2.5 Data Analysis

An average spectrum of each sample was composed of up to hundred scans to improve the signal/noise ratio. Data reduction of the XANES spectra involved energy calibration and normalization.

Peak Fitting: The XANES signal presents two components, 1) the edge (or threshold) itself and 2) well-defined peak(s) before the edge (pre-edge peaks) and/or after (the so-called “white-line, the intense peak after the edge).

1) The shape of the rising edge is usually assumed to be determined by the limited lifetime of the 1s core hole (for the K-edge) which has a Lorentzian shape. The edge is then the sum of all the transitions between this 1s level and the continuum states, i.e. the integral of a Lorentzian function, so an arctangent function. This function is used since a long time to describe conventional XAS process [186]. However, if the limiting resolution factor is not the core hole lifetime but the energy resolution of the spectrometer (which has a Gaussian shape), the edge can be seen as the integral of a Gaussian function, the so-called "error function". Practically, the shape of the edge is the consequence of both phenomena. For HERFD-XAS measurement, we have seen that the energy resolution of the spectrometer is the limiting parameter, not the initial and final states lifetime. In this case the edge shape should be then better fitted by an error function.

The transitions between the core hole and the localized states, which can give pre-edge and/or edge features such as the white-line (the intense peak after the edge) are usually adjusted with a Lorentzian or a Voigt function.

XANES have been fitted using Demeter software [187]. On this software, the two previously described step-like functions can be chosen to take into account the absorption edge, arctangent or

error function. The white-line peak and the shoulder on the high energy side of the white-line can be adjusted with either Gaussian or Lorentzian function. The quality of the adjustment was quantified by the R_{factor} value:

$$R_{factor} = \frac{\sum_{E_{min}}^{Emax}[S_{data(E)} - S_{fit(E)}]^2}{\sum_{E_{min}}^{Emax}[S_{data(E)}]^2} \tag{10}$$

We adjust the data using different sets of functions. Examples of adjustments are shown for the spectrum "Se-Supplemented Control" sample, experimental spectrum and spectral decompositions are given on Figure 45, main data obtained with such decompositions are given on Figure 46. The main results of this systematic decomposition study are that (i) the error function is slightly better than the arctangent function to describe the edge (which is in accordance with the fact that in HERFD measurements the experimental resolution is the limiting parameter, not the core-hole lifetime, the R_{factor} ranged from $1.1.10^{-3}$ to $1.8.10^{-3}$ for the decomposition with the error function and from $2.2.10^{-3}$ to $3.4.10^{-3}$ for the decomposition with the arctangent, (ii) independently of the used functions, the positions of the white-line and the shoulder are found to the same values within the error bare of the adjustment. The results we obtain is not dependent of the analysis.

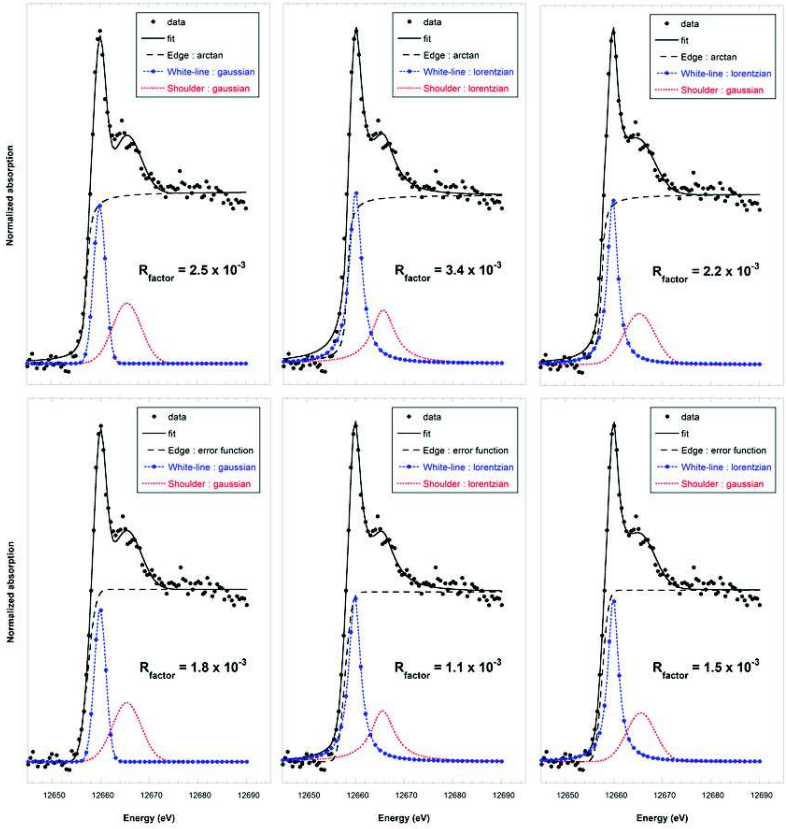

Figure 45: Example of spectrum decomposition using different sets of functions for the edge (Arctangent of error function) and the peaks (Lorentzian or Gaussian function). Data: spectra " Se-Supplemented Control"

Component		Edge	White-line	Shoulder	R_{factor} (x10^{-3})
1st adj.	Function	arctan	Gaussian	Gaussian	2.5
	Position (eV)	12657.4 (1.1)	12660.0 (0.4)	12665.6 (0.8)	
	area		2.28	2.10	
2nd adj.	Function	arctan	Lorentzian	Lorentzian	3.4
	Position (eV)	12658.2 (1.3)	12659.9 (0.6)	12665.6 (1.3)	
	area		3.83	2.29	
3rd adj.	Function	arctan	Lorentzian	Gaussian	2.2
	Position (eV)	12657.6 (1.2)	12659.9 (0.5)	12665.4 (0.9)	
	area		3.06	1.93	
4th adj.	Function	error function	Gaussian	Gaussian	1.8
	Position (eV)	12657.3 (1.0)	12659.9 (0.4)	12665.4 (0.7)	
	area		2.12	2.05	
5th adj.	Function	error function	Lorentzian	Lorentzian	1.1
	Position (eV)	12657.8 (0.8)	12659.9 (0.4)	12665.6 (1.0)	
	area		3.48	2.19	
6th adj.	Function	error function	Lorentzian	Gaussian	1.5
	Position (eV)	12657.6 (1.2)	12659.9 (0.5)	12665.6 (0.8)	
	area		3.09	1.70	

Figure 46: Main parameters deduced from spectrum decomposition using different sets of functions for the edge (Arctangent of error function) and the peaks (Lorentzian or Gaussian) . Example of the data analysis with the spectra "Se-Supplemented Control".

Linear Combination Fitting (LCF): In order to fit and identify the different component that composed the matrix of the analysed samples, linear combination fittings (LCF) have performed with Demeter (Athena) software [187] within an energy range of -20 eV below to $+40$ eV above the edge. LCF is a method that can be employed for the semi-quantification of oxidation states [252]. LCF is uded to reconstructs the sample spectrum using a combination of aselection of several reference spectra (reference that are already tabulated in the literature), and this combination of spectra should report a goodness of fit parameters (R_{factor} and reduced χ^2) along with the percent that each model contributes to the fit. The accuracy of this method depends on how well the spectra of the chosen reference compounds represent the components in the samples [187]. Every sample spectrum has to be fitted to the maximum number of standard spectra (usually no more that 5 reference spectra); the combination of standards that resulted in the best fit (smallest R_{factor} and reduced χ^2) was selected as the most likely representation of the sample. Combination that explained less than 5% of the fit were not considered.

Here, the references are coherent with several papers [168, 253, 254]. The most interesting analysis of the LCF for the sample set of data analysed is presented Figure 47 and Table 13.

Reference Compounds Samples	Selenodiglutathione	Selenocysteine	Glutathione Peroxydase	Se^{IV} selenite	R_{factor}(x10^{-3})
Se-Supplemented Control	76 %	-	-	24 %	9.5
Se-Supplemented FT-treated	74 %	-	-	26 %	13.4
ITS Control	47%	-	53%	-	28
ITS FT-treated	37 %	26 %	37 %	-	40.2

Table 13: The distribution of Se species determined by linear combination fitting of experimental spectra using the library of Selenium-based model compounds, described Figure 48.

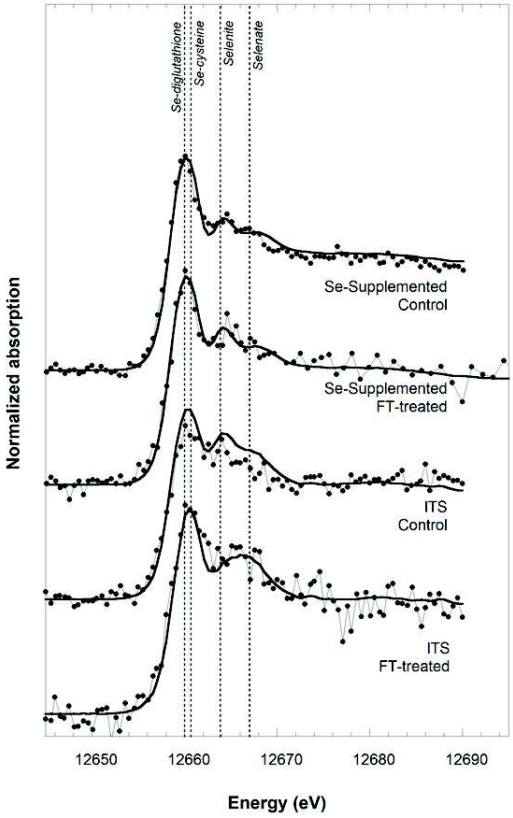

Figure 47: Linear combination fitting of experimental spectra using the library of Selenium-based model compounds, described Figure 48.

14.3 Results

Over the different experiments perfermed at FAME-BM30B beamline, a serie of Se-references has been realized: metals, biologic, as solid and liquid as described previously in the subsection 14.2.2. The goal of this experiment was to identify the selenium species present within articular cartilage explants cultured with different treatments in order to confirm or infirm our hypothesis "Selenocysteine should be a predominant Se-specie in articular cartilage because it is one of the main component of the selenoproteins". Using the new spectroscopic caracteristics of FAME beamline, high photon flux and analyser crystals detection systems, we measured high energy resolved fluorescence detected (HERFD) x-ray absorption near edge spectroscopy (XANES) spectra, from samples highly diluted ($<$ 2 ppm) and reference compounds. The HERFD spectra obtained for references (Figure 48) were successfully compared with the ones already measured by Sarret *et al.* [168]. The Figure 48 exposed their chemistry and spectral characteristics. This section has been used for the data analysis.Actually, hydrated samples have been analysed, nevertheless the dilution factor corresponding to the hydratation state of the sample correspond to a Se-concentration about 60 ppb reaching a limit in detection. Even if a trend and the step is present, a clear and statistically meaningful spectra was not achieved after 14h. This also explained why No Se samples were not analysed, their concentration being inferior at 200 ppb.

We tested this new method of Se speciation in an *in vitro* model of articular cartilage maturation where tissues undergo rapid remodeling to form adult-like tissue within three weeks, where the same process *in vivo* takes approximately six months. Cartilage explants from immature bovine metacarpophalangeal joints were cultured for 21 days in the presence of fibroblast growth factor-2 (FGF2) and transforming growth factor β1 (TGFβ1) to induce accelerated maturation [16]. For analysis, explants

were snap-frozen in precooled hexane and cryo-milled to obtain a homogeneous fine powder that was transferred under anoxic conditions to a He-cryostat for HERFD-XAS. Selenium concentration was determined by Triple Quadrupole Inductively Coupled Plasma Mass Spectrometry (ICP-QQQ, Agilent 8800) using MS/MS mode with hydrogen (H2) as reaction gas to avoid spectral interferences on Se at m/z 78, following acid digestion of the powdered samples, as described in the section 12.

Reference	State	Chemical representation	WL position (eV)
Se^{VI} (Sodium) selenate	Solid state	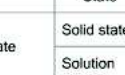	12667.1
	Solution		12667.1
Se^{IV} (Sodium) selenite	Solid state	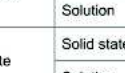	12664.0
	Solution		12664.0
Se^{-II} (Sodium) selenide	Solid state	Na_2Se 	12659.2 12663.7
	Solution	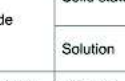	12664.0
Se-glutathione peroxidase	Solution	-	12664.8
Se-methionine	Solution	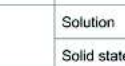	12661.3
	Solid state		12660.6
Se-cysteine	Solid state	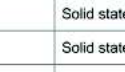	12660.7
Se-diglutathione	Solution		12660.0
Se-cystine	Solid state	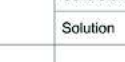	12660.0
	Solution		12660.0
Se-cystamine dihydrochloride $C_4H_{12}N_2Se_2 \cdot 2HCl$	Solid state		12659.8
Se-urea	Solid state	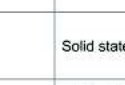	12659.4
(Elemental) Se^0 red	Solid state	Se-monoclinic	12659.1

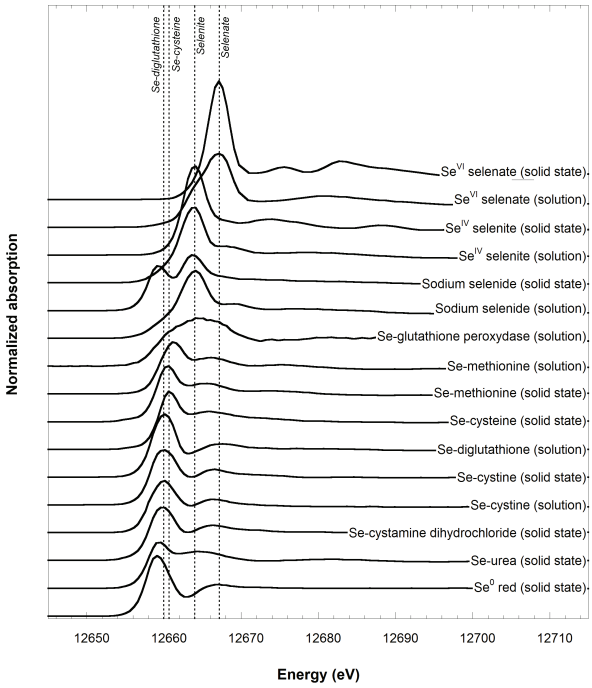

Figure 48: (*Left*) TTable of the database library of selenium compounds (organic and inorganic) analysed using 5 analyzer crystals. Selenium K-edge High energy resolution fluorescence detected x-ray absorption spectra of model Se compounds have been performed in solution and/or solid state. All references have been prepared in anoxic conditions. The references are presented with their oxidation state and their chemical representation. The position of the maximum of the white line is indicated in The WL-position column. (*Right*) Selenium K-edge High energy resolution fluorescence detected x-ray absorption spectra of model Se compounds (in solution except Se cysteine, in solid state) used in the linear combination fitting of experimental spectra.. The position of the maximum of the white line is indicated in parentheses.

Freshly isolated immature and mature cartilage had too low Se content (100-200 μg/kg or ppb, Figure 11) to collect good quality spectra with the current experimental set-up due to insufficient signal to noise ratios. Selenium content values for cartilage cultured in standard serum-free medium supplemented with insulin-transferrin-selenium (ITS) containing 6.7μg/L sodium selenite as the source of Se was in the range 400-500 ppb (Figure 11). In this concentration range, we demonstrated good signal-to-noise ratio spectra with our experimental HERDF-XAS techniques, whereas XAS method was not effective. We unambiguously identified major Se species present in cartilage using a least-squares fitting process of a linear combination of edge spectra from a library of inorganic and organoselenium reference compounds (Figure 48). The Se HERDF-XAS spectra of cartilage explants following culture-induced maturation was similar to untreated control explants. The biological activity of Se is related to its incorporation in the form of amino acid selenocysteine (Sec) into selenoproteins such as gluthatione peroxidase, iodothyronine deiodinases or thioredoxin reductase [69]. With Se concentrations as low as 400 ppb, we were able to identify alkyl selenide (RSeR) compounds (Sec and gluthatione peroxidase) as the major contributing components within the articular cartilage explants (Figures 49,

47 and 45). The importance of monitoring Sec levels is highlighted by studies showing the effects of deleting the Sec tRNA gene produce KBD-like phenotypes in mice, and, in humans where genetic polymorphisms in the gluthatione peroxidase-1 (GPX1) gene has been reported to be associated to higher risk of developing KBD [8].

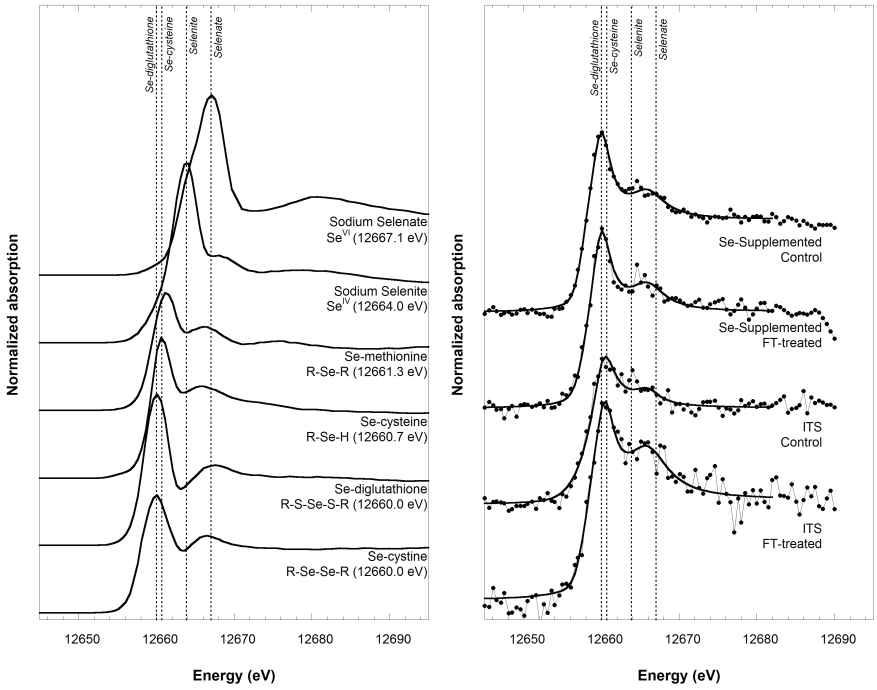

Figure 49: *Left:* Selenium K-edge High energy resolution fluorescence detected X-ray absorption spectra of model selenium compounds (in solution except the Selenocysteine in solid state) used in the linear combination fitting of experimental spectra. The position of the maximum of the white line is indicated in parentheses. *Right:* Selenium spectra of cultured cartilage explants which have matured *in vitro* during 3 weeks in medium supplemented with Insulin-Transferrin-Selenium (ITS) (which intrinsically contains 6.7 μg/L sodium selenite) [bottom spectra] or with both ITS and sodium selenite [upper spectra] for a total Se-concentration of 50 μg/kg, in presence (FT-treated) or absence (Controls) of growth factor . Energy calibration was achieved by setting the first inflection point of a Se metal foil K-edge spectrum at 12.658 keV. The scans were recorded in a step-by-step mode in the range of 12.6–12.8 keV and with a counting time of 15 s for each measured point. For each sample, between 2 (reference compounds) and 90 (diluted samples) scans were necessary to obtain an acceptable signal-to-background ratio.

The other contributing species is a thioselenide compound most probably in the form of selenodiglutathione (GSSeSG) (Figures 45 and 49). Selenodiglutathione is the major metabolite of selenite in mammalian tissues [188], an organic form of Se that is an important dietary source of Se [69]. Selenite and reduced glutathione spontaneously react to form GSSeSG, and reduced glutathione concentrations are known to be high in nearly all tissues [172]. Of note, GSSeSG is a highly reactive substrate for thioredoxin system [193], and recently it has been reported that thioredoxin reductase-2 deficiency induced impaired proliferation and chondrocyte cell death. This has been suggested to be another pathological mechanism for osteoarthropathy that occurs as a result of Se deficiency [194].

Dietary supplementation with sodium selenite (Na_2SeO_3) offers a potential treatment for KBD in children [195]. We noted that Se concentrations rose 5.5 -fold in cartilage cultured explants following 50 μg/L or 7.5 fold increase in sodium selenite supplementation in the culture medium when compared to normal culture conditions (ITS only), as quantified by ICP-QQQ analysis (Table 11). This is in line with the ~5 times greater Se-Kα X-ray fluorescence counts obtained in HERFD-XAS measure-

ments (data not shown). This is observed whether treated or not with growth factors. These results suggest that, under supplementation with sodium selenite, Se incorporation into tissues of articular cartilage explants reach some limits that are independent of the growth factor treatment known to regulate chondrocyte metabolism [196]. Under sodium selenite (oxidation state +4) supplementation, the fitting of Se HERFD-XAS spectra with a linear combination of spectra from a library of Se model compounds demonstrates that this inorganic form accounts for only 25% of Se species incorporated into the articular cartilage matrix. The predominant form of Se species identified was the redox active selenotrisulfide selenodiglutathione (GSSeSG), a primary Se metabolite. GSSeSG is an intermediate chemical species produced by a non-enzymatic reaction between selenite and reduced gluthatione [69], and is known to be metabolized further to hydrogen selenide (HSe^-) via selenopersulfide (GSSeSH) formation, two volatile and highly reactive compounds, by glutaredoxin systems in the presence of excess amounts of GSH, which leads to spontaneous oxidation of HSe^- to elemental Se (Se^0). These later species were not detected in our samples and data suggest that GSSeSG is preferential incorporated of into our model of articular cartilage maturation when exposed to elevated levels of exogenous sodium selenite.

Although beyond the scope of the present work, it would be of interest to obtain a spatially resolved distribution of these species and to explore the nature of Se bonding within chondrocytes or within the protein fraction of the articular cartilage matrix. We have demonstrated that up to now the limit of speciation using synchrotron X-ray microprobe for sub-cellular XAS analysis was 13 ppm for arsenic [169] an element with a K-edge close to that of Se. The proposed method could be coupled to synchrotron X-ray microprobe setup that uses Kirkpatrick-Baez mirror system as focusing optics, in order to bring spatially resolved speciation to the range of sub-ppm elemental concentration.

The present study demonstrates that HERFD-XAS analysis of highly-diluted elemental species in biological matrix is possible. Significantly, our work provides the opportunity to undertake highly-diluted elemental speciation studies in biological samples, overcoming previous technological bottlenecks that have existed until now. While hyphenated techniques provide specific molecular identification and are very sensitive techniques, liquid extractions are required as for any MS techniques, which likely change the speciation of the samples. On the contrary, frozen hydrated samples can be studied by HERFD-XAS. This analysis can be performed at low temperature (~ 10K) that allows to preserve at best the native state of the sample and drastically limit changes in speciation under the synchrotron X-ray beam. HERFD-XAS presently requires long acquisition times to obtain the required statistics for high quality spectra. Still, there is potential to further extend our novel technique. There is room for increased incident flux using optical elements along with larger collection angles and even higher sensitivity, alongside faster collection times with the possibility to couple more crystal analyzers. A CRG-FAME2 beamline is under construction that will provide the proposed improvements (higher incident flux and up to 12 crystal analysers for signal collection) paving the way for speciation analysis that has not been possible until now. The proposed method has the potential to allow the question of biochemical interconversion of ultra-diluted physiological elements such as Se or toxicants like mercury, lead or arsenic to be tackled directly. The advent of this method will clearly be of interest in many other domains such as environmental and material sciences.

Part VI
Characterisation of the Selenium Influence on the Extracellular Matrix Development and Organisation

In this part, a panel of techniques will be presented in order to visualize the selenium deficiency impact on the extracellular matrix development. These techniques explored the biochemistry and the biomechanics of the articular cartilage. A preliminary genetic study was also performed to provide some indications on the genetic variations induced by the Se-depletion of the culture medium.

15 Morphological Characterisations & Proteins Localisation Study

15.1 Histology

The reason for this histological study was to identify specific morphological changes occurring within the extracellular matrix of articular cartilage when cultured in the absence or presence of selenium. The global morphology, cellular distribution in the different zones and cell shapes are the most important parameters. This qualitative analysis provides interesting insights and can be useful to interpret our data generated through X-ray analysis and FTIR.

15.1.1 Principle

Histology is a technique to analyse cell/tissue physiology and morphology at the microscopic level. This provides good indications in order to understand the three-dimensional organization and structure at microscopic scale. This allows to assess tissue function at the cellular level. This technique includes two main stages: fixation of the cells and tissue of interest and staining. Sample are usually fixed with neutral buffer formalin, then embedded in paraffin blocks, which preserves the structure and morphology of the sample. In general, diverse features including subcellular structures within tissues are transparent and they are difficult to distinguish due to the low optical refractive indices differences. In order to better visualise the tissue composition such as cells, extracellular matrix and organelles, different stainings methods have been developed and used according to the target of interest. Staining is a coloured specific substance which relies on its binding, deposition, or partitioning within the sample based on chemical or physical properties. In this section, three different histological techniques will be employed: hematoxylin & eosin, safranin-O and toluidine blue.

Hematoxylin & Eosin: In general, the most common histologic stain is hematoxylin & eosin (H&E) and which is adequate for the visualisation of connective tissues, cartilage, carbohydrates, lipids and certain microorganisms. Hematoxylin when combined with specific metal ions mordants (aluminums salts) can be considered as a basic dye, called hematein when combined with Al^{3+}, forming a dye-metal complex. This induces a staining of negatively charged phosphate groups of nuclear DNA (acidic/basophilic structure) and a purplish-blueish-brownish color of the cellular nuclei is revealed. Usually, counterstaining is performed with eosin which is an acid dye hat effectively binds to positively charged arginine, histidine and lysine side chains of cellular proteins (basic/acidiphilic

structures). This stains acidophilic structures such as cellular cytoplasms, erythrocytes and collagen a pinkish-reddish colour.

For the following cartilage analysis, as noted in the paper of Schmitz *et al.* 2010 [189], the hematoxylin & eosin technique stains cell nuclei with a blueish-purple colour and the cartilage extracellular matrix in pinkish color with some blueish aspects in high proteoglycan content areas.

Safranin-O & Toluidine Blue: Two other staining methods using the basic dyes, safranin-O and toluidine blue, were used in order to extend and verify the qualitative analysis of the distribution of proteoglycans. Safranin-O and toluidine blue are both cationic dyes that stain acidic proteoglycans that are heavily glycosylated with glycosaminoglycans such as aggrecan. Toluidine blue exhibits an intense staining in cartilage (due to the large amount of sulfate-glycosaminoglycans - sGAG - compared to the safranin-O (Saf-O). Safranin-O technique is able to provide a tissue staining proportional to the proteoglycan content in normal cartilage but if a dysfunction appears in the GAG content which influences the proteoglycan content, Saf-O is not the ideal indicator [189]. Safranin O, also called Basic Red-2, is often used as a counterstain in order to colour all cell nuclei red. Safranin is mainly composed of dimethyl safranin but there is also trimethyl safranin. Safranin is also used as redox indicator. Safranin-O dye binds to glycosaminoglycan visualised by orange colour. Fast green, used as contrast stain of Safranin-O, is a sulfate-group containing acidic substrate. Fast green binds then strongly to the amino group on protein and thereby strongly stains the non-collagen sites. Generally, with safranin-O, nuclei are stained in blackish colour, cytoplasm bluish greenish colour and cartilage, mucin, mast cell granules in orangeish-redish colour. Toluidine blue present usually a subtle colour changes depending on the tertiary structure of the sample. Its properties are strongly influenced by several parameters such as pH gradient, temperature, light intensity, and solution concentration. Cytoplasm stains light blue, nuclear region dark blue, and mast cell purple.

15.1.2 Materials & Methods

Safranin-O & Toluidine Blue: After 3-week culture, all the treated explants samples were washed with DMEM-F12 and then twice with PBS. Then, they were fixed overnight at 4 °C in 10% NBF (Neutral Buffer Formalin). They were then paraffin-embedded following an automated protocol done in the Pathology Department of Singleton Hospital, Swansea. The paraffin-blocks were preserved at 4 °C. Samples were sectioned at 7 µ m thickness. These sections represent a transversal slice of the explant.

Safranin-O & Toluidine Blue: The staining protocols are based on standard laboratory protocols and are shown in figure 50. A light microscope is then used to collect images and attached digital camera used to collect these images. The cellular morphology and proteoglycan content were then evaluated.

Hematoxylin & Eosin (H&E)	Safranin-O (Saf-O)	Toluidine Blue (Tol-Blue)
	Deparaffinize & hydratation Xylene: 5min x1 Histochoice: 5min x1 100% ETOH: 2min x2 95% ETOH: 2min x1 70% ETOH: 2min x1 dH2O: 2min x1	
Stain with Hematoxylin Wash with runing tap water	Solution - 1min 30s until water become clear again	- -
Stain with Eosin Solution - 2min 30s Wash with running water Quick dip in 1% Acid ETOH Wash with running water	Stain with Fast Green FCF 0.05% - 5min Quick dip in 1% Acid ETOH Wash with running water Stain with Safranin-O (0.5%) - 5min Wash with running water	Stain with 0.5% Toluidine Blue - 1min 10s Wash with running water Quick dip in 1% Acid ETOH Wash with running water Counterstain with 0.05% Fast Green - 3min Wash with running water
	Dehydratation & Fixation 70% ETOH: 2min x1 95% ETOH: 2min x1 100% ETOH: 2min x2 Histochoice: 2min x1 Put slides in 37°C (incubator) 30 min Mounting using DPX Solution & Coverslip Let dry at 37°C for 1h	

Figure 50: Histological Staining Protocols for Hematoxylin&Eosin, Safranin-O and Toluidine Blue. Remark: ETOH stands for Ethanol

15.1.3 Results & Analysis

Cellular Morphology : In the following paragraph, the safranin-O staining sections is presented (Figure 52) because they exposed a better contrast than the other staining treatments applied on these same sections. The results are qualitative and allowed to obtain first insights of the effects of Se depletion and supplementation on explant cultures. The results are qualitative (N = 6) because the reproducibly and the strength of the stain strongly depends on the tissue section thickness (variation coming from the microtome calibration, cultures, bio-variability of the tissue, staining conditions and reagents). Before starting the analysis, representative sections of a fast-maturated tissue, where the development of the articular cartilage starts to take place are shown.

The sections presented Figure 51 are the typical reference images showing the native properties of the articular cartilage tissues (cellular morphology, cellular distribution and proteoglycan content) for immature and mature bovines. In the immature tissue, the cells do not have the typical stratified cellular organization as seen in the mature tissue. Instead they are randomly arrayed in the tissue. The size variation is observed as in the mature tissue, nevertheless they do not form the usual columnar pattern in the deep zone. The reduction of the tissue size is also normal because a second post natal ossification results in a reduction in tissue thickness [16-17].

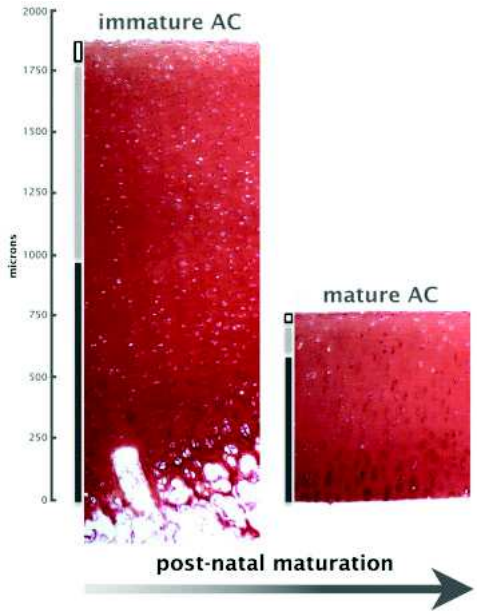

Figure 51: Postnatal developmental maturation of articular cartilage. Histologic sections of immature (7 days old) and mature (over 18 months old) cartilage samples taken from the metacarpophalangeal joint of male bovine calves were labeled with H&E to highlight proteoglycan content. The bar at the left of each section delineates the superficial (top; open), transitional (middle; shaded), and deep (bottom; darkly shaded) zones of the cartilage samples. [17-16]

Concerning the fast-maturation model, the results are presented Figure 52. As expected, the first micrometers at the surface are acellular which corresponds to the zone with the highest concentrations of lubricin, PRG4 are found. This layer remains present and intact for all the treated explants, so there is no effect on frictional properties. Nevertheless, it is within the tissue that the differences appear. In a first look, it is obvious to say that in explants of the selenium-depleted groups, the cell number is lower in regard to those of the ITS-groups.

Concerning the ITS groups (Figure 52 C) Control and D) Ft-treated), the cellular density is higher than in the No Se groups. The cells present in the superficial zone a flat-like shape for ITS control group and a strict flat shape for the ITS growth factor-treated group. The cellular activity in the ITS FT-treated group is important. There are obvious signs of cellular division at the surface with doublets of cells present in high numbers. The density is high and they are randomly arrayed in this zone. In the middle zone, cells tend to pack to each other with an increasing size and they appear rounder in shape. In the deep zone, the cellular size is augmented and columns appear in a disorganised way for ITS control and in more organized way for the ITS FT-treated group. Large aggregates of cells are present to the bone part (subchondral region), which correspond to remnants of hypertrophied chondrocytes. This represents a classic feature of endochondral ossification with the replacement of a pre-existing calcified cartilage by bone. The chondrocytes are in a hypertrophy stages and eventually die by apoptosis after the calcification of the cartilage matrix. As expected, this phenomenon is predominant in the tissue treated with growth factors. These observations correspond to the observations of precocious maturation of articular cartilage using these specific growth factor cocktail provided by the studies of Khan *et al.* 2011 [16].

For the group "No Selenium Control" (Figure 52A), there is a low number of cell in the superficial zone. The usual flat ellipsoidal shape is not really well defined and the chondrocytes remain quite round until the start of the middle zone. Then the cells become round and larger until forming cell-doublets. The cellular density decreases and there are some cell and nuclei-free lacunae-regions.

Once in the deep-zone, cells tend to pack together in order to form disorganized columns. In this particular regions, cells are larger and the cell-doublets are more numerous. As, in ITS groups, this is characteristic cellular hypertrophy with cell aggregate nearer to the subchondral bone appearing larger and rounder. This phenomenon is less remarkable than in the ITS groups. Cellular density continue to decrease and the size-variation is small in comparison of the usual variation that it can be observed in native tissues. In the No-Se growth factor treated group (Figure 52B), an interesting variations at the cartilage surface was seen, the appearance of chondrocyte clusters. These explants were placed in fast-maturation growth factor medium (FGF2-TGFβ1) that was depleted in selenium, a kind of clusterisation appears. The strong stain surrounding these aggregates tends to suggest chondron formation round independent units, although cell division and death could be a reason for the formation of these clusters. Apart this specific pattern at the surface, the same observation was apparent in the no-Se control, i.e no growth factor group of samples, where the cellular density was higher and the size variation still present.

Proteoglycans Assessments: In a global view, considering that proteoglycan content is set as proportional to the staining intensity, it is possible to say that the proteoglycan content is higher in the deeper zone that in the superficial regions as described to the literature [190-191]. This observation is less obvious in controls groups (No Selenium and ITS).

The intensity of the reddish, pinkish, orangeish colour refers to the proteoglycan (PGs) content. In ITS control (Figure 52C), we can observe a decrease of the collagen content from the surface toward the deeper zones. In No Se Control (Figure), the collagen content is relatively homogeneous in the middle and deep zones. Collagen content of the maturated AC (NoSe FT-treated (Figure 52B) and ITS FT-treated (Figure 52D) is found to be high mainly in the middle and deep zones. This is indicative of an improved collagen production under growth factor stimulation as it is expected in a mature tissue. This can be referred to the activation of the cellular activity related to the maturation process. Unexpectedly the No Se Control explant show an even higher collagen content than in ITS FT-treated for the middle and deep zones.

The ITS FT-treated samples (Figure 52D) show a dense and homogeneous PG content throughout the tissue (except the zone close to the subchrondral bone). This is also observed for ITS control (Figure52C), still, we can notice local variations with a less dense PG (ligher pink coloration) content in the middle and deep zones compared to ITS FT-treated explants. For No Se control (Figure 52A), the PG distribution is more complex and anarchic with mainly a high PG content (ponctual pinkish-redish coloration on a intense pinkish background) that superimpose to chondrocytes position in the deep zone. In Figure 52B, a high PG production is observed in middle and deep zones of No Se FT-treated explants with a intense orange coloration mainly expressed in the upper part of the tissue section.

This information related to the proteoglycan distribution is qualitative. Several factors such as staining protocols and conditions influence the staining. Furthermore, safranin-O can also be related to collagen content. Consequently, another technique such as infrared investigations has to be performed to discriminate the different matrix component contributions.

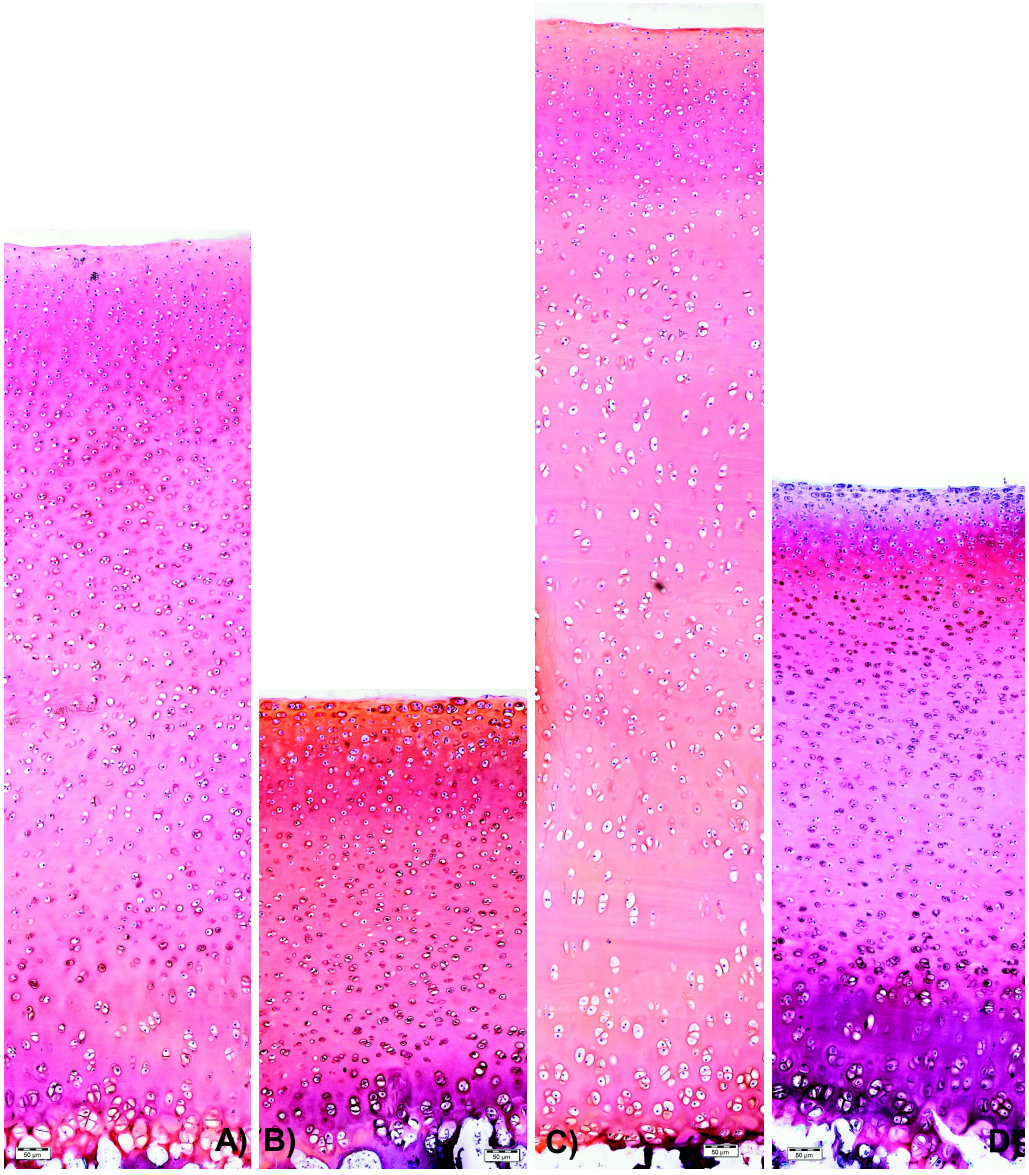

Figure 52: Postnatal developmental maturation of articular cartilage. Treated explants with a 7 μm-section thickness from cartilage samples taken from the metacarpophalangeal joint of male bovine calves were labeled with Safranin O to highlight proteoglycan content. Postnatal maturation results in a reduction of cartilage height, a decrease in cellular density, and changes in collagen fibril architecture. A) No Selenium Control AC qualified as immature, B) No Selenium Growth factors treated AC, tissue undergo a maturation, C) ITS serum treated AC Control, and D) ITS serum and growth factors treated AC, tissue is qualified as maturated tissue.

15.2 ImmunoFluorescence

To understand how the structural variations appear within the extracellular matrix of the articular cartilage, a protein localisation study was performed. We were interested to understand how (more precise where) selenium treatment, applied on explants during their maturation in culture, influences the protein distribution and expression of certain specific targets, indicator of the main component of the matrix or related to some specific differentiation processes. Consequently, Collagen type I, II, III, IX and X but also alpha-acetylated tubulin and BrDu (Bromodeoxyuridine) were selected to be investigated. Collagen type I is representative of the main component of bone, collagen type II for the

articular cartilage [15]. Collagen type III is crucial for collagen I fibrillogenesis and more synthetized in mature articular cartilage tissue, may be related to chondrocyte healing response [197-198]. Collagen Type IX is limitator of the type II collagen fibre aggregate and a potential regulator of the fiber diameter [199] and the collagen type X is set as an indicator of cellular hypertrophy [200]. BrDU is a common indicator in the detection of proliferation cells in living tissues. Alpha-acetylated tubulin is an antibody targeting some specific organelle involved in the mechanotransduction such as the primary cilium [201]. Actually, it also target microbules, centrioles and centrosomes, organelles involved in the cellular division and motion. In the following section, the results of the protein distribution of the Collagen II, III and IX will be presented. The other targets are shown due to the lack of reproducibility over the different experiments.

15.2.1 Indirect Immunofluorescence Principle

Immunostaining using antibodies is usually used confirm the presence and determine the exact location of protein epitopes. For example, for cartilage matrix composition and integrity studies, immunolocalization of proteins, protein fragments, cleavage sites and other epitopes can be performed in parallel with histological or histochemical investigations. This in-situ technology can provide interesting insights into the distribution, behaviour and cellular differentiation state. Nevertheless, the results can potentially vary depending on many factors such as the use of a predigestion steps (antigen retrieval methodology, extracellular matrix digestion) and fixation methods.

Briefly, the immunofluorescence or immunostaining is an experiment based on an antibodies targeting specific protein epitopes within the cells of a sample or tissue. It is necessary to be careful during the procedure because the staining is sensitive to harsh conditions required to unmask epitopes in formalin fixed tissue, or hidden within the extracellular matrix, as the specific epitopes of the protein targets must remain intact. It is why intermediate fixatives like cold alcohols such as acetone or ethanol are usually used to preserve these epitopes for recognition by antibodies. Consequently, the primary antibody recognize and bind the protein target within the sample. Generally, the primary antibody is then bound by secondary antibodies that are tagged with a fluorescent dye (fluorochome or enzyme) and the antibodies complex is then visualized using ultra-violet fluorescent microscope, confocal microscope, or histochemical reaction using peroxidase or alklakine phosphatase based reactions. This is based on the fluorescence principle. Here, fluorochromes (specific types of dye) absorb ultra-violet rays and emit visible light. In the following experiment, the most commonly used fluochrome called fluorescein (FITC) was chosen. The FITC characteristics are that it is excited by a blue light (wavelength of 488 nm) and it will emit a green colour (520 nm) which allow a visualisation of the protein of interest.

15.2.2 Materials & Methods

Samples: After 3-weeks culture, all the treated explants samples are washed with DMEM-F12 and then twice with PBS. They are then snap-frozen in precooled hexane and stored at $-80°C$. Later, the samples are then sectionned using a cryotome. Using a cryomatrix, transparent to fluorescence, sections with a thickness of $10\,\mu$m are produced. Between two to four sections are collected per slide in order to be sure that some sections will stay fixed to the slide after the several washes present in the immunofluorescence staining protocols. The slides are then perserved at $-20°C$ until undergo immunostaining. Cryofrozen sections have been selected in order to paraffin-embedded samples because for paraffin-fixed samples in important background is remaining which make difficult the analysis due

to a strong background.

Primary Antibody Labeling: Type II collagen is the main collagen component in the extracellular matrix of the articular cartilage. Its form and distribution is not the same with the depth of the tissue. The fibril size varies according to the zonal location in the cartilage. Consequently, it could be interesting to evaluate the expression and distribution changes of this major component when selenium is applied or not. The primary monoclonal antibody reacting against Col-II (II-II6B3;DSHB) was used on sample sections at a concentration dilution of 1:10 in 5% goat serum inPBS-Tween20 (PBST).

Type III collagen is related to type I collagen due to its similar protein composition and col-localisation in many tissues. It would be interesting to observe the variation of its expression relative to the maturation process applied on the treated sections. The primary antibody calls Col-III (3B2-s) anti-type 3 collagen antibody (DSHB) was used on sample sections at a concentration dilution of 1:2.5 using 5% goat serum in PBST.

Type IX collagen is often co-located with type II collagen due to its action as limitator of the type II collagen fibrillogenesis and as a regulator of fiber diameter. Selenium may play a role in its expression and localisation may provide useful information in conjunction with AFM and picrosirius red studys in order to determine the Se-impact in general fibrillation (size, diameter, density). The primary antibody called Col-IX (D1-9-s) anti-type 9 collagen antibody (DSHB) is then used on the diverse treated sections at a concentration dilution of 1:2.5 using 5% goat serum in PBST.

Secondary Antibody: The secondary antibody is a goat anti-mouse IgG FTIC conjugate (contains fluorochrome excited at 488 nm), prepared at a concentration (1:100) using 5% goat serum in PBST.

Immunofluorescence Staining Protocol for Cryosections:

1. On the day of staining, bring the frozen section (preserved at -20°C) up to room temperature
2. Label each slides. Negative controls (no primary antibody or no secondary antibody) in order to test for non-specific binding of the secondary antibody and autofluorescence.
3. Wet sections by adding drops of PBST for 2 min
4. Drop the excess and dry the slide without touching the tissue sections
5. Repeat step (3) and (4)
6. Put some drops of ice cold 95% ethanol between 10 sec to 1min
7. Drop off and wash PBST - twice
8. Drop off the liquid and clean the excess with tissue
9. Draw circle border around all section location using a wax Edge-pen
10. Add PBST to wash the sections
11. Put 200 μL per slide of a solution of 1 mg hyaluronidase and 0.1 U/mL chondroitinase ABC for 1h at 37°C
12. Wash 5 min with PBST at room temperature, in dark (closed box)
13. Drop off liquid, dry the slide and repeat step (12) twice
14. Put 200 μL per slide with a blocking solution composed of 10% goat serum in PBST - 6 hours

15. Drop of the liquid
16. Put 200 μL per slide of 1°Ab-solution (composition described previously). Negative control, 200 μL of 5% goat serum in PBST instead of the 1°Ab solution. Let Overnight at 4°C in a box close isolated from light.
17. Re do step (12) and (13)
18. Put 200 μL per slide of 2°Ab-solution (composition described previously) for all the samples included negative controls
19. Re do step (12) and (13)
20. Dry the slide as mush as possible without touching the sections
21. Put a tiny drop of DAPI in the middle of the slide and gently drop with a coverslip on it - becareful: avoid as much as you can bubbles
22. Place the slides in a specific rank and cover with Al-foil to protect slides from the light
23. Store at 4°C
24. Remark: Just before analyse, fix the coverslip to the slide with transparent nail gel and draw circle with a marker pen around sections to identity them

Remarks: Most of the incubations were carried out at room temperature and unless otherwise noted in a humid light-tight box or covered dish/plate to prevent drying and fluorochrome fading. Control and negative controls were used in order to verify the specificity of the labelling.

PBST is composed of PBS to which 0.5 % of the detergent Tween 20 is added to increase the binding specificity of the antibodies and is also used to neutralize the charges on the slides.

Cold 95% ethanol is used to fix and preserve membrane integrity, cellular structure and epitope in order to insure a good immunostaining. Due to their similar structure, ethanol compete with water for protein hydrogen bonds. Consequently it takes the water molecules in tissues and induces proteins precipitation at their isoelectric points by reducing their dielectric constant, and can block antibody-epitope binding due to changes in conformation. It usually stabilize the secondary structure of proteins.

Hyaluronidase and chondroitinase ABC re sugar-degrading enzymes are used to "degrade" the extracellular matrix in order for antibodies to have access to the target of interest and also to help reducing the intrinsic background fluorescence present in cartilage. This improves the image quality for a better visualisation of secondary bound fluorescent antibodies.

All the data that will be presented in this section were compared to the negative controls. As seen Figure 53, no fluorescence (green) signal is emitted from AlexaA488, only the nuclear counterstain DAPI (blue labelling) is present. All these different staining have been performed in the same run in order to produce a unique negative control for all the targets of interest.

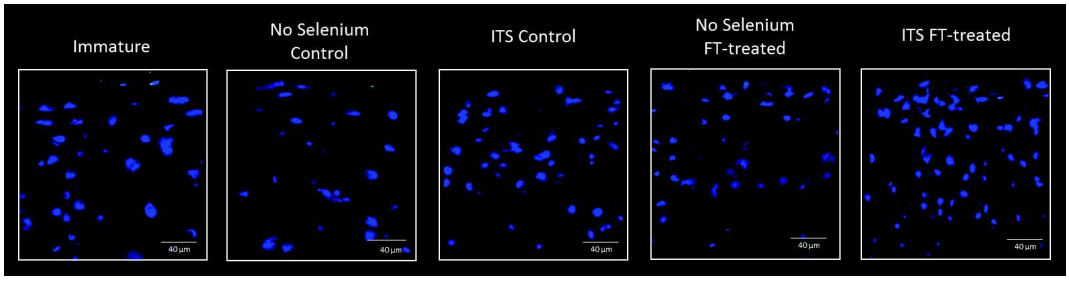

Figure 53: Representative negative controls in antibody labelling experiments using antibodies reactive against COL2/COL3/COL9.

15.2.3 Results

The localisation of collagen proteins is important to understand their functions and the general state of a tissue. In this study, the protein distribution will provide information about the influence of selenium on collagen protein production.

The type II collagen protein immunofluorescence analysis was performed on large tissue sections using a confocal light microscope. As observed in Figure 54, the protein is present throughout the section. In FT-treated samples, more labeling is revealed by the higher fluorescence signal intensity. In comparison, the fluorescence signal related to type II collagen 2 protein seems to be more localized in the controls. The signal appears to be associated to the cell borders as well visualized in the ITS control (Figure 54B). Nevertheless, this full depth investigation is difficult to use for the interpretation of the collagen location. Actually the tissue section was never perfectly flat and present some slight thickness variations. For each mosaic, the signal coming out of the confocal microscope was set to the maximum of the fluorescence. Consequently, a small shift in the focal depth can appear between the different images of the mosaic and then can introduce a bias in our analysis. This error is then difficult to evaluate. All the pictures have been treated with Fiji software to normalize and adjust the brightness of fluorescent signals to be comparable.

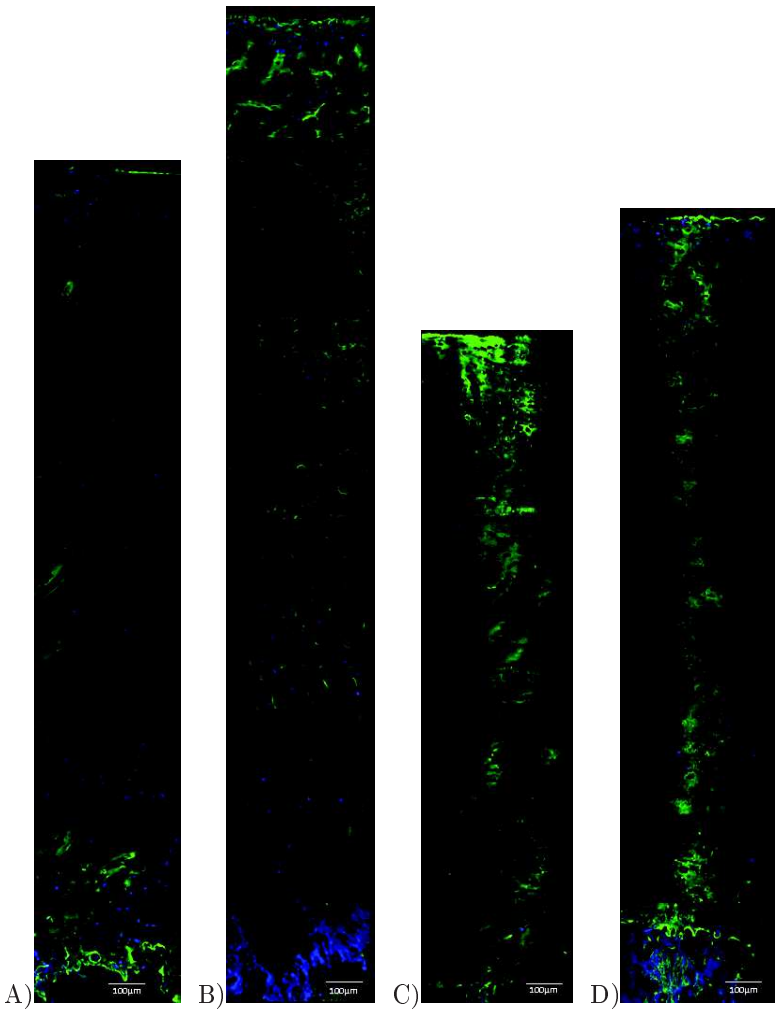

Figure 54: Immunofluorescence of the Collagen 2 (COL2a1; green labelling) for the samples: (A) NoSe Control, (B) ITS Control, (C) NoSe FT-treated and (D) ITS FT-treated. The blue color corresponds to the DAPI stain and is associated to nucleus. (From superficial zone (upper part of the section) to calcified zone (bottom part).

Collagen type II is present throughout the tissue, and this for all sample sections (Figures 55, 56, 57). The antibody labelling decreased from the surface to the deep zone. In the surface (Figure 55), the collagen type II protein is uniformly expressed in native tissues. The same pattern seems to appear in the explants treated with ITS. In the explants treated without any selenium and any growth factors, the fluorescent signal is extremely weak. Without selenium but with growth factor, the expression of the collagen type II is locally present in the upper part of the superficial zone. In the middle zone, the explants treated with selenium only present this protein in the pericellular matrix (Figure 56). In the deep zone, collagen type II appears to exhibit greater labelling in the explant growth factors-treated in the medium without selenium (NoSe FT-treated) (Figure 57).

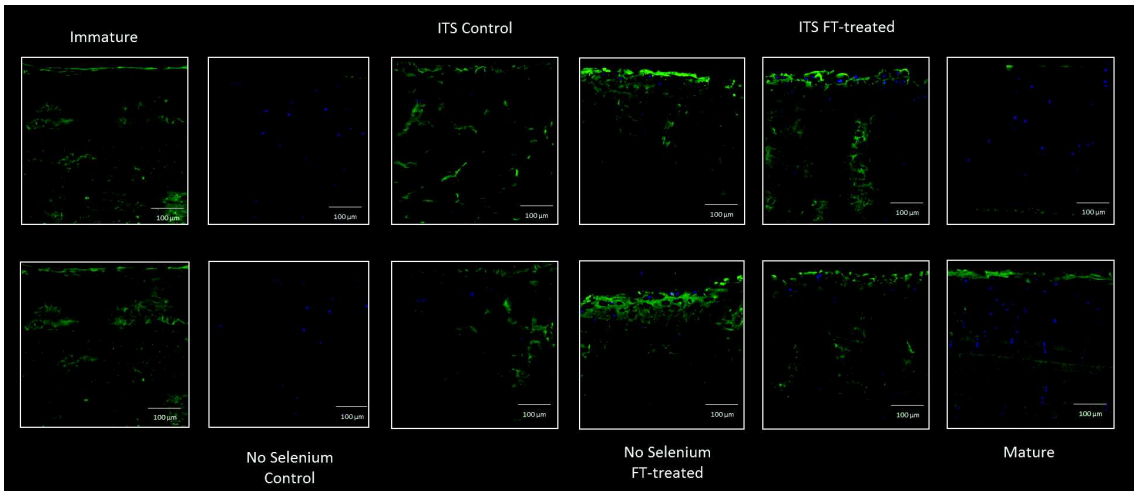

Figure 55: Immunofluorescence of the Collagen II (COL2a1) (in green) in the superficial zone of diverse AC samples (from the left to the right) Native Immature, NoSe Control, ITS Control, NoSe FT-treated, ITS FT-treated and Native Mature. The blue color corresponds to the DAPI stain and is associated to nucleus. (magnification X20)

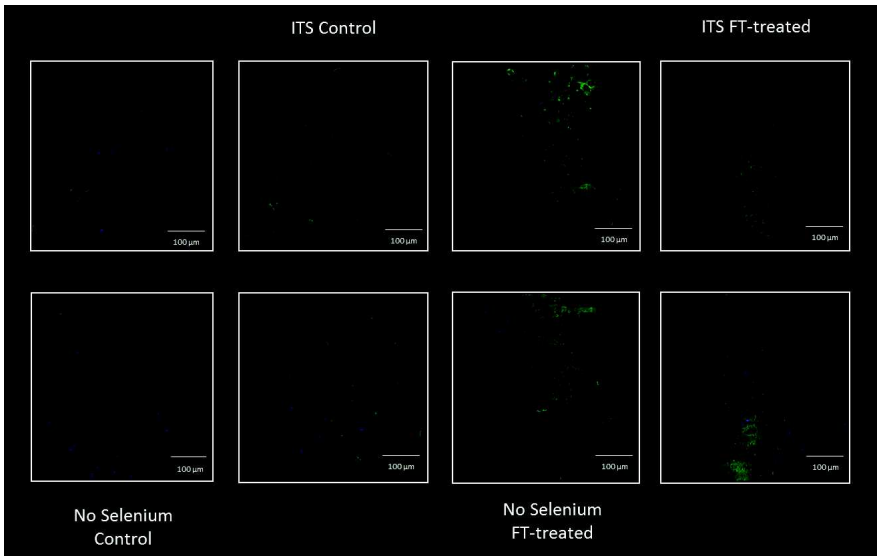

Figure 56: Immunofluorescence of the Collagen II (COL2a1) (in green) in the middle zone of diverse AC samples (from the left to the right) NoSe Control, ITS Control, NoSe FT-treated and ITS FT-treated. The blue color corresponds to the DAPI stain and is associated to nucleus. (magnification X20)

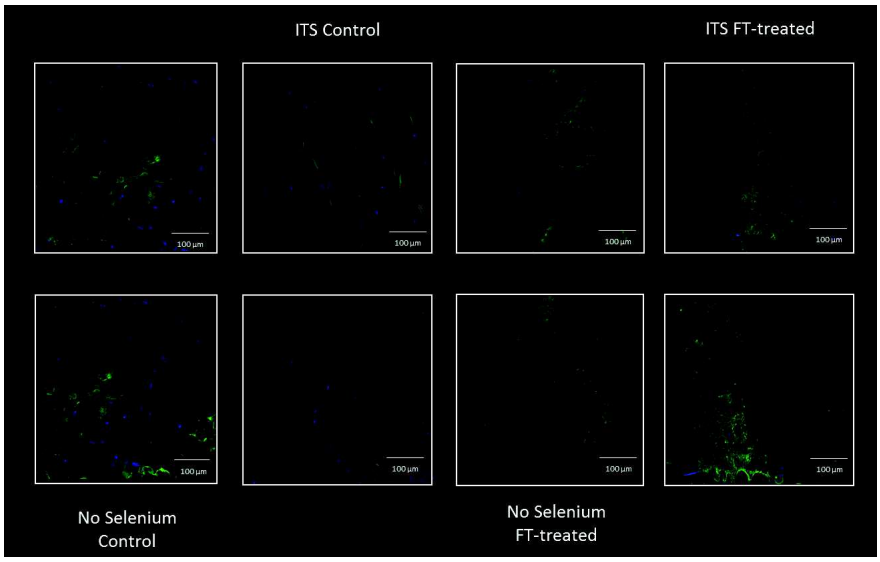

Figure 57: Immunofluorescence of the Collagen II (COL2a1) (in green) in the deep zone of diverse AC samples (from the left to the right)NoSe Control, ITS Control, NoSe FT-treated and ITS FT-treated. The blue color corresponds to the DAPI stain and is associated to nucleus. (magnification X20)

The collagen type III seems to be expressed in the periphery of some but not all cells, mainly in immature tissue such as native AC, explants NoSe Control and ITS control (Figure 58).In the mature tissue, the collagen type III is not expressed. A strong reduction is observed in the "maturated" tissues (NoSe FT-treated and ITS FT-treated).

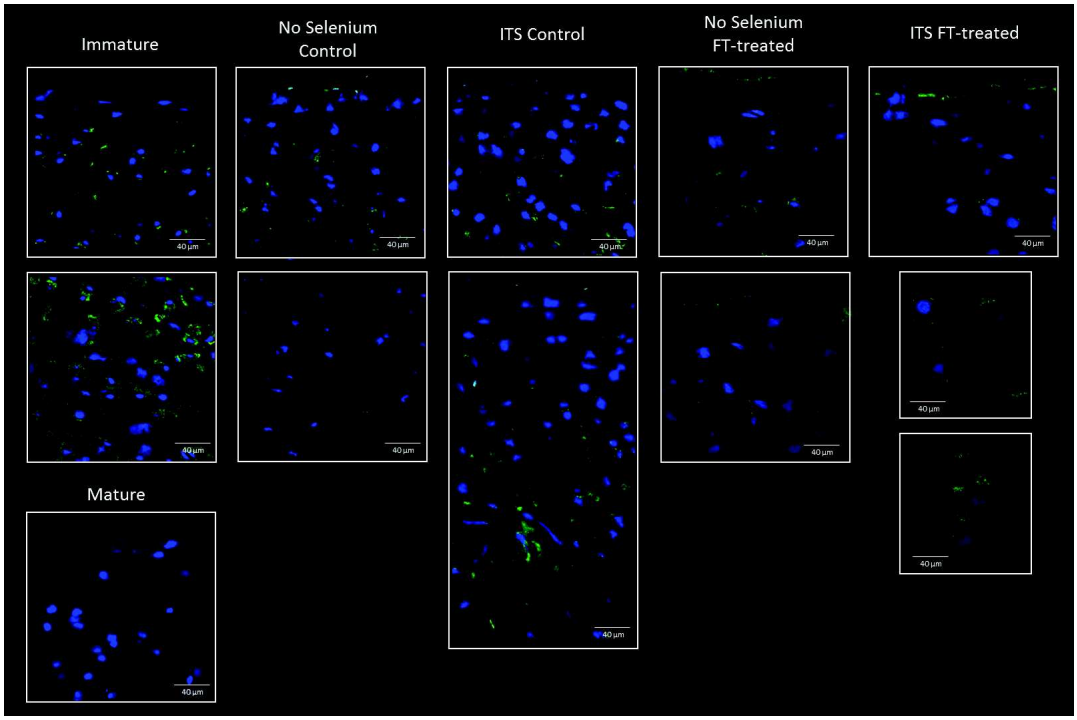

Figure 58: Immunofluorescence of the Collagen type III (in green) in the superficial zone of diverse AC samples (from the left to the right) Native Immature, NoSe Control, ITS Control, NoSe FT-treated, ITS FT-treated and Native Mature. The blue color corresponds to the DAPI stain and is associated to nucleus. (magnification X40)

The collagen type IX does not seem to be strongly labeled for in the surface, only certain cells how

a weak fluorescent signal (Figure 59). The expression is weaker in the samples in ITS samples. The mature tissue do not present any collagen type IX signal. In the deeper zones, the ITS FT-treated do not present any signal such as the mature tissue (Figures 60&61). The No Se samples presents a comparatively (more) higher signal.

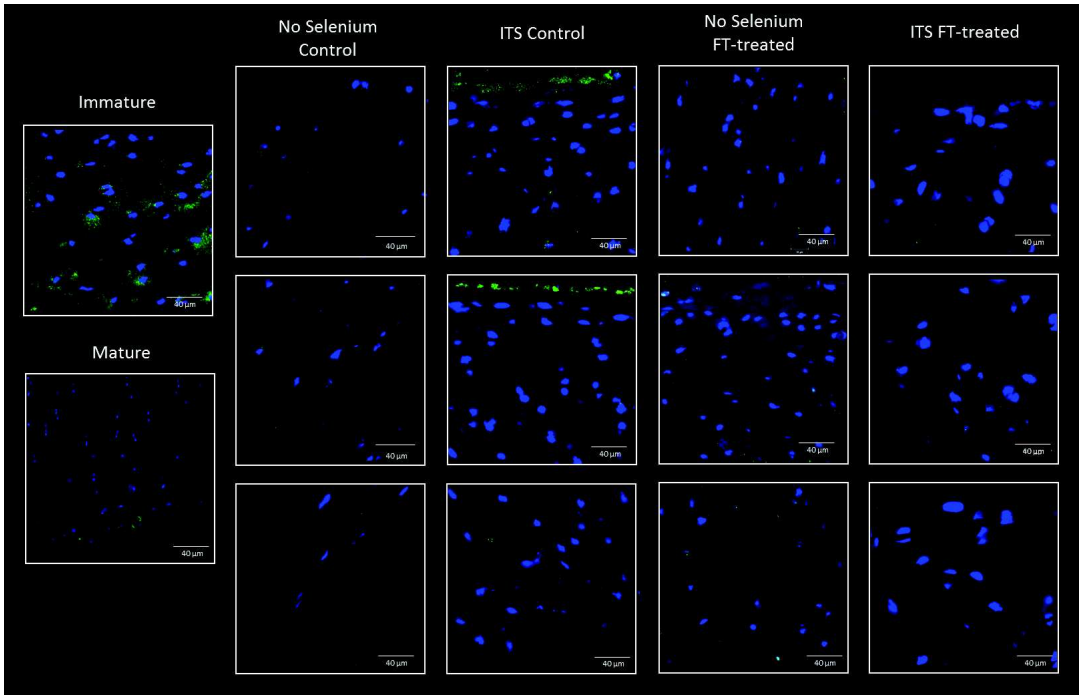

Figure 59: Immunofluorescence of the Collagen type IX (in green) in the superficial zone of diverse AC samples (from the left to the right) Native Immature, Native Mature, NoSe Control, ITS Control, NoSe FT-treated and ITS FT-treated. The blue color corresponds to the DAPI stain and is associated to nucleus. (magnification X40)

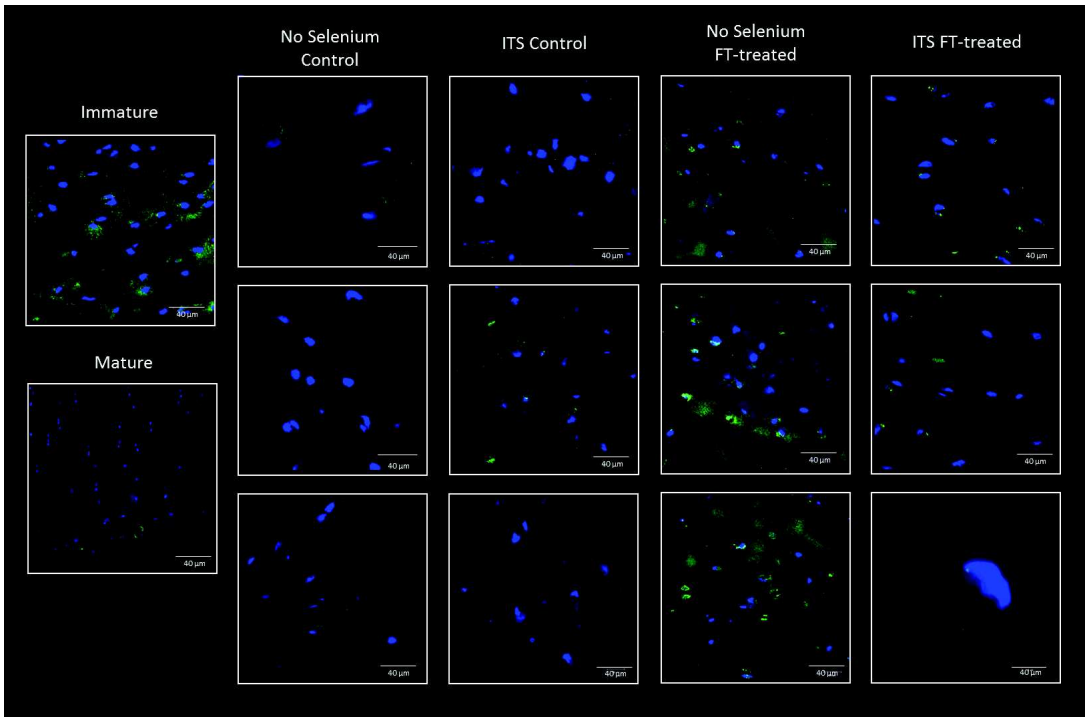

Figure 60: Immunofluorescence of the Collagen type IX (in green) in the middle zone of diverse AC samples (from the left to the right) Native Immature, Native Mature, NoSe Control, ITS Control, NoSe FT-treated and ITS FT-treated. The blue color corresponds to the DAPI stain and is associated to nucleus. (magnification X40)

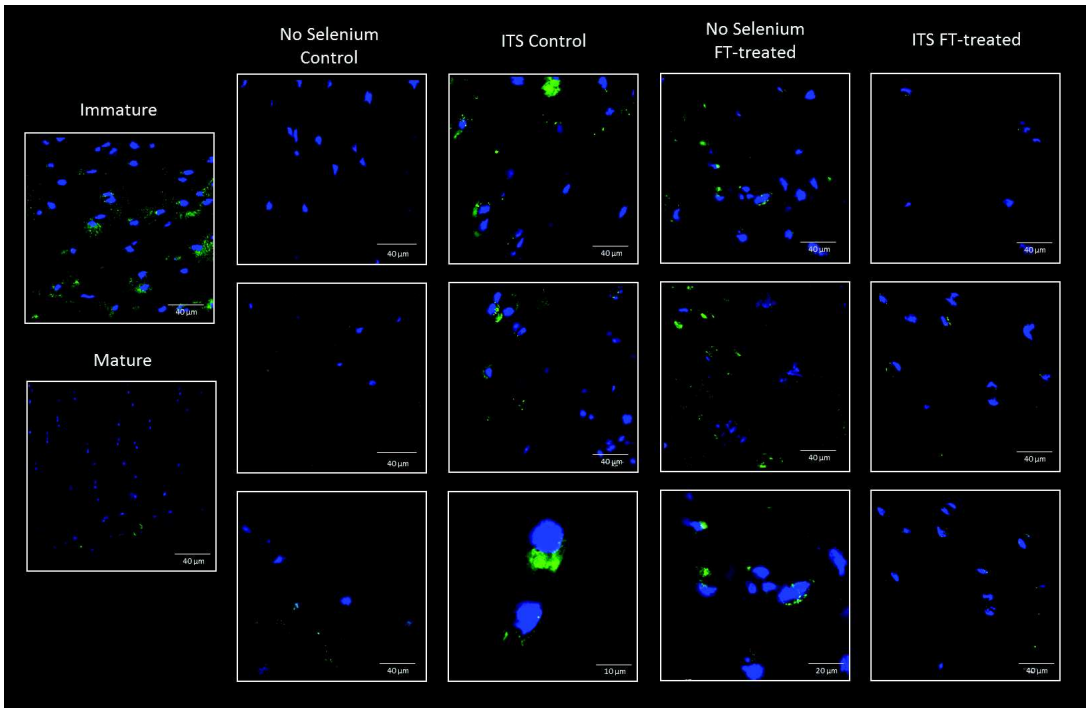

Figure 61: Immunofluorescence of the Collagen type IX (in green) in the deepzone of diverse AC samples (from the left to the right) Native Immature, Native Mature, NoSe Control, ITS Control, NoSe FT-treated and ITS FT-treated. The blue color corresponds to the DAPI stain and is associated to nucleus. (magnification X40)

16 Biological Investigations: Gene Expression Screening & Selenoprotein Expression in Articular Cartilage

16.1 Principle of the (Real-Time, quantitative) Polymerase Chain Reaction

The Polymerase Chain Reaction is a relatively simple technique to amplify DNA based on enzymatic reactions. This genetic amplification technique is characterized by high levels of sensitivity and specificity in bioanalysis. The normal PCR evaluates DNA as end-point analysis usually by visualising the amplified product in an agarose run in order to verify the size of the amplicon. This classical PCR-technique provides semi-quantitative information of the original starting material, when normalized to a housekeeping gene, in order to get a preliminary idea and allows rapid screening of genes of interest. Real-time quantitative PCR (RT-qPCR) monitors the progress of the amplification process from start to finish and allows accurate quantification of the amount of gene product in a sample when normalized to a housekeeping gene. The measurement of amplified products is made using the inclusion of fluorescent molecules that bind the DNA target. The amount of DNA is then evaluated regarding to the proportional increases in florescence signal. This technique defines the point in time during a cycle when the amplification of a specific target first passes a threshold, Ct. Thus the lower the Ct, i.e. the earlier the appearance of fluorescence signal above the threshold level, the more gene products are present.

DNA is composed of a pair of complementary polynucleotide strands conjugated together with hydrogen bonds to form a double helix. The strands are made up of the four bases: Adenine (A), Thymine (T), Guanine (G) and Cytosine (C) which pair with one other base, usually A to T, and C to G, on the complementary strand. When a DNA solution is heated, the non-covalent hydrogen bonds weaken and are destabilized and the two strands are then denatured (separation).

The amplification of nucleic acids for detection is achieved via a technique called the polymerase chain reaction. During this nucleic acid amplification process, a succession of repeated heating and cooling cycles take place. Under this temperature variation, target sequence specific primers, a thermostable DNA polymerase enzyme and 'free' nucleotides will interact and synthesize DNA to produce copies of a target DNA sequence. Because each copy is a template for two new copies the reaction is logarithmic in scale.

The following stages can be visualized on the Figure 62.

1. DNA samples is mixed with DNA polymerase and some nucleotides in the specific buffer solution
2. The original DNA, called target DNA, is then denatured due to the heating at 95 °C of the mixture
3. The complementary stands of the target DNA is then separated into two single strands due to the breaks of the hydrogen bonds (holding the complementary strands together)
4. The amplification phase starts. Short lengths of single stranded DNA (app. 10-20 bases long) called oligonucleotide primers added to the solution initiate to be directed towards the single strands.
5. The solution is cooled down to the annealing temperature (app. 55 °C). The primers are triggering to join to the complementary base sequences (using hydrogen bonding) on each of the single strands of DNA.
6. Small sections of these double-stranded DNA are then formed at either end of the sample. This induces a triggers DNA replication.

7. The DNA polymerase can bind to these double stranded sections.

8. The solution is then once more heated at app. 70°C (and not 90°C to do not denature again the DNA polymerase). The DNA polymerase extends the double stranded section by adding free nucleotides to the unwound DNA as it would be done in a natural DNA replication. The DNA polymerase catalyses the synthesis of a complementary strand for each of the single DNA-strands producing two identical double strands of DNA.

9. This process can be repeated many times by subsequent heat denaturation of the double stranded DNA, following of the same primer sequences to the resulting single-stranded DNE. The amount of DNA exponentially increases at each passage (x2, x4, x8, ...).

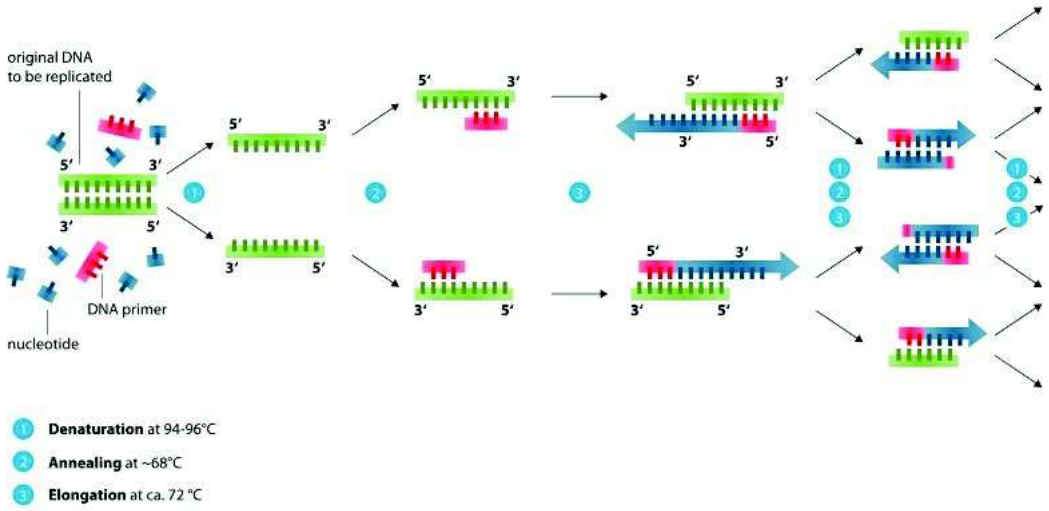

Figure 62: qPCR principle Illustration. PCR creates copies of a target section of DNA via a series of heating and cooling cycles. A target DNA sequence is added to a buffered PCR reaction mixture, comprising: primers, short sequences of DNA that are complimentary to the target sequence, nucleotides, and a thermostable DNA polymerase enzyme.
Source: http://www.elveflow.com/microfluidic-tutorials/microfluidic-reviews-and-tutorials/microfluidic-pcr-qpcr-rtpcr/

16.2 Materials & Methods

16.2.1 Sample Preparation

RNA extraction and cDNA conversion: Cultured or freshly isolated articular cartilage explants were frozen in hexane as described above and stored at 80°C prior to RNA extraction. Frozen explants were homogenised in the presence of frozen 0.5 ml TRI reagent using a mikrodismembrator U and chilled steel vessels (B. Braun Biotech International, Melsungen, Germany). The supernatant from the latter process was placed in an RNAEasy column for total RNA extraction with DNAseI digestion step (Qiagen, Crawley, UK). Total RNA was quantified using a NanoDrop 2000 spectrophotometer (NanoDrop, Wilmington, USA). One microgram of total RNA was used for reverse transcription reaction using the GoScript kit utilizing M-MLV reverse transcriptase and random primers (Promega, Southampton, UK).

Reverse Transcription PCR (RT-PCR) reaction was performed to synthetise cDNA on BioRad Real-time PCR analyser with the following thermal cycling program exposed Figure 63.

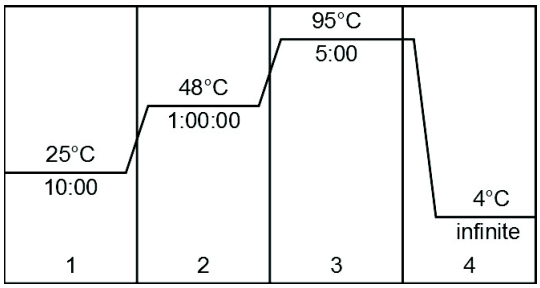

Figure 63: Reverse Transcription PCR routine

PCR & qPCR preparation: qPCR reactions were performed using the GoTaq qPCR mastermix (Promega), 12.5 ng cDNA and 0.3 mM forward and reverse primers.

Reagents	50 μL(1x)PCR reaction
5x Buffer SYBR Green	10 μL
$MgCl_2$ (25mM)	3 μL
dNTP (20mM)	0.5 μL
Forward Primer (F) (100 μM)	0.5 μL
Reverse Primer (R ou B)(100 μM)	0.5 μL
Taq-Polymerase	0.25 μL
Nuclease-free water	34.25 μL
cDNA Template (Sample)	1 μL

Reagents	20 μL(1x)qPCR reaction
2x GoTaq qPCR mastermix	10 μL
Forward Primer (F) (3 μM)	2 μL
Reverse Primer (R ou B) (3 μM)	2 μL
Nuclease-free water	2 μL
cDNA Template (Sample)	4 μL

Table 14: PCR and qPCR reaction receipes. The original DNA from which a specific sequence gene of interest will be amplified. Primers (F and R) are a pair of short nucleotides sequences (10-20 base pairs) corresponding to the partial sequences at the two extremities of the specific amplified DNA sequence. They identify and serve as starting point for the specific amplified sequence. Deoxynucleotide triphosphates nucleotides (dNTP) composed of 4 types of DNA bases (A,T,C,G) are used to synthesize the new DNA amplicons i.e. the new DNA samples resulting from the PCR process. DNA (Taq) polymerase is an enzyme that enables to create the new DNA strand from single-stranded DNA as a template by assembling specifically the nucleotides. qPCR Go-Taq Master Mix contain SYBR, Taq Polymerase, dNTP, $MgCl_2$.

Reactions were performed on a BioRad T100^{TM} ThermoCycler with the following thermal cycling program exposed Figure 64

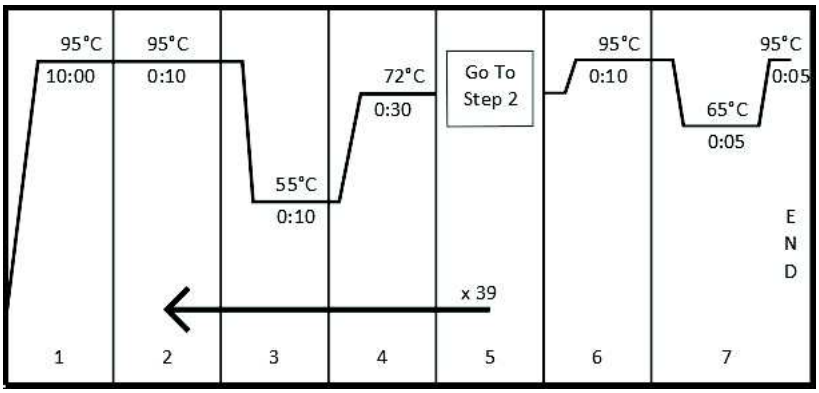

Figure 64: PCR routine

Reactions were performed on a BioRad Real-time PCR analyser with the following thermal cycling program exposed Figure 65.

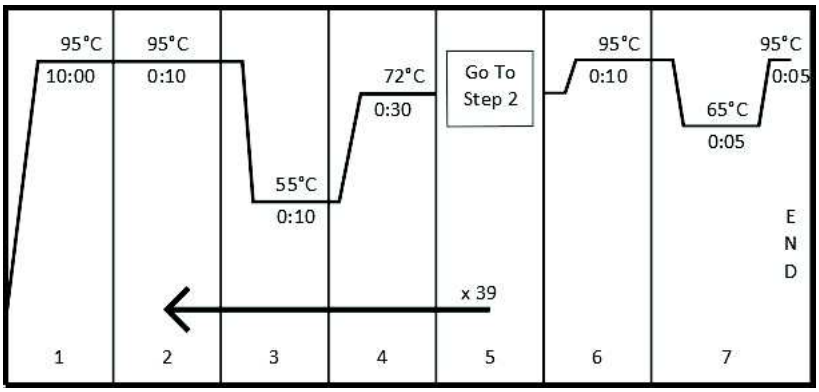

Figure 65: qPCR routine

Two controls have been realised:

- "-RT" - No reverse transcription: RNA followed the RT-PCR process without enzyme in the reaction, the cDNA cannot then be converted. If something remains, this corresponds to DNA coming from the original material which has not been eliminated in the RNA extraction mini-kit (Qiagen, Crawley, UK).
- "NTC" - No Template control: ddH_2O is used instead of the sample cDNA in order to verify the qPCR reaction specificity regarding to possible contaminations in reactions

Standard curves over the linear range of amplification were generated for all primer sets, and data was used where the efficiency of amplification was between 70% and 90% and the melt curves generated a single product. The data shown is the ratio of the concentration of the gene of interest (in nanograms, ng) and 18S rRNA (in ng).

The nucleotide sequences of primer sets used in this study are described in the Figure 66.

Family - Bos Taurus	Gene	Forward Primer	Reverse Primer	Amplicon (Bp)	Annealing (°C)	Accession (NCBI)
Gluthatione Peroxidase	GPX1	GCAACCAGTTTGGGCATCAG	TAGGGTCGGTCATGAGAGCA	210	60.04 / 60.03	NM_174076.3
	GPX1	AACGTAGCATCGCTCTGAGG	GATGCCCAAACTGGTTGCAG	121	59.9 / 60.04	NM_174076.4
	GPX2	AACAGCCTCAAGTACGTCCG	GAGGGAAAACGGGTCGTCAT	150	60.04	NM_001163139.1
	GPX3	GGAGGCCAAGGGGAAGTAAC	ATGGGAGTGTGGCGTAGTTG	116	60.04 / 60.03	NM_174077.3
	GPX4	TGTGGTGAAGCGGTATGGTC	GGAAGGCTTCTCGGAACACA	126	60.04 / 59.97	NM_174770.3
	GPX5	TTTTCCATGACACCCCACCC	AAAGAGGCTCTGACTGCCAC	137	60.18 / 59.96	NM_001025335.2
	GPX6	CGTCAGAGGTTGCCTCCCAT	TCATATGGAGGCTGGGTGGA	84	61.9 / 60.03	NM_001163142.1
	GPX6	GGGCCTCATGTCTTTTCCCA	TTGAGGGTGAGGGCTCCATA	130	59.96	NM_001163142.2
	GPX7	CCATCACTCCTACTGGGGGA	GGCTGGTGAGTCATTGGTCA	108	60.03 / 59.96	NM_001101113.2
	GPX8	GTCTCCATGGGGGTTTGGTC	AGAGTCGTTGGCTGCTGTTT	159	60.32 / 60.18	XM_015459069.1
Thioredoxin Reductase	TRXND 1	GCGAAAGGCTCTCGGGTTT	CACGAATCACCTCCCGCCT	89	60.67 / 62.02	NM_174625.3
	TRXND 2	GTGAAGTCCCTGACCTGGGG	TTGGAGACACCGCAAACTGT	110	61.84 / 60.11	NM_174626.2
	TRXND 3	CGAAATCCACGGAAGGGACA	TTGCCCGTCTTCTCACTGAC	133	60.04 / 59.97	XM_015468824.1
Deiodinase iodothyronine	DIO 1	GCCATGGGCGAGAAGACTGGC	TGGGGCCAGACCCCCTTGTT	153	65.96/65.86	NM_001122593.1
	DIO 1	GTACAGGACCCTGCCCTCCTGG	CCCGTGCCCCGTGGTGGTAG	103	66.04/67.37	NM_001122593.1
	DIO2	GCCCCCAATTCCAGCGTGGT	AGGTCAAGTGGCCGAGCCGA	162	65.57/ 66.12	NM_001010992.4
	DIO3	CTTGGGGGAGGATGCTTGAG	TGGTCGAGGCCAGTTAGAGA	115	60.11/ 59.96	NM_001010993.3
	DIO3	CGCGGTTGGTGGTCGGAGAG	AAGCGCGGGAAGAGCACGAG		65.5	
	DIO3	GTCGCGGTTGGTGGTCGGAG	TGGGCGCAGAGCCTCAAGGA		66	
Selenoprotein P	SEPP1	GCTCAGGGGGTGAGGTAAAC	TCTGTCCCTCCGGTTAGGAG	187	60	NM_174459.3
	SEPP1	TTCTGACTTTCGCTCAGGGG	TCTCTGTCCCTCCGGTTAGG	200	59.63/60.03	NM_174459.3
Selenophosphate synthetase 2	SEPHS2	AATAGAATTGCTGCCGGGCT	GTTCCTTGCAGGAGACCGAA	203	60.11/59.97	NM_001114732.1
	SEPHS2	GTCGGAGGCCTTGAAGAGAC	GTCTCAGGGGTATGACGCAG	115	60.11/59.90	NM_001114732.1
Selenoprotein 15	Sel15	AGGTTCCCTCAAGTCCAAGC	AGCAATGTTCCCACTGTCGT	126	59.60/59.89	NM_001034759.2
Selenoprotein K	SelK	CGGCCTGTGATGTAAGAGGG	TGCTGTCCAACACTTGTCCA	130	60.18/59.75	NM_001037489.2
Selenoprotein M	SelM	CTCCAGCTTGCGGATCATCT	GGCCTTGTAGACGGTTCCAG	134	59.89/60.39	NM_001163171.1
Selenoprotein N	SePN1	CTACCTGTCCAACAACCGCT	GCATGGATGCGGAACATCAC	183	59.97	NM_001114976.2
Ethanolaminephosphotransferase 1	Selenoprotein I - EPT1	CCTACTTGGCTGGCTCCAAA	GCCCACTACAATCCAGACCC	150	59.96/60.11	NM_001075257.1
Housekeeping gene - 18sRNA - Bos taurus ribosomal protein S18 (RPS18)		CAGTGGAGGCCTACACGCCG	AGGCAATTTTCCGCCGCCCA	119	65.26/65.84	NM_001033614.2
Bos taurus collagen type II alpha 1 - RNA transcript variant 2/1: qCol2a1		CTGGATGCCATGAAGGTTTT	GCTCCACCAGTTCTTCTTGG	93	56.27/58.47	NM_001113224.2
Bos taurus collagen type X alpha 1	qCol_10	CCCATGCTTGGGTAGGTCTG	CCATACCTGGTCGTTCTCGG	131	60.11/59.90	NM_174634.1
Proliferating cell nuclear antigen PCNA	pCNA	GTCAGGAGTCAACCAAGA	GGATACAGTGAGTTCTACCA	100	53.34/53.51	NM_001034494.1

Figure 66: Primer List

16.2.2 Real-Time quantitative PCR Analysis

At the end of qPCR reaction process, a typical amplification curve denoted with the PCR cycle number on the x-axis and the fluorescence from the reaction on the y-axis. On the figure 67, two principal reaction phases can be identified: first an exponential phase and secondly a non-exponential plateau phase. The amplification reaction are initiated but the fluorescence coming from the amplified product remains low and are not distinguishable from the fluorescence background levels. Nevertheless, after few cycles, the accumulation of the amplified product reach a level where a detectable fluorescence signal comes out. A cycle number determines this stage and is called quantification cycle Ct and it is used to accurately calculate the initial amount of template present in the sample at the start of the amplification reaction. The greater the amount of starting template present, the fewer amplification cycles will be required to yield a detectable fluorescent signal. Then an exponential phase starts where the amount of PCR product approximately doubles with each cycle. As the reaction proceeds, reaction components are consumed leading to one or more of the components becoming limiting, this causes the reaction to slow and enter the plateau phase.

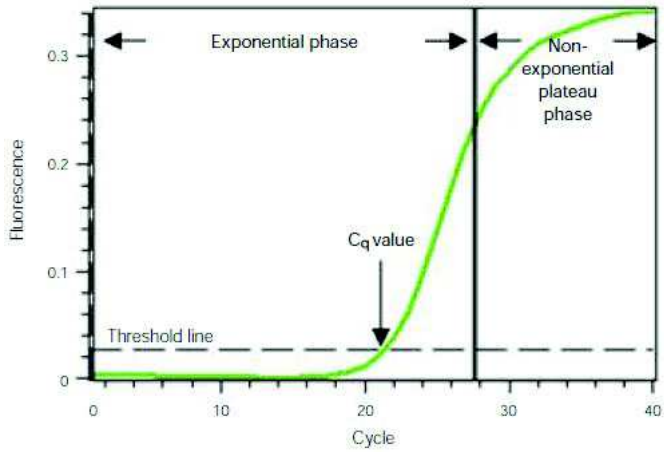

Figure 67: Typical amplification curve for a qPCR reaction (*BioRad website*). The plot shows the exponential and plateau phases of the reaction. Initially, fluorescence remains at background levels and increasing fluorescence is not detectable (cycles 1-18), even though product accumulates exponentially. Eventually sufficient amplified product accumulates to yield a detectable fluorescent signal. The cycle number at which this occurs is called the quantification (number, Cq). At the end, a plateau phase corrsponds to the end of the amplification process where the reaction components are then almost all consumed.

In order to proceed to the data analysis, some steps have to be verified. First, it is important to confirm that there is no fluorescent signal from the controls (-RT and NTC). If a positive fluorescence (Cq $<$ 38) appears for –RT control, this indicates the presence of genomic DNA contamination following mRNA extraction. If a positive fluorescence (Cq $<$ 38) appears for NTC control, this indicates the presence of contamination from the PCR setup procedure. Ideally, the control samples should not yield a fluorescent signal. However should this occur, samples that have Cq values close to, or above the Cq of the control must be disregarded. Secondly, the determination of the starting quantity (SQ) of template present in each sample has to be controlled (done using the Bio-Rad CFX manager software). The logarithm of the SQ values of the standards is plotted on the x-axis and their respective Cq values plotted on the y-axis The equation for the linear regression line ($y = mx + c$, or Cq = m(log quantity) + c) can then be determined. Based on the equation for linear regression, the following equation can be derived to determine the SQ of the unknown sample.

$$N_n = 10^{\frac{(n-c)}{m}}, \, where \, n = Cq \tag{11}$$

$$Quantity = 10^{\frac{(Cq-c)}{m}} \tag{12}$$

Here, at least four biological replicates should be used. The data will be presented in charts that show all biological replicates

Data Analysis: When a real-time qPCR is performed, the obtained results can then be analyzed according two different methods: absolute quantification and relative quantification.

Data Analysis: With absolute quantification, the concentration of the gene of interest normalized to the housekeeping gene is simply the ratio of the content of the gene of interest and housekeeping gene, both contents in ng (nanograms) as

$$\frac{\text{[gene of interest]}}{\text{[house keeping gene]}} \tag{13}$$

Data Analysis: The relative quantification method uses the difference between the tested gene and the housekeeping gene which means correlate the Ct values of the household gene and the gene of interest.

ΔCt is the difference between gene of interest and housekeeping gene [Cq $_{Gene\,of\,interest}$–Cq $_{House\,keeping\,gene}$]. Housekeeping genes often used are β-actin, GAPDH, β-2-microglobulin and 18S. Here, 18S have been selected. To visualize this difference, a plot can be made using the following calculation can be used:

$$\frac{1}{2^{-\Delta Ct}} \tag{14}$$

This value is can be further calculated into the $\Delta\Delta Ct$ corresponding to the difference between $\Delta Ct_{baseline}$ and ΔCt_{gene}. This value takes into consideration the differences between gene and household gene and also the difference in test conditions (example: differences between treated conditions and control condition). Consequently, the calculations have to be the following:

$Ct_{gene\,baseline} - Ct_{housekeeping\,genebaseline} = \Delta Ct_{gene\,baseline}$

$Ct_{gene\,treated} - Ct_{housekeeping\,gene\,treated} = \Delta Ct_{gene\,treated}$

$\Delta Ct_{gene\,treated} - \Delta Ct_{gene\,baseline} = \Delta\Delta Ct$

It is possible to visualize it using the formula:

$$\frac{1}{2^{-\Delta\Delta Ct}} \tag{15}$$

Statistical Analysis: Data range should be demonstrated via the standard deviation SD, not the standard error of the mean (SEM). The differences in gene expression of less than 10-fold should be reported with care, unfortunately a verification by more stringent mRNA QC and/or alternative scientific techniques (e.g. protein expression analysis) have not been performed related to timing problems.

Several tests (T-test, ANOVA, Tukey test) have been done in order to determine the insignificance of the results regarding to each independent groups.

Source: Real-Time PCR Applications Guide - BIORAD

16.3 Screening of the selenoproteins expression in articular cartilage tissue

PCR analysis was performed to determine the level of expression of selenoprotein genes in articular cartilage. This was followed by an identification of the amplified product by size in agarose gels by comparison with molecular weight standards to verify that the obtained amplicon corresponds to the genes of interest. This also allowed the selection of the most interesting targets.

PCR reactions were prepared as described previously Table 14 and then the 10 μL amplified product was run by electrophoresis in a 1% agarose gel at 75V. Images of the fluorescence of the amplified products trapped in gels have been taken using the ChemiDocTMMPSystem and the images were treated using the Image Lab version 5.2.

Preliminary experiments were performed to screen the presence of the range of selenoproteins present in bovine articular cartilage. Using a cDNA template coming from bovine immature and mature articular cartilage materials, a preliminary analysis of expression was determined. As seen Figure 68, the agarose gel evaluation of the potential targets according to the bovine AC cDNA presents some interesting targets to investigate such as GPX1, TRND1, Sel15, Sel M, Sel N, SPHS2 and potentially GPX 5 and 8.

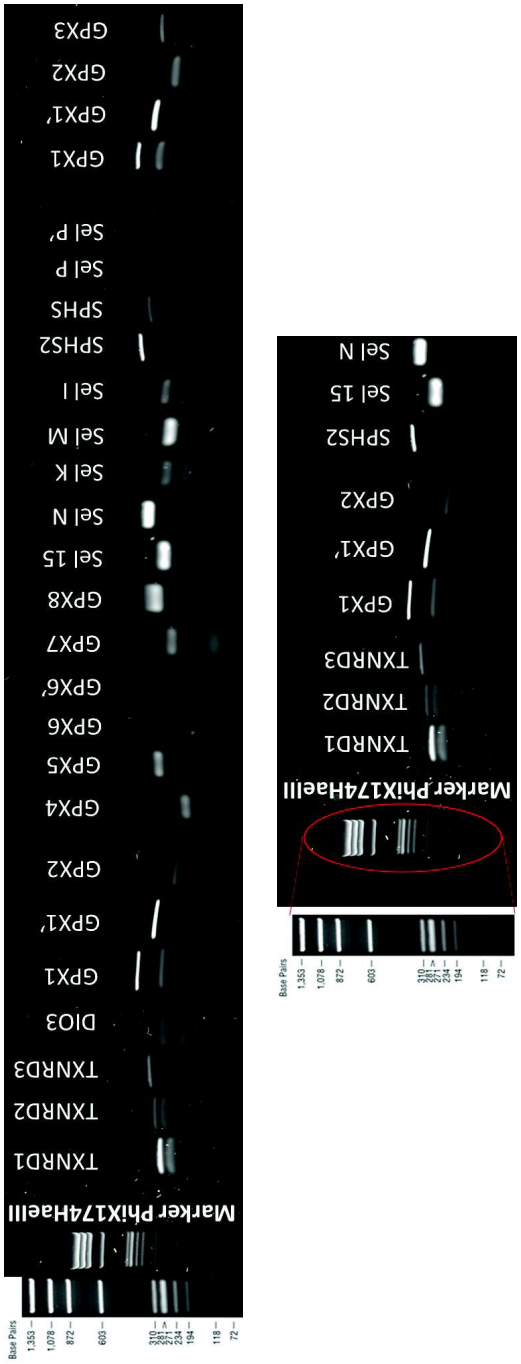

Figure 68: Screening of the selenoproteins expressed in articular cartilage (upper part). PCR amplified products selected (bottom part)

Other experiments were then conducted using cDNA made from cultured explants. The TRXND1 (Figure 69B) presents a band at 88 bp for all the treated sample cDNAs. Nevertheless, an unspecific band underneath appeared, this non-specific band was lost by adjusting the annealing temperature during a qPCR primer optimization step. The other members of the thioredoxin reductase family were positive for PCR bands, TRXND2 at 109 bp and TRXND3 at 132 bp (Figure 69B). The two primer pair sets for DIO1 PCR had a single band at the correct amplicon size and the bands were not specific. (Figure 69A). DIO2 primers amplified an intense band at 161 bp, specific to the gene of interest (Figure 69A). Concerning the three different DIO3 primer pair sets, only the primer pair F1/R1 presents a specific intense band at the correct molecular weight position (Figure 69A). In the glutathione peroxidase family, the GPX1 present bands at the right molecular weight and the primers sets displayed high specificity (Figure 70A). GPX 3, 4, 5, 7 and 8 primers also amplified bands corresponding to the size of the expected amplicon (Figure 70A). The same pattern is as seen with primers for SEPHS2, SelK, Sel15, SelI and SelN (Figure 70B). Concerning the GPX8 (Figure 70A), a double specific band appears and the lower band does not appear to be related to primer dimer formation as it is too large. The band may be the result of alternative splicing but we did not investigate further.

A)

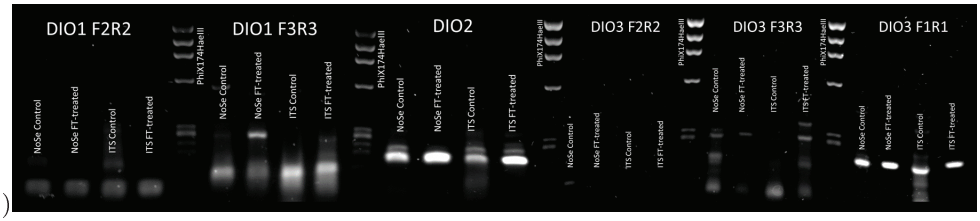

B)

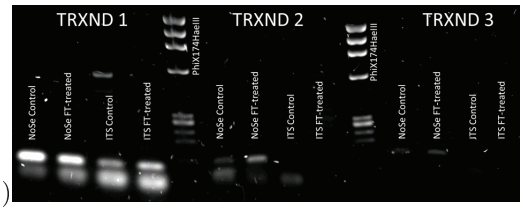

Figure 69: Screening of DIO (A) and TRXND (B) family expressed in Se-treated articular cartilage. From the left to the right each selenoprotein gene analysed: Ladder marker PhiX174HaeIII, NoSe Control, NoSe FT-treated, ITS Control and ITS FT-treated.

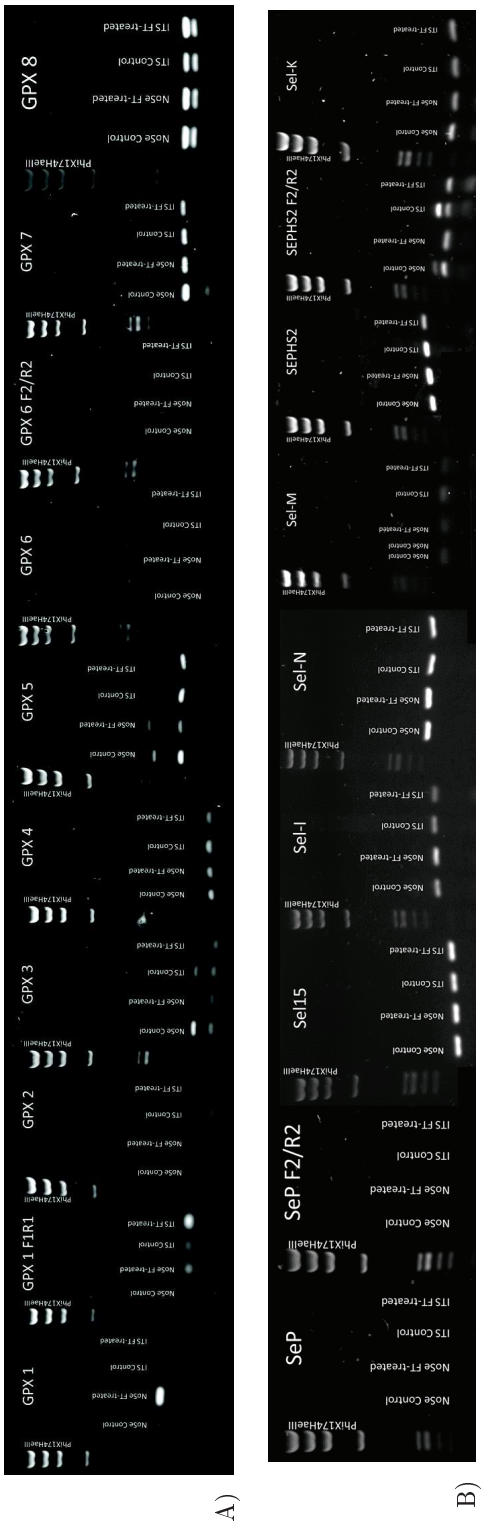

Figure 70: Screening of (A) GPX family and (B) selenoproteins (P, 15, I, N, M, H) expressed in Se-treated articular cartilage. From the left to the right each selenoprotein gene analysed: Ladder marker PhiX174HaeIII, NoSe Control, NoSe FT-treated, ITS Control and ITS FT-treated.

A qPCR experiment was performed in order to optimize the PCR conditions for primer pair sets. The thioredoxin reductase family, DIO1, DIO2, GPX1-7-8, SelN, SelK, Sel15 and SEPHS2 were optimized and were ready to use for further analysis.

16.4 Quantification of the gene expression for selenoproteins

Quantitative PCR analyses have performed on specific groups of genes. Specific targets have been selected in accordance to the literature where some genes appear to be differentially regulated during the postnatal maturational process in articular cartilage [202]. The genes that we have studied are the following: Aggrecans, Collagen II, PCNA, DIO2, TRXND1 and GPX1. 18S has been selected as housekeeping gene. This analysis have been performed with n=4 samples per group and for k=6 independent groups.

An increase in type II Iodothyronine deiodinase gene expression appears as explant matures from control to growth factor FT-treated: a 4.5-fold increase is observed for the sample group cultured in Se-depleted media (No Se), about 7.5-fold increase for the ITS media cultured samples and about 10-fold Se-supplemented sample group (Figure 71, $p<0.01$). No significative difference is observed between the FT-treated samples and the three groups. The controls (No Se Control and ITS Control) suggest a possible influence of the selenium on the gene expression ($p\tilde{}0.05$).

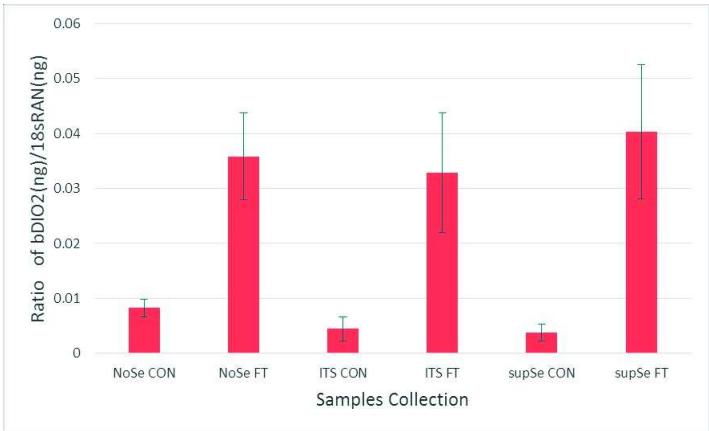

Figure 71: Transcript levels of DIO2 for the different explants treated in presence (FT) or absence (Control) of growth factors and in different Se-content composition (NoSe, medium depleted in Se, ITS, usual tissue culture media (and SupSe with add sodium selenite in the usual ITS media). All the groups are significatively different ($P < 0.01$) except the couples NoSe Control vs ITS Control, NoSe Control vs SupSe Control, No Se FT vs ITS FT, No Se FT vs Sup Se FT, ITS Control vs SupSe Control and ITS FT vs SupSe FT.

A 4.6-fold (No Se group), 9-fold (ITS group) and 8.8-fold (Se-supplemented group) increase of the gene expression from the control to the FT-treated samples is also observed for GPX1 (Figure 72, $p<0.01$). No significative difference is expressed between the diverse controls (NoSe, ITS, Se supplemented). An augmentation of the GPX1 transcript level is observed in the case of matured (growth factor treated) explants (different factor of 1.8 between No Se and ITS and 1.5 between No Se and Se-supplemented, $p<0.05$). This trend of the GPX1 presented data indicates that the growth factor induced-maturation influences the GPX1 level and is expressed by an up-regulation of its expression. Selenium content could have a potential impact on this gene level during the maturation process.

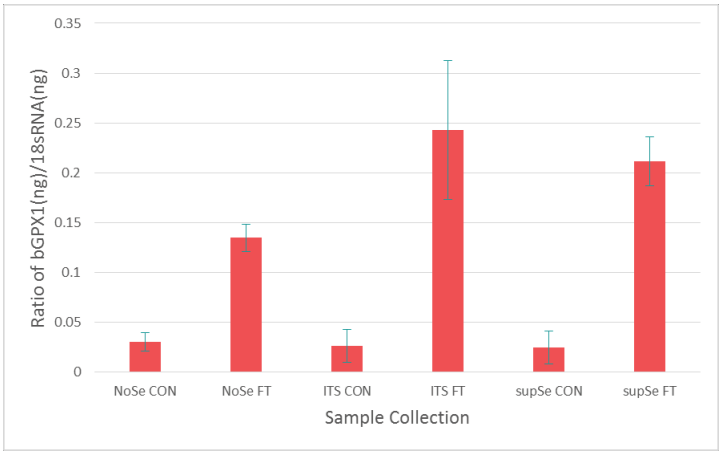

Figure 72: Transcript levels of GPX1 for the different explants treated in presence (FT) or absence (Control) of growth factors and in different Se-content composition (NoSe, medium depleted in Se, ITS, usual tissue culture media (and SupSe with add sodium selenite in the usual ITS media). All the groups are significatively different ($P < 0.05$) except the couples NoSe control vs ITS Control, No Se Control vs SupSe Control, ITS Control SupSe Control and ITS FT vs SupSe FT

The collagen II $\alpha 1$ gene expression is largely more dominant in the controls than in the growth factor FT-treated samples, with about 100-fold transcript gene level difference for No Se group, about 70-fold for ITS group and about 60-fold for Se-supplemented (Figure 73, $p<0.05$). The significative difference appears between NoSe controls and both Se-supplemented controls (without growth factor treatment) ($p<0.05$) collagen can be influenced by selenium content. Maturation influences the regulation of this gene, however due to the large standard deviation, no clear conclusion can be provided concerning the potential influence of the selenium in these culture explant treatments.

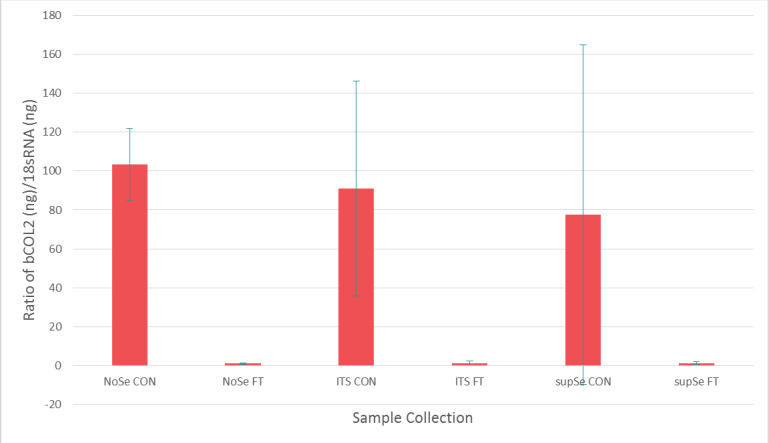

Figure 73: Transcript levels of COL2 for the different explants treated in presence (FT) or absence (Control)of growth factors and in different Se-content composition (NoSe, medium depleted in Se, ITS, usual tissue culture media (and SupSe with add sodium selenite in the usual ITS media). (Left red 2015 – Right green-blue2016). All the groups are significatively different ($P < 0.05$) except NoSe control vs ITS control, NoSe control vs SupSe control, NoSe FT vs ITS FT, NoSe Ft vs SupSe FT, ITS control vs SupSe control and ITS FT vs SupSe FT

An increase of the transcript level of aggrecans is observed in control (no growth factor treated) samples compared to the growth factor maturation induced-explants (FT) for each group of culture No Se cultured explants (about 7-fold increase), ITS cultured (about 5-fold increase) and Se-supplemented (about 3-fold increase) explants with a significative difference between controls and FT-treated samples

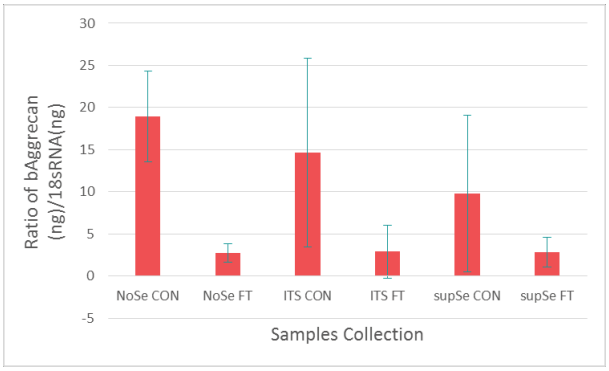

Figure 74: Transcript levels of bovine Aggrecans for the different explants treated in presence (FT) or absence (Control)of growth factors and in different Se-content composition (NoSe, medium depleted in Se, ITS, usual tissue culture media (and SupSe with add sodium selenite in the usual ITS media). No Se Control vs No Se FT, NoSe Control vs ITS FT, No Se Control vs SupSe FT, No SE FT vs ITS Control, ITS Control vs ITS FT and ITS Control vs SupSe FT are significatively different ($p<0.05$),

(Figure 74, $p<0.05$ for NoSe and ITS groups). A significative difference is also present between No Se Ft-treated and ITS control samples. No significative differences appear between controls and the FT-treated of the Se-supplemented group using Student T and Turkey tests for statistical analysis. Selenium may have an influence on condition (not fast maturated explants). Further repeats will be needed to state about a potential influence of the selenium in control conditions (without any growth factor supplementation). Due to a large variability in Se-supplemented samples, no statement can be made.

Further details are provided in annexe.

17 Synchrotron Microspectroscopy: Extracellular Matrix Characterisation of Articular Cartilage

17.1 Synchrotron Fourier Transform Infrared Microspectroscopy

When an infrared (IR) radiation passes through a sample, the radiation can be either absorbed or transmitted, depending on its frequency and the structure and state of the molecules in the sample. IR radiation excites certain molecular groups, producing vibration at fixed wavelengths. The IR spectrum reflects the chemical structure and three-dimensional orientation of the molecules in the sample. The most useful vibrational frequencies of most molecules correspond to the mid-IR spectrum (between 4 000 and 400 cm^{-1}, or from 2,5 to 25 μm). This allow IR spectroscopy to be used in sample identification and investigation of molecular structure. In the case of biological samples, we can found spectral windows that are commonly depicted within the mid-IR and assigned to particular functional groups: (i) the window between 3 000 - 2 800 cm^{-1} which reflects the dominance of the C-H stretching vibrations of -CH3 and >CH2 functional groups, which are abundant in membrane fatty acids, and the side-chain vibration from some amino acids, (ii) the window between 1 800 and 1 500 cm^{-1}, in which the peaks produced by amide I and amide II groups belonging to proteins and peptides are very intense and provide global information on protein structure. The bands near 1 740 cm^{-1} are caused by >C=O stretching vibrations of the ester functional groups in lipids, (iii) the window between 1 500 and 1 200cm^{-1} is a mixed region influenced by the bending modes of >CH2 and -CH3 groups in proteins, fatty acids, and phosphate-bearing compounds, and (iv) the window between 1 200 and 900 cm^{-1} is mainly due to the symmetric stretching vibration PO_2^- groups in nucleic acids and to C-O-C

and C-O-P stretching , which reveals the occurrence of carbohydrates and polysaccharides in the cell wall for example and also the influence of nucleic acids.

The corresponding amount of mid-IR radiation absorbed, A, by the pure sample substance at a particular wavenumber ν (cm^{-1}), with

$$\nu = 1/\lambda \tag{16}$$

is expressed as:

$$\mathrm{A}=\log(\tfrac{1}{T})=\log(\tfrac{I}{I_0}) \tag{17}$$

with I the intensity of mid-IR radiation passing through the sample, I_0 the intensity of mid-IR radiation reaching the detector in the absence of the sample (reference background spectrum), T the transmittance of the sample at a particular wavenumber ν .

Further, the Beer-Lambert law states that infrared absorption (at specific wavelength) is related to the concentration of the different molecular species in a sample following the formula:

$$\mathrm{A}(\lambda) = \epsilon(\lambda).\mathrm{b}.\mathrm{c} \tag{18}$$

where A is the wavelength-dependent absorbance (measured spectrum), ϵ is the wavelength-dependent absorptivity coefficient, b is the optical path length of light (sample section thickness), and c is the concentration of the investigated molecular species. ϵ is assumed to be material-specific when the absorbance is directly related to the chemical concentration of the molecules, provided that the sample thickness is constant.

Fourier-transform infrared (FTIR) spectroscopy, was developed in the early '70s and later a new class of spectrometers was commercially available, based upon the combination of a FFT (Fast-Fourier-Transform) algorithm and computers. In FTIR spectrometers, IR light is focused through an interferometer and then through the sample. A moving mirror inside the apparatus alters the distribution of infrared light (wavelength) that passes through the interferometer. The recorded signal, called an interferogram, represents light output as a function of mirror position, which correlates with wavelength. A FFT data-processing transforms the raw data into the sample spectrum. A major advantage of the FTIR spectrometers is that the information in the entire frequency range is collected simultaneously, improving both speed and signal-to-noise ratio (SNR). The absorbance is measured as a peak height, peak height ratio, peak area, or peak area ratio from the Fourier transform infrared (FTIR) spectrum. FT-IR absorbance spectroscopy without a microscope has no or very limited spatial resolution and the sample spectrum reflects the average biochemical and structural information referred only to the whole probed sample. The addition of an FT-IR microscope to the IR spectrometer opens the possibility to detect vibrational motions of molecules within very restricted regions of the sample allowing the development of microFT-IR spectroscopy. The FTIR microscope is used to associate the optical image of selected object, for instance an individual cell, with the corresponding IR spectrum or its chemical image and it has been used for the analysis of articular cartilage [22, 203].

The FT-IR microscope is similar to visible light microscope but it employ reflective microscope objectives that allow large collection angles without chromatic aberrations, which helps FTIR systems to achieve high spectral resolution over wide spectral ranges. FT-IR microscopy is often performed in transmission requiring samples deposited on optical windows (e.g. ZnSe, CaF2, and BaF2 crystals) that have very high values of transmittance within a wide range of frequencies in the mid-IR region. The IR microscope works like a standard optical microscope allowing the sample to be inspected and areas selected prior to FTIR analysis. The optical images can be recorded in order to associate the

image of selected object with its corresponding FT-IR absorbance spectrum detected through a single channel highly sensitive mercury cadmium telluride (MCT) photoconductive detector cooled in liquid nitrogen. Adjustable aperture slits of IR opaque material allow to delimit selected spot areas from which IR signals is acquired. Working with a conventional thermal source such as Globar, which emits mid-IR radiation in a 360 degrees distribution, and with aperture sizes reduced to $\sim 20\mu m \times 20\mu m$ or less, the photon throughput towards the detector significatively reduces while the detector noise remains constant and the value of signal to noise ratio (S/N) is strongly decreased independently on the duration of acquisition. Moreover, working with aperture sizes approaching the wavelength of mid-IR radiation (2.5μm-25μm) the recorded spectra become increasingly distorted due to diffraction effects increasing difficulties in spectra analysis and interpretation. Therefore, to increase S/N values to obtain high quality chemical image of a sample like a section of articular cartilage, one can take advantage of the much higher brightness source from Synchrotron Radiation (SR). This allow to use shorter aperture settings ($<20\mu m \times 20\mu m$ down to the diffraction limit of $\sim 3\mu m \times 3\mu m$) and thus higher spatial resolution compare to a conventional Globar source. This is mainly due to the fact that the flux of SR IR photons is not a limiting factor during the acquisition of IR signals. In this situation, spatial resolution becomes diffraction limited. The identification and assignment of major spectral components by "functional group analysis" is particularly useful for the qualitative analysis of pure organic molecules since the IR spectrum of each molecule is unique and it can serve as a signature to distinguish among different molecules, for instance pure proteins, nucleic acids DNA and RNA, lipids, and sugars. However biological samples are complex material and most often the IR spectrum of a sample like articular cartilage contains many mid-IR active molecular constituents resulting in a large number of overlapping bands and various spectral features. During spectra collection, spatial indication and chemical composition are stored pixel by pixel to provide a biochemical map of the sample section. Here, FTIRM determine the spatial composition of the main structural components of the organic matrix of the articular cartilage: proteoglycans and collagens. In literature, the ideal compromise for cartilage analysis is to set spatial resolution to 10μmx10μm [22] .

17.2 Methods & Materials

17.2.1 Sample Preparation

According to the Beer-Lambert law, it is required that tissues are sectioned sufficiently thin to ensure a linear response in absorbance as a function of concentration and avoid detector saturation. This results in spectra with well-defined absorption peaks. Sample sections can be made from both paraffin-embedded or frozen-hydrated cartilage samples. Here, cryosections from cryofixed cartilage explants were selected to prevent all risks of interferences with the paraffin IR absorption bands. Cryosectionning is mainly preferred in FTIRM because it does not require any fixation or complex processing. Paraffin-embedding process may alter tissue properties and affect or shift the signal of interest with concomitant artifacts in the quantitative analysis [204]. Furthermore, cryopreserved tissue allow to investigate hydrated biological samples in a close-to-native state compared to sample embedded into paraffin, a procedure that requires a succession of chemical baths. However, contrary to paraffin-embedding, cryo-sectioning may be prone to larger variations in section thickness. The section may not be perfectly flat and more difficult to maintain on the infrared window [205]. During measurements, samples may lift up under intense IR beam but also because of the LN2 purge of the microscope device required to remove atmospheric water and CO2 absorption bands from the optical path. They also have a tendency to wrinkle, being placed on the IR-window without any other treatments.

However, this technique allow to do imaging of functional groups from large area and to study the overall structure of the cartilage from its superficial zone down to the calcified area. In our study, we used thin section of the articular cartilage explants sections (sectioning perpendicular to cartilage surface). The recommended thickness for tissue sections investigated through FTIR microspectroscopy should be between $3-15\,\mu$m [22]. Indeed, to obtain an optimal sample thickness, a compromise have to be made in order to have enough tissue to get some interesting signals and not too much material to do not saturate the detector. Then, the adequate signal-to-noise ratio has to be maintain during experiments. The adequate section size for articular cartilage was found around $(10\pm2\,\mu$m) resulting in appropriate absorbance of the different IR bands over the entire mid-IR spectrum. The sectioning samples are then placed onto an infrared transparent window such as BaF_2 which have the largest interesting transmission range and allow to observe all the functional groups and molecular vibration of interest from 2 000 - 900 cm^{-1}[22].

17.2.2 Measurements of Articular Cartilage Samples and FTIR Imaging

Parameters:

For articular cartilage, it is really important to map a large specific area going from the surface of cartilage to the subchrondral bone zone because variations in the composition appear along the depth-wise direction. Generally, high quality spectral data is often required in order to proceed to a complex data analysis on the substructure and/or composition. These high quality data are time-consuming. In fact, it is important to maximize as best as possible the signal-to-noise ratio S/N in order to produce high-quality spectral data and several parameters also influence the acquisition time of the experiment: the spatial resolution define through IR apertures, the spectral resolution, number of co-added scans (signal-to-noise ratio) and the size of the area within the tissue section to be image. In general, the square root of the number of co-additions is proportional to the S/N, and therefore an increased number will enhance the S/N. We can mention that the interferometer mirror velocity may have an effect on S/N as does a weighting of the interferogram with an apodization function reducing the S/N. A synchrotron radiation light source is ~ 100–1,000-fold brighter than current benchtop thermal globar source and thus may still generate high S/N IR spectra when using apertures approaching the diffraction limit (down to 3x3 μm^2). Thus, a synchrotron source has a natural sampling aperture of 10–20 μm in diameter with a high S/N [206]. It is therefore possible to achieve spatial resolution compatible with tissue microstructure, allowing tissular molecular distribution analysis. Maps can be generated when point spectra are collected in a stepwise manner in a grid from a target area, which is useful for comparing the different region of interest of a tissue like articular cartilage. Generally, this can take several hours for a single sample even when using a synchrotron radiation (SR) source coupled to an IR microscope. The choice of resolution parameters is also a compromise between the S/N and the required level of information. For example, if we increase the spatial resolution the S/N will be lower. To compensate, the number of co-added scans can be increased to obtain higher S/N. It is possible to note that the raw absorption spectrum is only slightly affected by a decrease of the spectral resolution. $16\,\mathrm{cm}^{-1}$ resolution is often used to observe the features and analyse of simple data sets. Nevertheless, some fine spectral features can only be detected through the use of second-derivative spectra. In this case, the ideal spectral resolution generally used is between $4-8\,\mathrm{cm}^{-1}$ [22]. In our case, we selected the spectral resolution of $6\,\mathrm{cm}^{-1}$ with a spatial resolution of 10x10 μm^2.

Measurements and Acquisition:

FTIR measurements for articular cartilage are made in the spectral region, $900-2000\,\mathrm{cm}^{-1}$, related to most interesting AC feature changes [22]. In order to substrate of some external factors, a background spectrum has to be measured. This reference background spectrum is collected from

an empty area of the infrared window, where no material (biological sample or glue) is present on the window. The background spectrum take into account atmospheric effects (e.g. water vapour and carbon dioxide) and also the absorption generated by the infrared window itself, and uneven wavenumber distribution induced by the spectrometer. Nevertheless, it can also be useful to measure a spectrum of the emdebbing matrix of the sample (cryomatrix, resin...) to take into account a residual contribution of this embedding medium that can be spectrally substracted from the original spectra. In the AC study, the water vapour can be seen as the most problematic factor because it can absorb infrared light in specific regions for the FTIR spectroscopy of articular cartilage, i.e. the amide I and II spectral regions [22]. In order to unbalance this problem, the sample box is purged with dry air or nitrogen vapour to stabilize the atmospheric conditions and minimize the amount of water vapour and carbon dioxide. In the FTIR cartilage investigations, infrared light transmission is the most commonly used technique.

17.3 Data Analysis Methods: Semi-Quantitative Spectral Features of InfraRed Absorption of Articular Cartilage

In order to obtain a complete analysis of the variations in the AC explants cultured under different conditions, a semi-quantitative method was used, based on absorption band area. Spectral pre-processing is essential to normalize data sets and to allow direct comparison of data coming from different studies that are combined. Data have to be evaluated and filtered in order to minimize the non-biological variation between different measurements. A control of the data quality has to be done during this pre-processing phase which include the evaluation of signal-to-noise-ratio and water vapour limitations but also some corrupted data have to be removed from the analysis (for example, unwanted pixels where the Mie scattering is too high and the absorption induced saturation can corrupt the analysis). The same baseline correction has to be applied on the different data sets. Nevertheless, all pre-processing has to be applied in order to not alter biological information and has to reduce the variance caused by the measurement conditions. In this study, the "automatic baseline correction" of OMNIC software have been used. The correction [11] is done by first fitting a quadratic to the spectrum, Y(x), by linear least squares:

$$Y(x)\,Y^{'}(x) = ax^2 + bx + c \tag{19}$$

The maximum difference between $Y(x)$ and $Y'(x)$ is found. When the points from $Y(x)$ and $Y'(x)$ differ from the maximum difference divided by two, they are eliminated from Y(x) to provide a subset of the spectrum. After 20 iterations , the resulting $Y'(x)$ is subtracted from the original $Y(x)$ to provide a "baseline corrected" spectrum. The spectrum is then offseted by the value of its lowest point to give a spectrum with its minimum value of zero.

Collagen molecules constitute the major part of the articular cartilage solid matrix, collagen having stronger contribution to these absorption peaks [22]. According to the literature, the amide I region is traditionally used to evaluate the collagen content in AC samples [207]. In amide III region ($\approx$1200-1300 cm^{-1}), the absorption is related to combination of C-N stretching, N-H bending, C-C stretching, and sulfate stretching vibrations, as well as CH_2wagging vibrations [207]. The sulfate stretching vibrations are associated to PGs but the other vibrations are linked to the contributions of both collagen and PGs. The description of the amide III band contribution is very difficult,

[11] [from Using OMNIC Algorithms, Thermo electron corporation]

and it is assumed that its absorption is more strongly related to collagen molecules. Absorption in the region between amide II and amide III (≈1300-1500 cm^{-1}) is also mixed and relates to CH_2 bending vibrations, CH_3 asymmetric bending vibrations, COO^- stretching vibrations, and CH_2 side chains vibrations of collagen. The small CH_2 side chains vibration peak (≈1338 cm^{-1}) is an important characteristic feature of collagen [210]. However, this region also includes contributions from PGs. Absorption in the carbohydrate region (≈985-1140 cm^{-1}) is mainly related to the stretching vibrations of C-O and C-OH, as well C-C ring vibrations. Although both collagen and PGs contain vibrations in this region, it is believed to be more specific to PGs.

For this experiment, an univariate data analysis was used to evaluate these spectral features: a single variable was extracted from the absorption spectrum such as IR absorption peak height or the IR absorption band area after the baseline correction. Camacho *et al.* [207] identify and quantitatively evaluate the main components of the articular cartilage. Using the measurements of FTIR absorption spectra of pure Co-II, PGs (aggrecans) and some different mixtures of those two components, they provided a correlation table (see Table 15) between molecular functions and absorption peaks/wavelengths. They state that collagen content correlate to the amide I and amide II area regions, and proteoglycan to the carbohydrate region. The PG content is obtained by the ratio of carbohydrate region area normalized by amide I region area.

To enhance univariate analysis, derivative spectroscopic methods can be applied to reduce the noise remaining after the baseline correction. Usually, the second derivative is used on the baseline corrected absorption spectrum [208]. With this processing, positions of original maxima are conserved and correspond to the spectral position of the obtained minima in second derivative spectrum. This second derivative artificially enhance the resolution of the spectrum that can be used to study the secondary structures of proteins (alpha-helix, beta-sheet...) using the amide I or amide II bands. Second derivative method eliminates the baseline shifts and reduces other linear effects from the spectrum linked to the intrinsic property of the samples (e.g.,Mie scattering on cellular border). A smoothing is made using Savitzky-Golay filter to compensate the signal-to-noise ratio reduction related to the derivation. This smoothing was chosen not too strong (data points 5 and polynomial order 3) to avoid distortion and alter the information within the derivative spectrum [22]. In this experiment, a second derivative method was used to evaluate shifts and peak height modifications, if any. Using TQ-Analyst software, a small routine was made to obtain IR absorption map corresponding to the IR index of interest. All details of the method parameters are presented in Tables 15&17. The diverse IR indexes or bands presented in table 17 were chosen relative to the literature:

Interest	Bands - Index	Band Theory	Practical Bands	Baseline superior	Baseline inferior
Proteins - Collagen [203, 207, 209]	Amide I	$1590 - 1720\,\mathrm{cm}^{-1}$	$1590 - 1720\,\mathrm{cm}^{-1}$	$1780 - 1800\,\mathrm{cm}^{-1}$	$950 - 1000\,\mathrm{cm}^{-1}$
Collagen Feature [208, 210]	CH_2 side chains	$1338\,\mathrm{cm}^{-1}$	$1326 - 1350\,\mathrm{cm}^{-1}$	$1476 - 1486\,\mathrm{cm}^{-1}$	$1178 - 1186\,\mathrm{cm}^{-1}$
Collagen [207,210]	Amide III - N-H/C-H deformation	$1238\,\mathrm{cm}^{-1}$	$1232 - 1245\,\mathrm{cm}^{-1}$	$1295 - 1305\,\mathrm{cm}^{-1}$	$1175 - 1185\,\mathrm{cm}^{-1}$
Proteoglycans [203, 207, 208, 209, 211, 212]	Carbohydrates - Sugar Ring Band	$985 - 1140\,\mathrm{cm}^{-1}$	$985 - 1140\,\mathrm{cm}^{-1}$	$1130 - 1140\,\mathrm{cm}^{-1}$	$975 - 985\,\mathrm{cm}^{-1}$
Proteoglycans [208, 211, 213, 214]	C-O stretching	$1062 - 1064\,\mathrm{cm}^{-1}$	$1050 - 1076\,\mathrm{cm}^{-1}$	$1176 - 1186\,\mathrm{cm}^{-1}$	$950 - 960\,\mathrm{cm}^{-1}$
Lipides [215]	C-H stretching/$\nu_{as}CH_2$lipids	$2925\,\mathrm{cm}^{-1}$	$2913 - 2937\,\mathrm{cm}^{-1}$	$3005 - 2995\,\mathrm{cm}^{-1}$	$2800 - 2810\,\mathrm{cm}^{-1}$

Table 15: Absorbance Bands of the selected molecules of interest & TQ-analyst method parameters

17.4 Results

This experiment has been realised at SMIS beamline, SOLEIL Synchrotron (Paris, France). FTIR investigations on immature cartilage tissues are scarce. To properly characterize the extracellular matrix of the cultured explants using FTIR spectra, we have reviewed the different IR index used in the literature and validated some of them for the study of the organic matrix of AC; (table 15) these IR indexes were then applied to our sample collection. Native mature AC explants was obtained from the lateral aspect of the medial condyle of the metacarpophalangeal joints of 18-month old bovine. The Amide I band has often been discussed in literature for its collagen non-specificity relative to the significative PG contribution in this region [208] and alternative IR index based on spectral features rather than Amide 1 band area have been proposed [207, 208, 210]. After a careful analysis of the literature, four indexes have been selected as we found it as the most robust and representative of the AC biochemical composition. The results for mature explant can be found in Figure 108 in Annexes. Indeed, mature explant cannot be considered as a reference for our IR indexes so far the technique used for biopsy limits the punch only to the surface and a part of the middle zone; although, it provides a good indication for comparison to other FTIRM studies on mature cartilage.

The immature articular cartilage being a protein-rich tissue, multiple IR vibrational absorption bands related to the diverse protein characteristics and structures overlapped. Still, it is well-known that the position of the amide I absorption band is sensitive to protein conformation, hence, any shifts or broadening can be attributed to some protein conformational changes in the tissue. Here, the influence and the function of the selenium in this tissue is totally unknown consequently subtle shifts and variations in absorption bandwidth may appear. As seen in Figures 110,111 and 112 in annexes, no clear trend or differences (differences in spectral features, peak shifts...) can be established from the baseline-corrected or the second derivative spectra. Consequently, we decided to focus on the spatial distribution of selected molecular species. The IR absorption maps were processed on the basis of the selected IR indexes and further compared for the different experimental conditions.

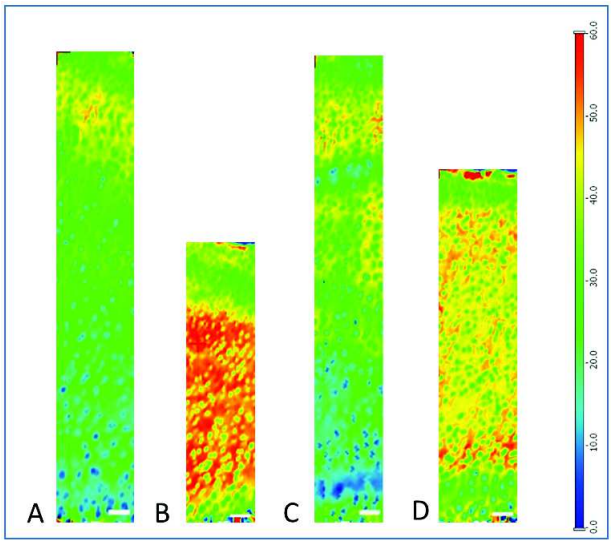

Figure 75: FTIR maps referring Amide I absorption band of the four cultured explants. Spatial resolution of 10μm x 10μm and spectral resolution of 6 cm^{-1}. A) No Selenium treated explant - No Se control, B) No Selenium and growth factors treated explant -No Se FT-treated, C) Selenium treated explant - ITS control and D) Selenium and growth factor treated explant - ITS FT-treated. The white line corresponds to a scalebar of 100 μm.

The amide I (A_I) band often refers to the protein content in most biological material. According

to literature [203, 207-210], the amide I band is strongly correlated to the collagen content of AC sample (Table 15). The collagen content in native immature explant is relatively low (superficial zone) and inhomogeneous, with a slight increase toward deeper zones (Figure 107 in Annexes). In ITS control (Figure 75C)), we can observe a decrease of the collagen content from the surface toward the deeper zones. In No Se Control (Figure 75A), the collagen content is relatively homogeneous in the middle and deep zones. Collagen content of the maturated AC (NoSe FT-treated (Figure 75B) and ITS FT-treated (Figure 75D)) is found to be high mainly in the middle and deep zones. This is indicative of an improved collagen production under growth factor stimulation as it is expected in a mature tissue. This can be referred to the activation of the cellular activity related to the maturation process. Unexpectedly the No Se Control explant show an even higher collagen content than in ITS FT-treated for the middle and deep zones.

The 1062 cm^{-1} band (as defined Table 15) has been shown to refers to the proteoglycan (PGs) content. Immature articular cartilage possesses overall a very low PGs content (Figure 107 in Annexes). The ITS FT-treated samples (Figure 76D) show a dense and homogeneous PG content throughout the tissue. This is also observed for ITS control (Figure 76C), still, we can notice local variations with a less dense PG content in the middle and deep zones compared to ITS FT-treated explants. For No Se control (Figure 76A), the PG distribution is more complex and anarchic with mainly a high PG content that superimpose to chondrocytes position in the deep zone. In Figure 76B), a high PG production is observed in middle and deep zones of No Se FT-treated explants that is found similar to FTIR images of the amide I absorption band used as a proxy for collagen content. As already reported in the literature [208], Amide I band appears then impacted by the more or less important presence of PG. This can consequently influence our interpretation for collagen distribution and content on the sole basis of the amide I absorption band area.

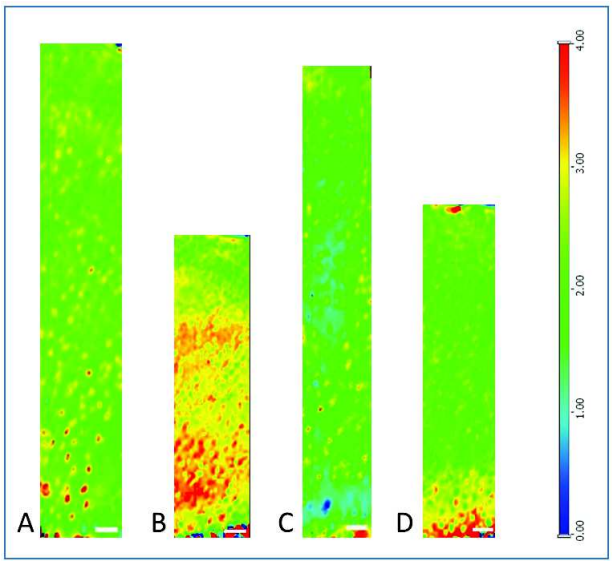

Figure 76: FTIR maps referring 1062 cm^{-1} absorption band of the four cultured explants. Spatial resolution of 10μm x 10μm and spectral resolution of 6 cm^{-1}. A) No Selenium treated explant - No Se control, B) No Selenium and growth factors treated explant -No Se FT-treated, C) Selenium treated explant - ITS control and D) Selenium and growth factor treated explant - ITS FT-treated. The white line corresponds to a scalebar of 100 μm.

Consequently, the spectral feature at frequency ~1338 cm^{-1}, has been selected and has been reported to be a good "collagen signature". [216]. The No Se content (Figure 77A) presents an alteration of the collagen distribution within the middle and deep zones compared to the native

immature tissue (Figure 107 in Annexes). This may be linked to the absence of Se within the medium. The ITS control (Figure 77C) present a reduction of the collagen signal, mainly in the deep zone. This support that the tissue does not reach a stable stage under classical culture conditions and maturation process. On the other hand, growth factor stimulated samples (No Se and ITS FT-treated, Figures 77B&D, respectively) show clearly an induced homogenous collagen distribution within the middle and deep zones. The No Se FT-treated display with decreased collagen content within the superficial zone while PG content appear to be high throughout the middle and deep zones. This confirms that the Amide I band was impacted by PG absorption band in our particular sample culture conditions.

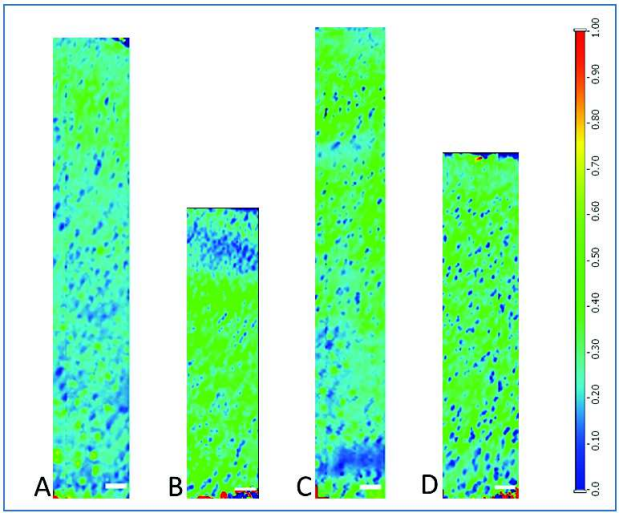

Figure 77: FTIR maps referring 1338 cm^{-1} absorption band of the four cultured explants. Spatial resolution of 10μm x 10μm and spectral resolution of 6 cm^{-1}. A) No Selenium treated explant - No Se control, B) No Selenium and growth factors treated explant -No Se FT-treated, C) Selenium treated explant - ITS control and D) Selenium and growth factor treated explant - ITS FT-treated. The white line corresponds to a scalebar of 100 μm.

Combining the collagen and proteoglycan information, growth factors are definitively important in the AC maturation process. The collagen content increases and tends to be homogeneous throughout the extracellular matrix in maturated AC tissues. However, Se-depletion appears to have an impact on the collagen distribution. When growth factor were added to this Se-depleted culture medium, we observe a balance of that distribution. ITS FT-treated explants presents a distribution of PG and collagen consistent with what can be expected from an accelerated maturation of the AC. contrast with No Se FT-treated explant that shows only a much denser and higher PGs content within the AC matrix. The infrared information provide a qualitative view of the biochemical variations of the AC matrix, however this cannot provide any formal information on the quality of the extracellular matrix. Further experiments have to be proceeded on the biomechanical properties of the AC tissue for this specific *in vitro* model.

17.5 Synchrotron Deep UltraViolet Microscopy

17.5.1 Deep UltraViolet Microscopy

In FTIR microscopy, IR-indexes related to the collagen crosslink in articular cartilage are still debated and not adapted in our case. Synchrotron DUV fluorescence microscopy analysis have been performed as it is fully complementary to FTIR microscopy and as far as it is a powerful technique for molecular histology or to follow metabolic processes in a biological sample [217]. In our model such study was

perform in order to investigate autofluorescent components of the maturated articular cartilage tissue. In particular, it is possible to study the collagen signal that originates from the crosslinks between the amino-acids. This experiment was a preliminary for studying cartilage for our model, this has never been reported while it has already been used to study bone [219] or liver [255]. We need to highlight tha the N-number per condition is limited, and further investigations will be required to be statistically significant, however some trend were observed.

This technique does not require any external probes or labelling, preserving samples from diverse chemical degradations [217]. However, at the microscopic scale, it is mostly limited to visible and near infrared excitation of the samples. Fluorophores naturally present in biological tissues can be excited in the deep UV (DUV, 200– 350 nm) [217-218]. Limitations exist in classic spectrofluorometric technique, mainly related to the lack of high-resolution and poor spectral resolution for which the wavelength range was limited to 350 nm [218]. DISCO beamline (SOLEIL Synchrotron, Paris, France) have developed a DUV fluorescence microscope for cell biology coupled to a synchrotron source which provides fine tunable excitation from 180 to 600 nm. A full spectrum can be acquired on each point of the image to study DUV excited fluorescence emitted from nanostructures [218]. DUV microscopy is very interesting technique to study some specific metabolic markers that do provide characteristic fluorescence emission spectra when excited with UV like nicotinamide adenine dinucleotide (NAD(P)H), collagen, tyrosine, Tryptophan, lipo-pigments, elastin, pyridoxins.

17.5.2 Methods & Materials

Sample Preparation: The samples, described section 10, are after three weeks cultures cryoembedded using precooled hexane in order to preserve as much as possible the structure and the chemical integrity of the tissues. Thin cryo-section of 20 μm were used for DUV microscopy and were mounted on 0.16 mm thick quartz coverslips (25 mm diameter) (ESCO-Optics, US, A1 fused Quartz coverslip, 0.984" +/-.005" DIA X 0.16mm +/- 0.01mm TK) that are free from autofluorescence and give no background. Cryosections have been used to avoid as much as possible the potential artefacts that often occurs during classical dehydration and diverse long embedding processes. The thickness has been fixed at 20μm in order to be within the linear range behavior of the detector.

Parameters and Data Analysis: The POLYPHEME microscope is composed of an Olympus IX71 inverted microscope which is standed homemade replacement of the intermediate lenses that were not transparent in UV. We used the Ultrafluar 40x NA 0.6 objective (Zeiss). We randomly collected spectra from each zone (superficial, middle and deep zones) for each sample (N= 2, per condition), in matrix and in chondrocytes distinctly. 16 points are selected randomly at each acquisition and have been averaged and normalised by an inhouse developped MathLab routine (DISCO beamline). Then, an average of the N number of samples per condition has been realised providing a total spectrum of the autofluorescence signal for each sample condition. Spectral deconvolutions performed by an inhouse developped MathLab routine (DISCO beamline). This routine corrects the baseline "offset" (the minimum is set at zero), then each spectrum is decomposed using the same parameters and 4 component positions were found in our samples: Tryptophan (335-355 nm, Trp), Tyrosine (301-311 nm, Tyr), Collagene (398-410nm, Col) and NaD(P)H. The fit is then calculated using an equation which gave different parameter (details in Annexes) values needed to calculate the peak integrals (area) of the regions of interest. An example of these deconvolution is provided in Figure 78.

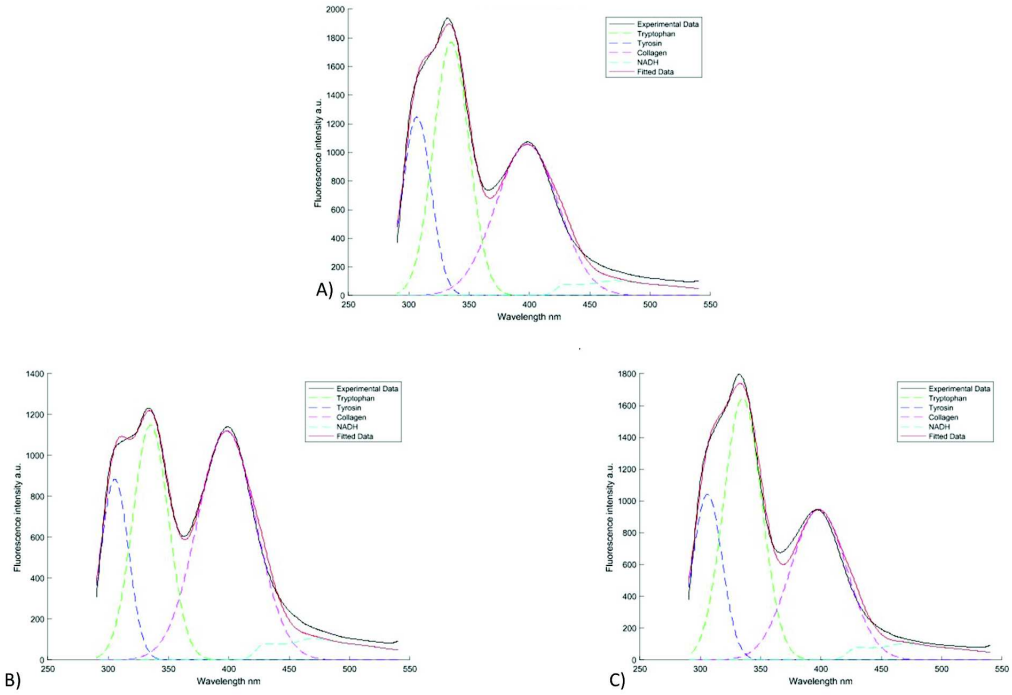

Figure 78: Example of spectral deconvolution of different samples (A) Immature in acellular zone, (B) NoSe Control in acellular zone, (C) ITS FT-treated in deep zone matrix four gaussian standing for Tryptophan (335-355 nm), Tyrosine (301-311 nm), Collagene (398-410 nm) and NaDH (experimental spectrum).

17.5.3 Results

DUV microscopy, using appropriate filters, can reveal all type of collagen, without any discrimination. Of note, we tested second harmonic generation microscopy that is more specific to some type of collagen, but our tests were unsuccessful. It is known that fibril-forming collagens display a strong emission in the DUV domain, attributed to emissions from collagen cross-links [256-257]. Indeed, the collagen signal originates from the crosslinks between the amino-acids. For example, the pyridinium crosslinks i.e., hydroxylysyl pyridinoline and lysyl pyridinoline are detected by means of their natural fluorescence at ~ 395-405 nm emission after excitation at 295 nm [258-259]. The variation of the ratios Tyr/Trp and Col/Trp in the cell domain seem to be interesting (Figure 79).It has been shown that for example phosphotyrosine levels in resting chondrocytes are regulated through activity of both tyrosine kinases and phosphatases [260]. We hypothesized that the Tyr/Trp would be informative on the metabolism of chondrocytes.We also hypothesized that the Col/Trp would be informative on the quality of collagen cross-links so far it has been shown that at least *in vivo* variations in cross-linking chemistry appear to be more related to the type of tissue than to the type of collagen [261]. Potentially, age-related changes in the collagen network, especially in the cross-links, can make the cartilage more brittle.

Both ratios, in cells and matrix have the same trend with a slight increase of these ratio within the ECM. In the superficial zone, for chondrocytes as for region within the matrix, it is difficult to state on a clear trend on the collagen signal, immature explant present a slight higher signal (1.2-fold increase) than the cultured explants. Middle and deep zones present the same sample expression, with a (1.25-fold) reduction of the autofluorescence signal of collagen in the deep zone. For both zones, immature and No Se Control (explant sample without selenium in culture medium, no growth factor treated) present a similar Tyr/Trp and Col/Trp values. Adding growth factors in the culture medium, samples

NoSe FT-treated present an increase of this signal compared to the superficial zone (2-fold increase and 1.8-fold for the middle and deep zone, respectively). In Se-rich culture medium (ITS medium), Control samples possesses 1.3-fold higher collagen crosslink expression that (ITS) FT-treated explants. In this middle zone, a strong difference (about 45%) appears between native immature and mature cartilage which is expected as the quality of the collagen cross-link should be superior. Chondrocytes do present a higher (about 5%) collagen to Tryptophan ratio than the matrix. Changes of collagen and tryptophan signal can be related to protein synthesis and/or degradation. Further analyses on these ratio could potentially provide a better understanding of the key role of chondrocytes in cartilage remodelling regulation during maturation and growth. Still, the data are too preliminary and there is no clear changes for tyrosine and collagen signal that could suggest any alteration of the collagen cross-links and/or degradation, and chondrocytes metabolism. The only clear change is for mature cartilage as it could be expected when compared to immature cartilage and *in vitro* matured explants.

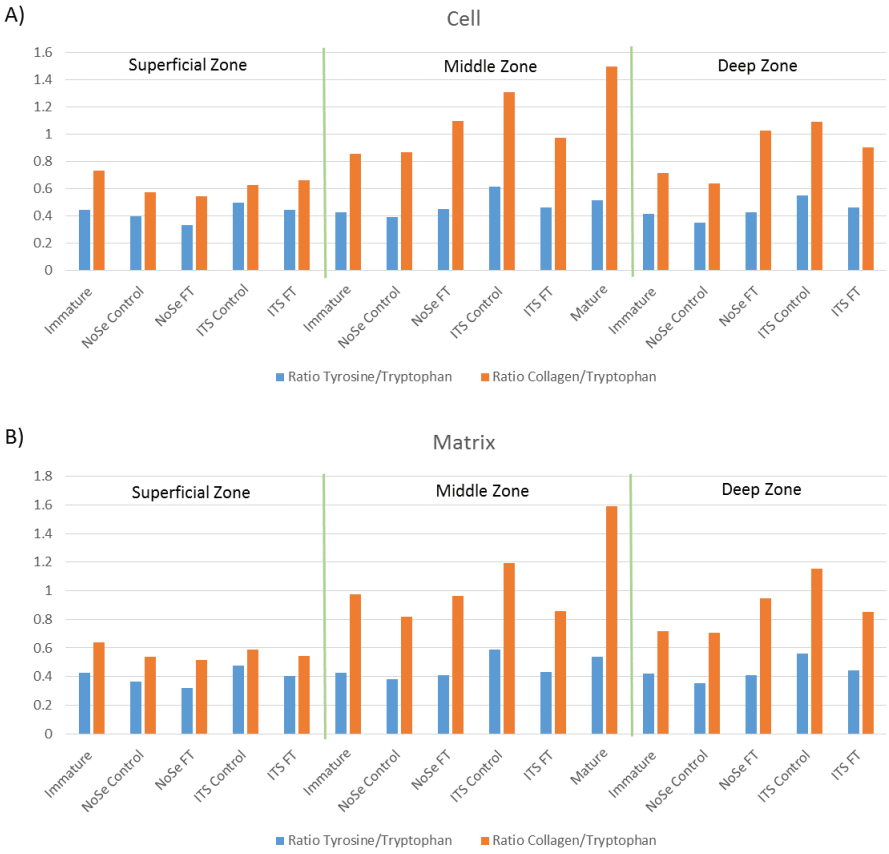

Figure 79: UV emission peak intensity ratios in native (Immature and Mature, no culture) and cultured articular cartilage explants (No Se Control, No Se FT-treated, ITS Control, ITS FT-treated) for (A) chondrocytes and (B) extracellular matrix. Blue stands for the ratio Tyrosine/Tryptophan and orange for ratio Collagen/Tryptophan.

This analysis is based on averaged data. A local measurement of these collagen, tyrosine and tryptophan levels combined with a multivariate analysis could potentially lead to finer analysis of the structural variations and of the Se-influence on cartilage maturation stages and to a better understand how the chondrocyte metabolism can lead to physio-pathological conditions such as osteoarthritis or KBD.

No error bars could be presented in these Figure 79 because the data from spectra acquired at

multiple random point location within AC region were pooled for only two articular cartilage sections.

18 Biomechanical Properties of Articular Cartilage: Selenium Influence

18.1 Principles of Atomic Force Microscopy (AFM)

AFM is a high-resolution scanning probe microscope, originally designed to interrogate any solid material surface [220]. Since its development, novel modes of analysis have enabled great strides in surface analysis, now providing ultra-high resolution (nanoscale in x, y and z) information about sample surface properties such as height, friction and stiffness [220]. A schematic of the typical AFM set up is shown in Figure 80.

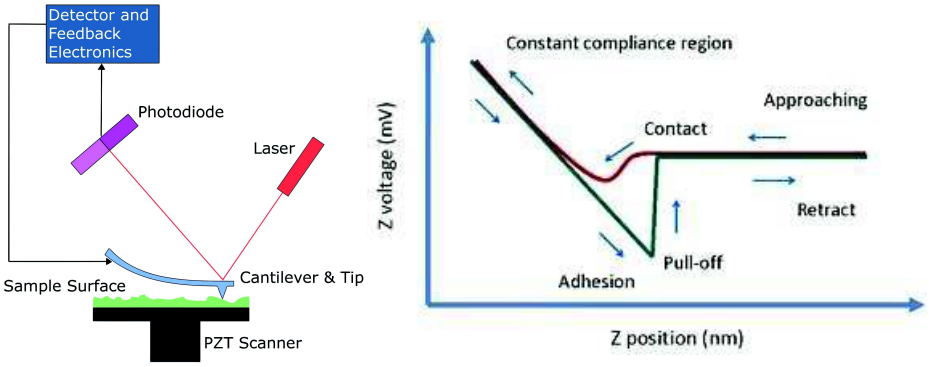

Figure 80: AFM set-up and principle overview. *(left)*The deflection of the cantilever is measured by reflecting a laser beam off the backside of the cantilever, which is displayed on a photodiode detector while it is scanning over the surface of the sample. *(right)* Red curve is the approach and the Green curve is the retract . Approach curve, from the right to the left of the picture: tip is far from the surface and there is no interaction; the tip contacts the surface in the "jump-to-contact" region (lower y values); once in contact, the cantilever is further approached to the surface and is bent, where now repulsive forces are predominant; Retract curve, from the left to the right of the picture: the cantilever is retracted from the surface and an adhesive (negative) interaction between the tip (green curve) and surface is measured (Pull-off force).

AFM principally involves accurately driving a sharp probe into contact with a sample surface. This probe is mounted onto the back of a flexible cantilever, with a given spring constant and resonant frequency (as described in Renner *et al.* 2012 [220]. At varying distances from the sample, the probe will undergo forces of repulsion (close to surface) and attraction (further away), causing the cantilever to bend or deflect. The cantilever bends at the surface because two major atomics forces appear, Van der walls and adhesion forces. Very strong repulsive forces (coulombian forces) are predominant between the tip and sample atoms due to exchange interactions as the electronic orbitals overlap at atomic distances. Once, the tip and the surface are in contact, other interactions appear. The friction when the cantilever bends laterally due to a friction force between the tip and the sample surfaces. The adhesion force which is related to the free energy change to separate unit areas of two media from contact to infinity in vacuum or in a third medium.

The amount of force between the probe and sample is dependent on a spring constant (relative to the stiffness of the cantilever) as well as the distance between the probe and the sample surface. This

force can be described using Hooke's Law:

$$F = -k.x \tag{20}$$

where F is the force, k the spring constant and x the cantilever deflection (nm). A closed-loop feedback control maintains a constant deflection measured by a semiconductor diode laser which is bounced off the back of the cantilever onto a position sensitive photo-detector. Vertical distances are evaluated by a conversion of the voltage required for the z-movement of the piezo-crystal into distances. Height topographical images of the samples can then be reconstructed from the movement of the x–y–z-piezo-crystal driven scanner, and using the recorded x–y-position, a 3D image of the sample surface can be reconstructed [220].

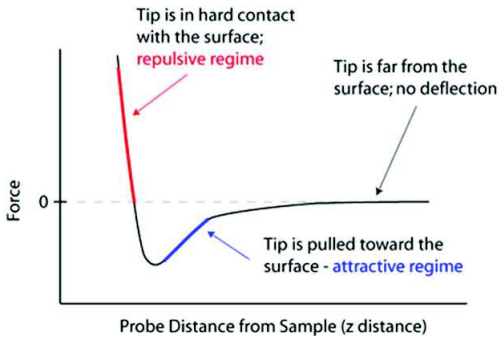

Figure 81: Atomic interaction force regimes governing the AFM measurement. A typical force curve representing the forces at work during tapping mode AFM, with the oscillating motion of the cantilever. Close to the surface, weak atomic attractive forces are felt (Van der Waals interactions). Reaching the minimum, the electron clouds of the tip and the sample surface electrostatically repel each other. Forcing the contact to happen, distance between atoms becomes extremely short. The repulsive force causes the cantilever to bend as the tip is brought closer to the surface.

AFM can be used in a diverse range of scanning modes, described in the papers of Jandt (2001) [221] and Butt *et al.* (2005) [222]. In contact mode, the probe is held in constant contact with the surface while it is scanned. In tapping mode, the cantilever oscillates at a fixed vibrational frequency close to its resonant frequency. The tip periodically contacts the sample surface at a predefined maximum vibrational amplitude. This non-permanent contact reduces the general stress imposed on the sample, thus mechanical wear and deformation of both the tip and the sample are minimized [223]. This mode is ideal for biological sample analysis, the lower energy transferred to the sample allows for reliable imaging of these soft samples [224].

PeakForce Tappingg^{TM} AFM (PFT) is a proprietary technique developed by Bruker Instruments. While in classic TM, only the cantilever is excited and oscillates at its resonance frequency (for air measurements, the range is usually between 70 and 400 kHz), in PFT it is the entire Z-scanner that oscillates at lower frequencies (0.25-2 kHz). This technique allows direct and precise control of the force applied to the sample (not possible with TM), thus allowing to scan delicate samples with controlled and lower forces that TM. Moreover, once the cantilever is adequately calibrated (spring constant and deflection sensitivity) it is also possible to obtain mechanical properties of the sample "on the fly", while imaging the surface. This allows to save time for sample analysis, as in classic AFM approaches, topography and mechanical properties have to be investigated separately AFM can be used to quantitatively measure the interaction of the cantilever tip with the sample using force-distance curves as a function of the tip-sample separation [227], Figure 81right, where the tip and sample are routinely brought in contact and separated. During each of these cycles, the cantilever

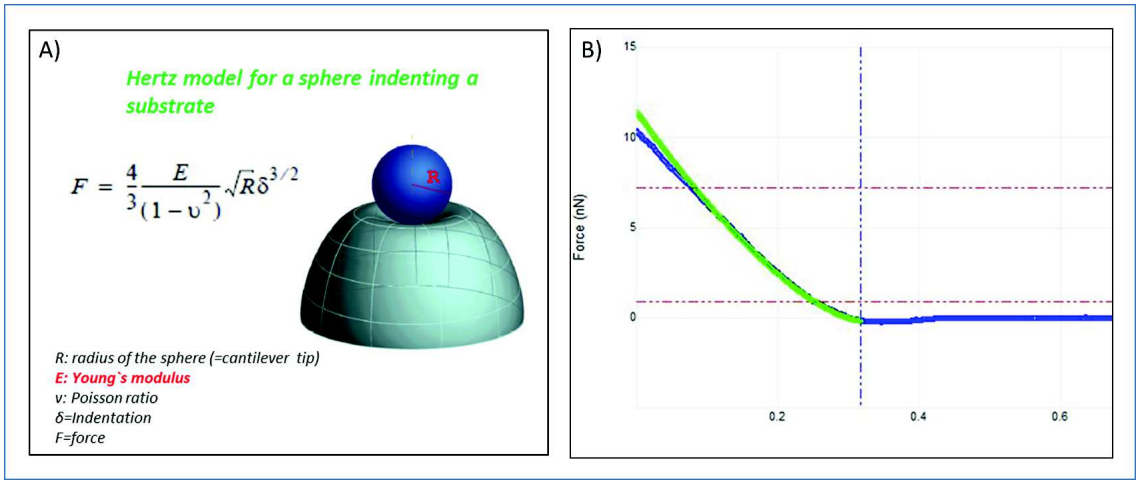

Figure 82: Figure 2. A) Hertz model. F is the force applied by the cantilever tip, E is the Young's modulus (fit parameter), ν is the Poisson's ratio and R the radius of the indenter, i.e. the cantilever tip. B) Fitting of an AFM force curve (blue) with Hertz model (green).

deflection, and hence the tip-sample interaction force, is measured at each point to obtain the curve displayed in Figure 81right. When the tip is approaching the sample, attractive forces between the tip and the cantilever at distances less than 10 nm attract the cantilever to the sample surface, in a phenomenon known as "jump-to-contact" [228], visible as a small negative-leading trend in the approach curve. Once the cantilever is in contact with the surface, further movement of the scanner causes the bending of the cantilever. During the retracting cycle, adhesion forces may often exist between the tip and the sample, and a pull-off force is required to detach the tip from the surface [229], which occur when the bending force of the cantilever is higher than the magnitude of the tip-sample force. Common applications of force curves include measuring the elastic modulus of the substrate via approach curves [230], adhesion properties of biological surfaces [231] and the study of molecular recognition events between two interacting molecules [262]. In the latter case, the AFM tip is functionalized with either one of these molecules, with the other deposited on a surface, and their interaction studied via force curves. In the present study, force curves are used to calculate Young's modulus and adhesion properties of explants. For Young's modulus, the Hertz model is adopted, which applies for the case of a spherical indenter pushing to deform flat surface (Figure 82A). The end of the cantilever tip can be approximated as a sphere with a nanometre-size radius (in this study, 20 nm) and the elastic modulus from each force curve is obtained by fitting the part of the curve in contact with the sample with the Hertz equation (Figure 82B). Adhesion was obtained from the pull-off force required to detach the cantilever tip from the surface during the retraction cycle (Figure 81right).

18.2 Methods

18.2.1 Explant Preparation

Following three weeks culture, in the presence or absence of selenium (ITS solution), and/or growth factors (TGF-β1 and FGF2 combination) treatments, the explanted punch biopsy cultures were ready and processed for surface topographical and nanomechanical analysis. Culture media was aspirated and explants were rinsed in pre-warmed (37°C) Hank's balanced salt solution (HBSS - Gibco by life technologies, Ref: 14175-053) for five minutes. HBSS was then replaced with pre warmed phosphate buffered saline (PBS; Gibco by life technologies, Ref:) for a further five minutes before mounting onto a sterile, dry petri dish (Corning, cell culture Dish,Sterile, Polystyrene Cat. No. 3295 LifeSciences).

The samples were each mounted using soft adhesive tac (Faber Castell tac). Following adhesion to the petri dish the explants were immersed in excess phenol red free DMEM-F12 (Gibco by life technologies, Ref: 21041-025) and incubated at 37˚C using a heater stage connected to Bruker/LakeShore 331S Temperature Controller . All preparation steps were performed in a sterile lamina flow hood (Labogene, Lynge, Allerod Municipality, Denmark - hood model is Scanlaf Mars). According to preliminary observations, after three hours in these specific conditions, the explants usually start to decay and become softer. Consequently, an analysis cannot exceed three hours.

Figure 83: Sample Preparation Stage. From left to right: Sample positioning, AFM calibration

18.2.2 Atomic Force Microscopy

All AFM analyses were performed using a BioScope Catalyst (Bruker Nano, Santa Barbra US) equipped with nano-positioning sensors in all three axis and closed-loop feedback for precise, repeatable scanning probe positioning with sub-nanometer resolution, mounted on a Nikon Eclipse Ti-S inverted optical microscope (Nikon Instruments, Netherlands).

Imaging:

AFM imaging was conducted using PeakForce Tapping mode (Bruker-nano) at 37˚C in physiological buffer. In this technique, which represents an evolution of the classic Tapping Mode, the cantilever oscillates in a sinusoidal mode over the sample surfaces at low frequencies (between 0.25-1 Hz). This technique allows for a better surface tracking of rough samples, coupled with a precise control of the force applied during scanning. Bruker MLCT Silicon nitride Si3N4 probes (MLCT-E tip, Bruker nano, Coventry, UK) of a nominal radius 20 nm with spring constants of [0.05-0.2] N/m (nominal value: 0.2 N/m) and resonant frequency [26-50] kHz (nominal value: 38 kHz) were employed. Surface coordinates acquired on a scan area of 5μmx5μm and 10 x10 points. A minimum of three areas per explant were analysed and two explants per sample group.

Sample Surface Roughness:

Roughness is quantified by the vertical spacing of a real surface from its ideal form. If these spacing are large, the surface is rough; if they are small the surface is smooth [232]. Quantitative assessment of the surface roughness through the values of Root Mean Square (RRMS), defined as the standard deviation of the asperity heights. Topography data were obtained in PeakForce Tapping mode and used to calculate roughness. The latter was determined both on entire cells and on three 400 μm^2 areas for each sample group. The roughness subroutine in the Nanoscope Analysis software, v1.50, was adopted, which calculates roughness $R_q or\, R_{rms}$ using the equation 21

$$R_q = \sqrt{\frac{\Sigma Z_i^2}{N}} \tag{21}$$

where N is the number of height points in the analyzed area and Z_i is the vertical distance of data point i from the mean image data plane.

Nanoindentation:

AFM stiffness measurements were based on recording the elastic modulus of the cartilage material by using the AFM tip as a nanoindentor. Explants were prepared as described previously. Bruker MLCT Silicon nitride Si3N4 probes (MLCT-E tip, Bruker nano, Coventry, UK) of a nominal radius 20

nm with spring constants of [0.05-0.2] N/m (nominal value: 0.2 N/m) and resonant frequency [26-50] kHz (nominal value: 38 kHz) were employed. Each cantilever used in the study was individually calibrated, calculating the sensitivity from a reference, hard force curve taken from the petri dish surface. The cantilever-specific spring constants were determined with the thermal tune subroutine of the Nanoscope analysis software (v1.50) which provided a value comprised between 0.1 and 0.14 N/m.

For Young's modulus determination, force curves were taken on different cells. 50-100 curves equally spaced on an area of 25 μm^2 were collected. For each sample 3-4 regions were analyzed. The approach curve in the contact regime of each force curve was fitted using the equation for a spherical indenter (Hertz model, 22), with the fitting module in the Nanoscope Analysis software v1.50, and only curves with a goodness of fit between 0.85 and 1 were considered for statistical analysis.

$$F = \frac{4E\sqrt{R}\delta^{\frac{3}{2}}}{3(1-\nu^2)} \tag{22}$$

In this equation 22, F is the force applied by the cantilever tip to the cell, E the Young's Modulus (fit parameter), ν the Poisson's ratio, R the radius of the indenter curvature, ie. the cantilever tip. F was calculated from the force curves and was of the order 200-500 pN. 0.5 was the Poisson's ratio used, while the nominal radius of the used tips was 20 nm.

18.2.3 Statistical Analysis

Normality of the data were analysed using the Kolmogorov Smirnov test. Normally distributed data were analysed with the one-way and two-way analysis of variance (ANOVA) and with the Mann-Whitney test for non-parametric data. In all cases in which ANOVA was significative, multiple comparison methods were used. Differences were considered significative for $P < 0.05$ (*$P < 0.05$, **$P < 0.01$, ***$P < 0.001$, ****$P<0.0001$). All data were analysed with the Minitab v14 statistical program.

18.3 Results

During this phase of the project AFM was used as a surface profiling techniques, to monitor topographical and nano-mechanical alterations in the apical surface matrix structure of explanted hyaline cartilage. Importantly, this technique provides the only apical surface data from our investigation, the site at which the cartilage must withstand high frictional forces within joints during movement. Excitingly therefore, the impact of selenium deficiency in the cartilage body can be assessed at the explant surface.

The surface zone is a very active region of articular cartilage metabolism where several matrix replenishment and re-organisation processes are undertaken. Previous data have shown that an explanted cartilage punch biopsy can be maintained in *in-vitro* culture in a dedicated culture medium, over a relatively long period of time, and induced to undergo a specific and physiologically relevant maturation process. This process results in a stiffening of the explant surface and specific collagen fibril re-arrangements, which can be detected using the AFM in conjunction with other techniques [17]. This model is adopted here in the presence and absence of selenium, to monitor the effect of selenium deficiency on the ex-vivo maturation process. A selenium deficiency could induce metabolic and/or structural disorder of the tissue surface, manifesting in AC biomechanical property defects, in turn generating a soft-like tissue more akin to their respective immature tissues.

The results presented in the following sections are robust preliminary results due to the large data generating capacity of modern AFM modes. The data set contains a minimum of 600 data points per sample group and is therefore interpreted as significative according to 95% confidence intervals. Excitingly, the data set is the first AFM investigations on such selenium-treated explants, providing an interesting first insight into the action of selenium on the biomechanical properties of cartilage.

18.3.1 Cartilage Topography

Following three weeks culture in the presence or absence of selenium (ITS solution) and/or growth factor (TGFβ1 and FGF2 combination) treatments, the explanted punch biopsy cultures were ready and processed for surface topographical and nano-mechanical analysis. Importantly, the nano-resolution provided by this instrument allowed the fine structural components of cartilage matrix such as collagen fibrils to be imaged without significative prior sample preparation [233-234]. AFM topography maps provide both qualitative and structural information based on height profiles and morphological presentation of the surface as well as quantitative analysis of surface roughness.

Distinct topographical differences were observed from native mature and native immature articular cartilage samples. Fibre like structures were distinguished in both sample references: immature and mature. Mature explants presented dense collagen fibers with a surface that seemed to be smother than that of their immature cartilage counterparts (Figure 84). This was confirmed by the assessment of surface roughness. Mature explants exhibited a median R_{rms} of 34.95 nm $\pm$ 20.95 nm, with an interquartile range between 26.60-47.55 nm, significatively lower than that of the immature samples, where a median R_{rms} of 50.90 nm $\pm$ 16 nm, interquartile range of 46.03-62.03 nm was observed ($p < 0.001$; Figure 84). A two fold increase in the surface height profile was also observed.

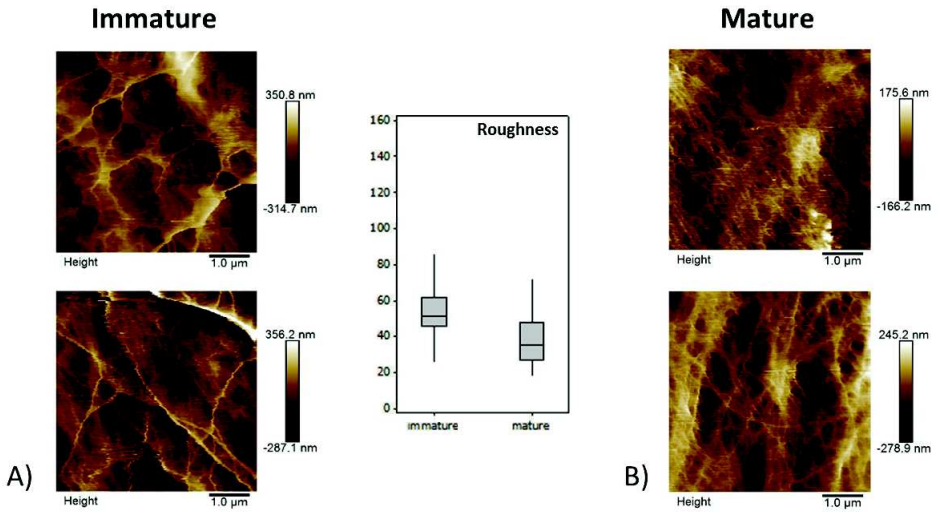

Figure 84: AFM Topography and Roughness of native immature (A) and mature (B) articular cartilage explants.

Following the analysis of immature and mature samples as control baselines for the project, the AFM analysis was established as a surface profile tool capable of monitoring apical surface changes during maturation. In order to assess the effect of ex-vivo stimulated maturation on the apical surface of the cartilage explants, both topographical and nanomechancial analysis were performed. FGF2 and TGFβ1 growth factor treatment seemed to result in a re-organised surface fibre pattern, with fibres more aligned along the x-axis in the images (Figure 85) compared to their untreated control

samples. In addition to the re-alignment the surfaces seems to be slightly smoother in appearance following growth factor treatment however this effect was far less pronounced than that seen in the mature cartilage samples. This observation was confirmed by surface roughness analysis, where no significative difference was observed following growth factor stimulation (Figures 85&86; $p>0.05$). However, all present a significative difference to mature reference ($p<0.005$).

In the sample pool cultured with ITS in the culture medium as Se-supplementation, controls and FT-treated cannot be distinguished from topographical images only, the height is also relatively similar. As previously reported, the collagen fibers are visible but they do not present any specific pattern variation across the total number of scan undertaken. No significative difference was observed in the surface roughness of the (FT-)treated explant surface (median of 88.90 nm$\pm$81 nm) with Se when compared to its relevant (FT-)untreated control sample (median of 47.80 nm $\pm$ 11.7 nm; $p>0.05$).

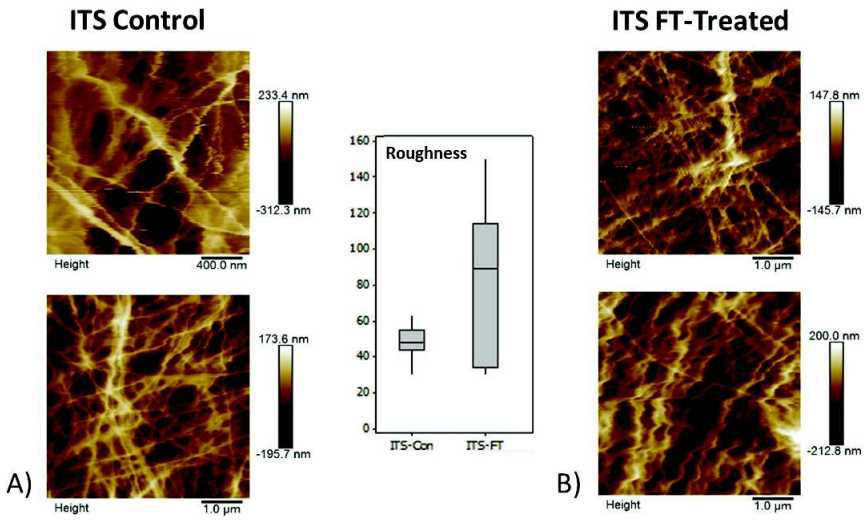

Figure 85: AFM Topography of Selenium treated (ITS) articular cartilage explants: (upper part) Control and (bottom part) FT-treated (growth factors treated)

The same observation can be made for the explants treated with a Se-depletion in the culture medium (Figure 86). Due to the high similarities, controls and FT-treated cannot be strictly distinguished from topographical images. As previously reported, the collagen fibers are visible but they do not present any specific pattern variation across the total number of scan undertaken. However, the fibers visually look slightly different than in ITS sample pool. No significative difference was observed in the surface roughness of the (FT-)treated explant surface (median of 51.33 nm$\pm$25.6 nm) without Se when compared to its relevant (FT-)untreated control sample (median of 53.35 nm $\pm$ 17.4 nm; $p>0.05$). No significative difference is either expressed between FT-treated samples in ITS and no selenium pools (median of 88.90 nm$\pm$81 nm and median of 51.33 nm$\pm$25.6 nm, respectively $p>0.05$) but it exists a significative difference between the No Se control and ITS control (median of 47.80 nm $\pm$ 11.7 nm and 53.35 nm $\pm$ 17.4 nm, respectively, <0.05).

The surface roughness of these four sample groups is in the same range [40-80] nm. Even if all the samples are statistically different, cartilage topographies and surface roughness cannot exhibit a clear and well-defined trend of the culture samples. No direct influence of the selenium can be (clearly) visible on the topographical structure of the extracellular matrix. This maturation model is based on biochemical processes using growth-factor stimulation, no biomechanical stimulations, required to a normal and correct tissue structuration, have been provided. Furthermore this treatment, being a tissue/cell culture model, might not exhibit an homogenous effect. Local regions of the explant surface

may possess slightly different structure to that of a juxtaposed region.

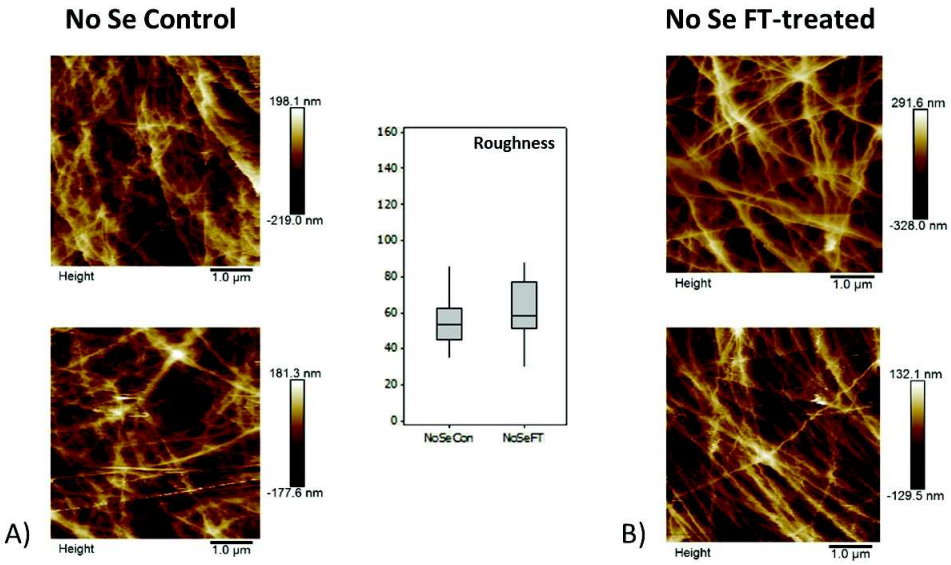

Figure 86: AFM Topography and Roughness of the No Selenium treated articular cartilage explants: (A) Control and (B) FT-treated (growth factors treated)

18.3.2 Nanoindentation and Cartilage Young's Modulus

Assessment of both biological and mechanical properties, are needed to understand and fully characterize, the effect of selenium on the functional properties of cartilage tissue. Mechanical properties are difficult to measure in small tissue regions and tissue level analysis has, for some time, relied on histological assessment. Nanoindentaiton using AFM has now become an established tool for the analysis of ex vivo cartilage [263]. Excitingly, using almost no sample preparation, this technique offers the opportunity to probe the structural integrity of cartilage surface and can be correlated with histological and other deep tissue techniques, providing whole tissue level structure function analysis.

Hyaline articular cartilage has been shown to observe a distinct, progressive increase in material stiffness during maturation [235]. Nanoindentation experiments were conducted on both native immature and mature cartilage explants in order to identify the baseline stiffness values. All AFM data was analysed using Hertzian mechanics, calculating the tissue Young's Modulus. Following maturation, immature punch biopsy samples were analysed for their mechanical properties and compared to those that underwent the same 'maturation' process in the absence of selenium supplementation.

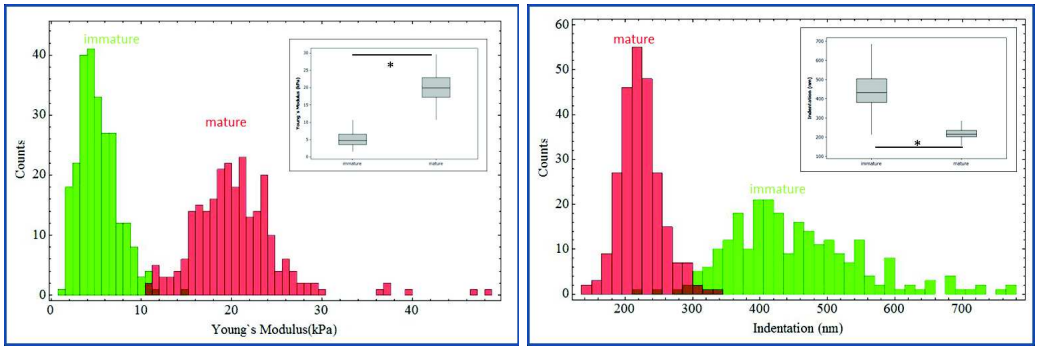

Figure 87: Native cartilage elasticity. Immature punch biopsy samples were not cultured and subjected to AFM nanoindentation analysis to assess their differing stiffness. (Left) Native tissue Young's Modulus from immature (Green) and mature (red) tissue shown as a histogram of value distribution and a boxplot (insert). (Right) Native tissue Indentation from immature (Green) and mature (red) tissue shown as a histogram and boxplot (insert). All data shown has been analysed for significance using 95% confidence intervals (* = $p<0.001$).

Tissue wide variations were observed in both the Young's Modulus and Indentation values recorded, in both the immature and mature samples. Consistent with previous observations this lead to non-parametric data sets (Anderson-Darling) for each sample [17]. Measuring the nanoscale compressive strength of cartilage using AFM (Figure 87Left), freshly isolated mature articular cartilage showed an increase in the median values for Youngs's modulus, and therefore a 4 fold stiffening of the apical surface compared to immature cartilage (19.95 kPa interquartile range 17.28-22.9 kPa versus 4.85 kPa interquartile range 3.6-6.62 kPa, respectively, $p < 0.001$). This observation was confirmed and validated by indentation depth analysis, showing that the more elastic immature cartilage explants have a greater indentation depth than those of the more stiff mature cartilage (Figure 87Right). A significative difference is expressed between mature and immature tissues with indentation median values of 217 $\pm$ 34 nm and 433 $\pm$125 nm, respectively ($p<0.001$).

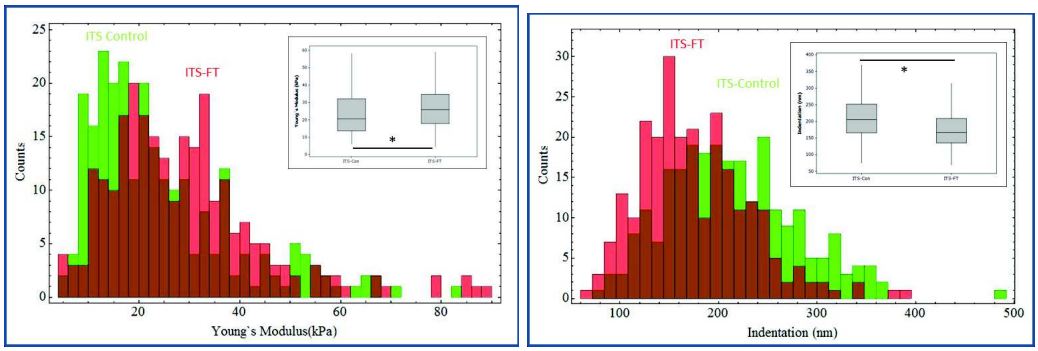

Figure 88: ITS group cartilage elasticity. Immature punch biopsy samples were cultured in ITS media over a period of three weeks and subjected to AFM nanoindentation analysis to assess their differing stiffness. (Left) Young's Modulus from ITS Control (Green) and ITS growth factor(FT)-treated (red) tissue shown as a histogram of value distribution and a boxplot (insert). (Right) Indentation from ITS Control (Green) and ITS FT-treated (red) tissue shown as a histogram and boxplot (insert). All data shown has been analysed for significance using 95% confidence intervals (* = $p<0.05$).

Immature explants cultured in ITS media and in the presence of growth factor (FGF2 and TGF β1) over 21 days exhibited an increased nanocompressive stiffness when compared to their untreated control samples. This increase however was less pronounced than that observed with native tissue comparisons. Treated explants showed a significatively increases Young's Modulus of 25.9kPa $\pm$ 16.825 kPa compared to 20.70 kPa $\pm$ 18.5 kPa observed in the growth-factor untreated controls sample (figure

88 left, p<0.001). As shown in figure 88left, wider value distributions were observed in both the treated and controls samples. Actually, the histograms present a large overlapping for nanoindentation of ITS controls (green) and FT-treated (red) samples. Interestingly, the distributions were more variable for the treated samples but with a median part containing the major indentation values (135 nm ±73.5 nm with a interquartile range of 68.40 - 167 nm) shifted compared to the ITS median indentation value. ITS control which present a normal distribution with a median 166.25 nm ± 86 nm (interquartile range 74 - 206 nm). The distributions of these control and growth-factors treated samples are then different which allow a significance of the results (p<0.001).

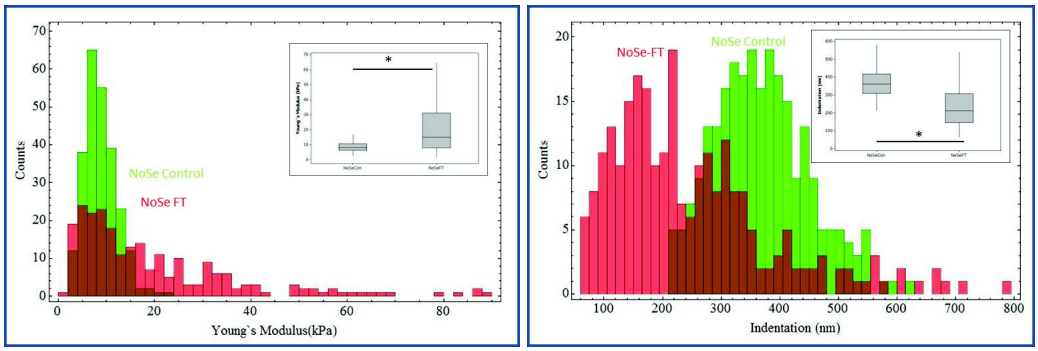

Figure 89: No Se group cartilage elasticity. Immature punch biopsy samples were cultured in Se-depleted media over a period of three weeks and subjected to AFM nanoindentation analysis to assess their differing stiffness. (Left) Young's Modulus from No Se Control (Green) and No Se growth factor(FT)-treated (red) tissue shown as a histogram of value distribution and a boxplot (insert). (Right) Indentation from No Se Control (Green) and No Se FT-treated (red) tissue shown as a histogram and boxplot (insert). All data shown has been analysed for significance using 95% confidence intervals (* = p<0.05).

A similar trend in explant cartilage elasticity was observed when the Se-depleted cultured samples were analysed. The immature explant cultured in the presence and absence of Se depleted growth factor cocktail (FGF2 and TGFβ1) exhibited significatively higher stiffness than that of the untreated (Se depleted media only) controls (p<0.001). Young's modulus values of 15.05 kPa ±23.33 kPa were observed in the treated samples, a near two fold increase in stiffness compared to the untreared control, which showed an average Young's modulus of 8.26 kPa ±4.43 kPa. Interestingly, the distributions were more variable for the treated samples (shown in Figure 89, red). Interquartile ranges between 7.87 and 31.20 kPa were observed following treatment – showing that the growth factor treatment, even in the absence of selenium induced region specific stiffness at the nanoscale. Indentation showed that the deformation is almost 40% lower for No Se Control with values of 362 nm interquartile range 309-418 nm and No Se FT-treated 212 nm interquartile range 147-307.75 nm (P < 0.001 respectively; as shown in Figure 89).

These two groups ITS and No Se samples also present different elasticity and indentation properties. A gradual increase of the stiffness appear from NoSe Control to growth-factor trated ITS samples as shown in Figure 90. ITS samples group present higher stiffness that the No Se sample group. The Young modulus for the growth factor treated samples is about 1.5-fold increased from the Se-deficient treated to ITS treated samples (median values of 15.05 kPa and 25.90 kPa, respectively, p<0.001). This ratio is also found the variation of the elasticity where a decrease of indentation values from 212 nm for No Se FT-treated samples to 167 nm for ITS FT-treated samples (p<0.001). The same observation can be made for the controls. The ITS control present a significative higher stiffness than the No Se control with an 2.5-fold increase in the Young's Modulus values (20.70 kPa for ITS control and 8.26 kPa for NoSe control, p<0.001) and almost 2-fold decrease in the indentation values (206 nm

and 362 nm, respectively, p<0.001). The absence of selenium can suggest a reduction of the stiffness however it is difficult to conclude on its impact on AC surface biomechanics.

Two main group trends can be observed in this preliminary data set. These trends were also replicated when maximal indentation median values of unstimulated immature cartilage explants were compared to growth factor-treated immature cartilage (ITS Control: 206 nm interquartile range 166.25-252.25 nm versus ITS-FT-treated 167 nm interquartile range 135.75-207.75 nm, $P < 0.001$). This was validated for Se-depleted treated samples (No Se Control: 362 nm interquartile range 309-418 nm versus No Se-FT-treated 212 nm interquartile range 147-307.75 nm, $P < 0.001$). As expected, the Young's modulus values also indicate that matured explants are much stiffer than immature/controls tissues (No Se FT-treated (15.05kPa)/No Se Control (8.26 kPa) (P<0.001), and ITS-FT-treated (25.90 kPa)/ITS Control (20.70kPa) (P<0.001)), although in this last case, the difference is smaller, possibly due to the large spread of data/local stiffness variations at the sample surface.

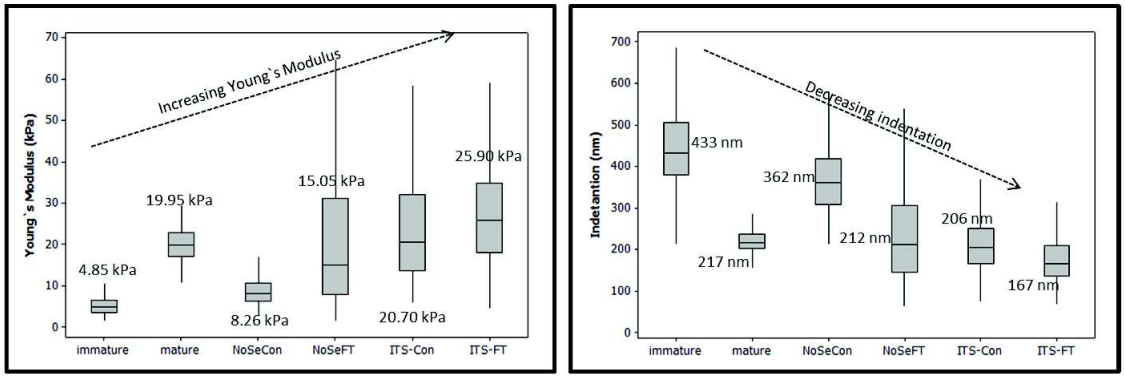

Figure 90: Summary of Young's Modulus and Indentation of the native immature and mature references and the four cultived explants (No Selenium treated explant - No Se control, No Selenium and growth factors treated explant -No Se FT-treated, Selenium treated explant - ITS control and Selenium and growth factor treated explant).

Another trend was observed, namely Se-treated explants (ITS group, with an average indentation value about 186 nm) are stiffer (less deformable) than No Se-treated explants (No Se group, with an average indentation value about 287 nm). Controls as growth factors-treated explants of these two sample sets possess a clear difference in Young's modulus, ITS samples are almost 2 fold stiffer than No Se samples (Figure 90). An interesting point is that a major difference (superior to 20%, P<0.001) is observed between No Se matured and matured ITS samples.

The Young's Modulus values obtained for native immature and mature tissue but also for ITS Control and FT-treated explants perfectly correlated the Young's modulus values range to the paper of Khan *et al.*2013 [17]. This work provides a good repeat and validates the reproducibility of the model developed in this paper [16-17]. Statistically significative, Selenium seems to influence the biomechanical properties of explant surface, decreasing the stiffness of this surface and inducing a higher deformation under strains compared to other Se-treated matured explants.

19 Tomographical Investigations for Articular Cartilage Development: 3D Visualization of Cartilage Channels

We used in the very end of this PhD work an innovative full-field x-ray imaging technique called phase contrast imaging (PCI). This modality is developed by INSERM research team based at the European Synchrotron Radiation Facility (ESRF), in Grenoble and particularly, E. Brun Inserm researcher in this team. The objective in the experiment was to investigate the potential of such method for the visualization of the collagen fibers and as a matter of fact the overall explants internal structure. This work also aims at developing imaging modalities articular cartilage with low (radiation, X-rays) dose at moderate spatial resolution for future potential clinical diagnostics and treatments. Indeed, regenerated cartilage obtained by 3D bio-scaffold and stem cells therapy have in the last years emerged [236] but no imaging modality allow a detail 3D tissular and cellular description of the articular cartilage to assess the potential benefits of these therapeutic strategies. However, some first promising insights have been reported about the potential enhanced differentiation identification between healthy and osteoarthritic cartilages [237]. The samples produced for this work were used as test samples and imaged in their fully hydrated state. Their size (4mm diameter and max. 2 mm height of ex-vivo cartilages, biopsy plugs) is ideal to evaluate the potential of this technique.

19.1 Synchrotron X-ray Phase Contrast Imaging Technique and Methods

One of the main properties of the synchrotron that can be exploited is the coherence of the X-ray beam produced. The spatial and temporal coherence allow to image such AC samples using an innovative full-field X-ray imaging technique called phase contrast imaging (PCI) [238]. PCI exploits the dual properties of X-ray absorbed and refracted when crossingmatter. The transmission of x-ray in matter can be modeled by the following equation: $n = 1 - \delta + i\beta$ where n is the complex index of refraction, δ its refraction part and β the absorption index. Using the typical wavelengths used in radiology, the real part of the refraction index of a material can be a thousand times greater than its absorption factor counterpart for light elements. This translates in a much greater contrast for soft tissues with X-ray imaging methods based on sensing the light phase (PCI) by comparison to traditional methods based on absorption. These unique characteristics allow high contrast 3D visualization of thick and complex samples even at high spatial resolution and still acceptable dose delivered. PCI is particularly adapted to visualize weakly absorbing details such as those often encountered in biology or medicine which become then a huge asset when one wants to image with high resolution a biological tissue sensitive to the (radiation) dose.

The principle of the PCI is to determine 3D distributions of the refractive properties of a sample by recording attenuation and phase changes of the transmitted x-ray beam induced by the matter. The final image contrast depends on several factors, including the spatial resolution of the detector, the image formation mechanism, the X-ray beam energy and the beam divergence. Using the simplest optical set-up, namely propagation based imaging, a coherent wave-front is passing through the sample and if the distorted wave-front propagates sufficiently far, the small differences in phase propagation cause interference, and variations of intensity which are observed in the image plane detected. At a distance z along the beam path within the sample, the X-ray attenuation is described by μ(x, y, z), refraction by the lateral phase gradient gradΦ (x, y, z), and scattering by the scattering (diffusion) coefficient σ (x, y, z) [240]. CT (Computed Tomography) imaging is based on the assumption that when the cumulative effects of these factors are recorded on a pencil beam and separated behind the sample, the values of μ, gradφ and σ can be reconstructed from a sufficient number of projections.

The ESRF-based INSERM team performed Propagation Based Imaging (PBI) in equivalent con-

ditions so that both the Laplacian and the gradient of the phase can be collected. Such combination is used in a special algorithm to increase the phase recovery fidelity. During the image reconstruction stage, specific pre-processing image procedures and filters are applied for denoising and image normalization. Quantitative PCI image analysis are performed after CT reconstruction of the different signals (index of refraction, dark signal, absorption map). A Fourier based algorithm is used to integrate in the same phase reconstruction both the gradient and Laplacian phase signal recorded. 3D image analysis are performed on iMorph [265] to perform a 3D topological analysis of cells distribution as well as of nourishing canals.

As already described in this work, the articular cartilage punches samples of bovine metacarpophalangial joint had undergone accelerated maturation through incubation with a cocktail of growth factor (Fibroblast Growth Factor 2 and Transforming Growth Factor $\beta 1$) enriched growth culture medium. Controls (serum-free medium) had also been imaged. One set of explants cultured in presence or absence of growth factor but in a medium totally depleted in selenium were also analysed. These small volumes of ex-vivo cartilages (biopsy plugs) were fixed in 10% Neutral buffer formalin during 12h and then stored at 4°C in PBS solution in sealed container so that no sample damage occurred during data acquisition. Theses samples were imaged at high spatial resolution (~1 μm) to achieve a better understanding of the cellular transformation during cartilage maturation. The evaluation of structural changes in the matrices allow a better identification of cartilage reconstruction strategies.

19.2 Preliminary results: Observations and Perspectives

In the case of cartilage samples, PCI presents the tremendous advantage of being sensitive to the different tissues constituting a joint [239, 264]. Such imaging approach makes possible the simultaneous detailed visualization of both the high absorbing tissues, like bone, and the softer materials, like chondrocytes. PCI-CT clearly outperforms conventional X-ray CT with the clear depiction of the soft tissues. Moreover, PCI-CT was shown to surpass as well MRI when visualizing the bone matrix [239]. We conducted a PCI experiment at the ESRF on BM05.

We analyzed 7 days-old bovine cartilage explants by PCI technique. Figure 91 shows an example of a 3.5μm thick slice PCI computed tomography (isotropic voxel: 3.5μmx3.5μmx3.5μm). In Figures 91&92, the chondrocytes are clearly visible as well as specific cells and bone extra cellular matrix in formation (possibly bone-forming osteoblast). Previous studies have been performed on the visualisation of cartilage canals [241], however nourishing canals present in the maturing part of the cartilage are only visible for the first time in 3D with high precision regarding morphological parameters.

Using this technique, a better understanding of selenium influence on the maturation and growth process in our model conditions is now made possible. The 3D-structure representation of the tissue allow to visualise the morphological variations of the cartilage channels (Figure 92), essential to nutritional and growth factor supply. These canals have for function to provide by passive diffusion to the cartilage extracellular matrix the elements required to future bone generation. This process induces the vascularisation of the growth cartilage, initiating the start of the calcification/ossification as reported in literature [241-244]. A quantification of several parameters such as cartilage thickness, chondrocytes homogeneous topographic distribution, zone height and surface and transversal damage or structure changes can be now performed. These channels could have for function to provide the cartilage extracellular matrix with the elements required to the future cartilage growth calcification. Cellular distribution and matrix density changes permit the visualisation of the impact on growth and maturation of further treatments (nuxious for Se-deficiency or beneficial as remedy).

This proof of concept study is in its preliminary stage and a more extensive study using at first

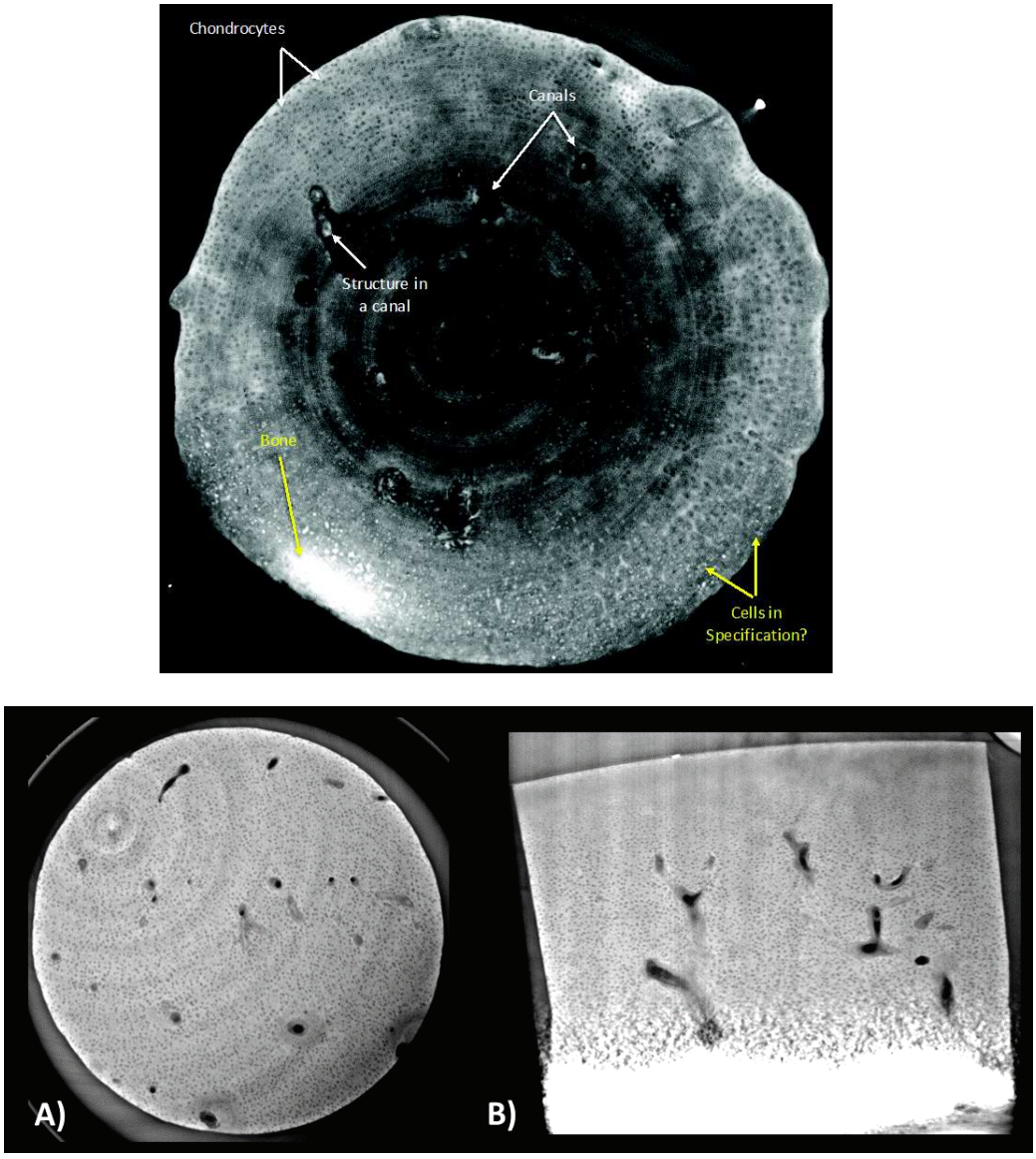

Figure 91: Tomographical Phase Contrast Images performed at BM05 at the ESRF. *Upper picture*: Reconstructed slice from PCI of a 4mm diameter maturating cartilage explant. *Bottom picture*: (A) Horizontal (4mm diameter explant) and (B) transversal (1.5 mm height explant) reconstructed slice from PCI of a native immature cartilage fragment.

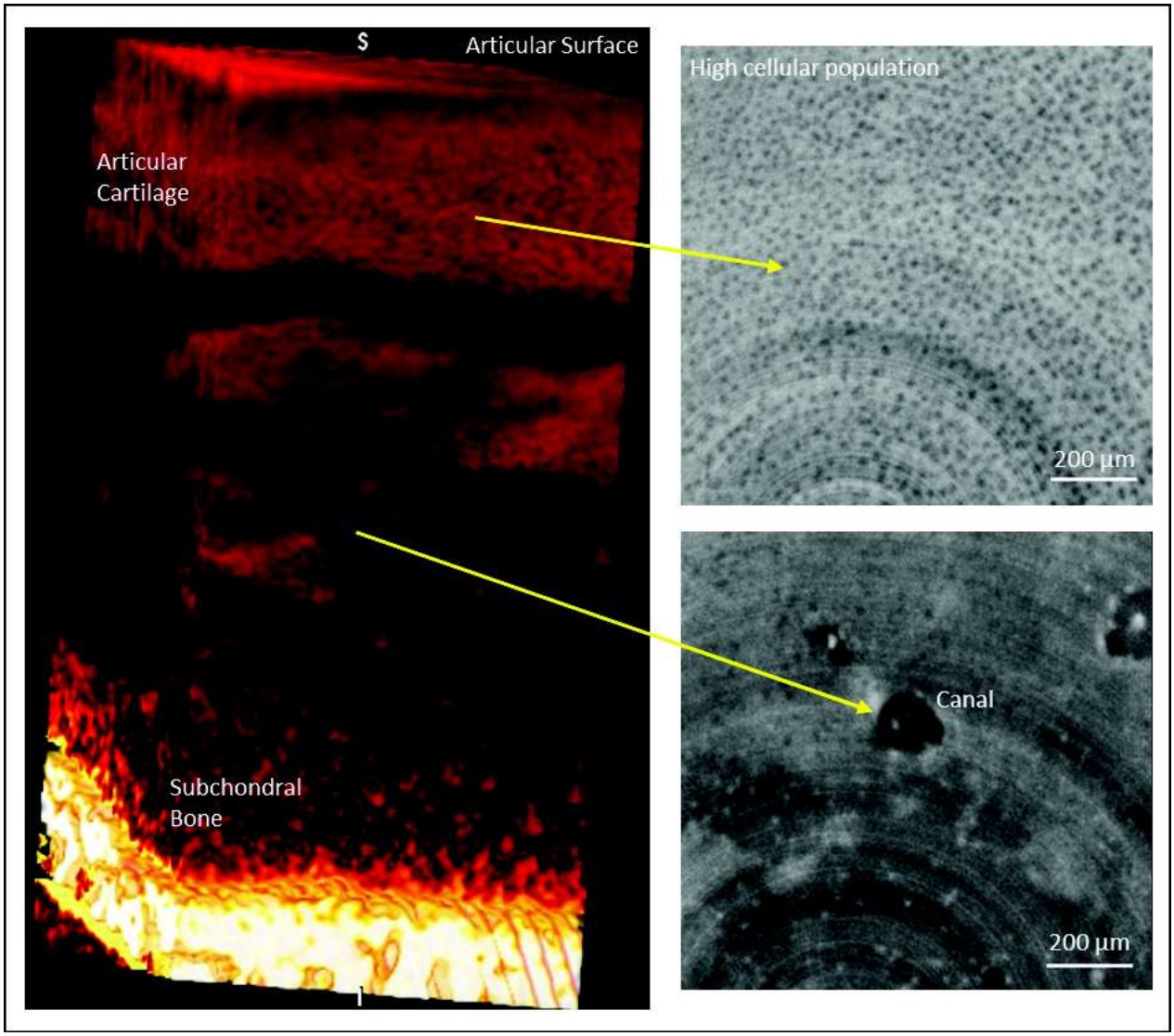

Figure 92: 3D-Block reconstruction of ITS Control explant with a transversal reconstructed slice from PCI of the articular cartilage surface presenting an extremely large cellular density and the visualisation of cartilage channels present in the growth cartilage.

image analysis has to be carried out. In addition, CT-imaging and histological studies have to be performed on the very same analysed samples in order to provide complementary information. Numerous strategies for articular cartilage repair are studied by many groups worldwide, all facing the difficulty to evaluate the effect of various strategies endeavour for cartilage regeneration. The establishment of the morphological variations during treatment studies is often realized using 2D histological approaches and exceptionally lengthy 3D histomorphometry had been carried out. Histological techniques present limitations such as potential damage of the cartilage structure and artefacts (during staining, dehydration and fixation processes, sectioning) giving rise to misinterpretation. Until today, no other specific non-invasive imaging approach than X-ray phase contrast imaging (XPCI) allow the 3D rendering of both soft (collagen matrix) and harder tissues (subchondral bone), and provides a global vision of the tissue at cellular scale.

Part VII
General Discussion

Selenium definitely has its importance in articular cartilage metabolism and homeostasis. As suggested in our general hypothesis, selenium depletion in the surrounding nutritional environment contribute to articular cartilage tissue degeneration. Evidences that the lack of selenium causes quite important changes have been presented. The biological activity of Se is related to its incorporation in the form of amino acid selenocysteine (Sec) into selenoproteins such as gluthatione peroxidase, iodothyronine deiodinases or thioredoxin reductase [69]. By using immature articular cartilage from the metacarpophalangeal joint of bovine steers, Khan *et at.* (2011) [16] have used growth factors fibroblast growth factor-2 and transforming growth factor β1 to induce precocious maturation of this cartilage [16-17]. Tests relative to Se depletion, through its absence in culture medium or its presence through Se-supplementation, were used to determine how selenium affect the articular cartilage tissue development during this critical window of growth which coincides with age-related incidence of KBD. This project aims to characterize the selenium implication in the articular cartilage development in a biological, biochemical and biophysical points of view. Selenium studies in biological materials is extremely complex as it is mentioned all along this work due to its known infime concentration within tissues. Consequently it is important to determine the selenium involvement into tissue organization and function. The identification (speciation) and definition of the spatial distribution of Se in articular cartilage will extend our understanding of selenium impact in articular cartilage. Once, elucidated, the characterization of the ECM of AC in presence or absence of Se during the maturation processes can be investigated using microspectroscopic techniques and molecular biology tools.

Characterisation of the Selenium in Articular Cartilage

In order to study Se speciation in an *in vitro* model of articular cartilage maturation and select the most adequate technique to use, Se concentration and Se location have to be evaluated. Cartilage explants from immature bovine metacarpophalangeal joints were cultured during 21 days in the presence of fibroblast growth factor-2 (FGF2) and transforming growth factor β1 (TGFβ1) to induce accelerated maturation [16]. We tried to minimize the sample preparation in order to preserve the cultured cartilage explant close to their native hydrated state and avoid changes in Se spatial distribution and Se species. The cryopreservation of the sample and storage under anoxic conditions prior analysis guarantee at best the chemical integrity of the samples. We could not find publications that have tried to determine Se content within cartilage. We provide first data and confirm the expected very low level of Se generally found in tissues and in the range of 100-200 μg/kg or ppb in average, for immature or mature bovine cartilage as determined by ICP-QQQ. Low Se content makes difficult X-ray fluorescence imaging even using high flux synchrotron nanoprobe for which detection limit for Se is ~600 ppb for a 100 ms acquisition time with an X-ray spot of ~50-100 nm. To go below the 100 ppb detection limit an acquisition time of 500s would be necessary but is not realistic to map even small cartilage region of only 100 x 100 μm with a 1 to 0.2 μm spatial resolution. Thus, compromise has to be made between reasonable acquisition time, spatial resolution to be achieved and elemental concentration to be detected. For our samples, the X-ray fluorescence nanoanalysis demonstrate that we were able to detect has a punctual localization of Se recurrently found in all sample that we could image. To the best of our knowledge, there are no studies that report the spatial distribution of Se in a cryosection of articular cartilage. The same conclusion can be drawn with regards to our study of Se bulk analysis

of articular cartilage. This was observed for all maps and specifically located at chondrocytes site. This suggests that it cannot account for a contaminant. The fraction of Se that could be detected and imaged appears to have a "single spot" pericellular location. The spectrum derived from these Se-rich regions indeed display a clear X-ray fluorescence emission Se peak relative to the K_α X-ray emission line. This is further confirmed with higher resolution scan of single chondrocytes (0.2 μm spatial resolution and 1s integration time/s) where the same punctual Se location is detected. This does not rule out the presence of Se elsewhere within the ECM but most probably we were not able to image it with the experimental setup used for our experiment and a too low Se concentration. We did not get any further beamtime accepted despite the submission of several proposal at Synchrotron source. It would be of interest to pursue these analysis to confirm the observed Se distribution in chondrocytes. Similar studies on cartilage samples supplemented with Se would be of particular interest too. The specific pericellular localization of Se within AC tissue (cell-ECM interface location) can suggest that Se can be related to a specific organelles location. This organelle should be placed at the interface of the cell and the ECM. According to the observed pattern, it can be suggested that it could be a primary cilium or a centriole [250]. Every chondrocyte possesses a primary cilium which can have a length up to 5 microns [201]. The primary cilium is an immobile, solitary and microtubule-based structure that projects from cell surface into the extracellular environment. It has a dual sensor, an antenna acting as a mechanosensor and chemosensor. In chondrocytes, primary cilia have a role in the mechanotransduction of events related to the stimuli happening in the cartilage extracellular matrix. It is required for the intercellular activation of the dynamical mechanical loading like compression-induced Ca^{2+} signaling mediated by ATP-release [249]. It appears that the primary cilia play a role in the regulation of the joint development processes. Although still hypothetic, the observed Se localization at chondrocytes could be associated to an organelle involved in the mechanotransduction of the cells within the ECM. Of note, sperm capsule selenoproteins are localized in the mid-piece portion of spermatozoa where it stabilizes the integrity of the sperm flagella [266]. The present PhD has required several accesses to synchrotron sources. As any other worldwide user, project has to be submitted each 6-month prior being peer-reviewed and eventually granted for access to synchrotron beamtime, generally 1 to 5 days of experiments. We were most often successful, but in the case of X-ray fluorescence studies, we were successful only once and get access for 3 days. This precludes our wishes to better identify the intracellular Se location and hypothetic associated organelle. Thus, further studies are required to confirm these hypotheses. It would be necessary to perform immunohistochemistry (immunofluorescence of the acetylated α-tubulin (referring to primary cilium and centriole), NanoSIMS and/or synchrotron X-ray fluorescence imaging and nanoanalysis of chondrocytes where the primary cilia could be labeled using secondary gold-labeled antibody for example. Such approach would allow to get a merge image of both Se and gold distribution at the subcellular level and confirm or not the Se co-localization with part of the primary cilium. Although the main objective was Se distribution within the AC tissue; the techniques being multielemental, we could also observed that, as expected, sulfur distribution depict well the surrounding ECM as it mainly corresponds to sulfated GAGs and PGs, the major components of articular cartilage ECM. Interestingly, we show that Ca (the technique can only account for the Ca that is intracellularly bound) seems to correlate to the chondrocytes nuclear location or the reticulum endoplasmic while iron appears to be more cytosolic. The presence of these elements within chondrocytes is of importance. Iron appears to be found in a non-negligible concentration that is quite unusual at the intracellular level. These observations deserve further studies of AC tissue at different stages of maturation. This will help to understand the role of these elements towards the metabolic activity of chondrocytes.

No information is available regarding Se chemical form in cartilage or the impact of Se supplementation during cartilage maturation. A major obstacle to such investigations has been the absence of

suitable sensitive analytical methods. Overcoming resolution limits using conventional synchrotron-based X-ray absorption spectroscopy (XAS), we have developed HERFD-XAS based on an array of crystal analyzers, providing a novel, highly sensitive in situ method for element probing that breaks the ppm concentration barrier for speciation within native or physiologically relevant tissue. Currently, studies using XAS in transmission mode are limited to probing elements at concentrations of a few tenth of μg/g or ppm. The major limitations for optimal XAS acquisition such as solid-state detector saturation resulting in failure to filter unwanted contributions (elastic and inelastic scattering signals for example) have not been overcome to date, despite continuing efforts. Our proposed HERFD-XAS technique clearly demonstrates that speciation can be conducted in such complex matrix with Se content as low as ~400 ppb. To our knowledge this has not been reported so far for any XAS technique. The biological activity of Se is related to its incorporation in the form of amino acid selenocysteine (Sec) into selenoproteins such as gluthatione peroxidase, iodothyronine deiodinases or thioredoxin reductase [69]. With Se concentrations as low as 400 ppb, we were able to identify alkyl selenide (RSeR) compounds (Sec and gluthatione peroxidase) as the major contributing components within the articular cartilage explants. The importance of monitoring Sec levels is highlighted by studies showing the effects of deleting the Sec tRNA gene produce KBD-like phenotypes in mice, and, in humans where genetic polymorphisms in the gluthatione peroxidase-1 gene has been reported to be associated to higher risk of developing KBD [8]. The other contributing species is a thioselenide compound most probably in the form of selenodiglutathione (GSSeSG. Selenodiglutathione is the major metabolite of selenite in mammalian tissues [69,188]. Selenite and reduced glutathione spontaneously react to form GSSeSG, and reduced glutathione concentrations are known to be high in nearly all tissues [192]. Of note, GSSeSG is a highly reactive substrate for thioredoxin system [193], and recently it has been reported that thioredoxin reductase-2 deficiency induced impaired proliferation and chondrocyte cell death. This has been suggested to be another pathological mechanism for osteoarthropathy that occurs as a result of Se deficiency [194]. We also perform speciation studies for cultured AC explants exposed to exogenous sodium selenite supplementation. Indeed, dietary supplementation with sodium selenite has been shown to offer a potential treatment for KBD in children [195]. The results we could obtain suggest that, under supplementation with sodium selenite, Se incorporation into tissues of articular cartilage explants is limited and independent of the growth factor treatment known to regulate chondrocyte metabolism [196]. Under sodium selenite (oxidation state +4) supplementation, the fitting of Se HERFD-XAS spectra with a linear combination of spectra from a library of Se model compounds demonstrates that this inorganic form accounts for only 25% of Se species incorporated into the articular cartilage matrix. The predominant form of Se species identified was the redox active selenotrisulfide selenodiglutathione (GSSeSG), a primary Se metabolite. GSSeSG is an intermediate chemical species produced by a non-enzymatic reaction between selenite and reduced gluthatione [69], and is known to be metabolized further to hydrogen selenide (HSe^-) via selenopersulfide (GSSeSH) formation, two volatile and highly reactive compounds, by glutaredoxin systems in the presence of excess amounts of GSH, which leads to spontaneous oxidation of HSe^- to elemental Se (Se^0). These later species were not detected in our samples and data suggest that GSSeSG is preferentially incorporated into our model of articular cartilage maturation when exposed to elevated levels of exogenous sodium selenite. It would be of interest to obtain a spatially resolved distribution of these species and to explore the nature of Se bonding within chondrocytes or within the protein fraction of the articular cartilage matrix. It has been demonstrated that up to now the limit of speciation using synchrotron X-ray microprobe for sub-cellular XAS analysis was 13 ppm for arsenic [169] an element with a K-edge close to that of Se. The proposed method could be coupled to synchrotron X-ray microprobe setup that uses Kirkpatrick-Baez mirror system as focusing optics, in order to bring spatially resolved speciation to the range of sub-ppm elemental concentration. The

present study demonstrates that HERFD-XAS analysis of highly-diluted elemental species in biological matrix is possible. Significantly, our work provides the opportunity to undertake highly-diluted elemental speciation studies in biological samples, overcoming previous technological bottlenecks that have existed until now. While hyphenated techniques provide specific molecular identification and are very sensitive techniques, liquid extractions are required as for any MS techniques, which likely change the speciation of the samples. On the contrary, frozen hydrated samples can be studied by HERFD-XAS. This analysis can be performed at low temperature (~ 10K) that allows to preserve at best the native state of the sample and drastically limit changes in speciation under the synchrotron X-ray beam. HERFD-XAS presently requires long acquisition times to obtain the required statistics for high quality spectra. Still, there is potential to further extend our novel technique. There is room for increased incident flux using optical elements along with larger collection angles and even higher sensitivity, alongside faster collection times with the possibility to couple more crystal analyzers. A CRG-FAME2 beamline is under construction that will provide the proposed improvements (higher incident flux and up to 12 crystal analysers for signal collection) paving the way for speciation analysis that has not been possible until now. The proposed method has the potential to allow the question of biochemical interconversion of ultra-diluted physiological elements such as Se or toxicants like mercury, lead or arsenic to be tackled directly.

Characterisation of Selenium Influence on the Articular Cartilage Extracellular Matrix

We investigated the level of expression of selenoprotein genes in our *in vitro* model of articular cartilage. These genes encoding for selenoproteins (Thioredoxin Reductase TRNDX1, Glutathione Peroxidase GPX1, Iodothyronine deiodionases DIO2) were selected based on a review of the literature that encompasses the different gene appearing in patients suffering of the KBD or osteoarthritis and also some studies that have been performed *in vitro* on chondrocytes cultures [5, 8, 11, 12]. qPCR analyses allow to study the up and down regulations of diverse genes related to selenoproteins expressed in bovine AC upon diverse maturation treatments. Analyses of first set of data are still mostly qualitative and semi-quantitative. An increase in DIO2 gene expression appears as explant matures. The upregulation of DIO2 appear to be related to the use of the growth factor. Indeed, in our *in vitro* model, we use transforming growth factors beta and fibroblast growth factors families of cytokines being known to regulate chondrocyte metabolism [196]. The same observation can be made for GPX1 gene expression and apparently without any significant effect of Se-depletion or Se-supplementation on both expression level. Still, this would require confirmation with appropriate number of replicate with additional western blot analysis for the associated protein level. Concerning the collagen II a 1 gene expression, we have the opposite behaviour with a strong downregulation of the COL2 gene expression in presence of the growth factors that is in agreement with previous work showing synergistically action of FGF2 and TGFβ1 on chondrocytes by repressing collagen type II gene expression [267]. We did not found any significant influence of the Se-depletion/supplementation. This deserves further experimentation and particularly proteomic on selenoproteins to evidence in more details the impact of either Se-depletion, Se-supplementation or the FGF2 and TGFβ1 association on the AC maturation in this *in vitro* model. Histological sections of maturated AC explants treated with different Se-level were labelled with Safranin O to highlight proteoglycan content. The histological section corresponding to the usual ITS treatments provides the same information that the explants with a postnatal maturation as described in Khan *et al.* 2011 [16] (results in a reduction of cartilage height, cell density variations, cell morphological changes) [29,47]. An interesting singularity appears in the explants cultured in a

serum totally depleted in selenium. The results have shown that explants underwent a fast maturation development (growth factors treatment). We suggested that the observed clusters formed could be chondrons independent units. The morphology is closed to what is observed in early-middle stages of osteoarthritis [251]. Of course, this does not reproduce the importance of the effects observed in OA-tissue, the number of cells in a clusters being well inferior to 20 as observed in total for OA-cartilage. In the surface zone there is a light staining in the extracellular matrix compare to the much stronger one in the cellular border and pericellular region. This can be associated to the possible metabolism of chondrons.

Indeed, the chondrons could be identified as a kind of hypertrophic stage and this would induce a non-promotion the proteoglycan and collagen components as described in literature [268-269, 281]. Interestingly, a potential reduction of the type VI collagen concentration has been observed in the superficial zone and could be correlated with the potential loss of mechanical properties [39, 270] as it is observed in AFM studies. These hypotheses could be confirmed by immunofluorescence for the type-VI collagen protein localization. Experiments have been scheduled, but due to some protocols and reagents problems, we are not able to provide any validated data. However, it appears to us not too speculative that a Se-deficiency would be a favourable environment for the development of osteoarthritis-like pathology. In addition, we have to highlight that our *in vitro* model is static whereas *in vivo* mechanical constraints play an important role in AC maturation. Our last experiments using synchrotron X-phase tomography is thus of importance for future studies where mechanical compression could be additionally applied to the explants. The capabilities of the X-ray phase tomography could thus be exploited for a nearly 3D histological resolution of the AC explants. Such 3D visualization of the explants could provide interesting complementary and more precise information about the spatial organisation of the tissue, the cellular density and distribution (differentiation stage of chondrocytes, calcification...). This will allow a direct 3D histomorphometry of the explants and we expect to better highlight the impact of Se-depletion on AC maturation.

The complementary use of the synchrotron FTIR microspectrocopy was interesting as it allows molecular mapping and consequently provide information on the ECM. As mentioned previously, Amide I band has often been discussed in literature for its collagen non-specificity relative to the significant PG contribution in this region [208] and alternative IR index based on spectral features rather than Amide 1 band area has been proposed [208, 210]. The amide I (AI) band often refers to the protein content in most of biological material and especially the collagen content in the case of articular cartilage tissue [203, 207-209]. Histological experiments using safranin O refers to proteoglycans (orange color) as described in the literature [189]. However, in some protocols Safranin-O staining can also provide a red-orange colour assign to collagen. Still, an interesting correlation appears between histological staining and the FTIR map obtained for the different cultured AC samples. From stained sections, it is possible to say that the proteoglycan content is higher in the deeper zone that in the superficial regions as described in the literature [190, 191]. When IR molecular maps were generated by the use of the 1062 cm^{-1} band, an IR index that has been shown to refers to the proteoglycan (PGs) content, we can observed that the color and intensity gradient in the staining intensity refers to the proteoglycan (PGs) content. The ITS FT-treated samples show a dense and homogeneous PG content throughout the tissue. A high PG production is observed in middle and deep zones of No Se FT-treated explants that is found similar to FTIR maps based on the amide I absorption band used as a proxy for collagen content. This is also confirmed by safranin o staining of AC sections with an intense orange coloration mainly expressed in the upper part of the tissue section. As already reported in the literature [208], Amide I band appears to be impacted by the presence of PG. This can consequently influence our interpretation for collagen distribution and content on the sole basis of the amide I absorption band area. Collagen spectral feature has been associated to an IR index using frequency ~1338 cm^{-1}

[216]. We correlated these results with histological and immunofluorescence analyses. We confirmed that No Se samples present an alteration of the collagen distribution within the middle and deep zones and could be linked to the absence of Se within the medium. The ITS control present a reduction of the collagen signal, mainly in the deep zone. This support that the tissue does not reach an advanced maturation stage yet. As expected, the AC explants that were cultured with combined growth factor show clearly an induced homogenous collagen distribution within the middle and deep zones. The No Se FT-treated display with decreased collagen content within the superficial zone while PG content appear to be high throughout the middle and deep zones. In immunofluorescence, without selenium but with growth factor, the expression of the collagen type II is locally present in the upper part of the superficial zone. In the middle zone, the explants treated with selenium only present this protein in the pericellular matrix. In the deep zone, le collagen type II appears to exhibit greater labelling in the explant growth factors-treated in the medium without selenium (No Se FT-treated). Theses combined observations are coherent with literature where it was shown that in KBD (and OA) a lower level of collagen type II was found in chondrocytes, highlighting some dysfunction in the ability to correctly synthesize and secrete collagens [5, 282]. However, chondrocytes could produce type I collagen which are usually present in the bones. It can be a potential explanation of the relatively important collagen distribution in No Se FT-treated. Combining the collagen and proteoglycan information from FITRM, histology and immunofluorescence, growth factors are definitively important for the characterization of the AC maturation process. The collagen content increases and tends to be homogeneous throughout the extracellular matrix in maturated AC tissues. However, Se-depletion appears to have an impact on the collagen distribution. When growth factors were added to this Se-depleted culture medium, we observe a balance of that distribution. ITS FT-treated explants show a distribution of PG and collagen consistent with an accelerated maturation of the AC. This contrast with No Se FT-treated explants that show only a much denser and higher PGs content within the AC matrix. The infrared information provide a qualitative view of the biochemical variations of the AC matrix, however this cannot provide any formal information on the quality of the extracellular matrix.

We finally explored, at nanoscale, the biomechanical properties of our model of AC. These preliminary results provide a novel first insight of the potential of AFM investigations on the articular cartilages, even if a limitation of this study is that all AFM results came from a single batch of samples with a low number of repeats. Further experiments should be done in order to verify the biological reproducibility of the results obtained for different culture replicates and also to increase the statistics by analysing a larger number of area per sample. The obtained information are coherent with the established hypotheses and the analysed references (native immature and mature explants) are in agreement with the data reported in the literature [17,271] and previous analyses made by some researchers in the CHN department (unpublished data). The collagen organisation has an important role in regulating cartilage mechanical properties during maturation process. Any alterations in the mechanical properties of the AC may have important consequences on cartilage ECM synthesis with direct consequences on the mechanical integrity of the AC. Even if cartilage topography and roughness estimation do not present significant difference ($P>0.05$), subtle changes in the fibrillary distribution can be observed from the images. Further analyses are in progress to evaluate the fibril size and density at the sample surfaces in order to establish some preliminary trend. Another trend was observed through the studies of the young's modulus and indentation. Se-treated explants (ITS group, with an average indentation value about 186 nm) are stiffer (less deformable) than No Se-treated explants (No Se group, with an average indentation value about 287 nm). The latter when also exposed to growth factor get even stiffer by almost 2-fold compared to AC cultured in Se-depleted conditions. The Young's Modulus values obtained for native immature and mature tissues but also for ITS Control and FT-treated explants perfectly correlate to Young's modulus values reported by Khan *et al.*

2013 [17]. On the overall, we provide an important information about the absence of Se with the consequence of decreasing the stiffness of the AC surface and inducing a higher deformation under strains compared to other Se-treated matured explants.

As reported in Khan *et al.* 2013 [17], the specific increase in stiffness for treated samples could be induced by a reduction in glycosaminoglycan content in *in vitro* cultured explants compared to freshly isolated native cartilages. This GAGs reduction generally induced an increase in the sample stiffness. This can also be associated to a normal phenomenon occurring as in human cartilage during aging [153]. As hypothesised in Khan *et al.* 2013 [17], the differences in surface stiffness during cartilage maturation measured at the nanometer scale represent changes in collagen structure, particularly in the thickness or density of fibres that can be modulated by fibril associated proteoglycans such as biglycan or decorin [272-274]. The selenium depletion in the culture medium has the effect of increasing this difference, exhibiting biomechanical properties closest to the native immature tissue. It can be suggested that during cartilage maturation, the surface becomes stiffer and exhibits smoother surface as observed in Khan *et al.* 2013 [17] and Ghadially *et al.* (1978) [275]. It is evident that Se depletion impairs the nanomechanics in surfaces of the AC explant samples. However, the exact mechanism inducing these phenomena remains unknown.

Part VIII
General Conclusion & Perspectives

This project was a real challenge to promote the importance of the medical geology studies within a complex biological topic. The relationship existing between environment and health is tenuous and extremely important. This project tends to confirm that Selenium is an essential element in the development of the human body. As seen all over the manuscript, selenium deficiency has some impact on cartilage matrix component distributions and organisation. Se-action is also controlled at the genomic levels. This knowledge provides already good insights on how a selenium deficiency negatively impacts the articular cartilage metabolism. This project also provides information about the use of several advanced techniques in order to offer a panel of complementary information on the impact of Se over the AC maturation processes.

To assess the importance of the Selenium in AC tissues, it was necessary to determine the Se-concentration in articular cartilage. This was for first time provided using state of the art ICP-MS techniques and spatial distribution in the AC tissues was tackle through the use of Synchrotron-based X-ray fluorescence nanoimaging technique. A recurrent Se patterns with point location that correlate to cellular/matrix interfaces, potentially revealing an involvement of Se in a particular chondrocyte organelle, putatively primary cilium. We could for the first time push the X-ray absorption spectroscopy speciation technique to unprecedented 400 ppb (μg/kg) detection level. The speciation investigation confirmed the Se present in articular cartilage to be Se^{-II} related to selenocysteine, an amino acid present in the active site of most selenoproteins. Under supplementation with inorganic form of Se i.e. sodium selenite were discovered that the main Se-form was selenodigluthatione with a 25 % of Se stored as sodium selenite in the AC matrix.

Complementary investigations of selenium involvement on the ECM were performed using diverse techniques to study the impact of selenium on biochemical and biophysical tissue properties. All the histological, immunofluorescence and FTIR analyses tend to confirm that a selenium deficiency impacts the articular cartilage development. Even if the results are subtle, they tend to show that selenium deficiency in the culture environment induce negative changes in metabolism and maturation process, namely the dissociation of bone from AC. Mechanical tests have been realized and tend to confirm that selenium deficiency induces a decrease in tissue stiffness with possibly a compromised mechanical role of the cartilage in the joint. A better understanding of selenium's role in the articular cartilage growth and metabolism is fundamental to establish preventive solutions adequate to tissue degradation and to potentially enhance different treatments in progress. Results are encouraging but several experiments have to be performed to confirm and validate the mechanistic role of Se in the AC growth.

The present project is a basis that highlights Se as a interesting element to be taking into account for future strategies aimed at regeneration of the articular cartilage. Articular cartilage is extremely difficult to regenerate regarding to its low replenishment rate. Selenium could be an additional factor playing an essential role to enhance and boost actual regenerative techniques (stem cells, 3D bio-printing, grafts). The comprehension of the fundamental mechanisms and the given methodology can provide interesting lines of research for other diseases where selenium is potentially implicating, such as cancer, diabetes and Alzheimer disease [18]. This work can be extented to the study of the present model exposed to mechanical load or, to upcoming engineered cartilage system.

This prospective project has encountered many difficulties. The study about selenium in articular cartilage is scarce. Selenium impact on articular cartilage tissues started to be investigated when some geological and epidemiological studies have shown the strong link between Se deficient soils and

Kashin-Beck disease occurrence in China. Se-deficient soils are cultivable, consequently the cereals, like rice produce on these soils are also Se-deficient. The population that are eating these cereals can be chronically Se-deficient with negative effects on their cellular functions and more generally on their general metabolism. The proportion of people affected by this disease is important, and several biologists tried to identify the Se-involvement at protein and genetic levels. Some of them established relationship between this disease and variations of selenoprotein expressions. Nevertheless, the impact of selenium on articular cartilage has never been precisely defined, and all the methods and techniques applied during this thesis aim to provide some answers and guidelines for further works. Non classical laboratory techniques have been developed and used. The biological, biomechanical and biochemical properties of these particular samples have been explored. It is important to keep in mind that technique can slightly change according to the model being analysed.

This project finally opens on a variety of further explorative works. Diverse objectives could be investigated:

(a) repeat of this AC model under mechanical load

(b) biological investigations of selenoproteins expression

(c) 3D imaging of articular cartilage.

Dynamic AC in-vitro Model: The development of this AC model under mechanical load will allow to validate the necessary constraints to structure tissues in *in-vitro* conditions. This can also extend the lifetime of the sample in culture because in a static condition, cultured samples start to degrade in the center of the plug after three weeks. Dynamic conditions can enhance the transfer of nutriment of the culture medium to the entire explants. The impact of the selenium can also be evaluated in conditions closer to the "real one". In static conditions, the results are subtle but they tend to show that selenium deficiency in the culture environment induce negative changes in metabolism and maturation processes. Loading on these explants can enhance the visualization of these variations and help to better identify the impact of Se on the articular cartilage development.

Selenogenomic and Selenoprotein Investigations: A full biological study can be explored as well. Preliminary studies have shown that various Se concentrations induce variations in selenoprotein expressions. Regarding the obtained results, a large proteomic investigation could allow to identify the key player related to the selenium involvement in the AC cellular metabolism.

3D-Dynamics and Tribology of AC: Tribological tests should further be investigated. With using geophysical techniques, a friction study can be performed. Adapting a friction instrument developed to study rock rupture, articular cartilage/bone system ruptures and dynamics would lead to the identification of fragile axis present in articular explants. Phase-contrast X-rays tomography combined to a small press to load charges on the explants can be performed at ESRF to determinate the exact location of the rupture. Tomographical images will allow a correlation of the rupture point to the fragile component. This study can be used to enhance 3D-bioprinting structure study. This project can also be combined to synchrotron phase-contrast tomography on explants coming from dynamic explant cultures (as described previously) to assess the weakness of the articular cartilage which means identify the elements the most sensible and susceptible to break under strong mechanical strains. Selenium impact on articular cartilage biomechanics can be established.

Tomographical 3D Imaging of AC: Synchrotron-based tomography can be an amazing tool for future experiments. Up to now, most results comes from AC section as complete 3D histomorphometric studies are scarce. Full 3D analysis are necessary to be the most representative view for the characterisation of the AC. Cryosections usually preserve the "native" sample conditions without any alterations linked to post-culture treatment. However, some sectioning artefacts can alter the information of the samples. Analyses on the entire samples (explants) can solve these problems. X-ray phase-contrast tomography can provide a better understanding of articular cartilage growth and maturation in native conditions. As described in the previous section, synchrotron-based phase-contrast tomography is an on-going project to be developed for 3D-imaging of cartilage tissues. Preliminary experience already gave the visualisation of 3D-structure of the tissue. This highly promising technique gives access to a better visualisation of the cartilage channels with complementary structural information (density changes, cell distribution). Actually, cartilage channels have been observed and studied long time ago, however their functions remain unclear. This technique can be used to be highly complementary to histological analysis. Combined with biological investigations and histology, a precise analysis can be performed to determine the role of these channels. Channels being in the growth cartilage (future bone), modifications of the cellular and channel morphology can allow to assess any impact of selenium-deficiency on articular cartilage maturation.

Osteoarthritis, Kashin Beck and all the other joint degradation-related diseases represent a major human health and economical burden in our society that needs to be solved. The medical geology field could be a new direction to investigate such diseases. It reveals environmental factors leading to a given disease. It requires a good understanding of the interconnections between soils, air, water, pollution, health and diseases. The link between soils, agriculture and food is obvious and relatively well known. Cultivated on specific soils, plants and cereals ingest all necessary nutriments from soils. Soil Se-deficiency induces Se-deficient diet, thus Se-deficiency in organisms and human body. Furthermore, even if direct observations linking Se-deficiency and certain joint diseases are now established, the exact implication of selenium in the onset and propagation of these diseases remains unclear. Se-supplementation (food) seems to be beneficial to health improvement but its long-term effect is still not yet confirmed. Selenium can be a key element in new strategies to increase the resistance of cartilage to degradative processes. It could be an additional factor playing an essential role in the bio-compatibility and incorporation of new transplanted tissue and can be a source of stimulation for stem cell therapy by its cellular protective action. Control and understanding of selenium intake could therefore become in the future the "natural" remedy for several diseases such as osteoarthritis.

Part IX

Annexes

20 Quantitative Polymerase Chain Reaction

To perform the optimal qPCR, two controls have been realized. After RNA extraction, a "-RT" no reverse transcription has been performed. RNA followed the RT-PCR process without enzyme in the reaction, the cDNA cannot then be converted. If something remains, this corresponds to DNA coming from the original material which has not been eliminated in the RNA extraction mini-kit. Then, during the qPCR plate preparation, a "NTC" no template control has been produced.dd H_2O or RNAse free water is used instead of the sample cDNA in order to verify the qPCR reaction specificity which can be compromised with a possible contaminations in reactions. In following presented reactions, the two controls were negative (no remaining DNA from the RNA extraction, no contamination).

Standard curves over the linear range of amplification were generated for all primer sets, and data was used where the efficiency of amplification was between 70% and 90% and the melt curves generated a single product. The data shown is the ratio of the concentration of the gene of interest (in nanograms, ng) and 18S rRNA (in nanograms).

The efficiency E refers to the amount of PCR product increase after each cycle ($E = 10^{(-\frac{1}{Slope})}$). Ideally, a reaction should reach an efficiency E close to 100% (reaction efficiency 90-105%). For all these reactions, E was a little low. Usually a low E value is related to poor primer design, bad reaction conditions, pipetting error. However, here the more probable reason is the primer sets coming from cloning which underwent several frozen-thaw series. The R^2 value refers to the goodness of the fit of the regression line which means that if all dots were perfectly lying on the line, the R^2-value would be equal to 1. Values superior to 0.97 are considered as good.

This analysis have been performed in two times due to the PhD schedule. During the two and third journeys in Swansea, the qPCR investigations have been performed for only six genes because of cloning problems. Quantitative PCR analysis of groups of proteins that seemed to be interesting to analyse and which seemed according to the literature are differentially regulated during the postnatal maturational process in articular cartilage with or without selenium [202]. The genes of interest are then the following: Aggrecans, Collagen II, PCNA, DIO2, TRXND1 and GPX1. 18S has been selected as housekeeping gene. The first study provides guidelines for a second trial. The first qPCR analysis has been done with n=4 samples per group and for k=6 independent groups, the second one with k=4 with n=5 samples per group.

Here, found all the standard curves, melt peak and melt curves of the qPCR reactions.

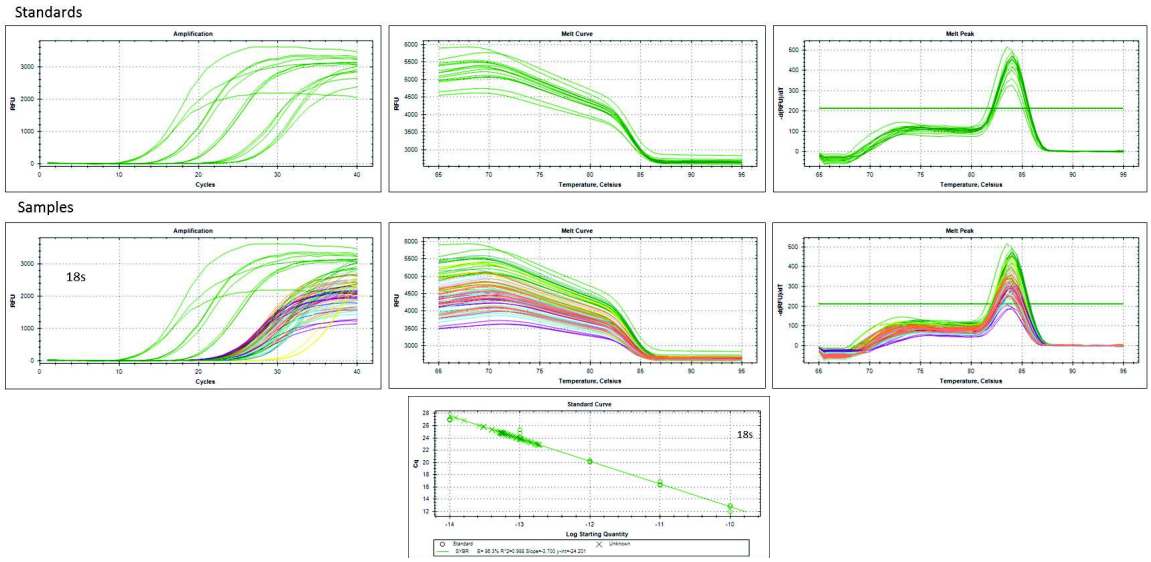

Figure 93: Amplification Plot , Melt Curve, Melt Peak and Standard Curve for 18SRNA gene-analysed Absolute Quantification on articular cartilage samples (NoSe Control, NoSe Ft-treated, ITS Control and ITS FT-treated)

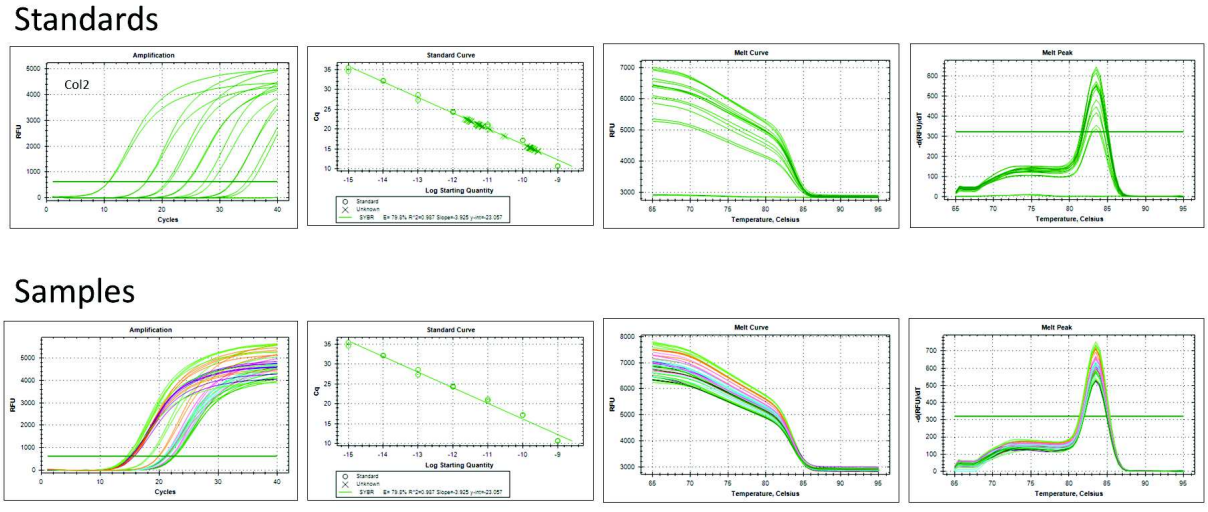

Figure 94: Amplification Plot , Melt Curve, Melt Peak and Standard Curve for COL2-analysed Absolute Quantification on articular cartilage samples (NoSe Control, NoSe Ft-treated, ITS Control and ITS FT-treated) (2015)

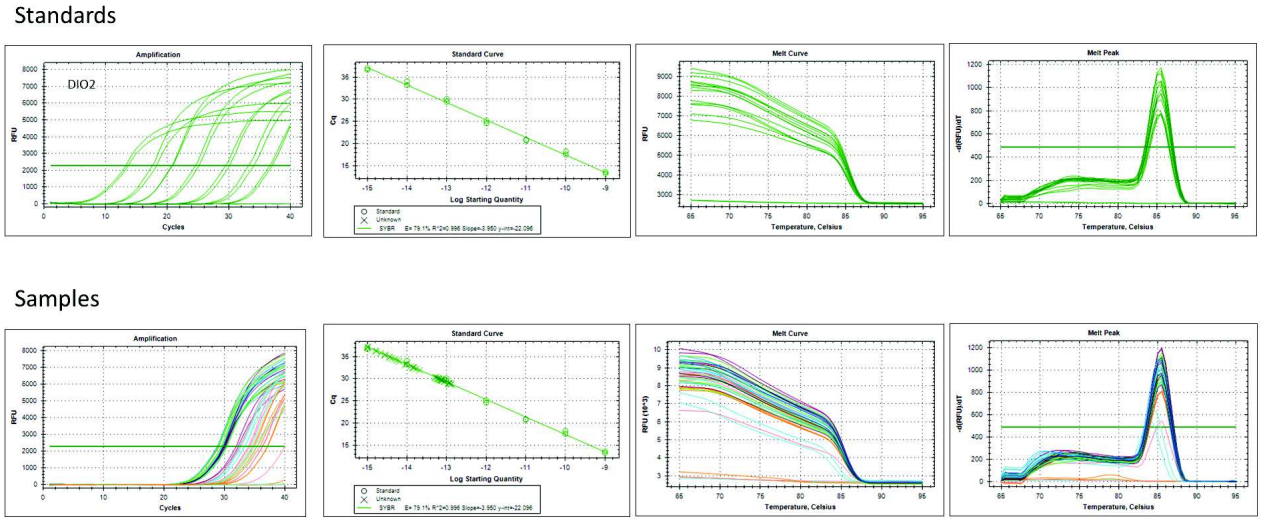

Figure 95: Amplification Plot , Melt Curve, Melt Peak and Standard Curve for DIO2-analysed Absolute Quantification on articular cartilage samples (NoSe Control, NoSe Ft-treated, ITS Control and ITS FT-treated) (2015)

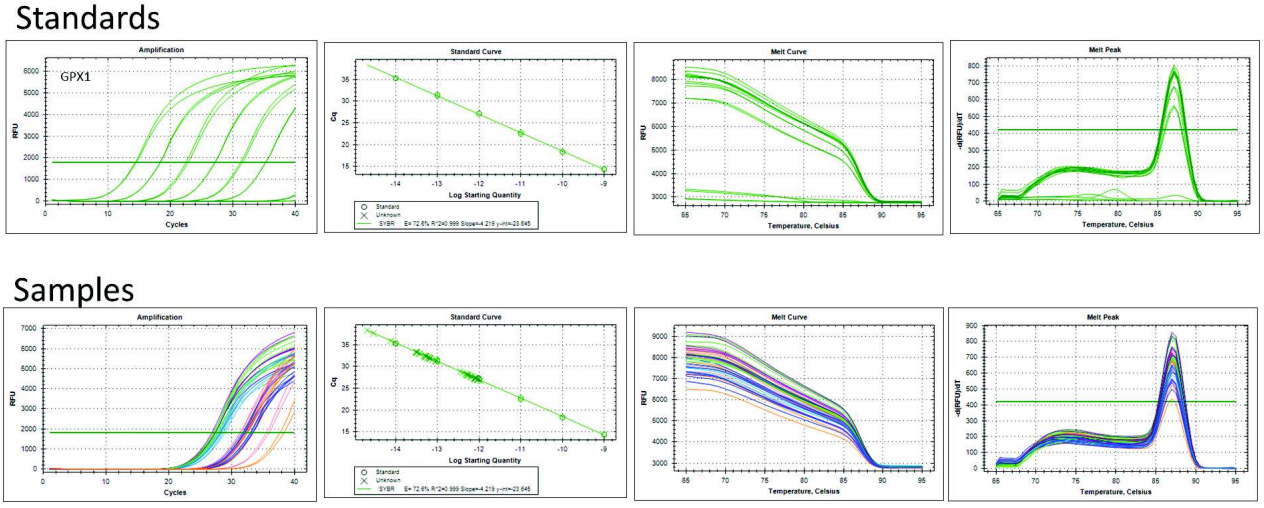

Figure 96: Amplification Plot , Melt Curve, Melt Peak and Standard Curve for GPX1-analysed Absolute Quantification on articular cartilage samples (NoSe Control, NoSe Ft-treated, ITS Control and ITS FT-treated) (2015)

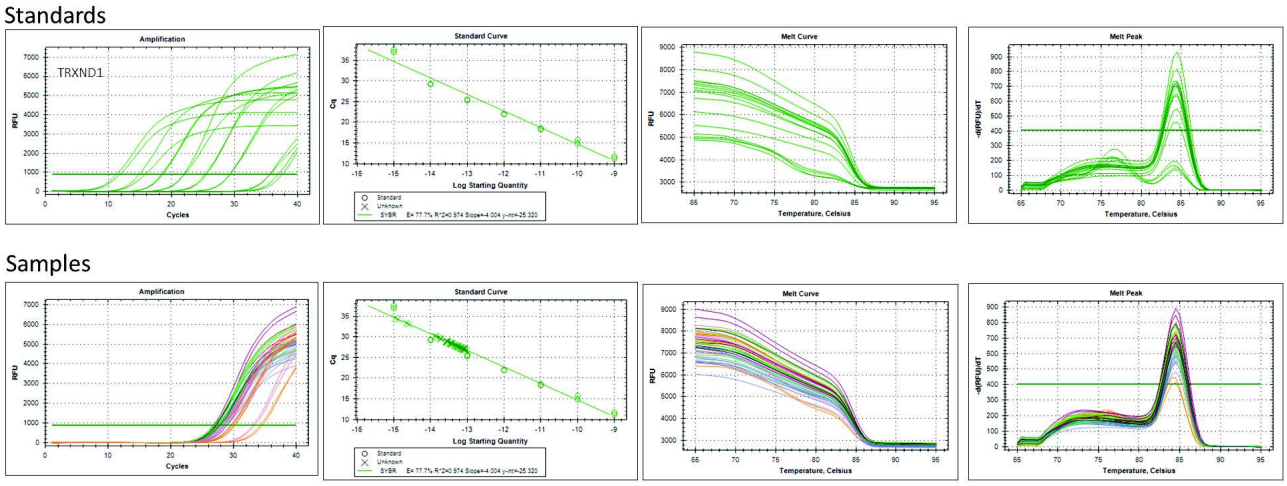

Figure 97: Amplification Plot , Melt Curve, Melt Peak and Standard Curve for TRXND1-analysed Absolute Quantification on articular cartilage samples (NoSe Control, NoSe Ft-treated, ITS Control and ITS FT-treated) (2015)

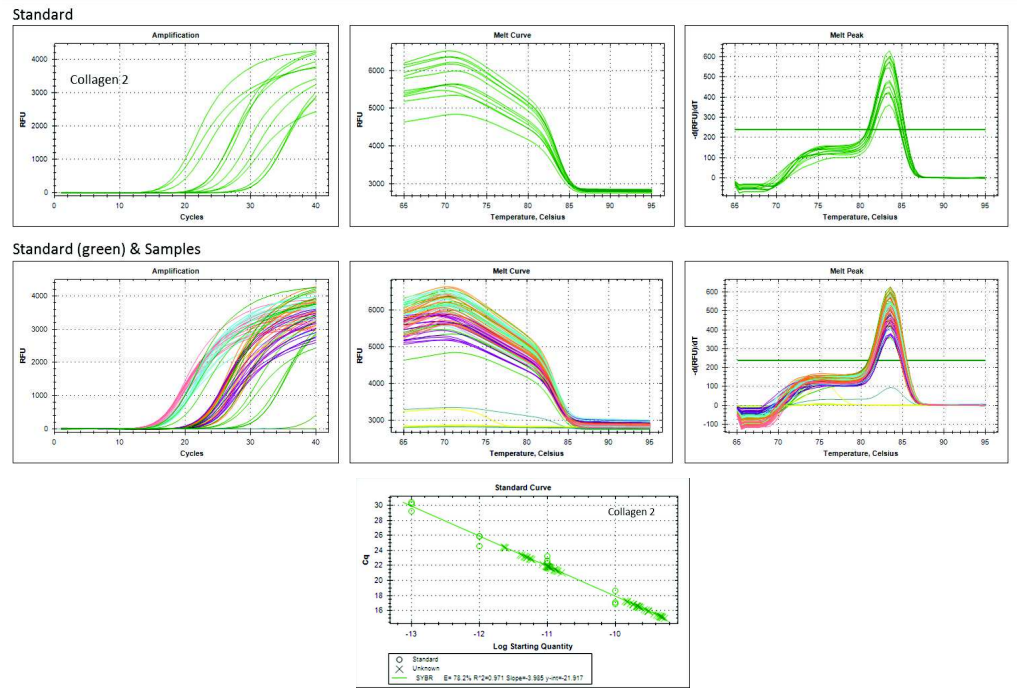

Figure 98: Amplification Plot , Melt Curve, Melt Peak and Standard Curve for COL2-analysed Absolute Quantification on articular cartilage samples (NoSe Control, NoSe Ft-treated, ITS Control and ITS FT-treated) (2016)

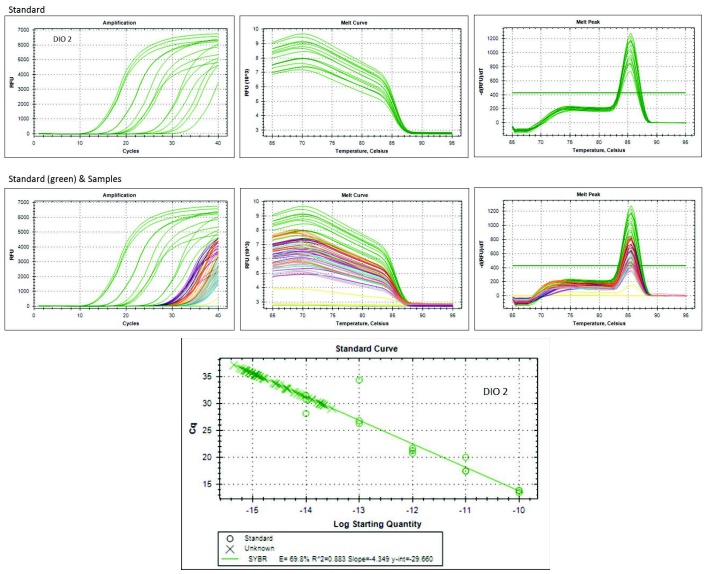

Figure 99: Amplification Plot , Melt Curve, Melt Peak and Standard Curve for DIO2-analysed Absolute Quantification on articular cartilage samples (NoSe Control, NoSe Ft-treated, ITS Control and ITS FT-treated) (2016)

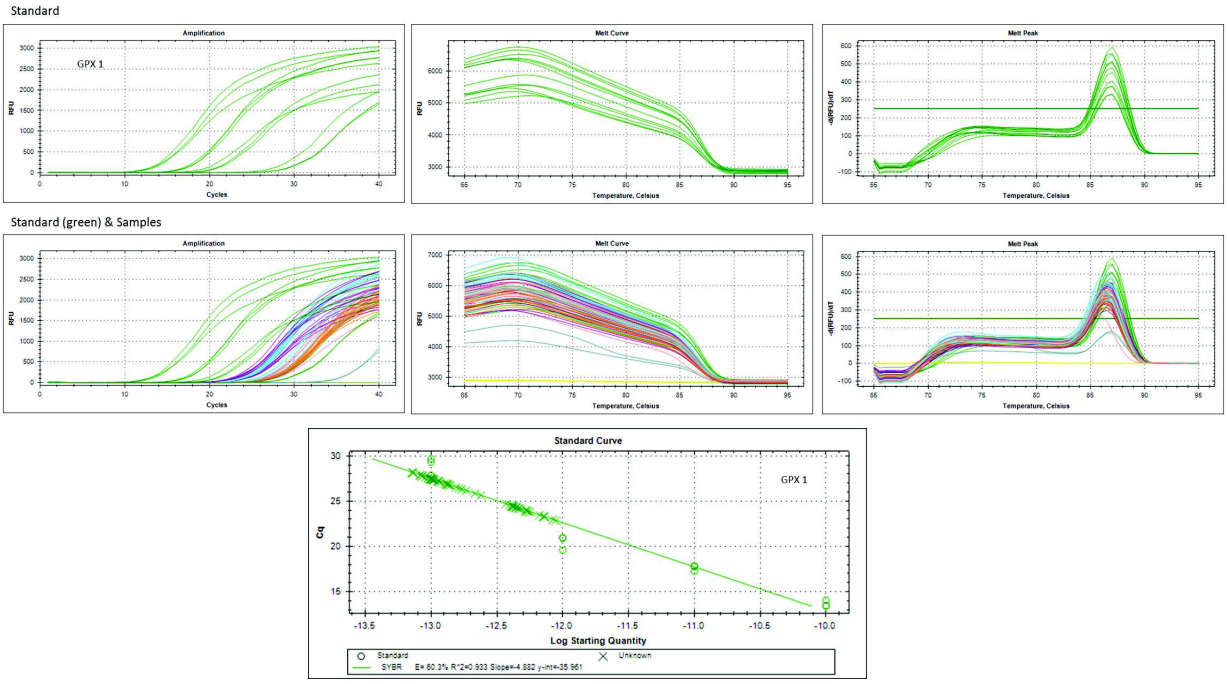

Figure 100: Amplification Plot , Melt Curve, Melt Peak and Standard Curve for GPX1-analysed Absolute Quantification on articular cartilage samples (NoSe Control, NoSe Ft-treated, ITS Control and ITS FT-treated) (2016)

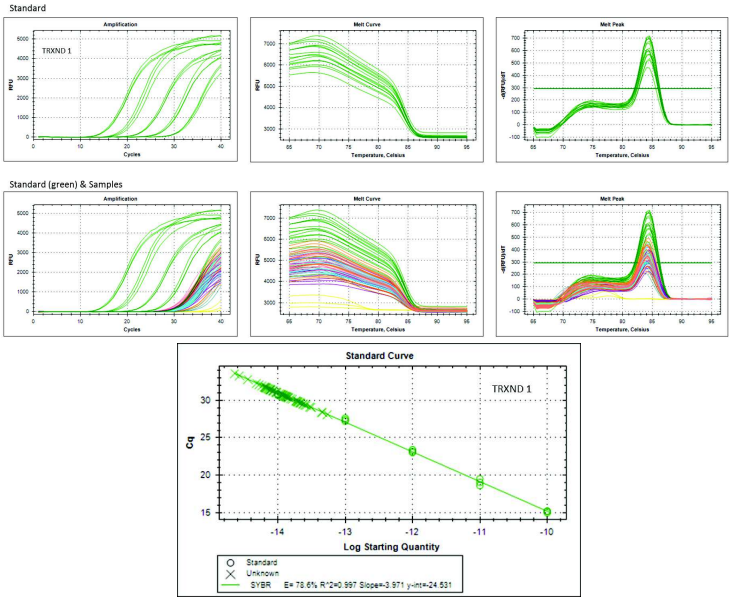

Figure 101: Amplification Plot , Melt Curve, Melt Peak and Standard Curve for TRXND1-analysed Absolute Quantification on articular cartilage samples (NoSe Control, NoSe Ft-treated, ITS Control and ITS FT-treated) (2016)

Some variations appears over the qPCR repetitions, especially for TRXND1 gene (Figure 102). It is then important to further reproduce these experiences in order to evaluate the reproducibility of the new Se-depleted AC fast maturation model. Potential pipetting errors and the experimenter can be a reason of these problems. However, the other studied genes (Figures 103-105) such as DIO2 (Figure 103) reproduce the same trend for the different experiments, which let suggest a potential error related to this primer set. The results seems more accurate for the second trial (2016) due to the higher purity of the RNA extracted.

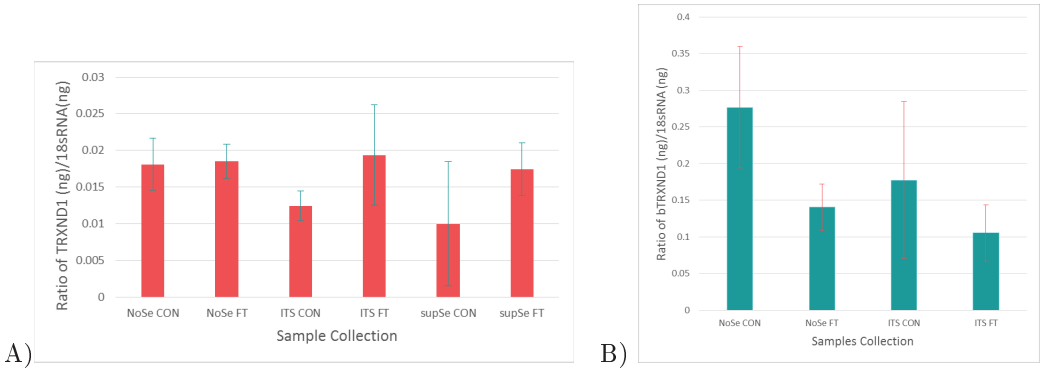

Figure 102: Transcript levels of TRXND1 for the different explants treated in presence (FT) or absence (Control)of growth factors and in different Se-content composition (NoSe, medium depleted in Se, ITS, usual tissue culture media (and SupSe with add sodium selenite in the usual ITS media).(Left red 2015 – Right green-blue2016) A) None significative difference between the samples is observed using Turkey Test, B) All the groups are significatively different ($P < 0.01$) except the couples NoSe control vs ITS Control and NoSe FT vs ITS FT.

The two experiences related to the TRXND1 gene expression analysis are contradictory, presenting a inverse trend. In the first experiment, the data do not exposed significative difference which can permit to state on some conclusion (Figure 102A). Nevertheless, the second trial seems to be more coherent with the experiments investigated during the design of the ITS model (Unpublished data,

Khan). The trend seems to present a decrease gene expressed during the maturation (about 2-fold reduction from control to FT-treated samples for No Se group and about 1.6-fold decrease for ITS group). The controls and the Ft-treated cDNA expression of the same group are significatively different (Figure 102B, NoSe $p<0.05$,ITS group: $p<0.01$). However, no statement can be made due a lack of significative difference between controls or FT-treated samples of these two groups. A new primer design is then first required.

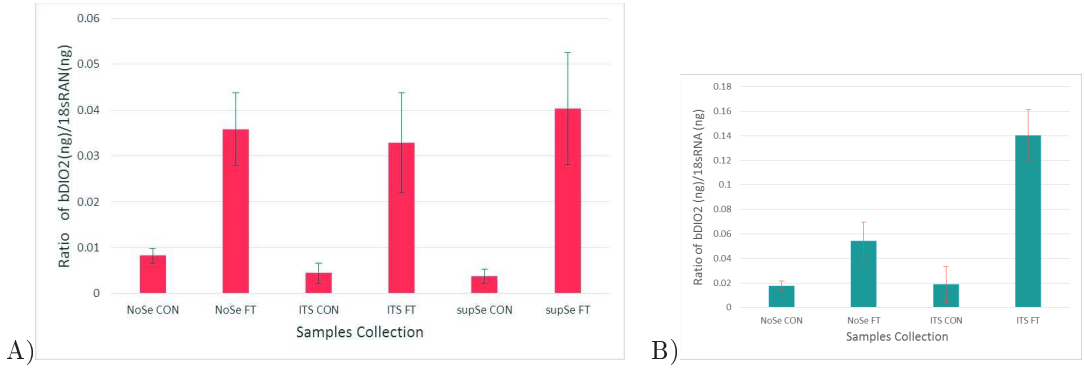

Figure 103: Transcript levels of DIO2 for the different explants treated in presence (FT) or absence (Control)of growth factors and in different Se-content composition (NoSe, medium depleted in Se, ITS, usual tissue culture media (and SupSe with add sodium selenite in the usual ITS media).(Left red 2015 – Right green-blue2016) A) All the groups are significatively different ($P < 0.01$) except the couples NoSe Control vs ITS Control, NoSe Control vs SupSe Control, No Se FT vs ITS FT, NO Se FT vs Sup Se FT, ITS Control vs SupSe Control and ITS FT vs SupSe FT, B) All the groups are significatively different ($P < 0.01$) except the couple NoSe control vs ITS Control.

An increase in type II Iodothyronine deiodinase gene expression appears as explant matures from control to growth factor FT-treated: a 4.5-fold increase is observed for the sample group cultured in Se-depleted media (No Se), about 7.5-fold increase for the ITS media cultured samples and about 10-fold Se-supplemented sample group (Figure 103A, $p<0.01$). No significative different is observed between the FT-treated samples of the three groups. The controls (No Se Control and ITS Control) tend to suggest that a possible influence of the selenium on the gene expression ($p\tilde{}0.05$). However, the general evolution of type II Iodothyronine deiodinase gene expression is better exposed in a second repeat (Figure 103B). Here, also appears as explant matures from control to growth factor FT-treated: about 3-fold increase is observed for the sample group cultured in Se-depleted media, and about 7.5-fold increase for the ITS media cultured samples (Figure 103B, $p<0.01$). It is interesting to notice that about 2.5-fold increase in this gene transcript level is also found in maturated (growth factors treated) explants which grown in ITS media ($p<0.01$). Selenium appears to impact this gene expression during the maturation process.

A 4.6-fold (No Se group), 9-fold (ITS group) and 8.8-fold (Se-supplemented group) increase of the gene expression from the control to the FT-treated samples is also observed for GPX1 (Figure 104A, $p<0.01$). No significative difference is expressed between the diverse controls (NoSe, ITS, Se supplemented). An augmentation of the GPX1 transcript level is observed in the case of matured (growth factor treated) explants (different factor of 1.8 between No Se and ITS and 1.5 between No Se and Se-supplemented, $p<0.05$). This trend of the GPX1 presented data indicates that the growth factor induced-maturation influences the GPX1 level and is expressed by an up-regulation of its expression. Selenium content could have a potential impact on this gene level during the maturation process. For the second experiment, the gene expression also increases from the control to the FT-treated samples is also observed for GPX1 (Figure 104B, $p<0.01$). No significative difference is expressed between the diverse controls (NoSe, ITS) and a non-negligible increase of the transcript

level of GPX1 in the case of matured explants (4-fold increase for No Se group and 2.3-fold increase for ITS group from control to FT-treated samples, $p<0.01$). Data tend to indicate that the growth factor induced-maturation influences the GPX1 level and is expressed by an up-regulation of its expression. Further repeats on other sample sets have to be performed to clarify this trend that have been found in the first experiment where selenium content could have a potential impact on this gene level during the maturation process.

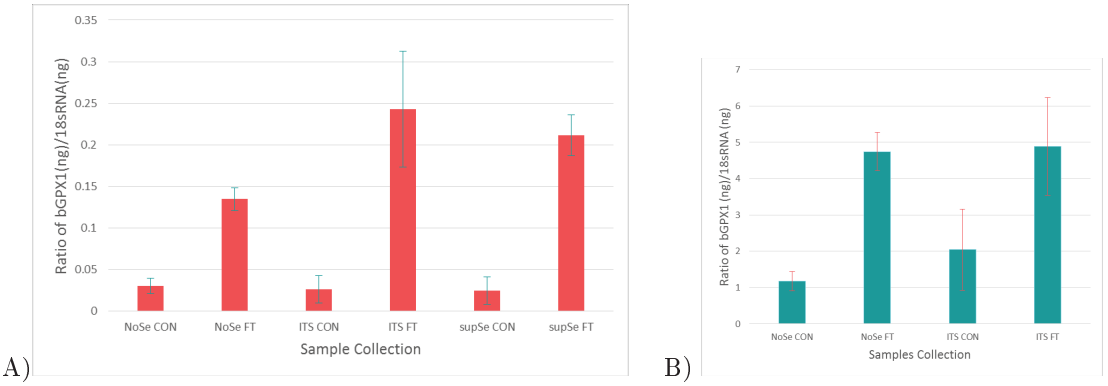

Figure 104: Transcript levels of GPX1 for the different explants treated in presence (FT) or absence (Control) of growth factors and in different Se-content composition (NoSe, medium depleted in Se, ITS, usual tissue culture media (and SupSe with add sodium selenite in the usual ITS media). (Left red 2015 – Right green-blue2016) A) All the groups are significatively different ($P < 0.05$) except the couples NoSe control vs ITS Control, No Se Control vs SupSe Control, ITS Control SupSe Control and ITS FT vs SupSe FT, B) All the groups are significatively different ($P < 0.01$) except the couples NoSe control vs ITS Control and NoSe FT vs ITS FT.

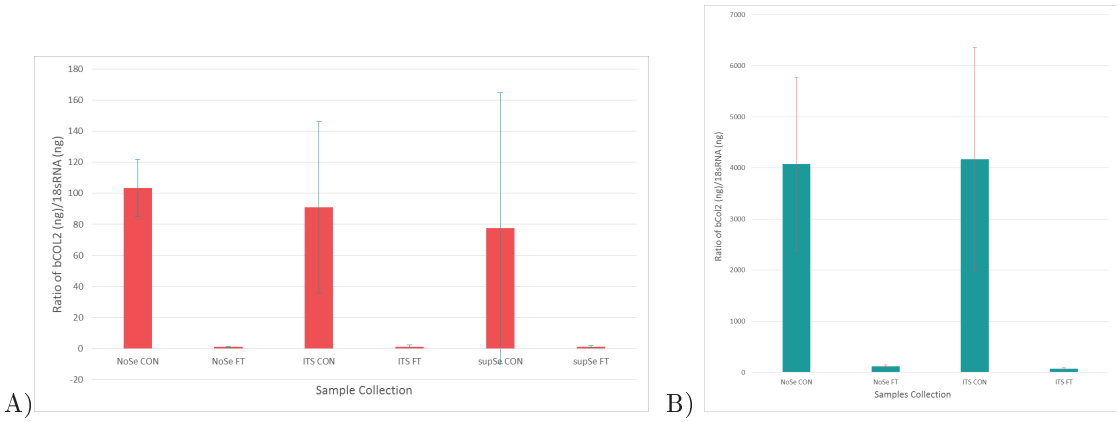

Figure 105: Transcript levels of COL2 for the different explants treated in presence (FT) or absence (Control)of growth factors and in different Se-content composition (NoSe, medium depleted in Se, ITS, usual tissue culture media (and SupSe with add sodium selenite in the usual ITS media). (Left red 2015 – Right green-blue2016) A) All the groups are significatively different ($P < 0.05$) except NoSe control vs ITS control, NoSe control vs SupSe control, NoSe FT vs ITS FT, NoSe Ft vs SupSe FT, ITS control vs SupSe control and ITS FT vs SupSe FT, B) All the groups are significatively different ($P < 0.01$) except the couples NoSe control vs ITS Control and NoSe FT vs ITS FT.

The collagen IIα1 gene expression is largely dominant in the controls than in the growth factor FT-treated samples, with about 100-fold transcript gene level difference for No Se group, about 70-fold for ITS group and about 60-fold for Se-supplemented (Figure 73A), $p<0.05$). The significative difference appears between NoSe controls and both Se-supplemented controls (without growth factor treatment) ($p<0.05$) collagen can be influenced by selenium content. In the second experiment, the

gene expression is also dominant in the controls than in the growth factor FT-treated samples, with about 35-fold transcript gene level difference for the No Se group and 56-fold in ITS group (Figure 105B), $p<0.01$). The maturation influences the regulation of this gene, however due to the large standard deviation, no strict conclusion can be provided concerning the potential influence of the selenium in these culture explant treatments. The trend remains the same in both experiments and is confirmed.

A 2-fold decrease of the transcript level of PCNA is exposed in growth factor maturation induced-explants (FT) compared control (no growth factor treated) samples for the group of culture No Se cultured explants with a significative difference between controls and FT-treated samples (Figure 106, $p<0.05$). No significative differences appears between controls and FT-treated of the two other groups using Student T tests for statistical analysis. We cannot state on the selenium or growth factor treatment in our case. However, unpublished data attest that a difference should be present between ITS control and ITS FT-treated. Consequently, further repeats and analyses have to be performed, and maybe required a new primer design.

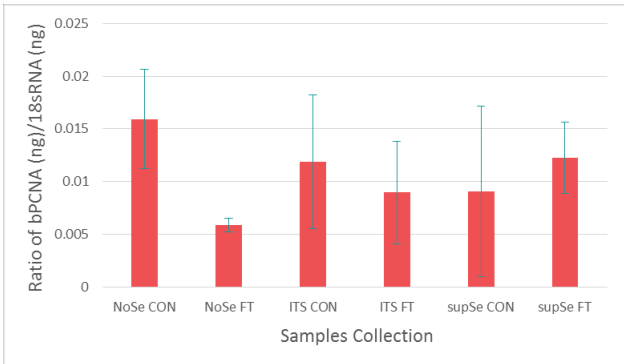

Figure 106: PCNA

21 Synchrotron Fourier Transform InfraRed Microspectroscopy

Classical laboratory techniques (immunofluorescence, histology) have been used to preliminary and qualitatively assess potential variations proteoglycans and collagen contents and distributions in the extracellular matrix. However, selenium being present in microquantity in the organism, changes in matrix can be subtle. Quantitative analysis were then required to quantify these particular changes related to these matrix components; the synchrotron FTIR appears to be an interesting option to finely characterise our model and discriminate both the influence of the selenium and the growth factor stimulation treatment. As mentioned previously, growth factor treatment have an impact of the extracellular matrix by stimulating cells producing a coherent content of the diverse matrix components. Selenium seems to have an influence on this matrix production. When a Se-deficiency is present in the explant culture, a degradation of the collagen content and an overexpression of proteoglycans are observed in control and growth factor treated conditions, respectively. It remains not possible to determinate precisely which is the Se-impact on the quality of the extracellular matrix.

Fresh 7 days-old articular cartilage from the metacarpophanlageal joint is used in this model to evaluate the selenium influence in the protein (collagen and proteoglycan) distribution. The collagen content in native immature explant is relatively low (surface) and inhomogeneous, with a slightly increase with depth and immature articular cartilage possesses an extremely low PGs composition (Figure 107), as previously discussed in the FTIR section. A strict comparison with the literature

is difficult, this one being mainly based on mature or mature degraded (osteoarthritic) AC tissues coming from different joints that those we are using. No exhausitive literature exists on immature cartilage FTIRM or FTIR imaging [22, 209] and it is complicated to compare the tissue and results between each other. Immature articular cartilage is an interesting template upon which biomechanical and biochemical cues act in adapting the tissue to joint-specific functions through induction of morphological, structural and biomolecular heterogeneity [148]. All the necessary components for tissue structure are present but they are extremely disorganised. Consequently, the different tissues used in literature coming from diverse biopsy punch locations and from different species and ages (old bovine or ages not specified) [22, 209, 212 276], it is then no possible to perform a strict and linear comparison with our highly immature 7 days-old tissues that we are using.

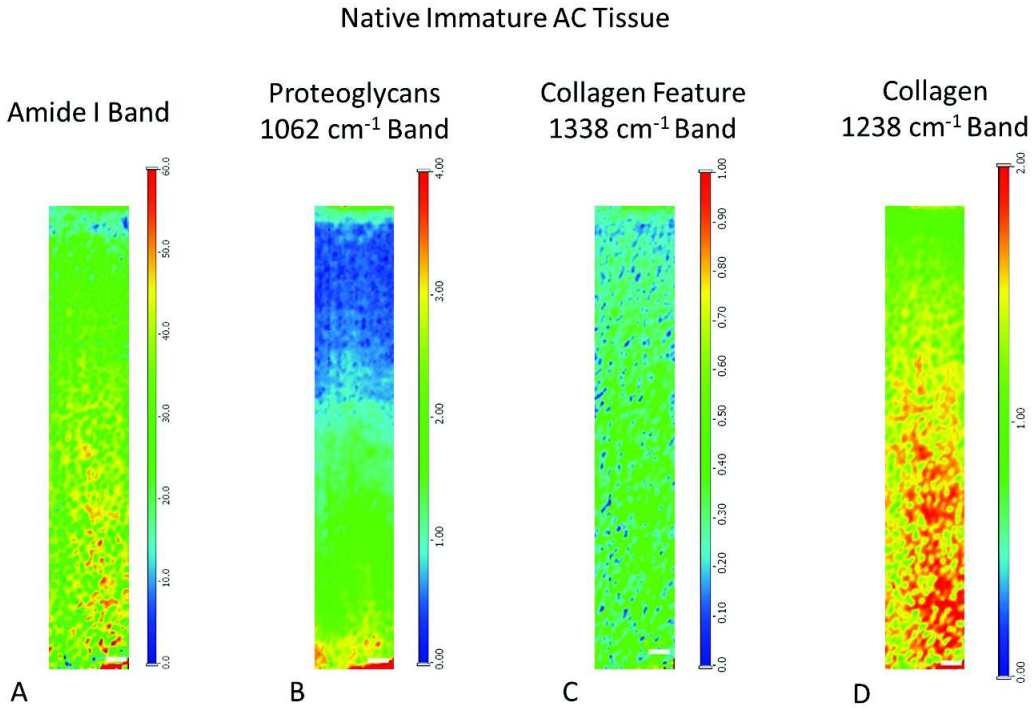

Figure 107: FTIR-Map of native immature explants (no cultured - fresh fixed) for four different indexes with a spatial resolution of 10μm x 10μm and spectral resolution of 6cm^{-1}: Amide I (A) and feature band 1338 cm^{-1} (C) and 1238 cm^{-1} (D) bands for collagen content, 1062 cm^{-1} (B) for proteoglycan content. The white line corresponds to a scalebar of 100 μm.

To determinate the better indexes to semi-quantitatively evaluate the matrix component distributions and concentrations, native and fresh mature AC tissues have been used. . Indeed, mature explant cannot be considered as a reference for our IR indexes so far the technique used for biopsy limits the punch only to the surface and a part of the middle zone; although, it provides a good indication for comparison to other FTIRM studies on mature cartilage. The Amide I , 1338 cm^{-1} and carbohydrate (sugar-ring) (1140-985 cm^{-1}) absorption bands related to collagen and proteoglycan contents appear to be the best indexes to use, being in good concordance with the literature [22, 203, 208, 209, 212, 276, 277] contrary to the rest of the large collection of indexes tested (Table 16). The results for mature explant can be found in Figure 108.

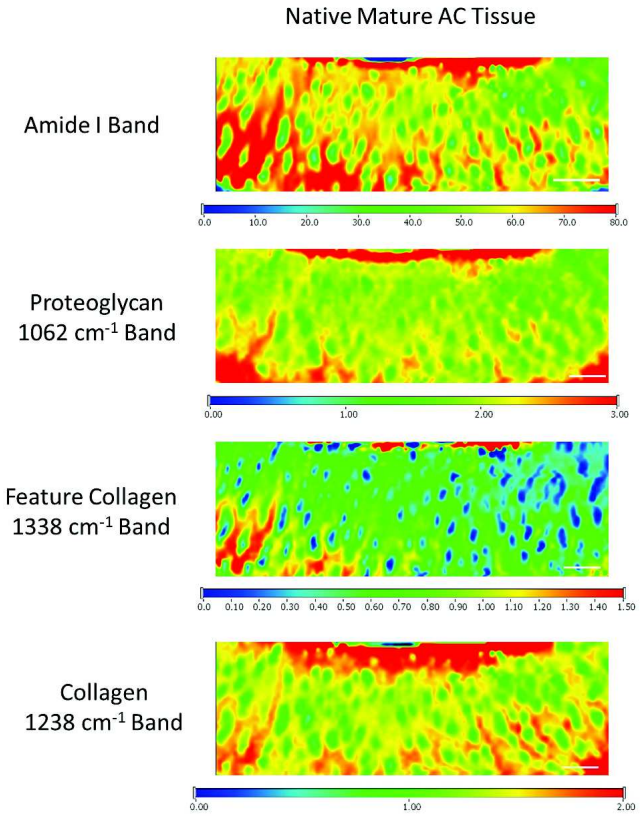

Figure 108: FTIR-Map of native mature (no cultured - fresh fixed) explants for four different indexes with a spatial resolution of 10μm x 10μm and spectral resolution of 6cm^{-1}: Amide I, 1338 cm^{-1} and 1238 cm^{-1} bands for collagen content, 1062 cm^{-1} for proteoglycan content. The white line corresponds to a scalebar of 100 μm.

Interest	Bands - Index	Band Theory	Practical Bands	Baseline superior	Baseline inferior
Proteins-Collagen [203, 207-209, 276]	Amide I	$1590 - 1720\,cm^{-1}$	$1590 - 1720\,cm^{-1}$	$1780 - 1800\,cm^{-1}$	$950 - 1000\,cm^{-1}$
Proteins [207, 210]	Amide II	$1510 - 1595\,cm^{-1}$	$1510 - 1595\,cm^{-1}$	$1780 - 1800\,cm^{-1}$	$950 - 1000\,cm^{-1}$
Proteins [207]	Amide III	$1200 - 1300\,cm^{-1}$	$1200 - 1300\,cm^{-1}$	$1780 - 1800\,cm^{-1}$	$950 - 1000\,cm^{-1}$
Feature Collagen [208, 210]	$1338\,cm^{-1}$	$1338\,cm^{-1}$	$1326 - 1350\,cm^{-1}$	$1476 - 1486\,cm^{-1}$	$1178 - 1186\,cm^{-1}$
Collagen [208, 213, 284]	$1204\,cm^{-1}$	$1204\,cm^{-1}$	$1192 - 1216\,cm^{-1}$	$1295 - 1305\,cm^{-1}$	$1175 - 1185\,cm^{-1}$
Collagen [207, 210]	$1238\,cm^{-1}$	$1238\,cm^{-1}$	$1232 - 1245\,cm^{-1}$	$1295 - 1305\,cm^{-1}$	$1175 - 1185\,cm^{-1}$
Collagen [210]	$1227\,cm^{-1}$	$1227\,cm^{-1}$	$1220 - 1232\,cm^{-1}$	$1295 - 1305\,cm^{-1}$	$1175 - 1185\,cm^{-1}$
Collagen [210, 285]	$1640\,cm^{-1}$	$1640\,cm^{-1}$	$1628 - 1652\,cm^{-1}$	$1780 - 1800\,cm^{-1}$	$950 - 1000\,cm^{-1}$
Collagen [285]	$1660\,cm^{-1}$	$1660\,cm^{-1}$	$1648 - 1672\,cm^{-1}$	$1780 - 1800\,cm^{-1}$	$950 - 1000\,cm^{-1}$
Proteoglycans [203, 207-212, 276]	Carbohydrates - Sugar Ring Band	$985 - 1140\,cm^{-1}$	$985 - 1140\,cm^{-1}$	$1130 - 1140\,cm^{-1}$	$975 - 985\,cm^{-1}$
Proteoglycans [208, 211, 213, 214]	1062 or $1064\,cm^{-1}$	1062 or $1064\,cm^{-1}$	$1050 - 1076\,cm^{-1}$	$1176 - 1186\,cm^{-1}$	$950 - 960\,cm^{-1}$
Proteoglycans [208, 211, 214]	$1374\,cm^{-1}$	$1374\,cm^{-1}$	$1362 - 1386\,cm^{-1}$	$1470 - 1490\,cm^{-1}$	$1317 - 1327\,cm^{-1}$
Proteoglycans	$1245\,cm^{-1}$	$1245\,cm^{-1}$	$1233 - 1257\,cm^{-1}$	$1295 - 1305\,cm^{-1}$	$1175 - 1185\,cm^{-1}$
Proteoglycans	Chondroitin sulfate related band	$1027 - 1016\,cm^{-1}$	$1039 - 1004\,cm^{-1}$	$1176 - 1186\,cm^{-1}$	$950 - 960\,cm^{-1}$
Lipides	$2925\,cm^{-1}$	$2925\,cm^{-1}$	$2913 - 2937\,cm^{-1}$	$3005 - 2995\,cm^{-1}$	$2800 - 2810\,cm^{-1}$
Glycogene	$1025\,cm^{-1}$	$1025\,cm^{-1}$	$1010 - 1040\,cm^{-1}$	$1192 - 1182\,cm^{-1}$	$966 - 957\,cm^{-1}$
OH	$3396\,cm^{-1}$	$3396\,cm^{-1}$	$3384 - 3408\,cm^{-1}$	$3645 - 3655\,cm^{-1}$	$2745 - 2755\,cm^{-1}$
NH	$3300\,cm^{-1}$	$3300\,cm^{-1}$	$3288 - 3312\,cm^{-1}$	$3645 - 3655\,cm^{-1}$	$2745 - 2755\,cm^{-1}$
Hydratation	OH-Band	$3200 - 3600\,cm^{-1}$	$3200 - 3600\,cm^{-1}$	$3645 - 3655\,cm^{-1}$	$2745 - 2755\,cm^{-1}$
Mineralisation [209]	Phosphate	$900 - 1200\,cm^{-1}$	$900 - 1200\,cm^{-1}$	$1780 - 1800\,cm^{-1}$	$950 - 1000\,cm^{-1}$
Phosphate [286]	PO4v3	$1030 - 1070\,cm^{-1}$	$1030 - 1070\,cm^{-1}$	$1176 - 1186\,cm^{-1}$	$950 - 960\,cm^{-1}$
Mineralisation [209]	Carbonates	$850 - 850\,cm^{-1}$	$850 - 850\,cm^{-1}$	$1780 - 1800\,cm^{-1}$	$950 - 1000\,cm^{-1}$

Table 16: Complete table of all the tested Absorbance Bands of molecules of interest & TQ-analyst method parameters

As reported in literature and as observed here, the amide I absorption band cannot strictly used to refer to the collagen content of the AC tissue, this band being impacting by proteoglycans. The 1338 cm^{-1} absorption band is reported to be related to collagen feature in AC tissue. However to confirm the collagen information, another index related to the Amide III (supposed to be less impacting to proteoglycan) has been chosen regarding to the literature [278-279]: the 1238 cm^{-1} absorption band. As observed Figure 109, the collagen distribution pattern observed in the cultured and treated samples for 1338 cm^{-1} is also obtained for 1238 cm^{-1} band. The colors are not the same because the absorbance intensity is differently scaled, it remains that the distribution pattern is highly similar. The No Se content (Figure 109A) presents an alteration of the collagen distribution within the middle and deep zones compared to the native immature tissue (Figure 107). This may be linked to the absence of Se within the medium. The ITS control (Figure 109C) present a reduction of the collagen signal, mainly in the deep zone. This support that the tissue does not reach a stable stage under classical culture conditions and maturation process. On the other hand, growth factor stimulated samples (No Se and ITS FT-treated, Figures 109B&D, respectively) show clearly an induced homogenous collagen distribution within the middle and deep zones. The No Se FT-treated display with decreased collagen content within the superficial zone while PG content appear to be high throughout the middle and deep zones. This confirms that the 1338 cm^{-1} absorption band is a good indicator of the collagen content (concentration and distribution) for this model.

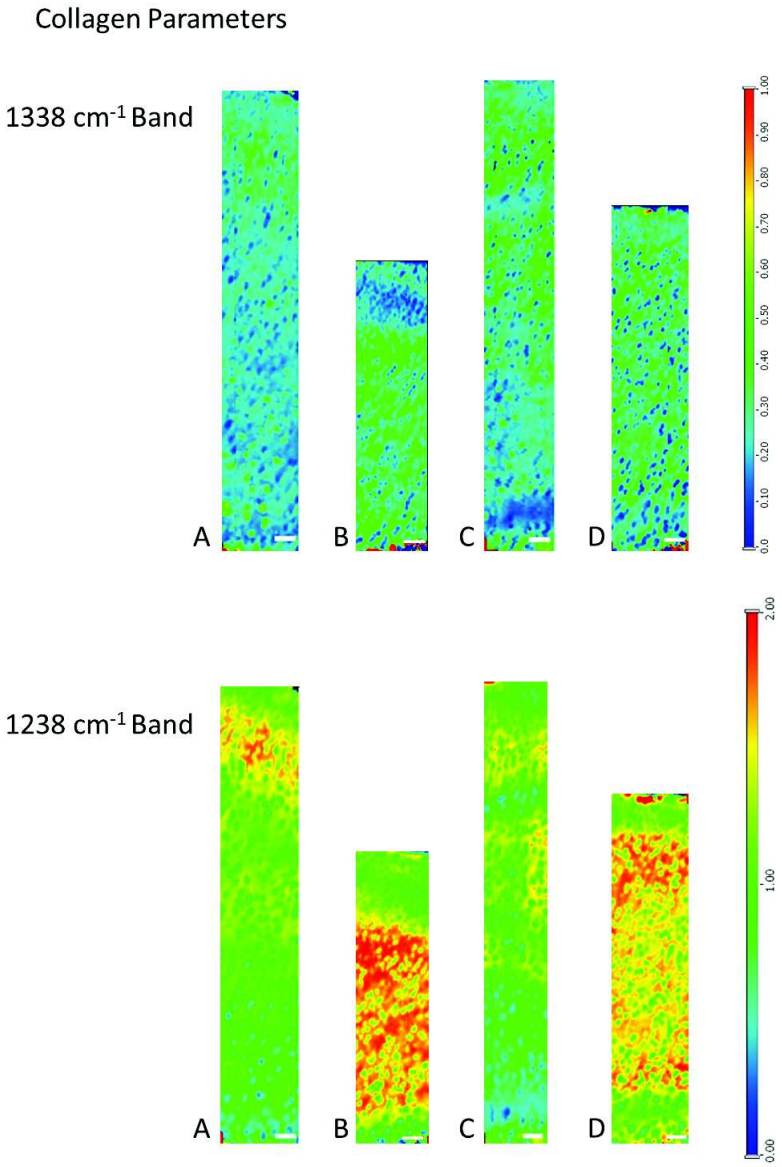

Figure 109: FTIR maps referring to the collagen content and distribution within diverse cultured explants: special collagen feature 1338 cm^{-1} (upper part) and 1238 cm^{-1}(bottom part) absorption bands. Spatial resolution of 10μm x 10μm and spectral resolution of 6 cm^{-1}. A) No Selenium treated explant - No Se control, B) No Selenium and growth factors treated explant -No Se FT-treated, C) Selenium treated explant - ITS control and D) Selenium and growth factor treated explant - ITS FT-treated. The white line corresponds to a scalebar of 100 μm.

Several indexes (ratio of absorption bands, Table 17) related to specific information such as collagen degradation, collagen integrity have been investigated during the univariate analysis of the different samples. Information of the collagen integrity of the extracellular matrix of explant cultured in Se-depleted media could provide good insight of the selenium influence on the quality of the cartilage matrix. Most of the indexes related to collagen integrity or degradation refer to Amide I or Amide II bands which are highly impacted by the proteoglycan content. Consequently, regarding to our model, these indexes cannot be used. The "collagen degradation" index (1238 cm^{-1}/1227 cm^{-1}) could be an interesting solution. The integrating of the frequencies is made over 4x(spectral resolution) area centered to these peaks. Thus, the ratio corresponds to the division of two similar zones. The results cannot then present subtle variations appearing within the extracellular matrix and the result can be

discussed for it non-significance.

Index	Bands - Index	Band Ratio	Practical Bands
Collagen Degration [203, 276]	$\frac{1338\,cm^{-1}}{\text{Amide II}}$	$\frac{1338\,cm^{-1}}{1510-1595\,cm^{-1}}$	$\frac{1326-1350\,cm^{-1}}{1590-1720\,cm^{-1}}$
Collagen Integrity [210, 285]	$\frac{\text{Amide II}}{1338\,cm^{-1}}$	$\frac{1510-1595\,cm^{-1}}{1338\,cm^{-1}}$	$\frac{1590-1720\,cm^{-1}}{1326-1350\,cm^{-1}}$
Collagen Integrity Breakdown [285]	$\frac{1640\,cm^{-1}}{1660\,cm^{-1}}$	$\frac{1640\,cm^{-1}}{1660\,cm^{-1}}$	$\frac{1628-1652\,cm^{-1}}{1648-1672\,cm^{-1}}$
Collagen Degradation [210]	$\frac{1238\,cm^{-1}}{1227\,cm^{-1}}$	$\frac{1238\,cm^{-1}}{1227\,cm^{-1}}$	$\frac{1232-1245\,cm^{-1}}{1220-1232\,cm^{-1}}$
Proteoglycan Content [207-209]	$\frac{985-1140\,cm^{-1}}{\text{Amide I}}$	$\frac{985-1140\,cm^{-1}}{1590-1720\,cm^{-1}}$	$\frac{985-1140\,cm^{-1}}{1590-1720\,cm^{-1}}$
Lipid Content	$\frac{2925\,cm^{-1}}{\text{Amide II}}$	$\frac{2925\,cm^{-1}}{1510-1595\,cm^{-1}}$	$\frac{2913-2937\,cm^{-1}}{1510-1595\,cm^{-1}}$
Glycogene Content	$\frac{1025\,cm^{-1}}{\text{Amide II}}$	$\frac{1025\,cm^{-1}}{1510-1595\,cm^{-1}}$	$\frac{1010-1040\,cm^{-1}}{1510-1595\,cm^{-1}}$

Table 17: Ratio of Absorbance bands related to indexes

The immature articular cartilage is a protein-rich tissue, multiple IR vibrational absorption bands related to the diverse protein characteristics and structures overlapped. Still, it is well-known that the position of the amide I absorption band is sensitive to protein conformation, hence, any shifts or broadening can be attributed to some protein conformational changes in the tissue. Here, the influence and the function of the selenium in this tissue is totally unknown consequently subtle shifts and variations in absorption bandwidth may appear. The spectra presented in Figures 110, 111 and 112 refer to a average of several independent spectra. They have been selected per zone (superficial, middle or deep zones) and per regions (cells or extracellular matrix) and average using the OMNIC statistical spectra tools. This provided a total spectrum corresponding the arithmetic mean of the Y values for each point; all Y values for a data point are added together and the total is then divided by the number of spectra (OMNIC UserGuide). The second derivative are also the average of a collection of spectra twice-derivated to show the change in the rate of change across the spectrum with significatively narrower bands. The second derivative is used here to determinate if any subtle peak location changes appears between the samples. The exact (negative) peak locations in the second derivative are placed at the same (position) peak locations that in the original spectrum. The second derivative spectrum formula is

$$D'(i) = \left(\frac{Y(i-2) - 2 * Y(i) + Y(i+2)}{(X(i-1) - X(i+1)} \right)^2 \tag{23}$$

with $D\prime(i)$ is the second deriv ative at each point$i$, $Y(i)$ is the absorbance at each point i, $X(i)$ is the location of each point i where i is the integer value of the point. (OMNIC Algorithm Guide). The number of spectra used to the average was about 440 spectra for the superficial zone, 500 for the middle zone and 450 for the deep zone and calcified cartilage zone.

The immature articular cartilage is a protein-rich tissue, multiple IR vibrational absorption bands related to the diverse protein characteristics and structures overlapped. Still, it is well-known that the position of the amide I absorption band is sensitive to protein conformation, hence, any shifts or broadening can be attributed to some protein conformational changes in the tissue. Here, the influence and the function of the selenium in this tissue is totally unknown consequently subtle shifts and variations in absorption bandwidth may appear. As seen in Figures 110, 111 and 112 in annexes, no clear trend or differences (differences in spectral features, peak shifts...) can be established from the baseline-corrected or the second derivative spectra. Consequently, we decided to focus on the spatial distribution of selected molecular species. The IR absorption maps were processed on the basis of the selected IR indexes and further compared for the different experimental conditions. The absorption maps present large differences for all the analysed samples, however this can be found in the spectra with the variation of some particular parameters such as bandwidths and peak intensities.

All the spectral analysis presented here is focused on the extracellular matrix due to the interest of the cartilage structuration changes in present or absence of selenium. However, is could also be interesting to analyse the cell metabolism variations in the diverse zones of the different Se-treated explants. Cellular variation is difficult to interpret all cells being in a different stage at the moment of the fixation. Averaging several spectra of different cells in a zones will smoothing all fine molecular structural modifications.

This discrimination was difficult to perform with the maps due to the high interconnection of the molecular vibration bands, and no obvious different in the spectral data, in regard to the time only distribution maps have been analyses in the semi-quantitative way. Consequently to enhance the analysis that has been presented in this thesis, a multivariate analysis such as principal component analyses (PCA) has to be performed. This will permits a precise discrimination of the different trends present in the samples. This is then the following step to finely explore the potential local and subtle variations appearing in the maturated articular cartilage tissue treated with or without selenium.

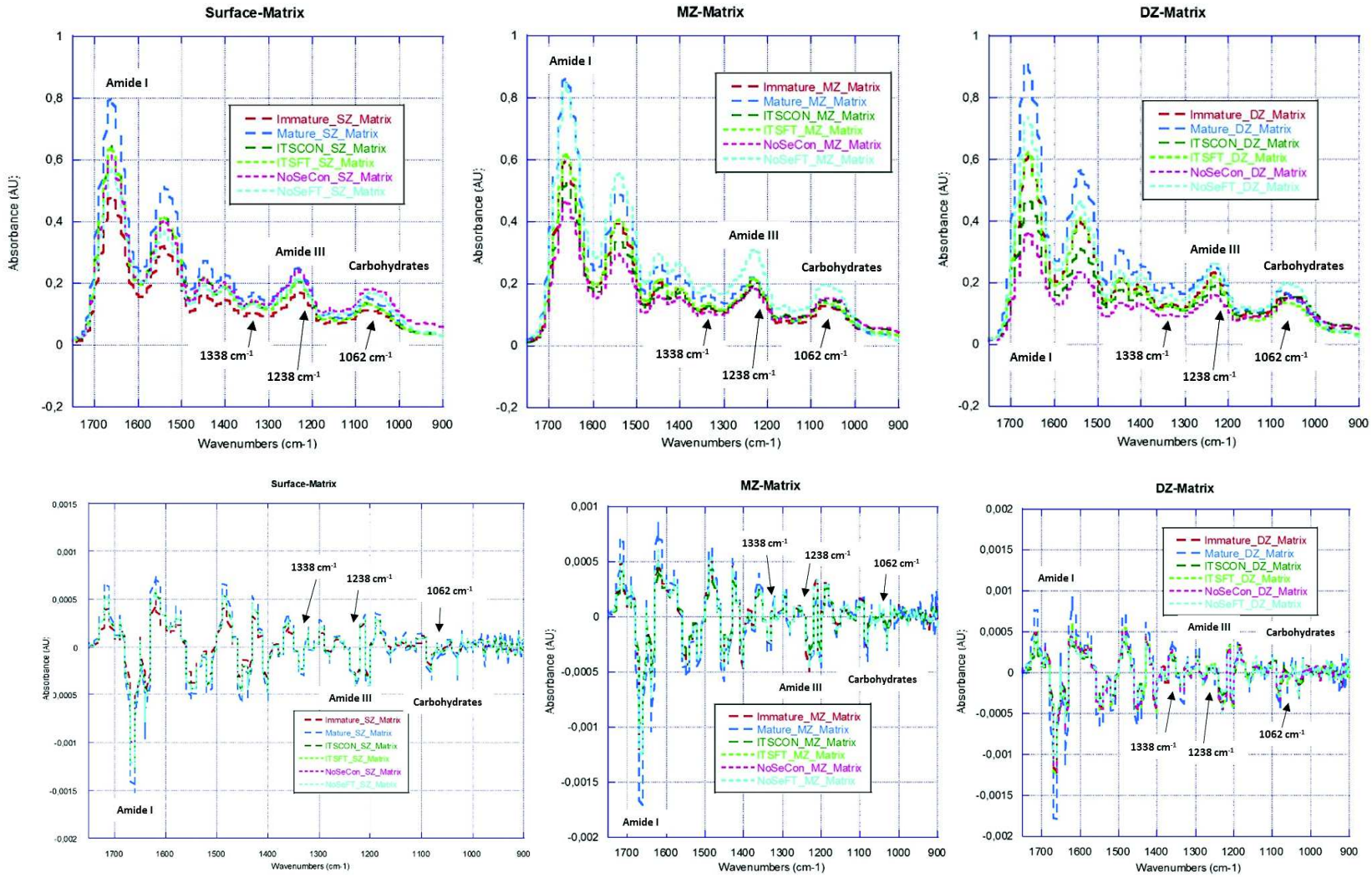

Figure 110: Characteritic FTIR spectrum (upper figure) and second derivative spectrum (botton figure) for the different samples for each tissue regions (left) surface, (middle) middle zone and (right) deep zone. Spatial resolution of $10\,\mu$m x 10μm and spectral resolution of 6 cm^{-1}. (red) Native immature explant (no culture), (pink) No Selenium treated explant - No Se control, (cyan) No Selenium and growth factors treated explant -No Se FT-treated, (green) Selenium treated explant - ITS control, (light green) Selenium and growth factor treated explant - ITS FT-treated and (blue) native mature explant (no culture). Note: Amide I ($1590 - 1720\,\mathrm{cm}^{-1}$), Amide III ($1200 - 1300\,\mathrm{cm}^{-1}$) bands and $1338\,\mathrm{cm}^{-1}$ and $1238\,\mathrm{cm}^{-1}$ peaks referring to collagen, carbohydrate (sugar ring) (1140-985 $\mathrm{c}m^{-1}$) region referring to total proteoglycan content with sulphated proteoglycan peak at 1062 $\mathrm{c}m^{-1}$.

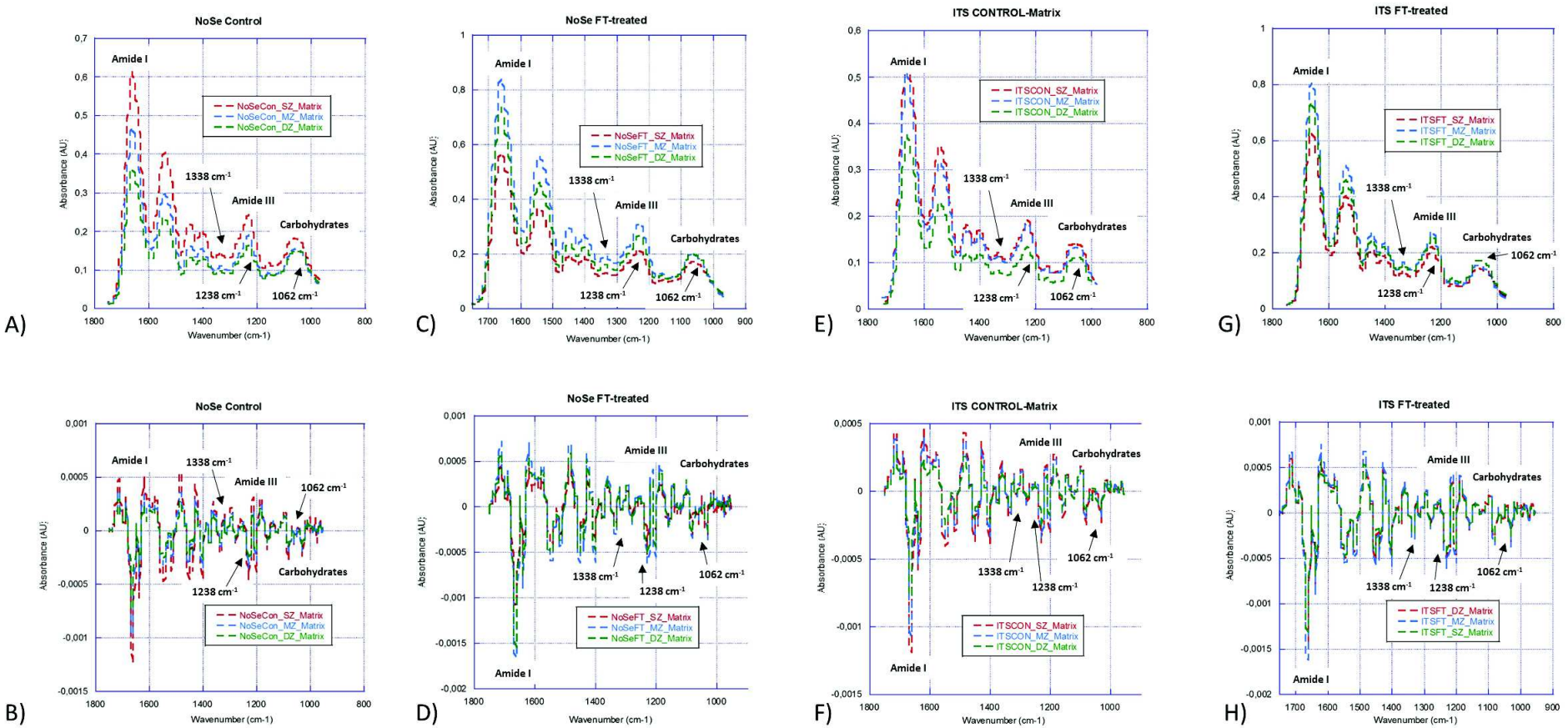

Figure 111: Characteritic FTIR spectrum (A, C, E, G) and second derivative spectrum (B, D, F, H) of the different regions of the tissue for all articular cartilage (AC) samples (From the left to the right: No Se control AC (A, B), No Se FT-treated AC (C, D), ITS control AC (E, F) , ITS FT-treated AC (G, H): (red) surface, (blue) middle zone and (green) deep zone. Spatial resolution of $10\,\mu$m x 10μm and spectral resolution of 6 cm^{-1}. Note: Amide I ($1590 - 1720\,\mathrm{cm}^{-1}$), Amide III ($1200 - 1300\,\mathrm{cm}^{-1}$) bands and $1338\,\mathrm{cm}^{-1}$ and $1238\,\mathrm{cm}^{-1}$ peaks referring to collagen, carbohydrate (sugar ring) (1140-985 cm^{-1}) region referring to total proteoglycan content with sulphated proteoglycan peak at 1062 cm^{-1}.

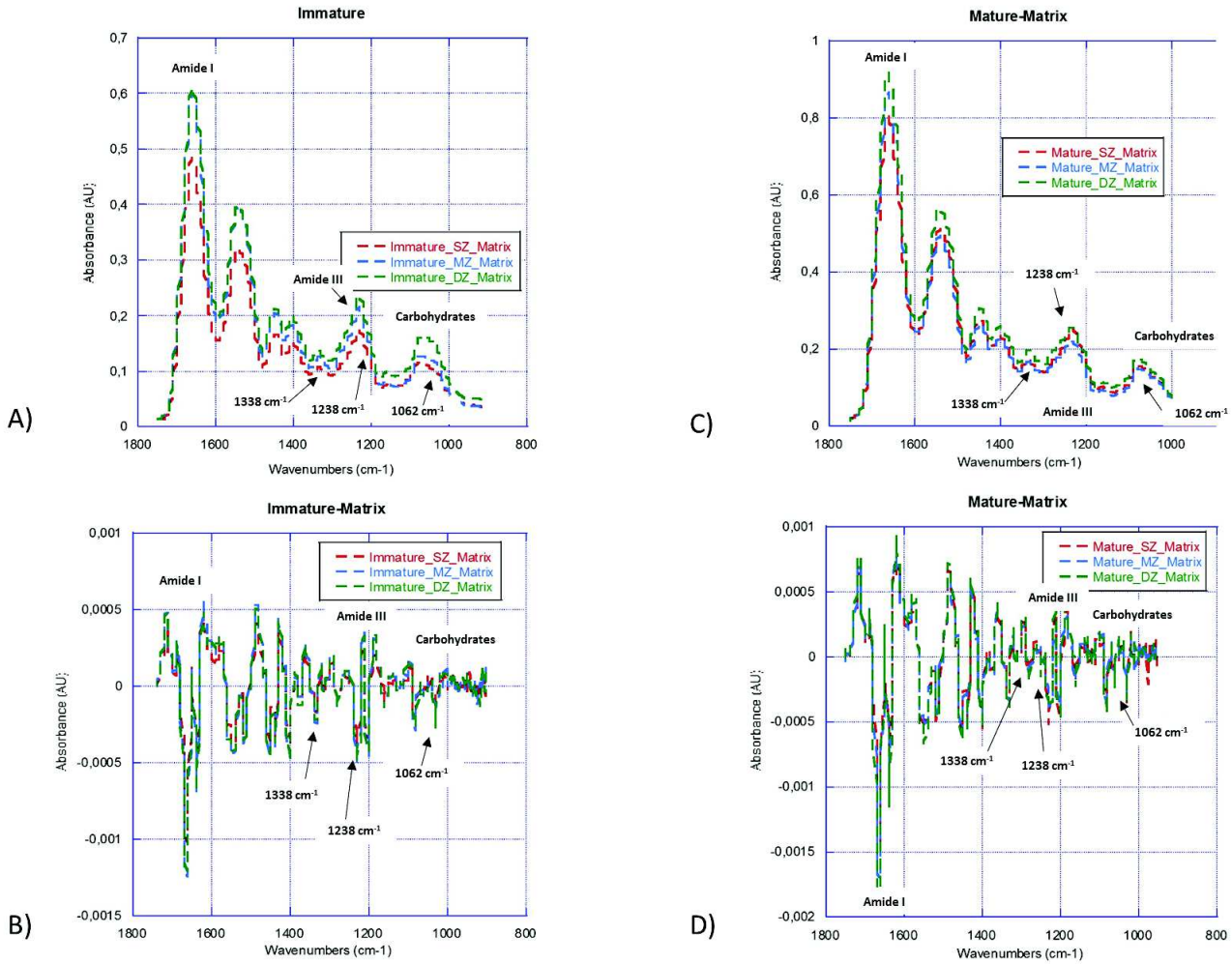

Figure 112: Characteritic FTIR spectrum (A,C) and second derivative spectrum (B,D) of the different regions of (A, B) Native immature explant (no culture) and (C, D) Native mature explant (no culture): (red) surface, (blue) middle zone and (green) deep zone. Spatial resolution of 10 μm x 10μm and spectral resolution of 6 cm^{-1}. Note: Amide I ($1590 - 1720\,\mathrm{cm}^{-1}$), Amide III ($1200 - 1300\,\mathrm{cm}^{-1}$) bands and $1338\,\mathrm{cm}^{-1}$ and $1238\,\mathrm{cm}^{-1}$ peaks referring to collagen, carbohydrate (sugar ring) (1140-985 cm^{-1}) region referring to total proteoglycan content with sulphated proteoglycan peak at 1062 cm^{-1}.

22 Synchrotron Deep UltraViolet Microscopy

The preliminary study need to be complete. The data analysis has been restricted. Further analyses on this data set have to do done. However, here is presented the preliminary results which show a huge potential of this technique on these AC samples and provide a trend on the selenium influence in the sample collagen variations. Being a test, the fundamental data are missing. Further repeats would be necessary to complete this study.

Spectral deconvolutions performed by MathLab routine (DISCO). This routine corrects the baseline "offset" (the minimum is set at zero), then each spectrum is decomposed using the same parameters (4 component positions: Tryptophan (335-355 nm), Tyrosine (301-311 nm), Collagene (398-410nm) and NaDH provided by an experimental spectrum). The fit is then calculated using an equation which gave different parameter (a1, a2, a3, a4, b1, b2, b3, b4, c1, c2, c3) values need to calculate the peak integrals (area) of the regions of interest. The equation of the fit is:

ftype = ('a1*exp(-((x-b1)/c1).*((x-b1)/c1))+ a2*exp(-((x-b2)/c2).*((x-b2)/c2)) + a3*exp(-((x-b3)/c3).*((x-b3)/c3)) + a4*(0.3208*exp(-((x-430.9+b4)/10.9).*((x-430.9+b4)/10.9)) + 0.6512*exp(-((x-453.8+b4)/24.03).*((x-453.8+b4)/24.03)) + 0.3282*exp(-((x-420.6+b4)/5.586).*((x-420.6+b4)/5.586)) + 0.536*exp(-((x-485.8+b4)/39.65).*((x-485.8+b4)/39.65)) + 0.3142*exp(-((x-415+b4)/2.344).*((x-415+b4)/2.344)) + 0.156*exp(-((x-544.1+b4)/72.97).*((x-544.1+b4)/72.97)))')

with options

option = fitoptions(ftype);

option.Lower = [0,0,0,0,335,301,398,-10,0,0,0]; % lower values option.Upper = [10000,10000,10000,100,355,311,410,10
% upper values option.Exclude

= outliers; %outliers option.StartPoint = [0,0,0,0,345,306,405,0,10,10,10]; % init values.

Here, it is possible to see the expression of average fluorescence spectrum for each sample type per zones and according different regions (cells or matrix) (Figures 114, 113 and 115). The variations of the peaks related to tyrosine, Tryptophan and collagen between the different sample are subtle, ratios of peak area are then required to establish trend of collagen content changes (section 17.5).

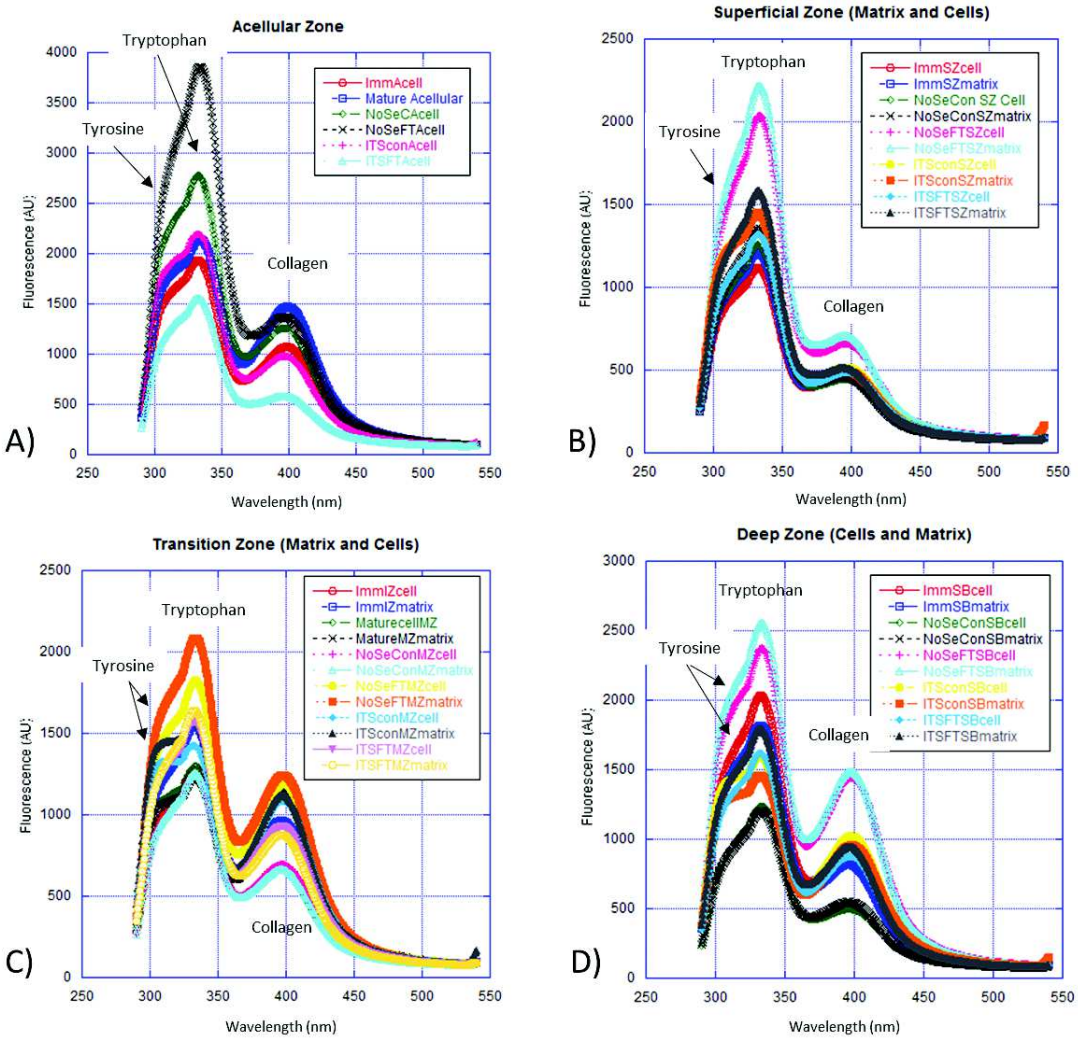

Figure 113: Fluorescence spectra per zones of all samples (native immature and mature references and cultured explants): A) Acellular Zone, B) Superficial Zone, C) Middle Zone, D) Deep Zone and Subchrondral Bone boundary. Note: Tyrosine ($307-322\,\mathrm{nm}$), Tryptophan ($327-353\,\mathrm{nm}$) and Collagen (412-436 nm). Signal coming from cells and matrix have been separated.

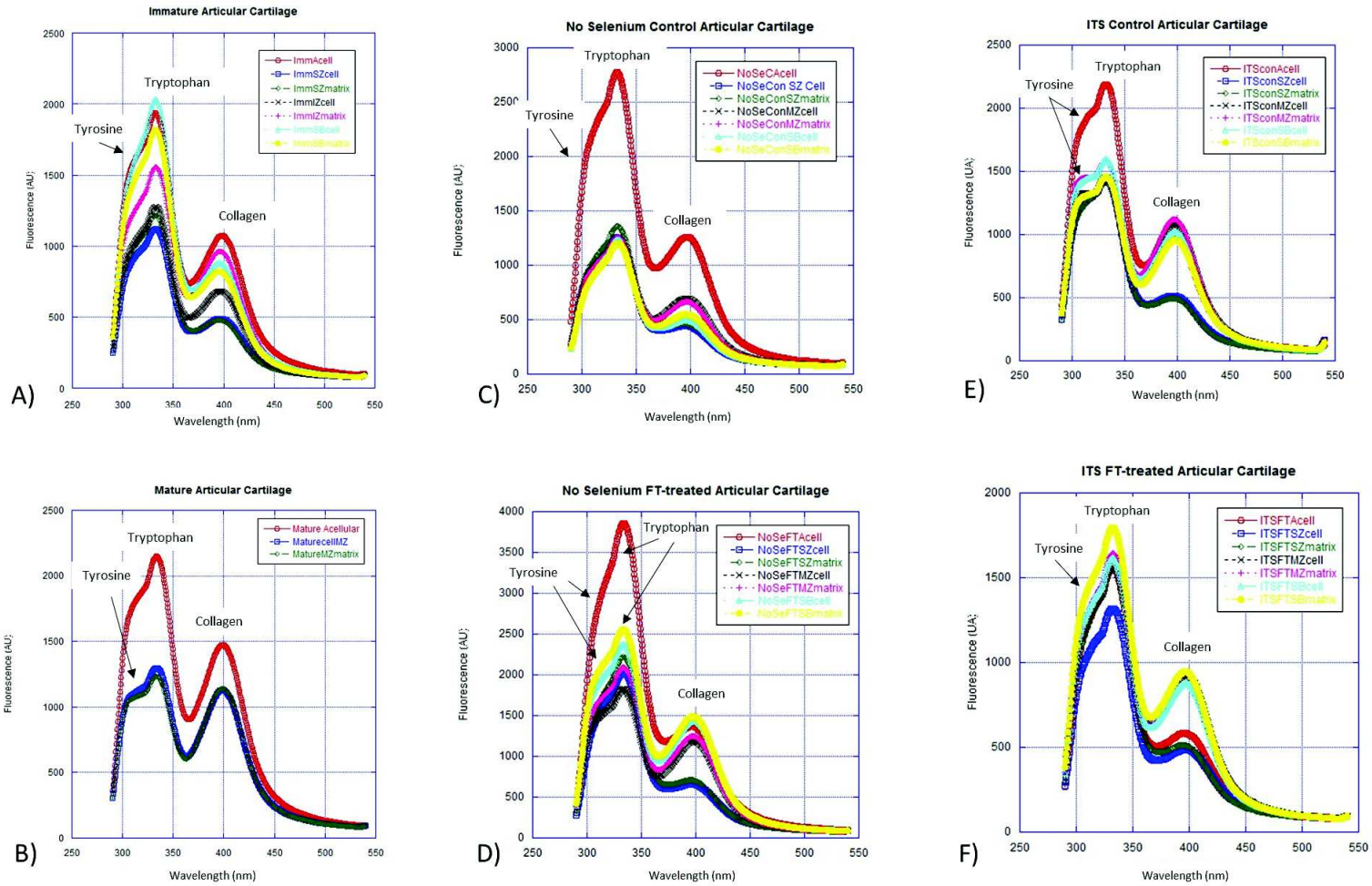

Figure 114: Fluorescence spectra for the different samples A) Native immature explant (no culture), B) native mature explant (no culture), C) No Selenium treated explant - No Se control, D) No Selenium and growth factors treated explant -No Se FT-treated, E) Selenium treated explant - ITS control, F) Selenium and growth factor treated explant - ITS FT-treated and (blue) . Note: Tyrosine ($307-322\,\mathrm{nm}$), Tryptophan ($327-353\,\mathrm{nm}$) and Collagen (412-436 nm). Signal coming from cells and matrix have been separated.

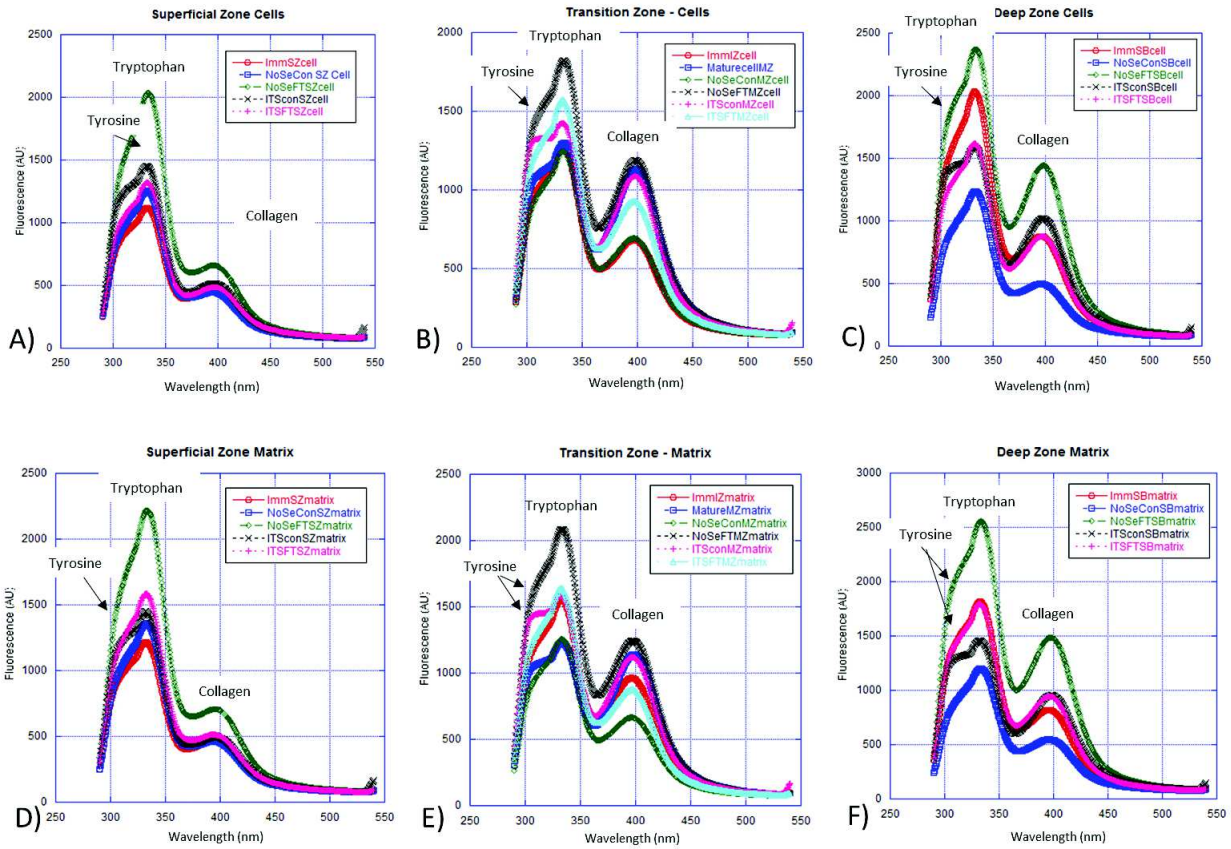

Figure 115: Fluorescence spectra per zones of all samples (native immature and mature references and cultured explants) where signal coming from cells and matrix have been separated: A) Superficial Zone for Cells, B) Middle Zone for Cells, C) Deep Zone and Subchrondral Bone boundaryfor Cells, D) Superficial Zone for Matrix, E) Middle Zone for Matrix, F) Deep Zone and Subchrondral Bone boundary for Matrix. Note: Tyrosine ($307-322\,\text{nm}$), Tryptophan ($327-353\,\text{nm}$) and Collagen (412-436 nm).

Concerning the acellular zone, it is interesting to observe that cultured explants present a decrease of the ratio Col/Trp compared to the native (no culture tissue). In native condition, this ratio is inferior for immature samples than for mature samples. Surprisingly, the opposite trend appears, maturated (growth factor FT-treated) samples have a Col/Trp ratio lower than the control conditions (without growth factors). For the ratio Tyr/Trp, the values are relatively constant except for the maturated samples NoSe FT-treated and ITS FT-treated (growth factor "FT" treatment) which are reduced by 32% and 12% respectively compared to the others.

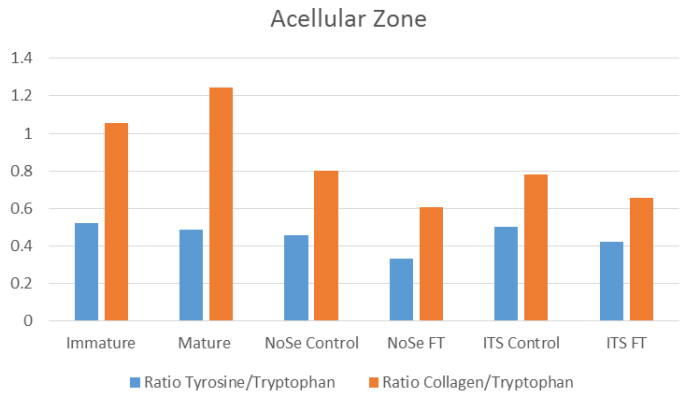

Figure 116: UV emission peak intensity ratios in native (Immature and Mature, no culture) and cultured articular cartilage explants (No Se Control, No Se FT-treated, ITS Control, ITS FT-treated) in the laminae acellular zone. Blue stands for the ratio Tyrosine/Tryptophan and orange for ratio Collagen/Tryptophan.

Full field imaging has been performed using TELEMOS microscope. bandpass filters Tyrosine ($307-322\,\mathrm{nm}$), Tryptophan ($327-353\,\mathrm{nm}$) and Collagen (412-438 nm) (excitation at 290 nm). The collagen signal is originating from the crosslinks between the amino-acids. TELEMOS images corresponding to the autofluorescence signal of the different treatments have been reconstructed with MathLab routine (DISCO). For each mapping, the ratios Tyrosine/Tryptophan (Tyr/Trp) and Collagen/Tryptophan (Col/Trp) were calculated. ImageJ treatment have been made to establish the ratio of the images filtered for collagen normalised by those filtered for Tryptophan. The brightness had been adjusted to be coherent for all samples. The Tryptophan reveals the protein distribution in tissues [255] and is used here to normalize the signal of other more specific proteins such as collagen. DUV fluorescence imaging provides interesting information concerning the collagen repartition in tissues. The differences in signal intensities between the two channels (red filters at 327–353 nm and green at 412–438 nm) allow the detection of collagen abundance. The images relative to the ratio Col/Trp are difficult to analyse. No major difference appears and the "vignet" problem has to be solved (Figure 118). Further image treatments have to be performed to extract information.

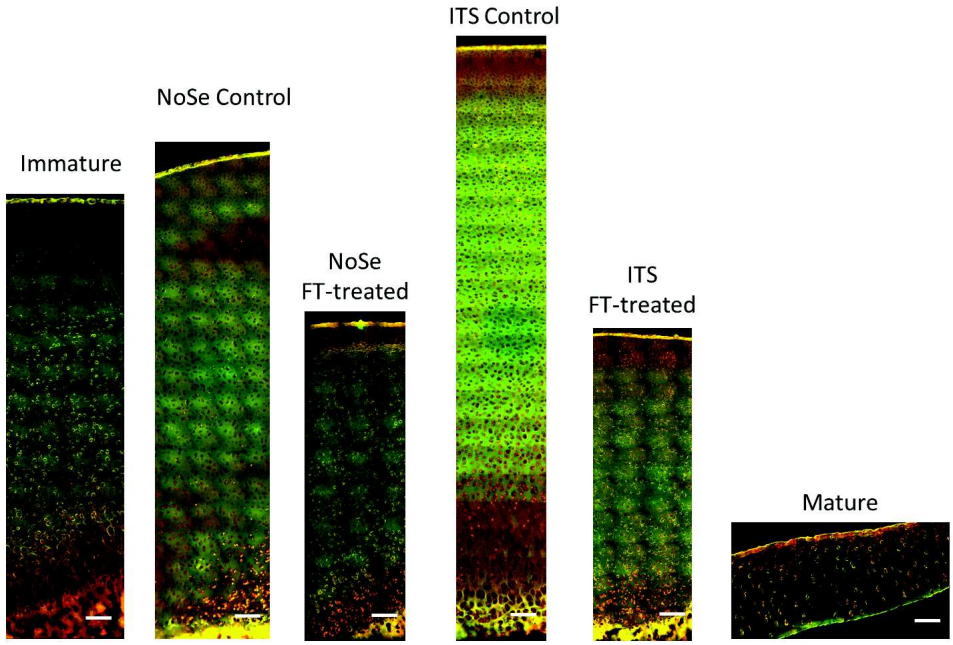

Figure 117: Merge of DUV fluorescence image corresponding to the ratio (Col/Trp) between the image related to the collagen (green) bandpass filter (412-438 nm) and the image of the Tryptophan ($327 - 353\,\text{nm}$) (red). White scalebar: 170 μm.

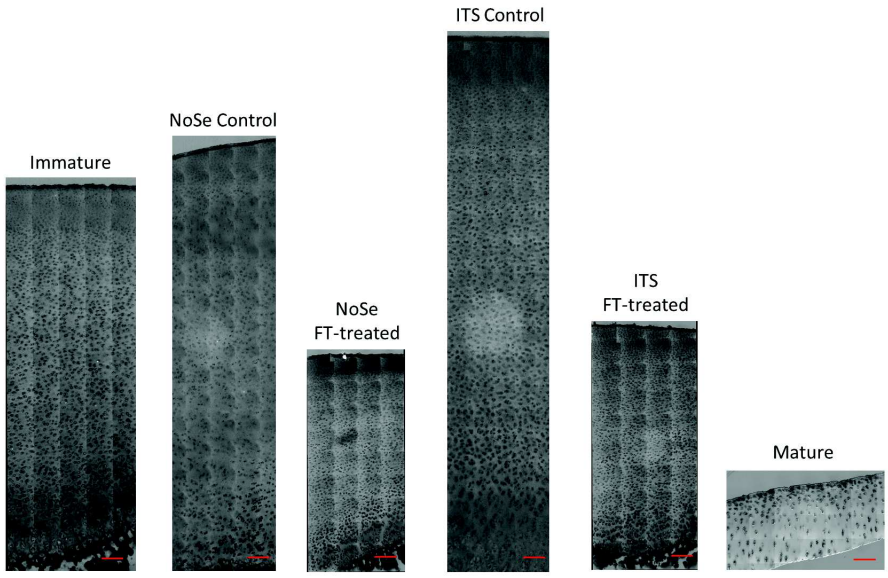

Figure 118: DUV fluorescence image corresponding to the ratio (Col/Trp) between the image related to the collagen filter (412-438 nm) and the image of the Tryptophan ($327 - 353\,\text{nm}$). Red scalebar: 170 μm.

Part X
References

[1] X.L. Lu and V.C. Mow. Biomechanics of Articular Cartilage and Determination of Material Properties. Official Journal of the American College of Sports Medicine. 2008. 193-199131

[2] R. Stone. A Medical Mystery in Middle China. Science. 2009 Vol. 324, Issue 5933, pp. 1378-1381

[3] J. Tan, W. Zhu, W. Wang, R. Li, S. Hou, D. Wang, L. Yang. Selenium in soil and endemic diseases in China. Science of The Total Environment. Volume 284, Issues 1–3, 4 February 2002, Pages 227–235

[4] F. Fordyce. in Essentials of Medical Geology. (ed. Selinus, Olle.) Chapter 16 Selenium, 375–416. Springer Netherlands (2013)

[5] A. Zhang, J.L Cao, B. Yang, JH Chen, ZT Zhang, SY Li, Q. Fu, C.E. Hugnes, and B. Caterson. Effects of mycotoxin moniliformin and selenium deficiency on human articular cartilage metabolism and their potential relationships to the pathogenesis of Kashin-Beck disease have been demonstrated. Biomedicine & Biotechnology. 2010. 11(3):200-208.

[6] X. Wang, S. Wang, S. He, F. Zhang, W. Tan, Y. Lei, H. Yu, Z. Li, Y. Ning, Y. Xiang, X. Guo. Comparing gene expression profiles of Kashin-Beck and Keshan diseases occurring within the same endemic areas of China. Sci China Life Sci. 2013 Sep;56(9):797-803.

[7] YF. Yao, FX Pei, XB Li, J Yang, B Shen, ZK Zhou, L Li, PD Kang. Preventive effects of supplemental selenium and selenium plus iodine on bone and cartilage development in rats fed with diet from Kashin-Beck Disease endemic area. Biol Trace Elem Res. 2012 May;146(2):199-206.

[8] YM. Xiong, XY Mo, XZ Zou, RX Song, WY Sun, W Lu, Q Chen, YX Yu, WJ Zang. Association study between polymorphisms in selenoprotein genes and susceptibility to Kashin-Beck disease. Osteoarthritis Cartilage. 2010 Jun;18(6):817-24.

[9] JM. Jordan. Ongoing Assessment of Osteoarthritis in African Americans and Caucasians in North Carolina: The Johnston County Osteoarthritis Project. Trans Am Clin Climatol Assoc. 2015;126:77-86.

[10] JH Chen, S.Xue, S. Li, ZL Wang, H. Yang, W. Wang, D. Song, X. Zhou, C. Chen. Oxidant Damage in Kashin-Beck Disease and a Rat Kashin-Beck Disease Model by Employing T-2 Toxin Treatment Under Selenium Deficient Conditions. (2012) Journal of Orthopaedic Research

[11] J. Yan, Y. Zheng, Z. Min, Q. Ning, S. Lu. Selenium effect on selenoprotein transcriptome in chondrocytes, Biometals (2013) 26:285–296

[12] M. Roman, P. Jitarub and C. Barbante. Selenium biochemistry and its role for human health. Metallomics. 2014 Jan;6(1):25-54

[13] T. Masahiko, S. Damle, M. Penmatsa, P. West, X. Yang, M. Bostrom, C. Hidaka, M. Yamauchi, N. Pleshko. Temporal changes in collagen cross-links in spontaneous articular cartilage repair. Cartilage. 2012 Jul;3(3):278-287.

[14] A. Hanifi, JB. Richardson, JH. Kuiper, S. Roberts, N. Pleshko. Clinical outcome of autologous chondrocyte implantation is correlated with infrared spectroscopic imaging-derived parameters. Osteoarthritis Cartilage. 2012 Sep;20(9):988-96.

[15] JA. Buckwalter, HJ. Mankin, AJ. Grodzinsky. Articular Cartilage and Osteoarthritis. AAOS Instructional course lectures2005;54:665-480 - Chapter45

[16] IM. Khan, SL. Evans, RD. Young, EJ. Blain, AJ. Quantock, N. Avery. FGF2 and TGFβ1 induce precocious maturation of articular cartilage. Arthritis Rheum 2011;63(11):3417e27.

[17] IM. Khan, L. Francis, PS. Theobald, S. Perni, RD. Young, P. Prokopovich, RS. Conlan, CW. Archer. *In vitro* growth factor-induced bio engineering of mature articular cartilage. Biomaterials 34, 1478-1487 (2013). doi:10.1016/j.biomaterials.2012.09.076

[18] DL. Hatfield, MJ. Berry, N.Vadim. Selenium: Its Molecular Biology and Role in Human Health -Springer -3rd edition (2012)

[19] Mansour. Biomechanical of Cartilage - Chapter 5 - 66-75 from Biomechanics of Cartilage by Eric Urbina Santibañez

[20] J. Martel-Pelletier, C. Boileau, JP. Pelletien, PJ. Roughley. Cartilage in normal and osteoarthritis conditions (Ch°11) Best Pract Res Clin Rheumatol. 2008 Apr;22(2):351-84.

[21] JA. Buckwalter, HJ. Mankin, AJ. Grodzinsky. Articular Cartilage and Osteoarthritis. AAOS Instructional course lectures2005;54:665-480 - Chapter45

[22] S. Saarakkala, L. Rieppo, J. Rieppo, and J.S. Jurvelin. Fourier Transform Infrared (FTIR) Microspectroscopy of Immature, Mature and Degenerated Articular Cartilage. Microscopy: Science, Technology, Applications and Education A. Méndez-Vilas and J. Díaz (Eds.)

[23] EB Hunziker, TM Quinn, HJ Häuselman. Quantitative structural organization of normal adult articular cartilage. Osteoarthritis and cartilage. 2002Jul;10(7):564-572

[24] JJ Sopena-Juncosa, J.M. Carrillo-Poveda, M. Rubio-Zaragoza, J. I. Redondo-García, I. Serra-Aguado, I. Soleri-Canet. Estructura y función del cartílago articular. Portada: Armas Frente a la Patología Articular. (2000)

[25] NS Landínez-Parra, DA. Garzón-Alvarado and JC Vanegas-Acosta. Chapiter 11 Mechanical Behavior of Articular Cartilage 2012, licensee InTech

[26] GM LEE and RF. Loeser. Interation of the chondrocyte with its pericellular matrix.Cells and Materials, Volume 8, 1998 (Pages 135-149)

[27] AD Pearle, RF Warren, SA Rodeo. Basic science of articular cartilage and osteoarthritis. Clin Sports Med. 2005 Jan;24(1):1-12.

[28] VC Mow, A Ratcliffe, AR Poole. Cartilage and diarthrodial joints as paradigms for hierarchical materials and structures. Biomaterials. 1992;13(2):67-97.

[29] A. Benninghoff (1925). Form un Bau der Gelenkknorpel in ihren Beziehungen zur Funktion. II. Der Aufbau des Gelenkknorpels in seinen Bezeihungen zur Funktion. Zeit Zellforsch und Mikroskop Anat 2 : 783-862.

[30] Articular Cartilage Repair. Am J Sports Med March 1998 26 309-324

[31] EB Hunziker, M Michel, D Studer. Ultrastructure of adult human articular matrix after cryotechnical processing. Microsc Res Tech (1997) 37 : 271-284 & EB Hunziker, J Wagner, D Studer. Vitified articular cartilage reveals novel ultrastructural features respecting extracellular matrix architecture. Histochem Cell Biol (1996) 106 : 375-382

[32] AR Poole, T Kojima, T Yasuda, F Mwale, M Kobayashi, S Laverty. Composition and structure of articular cartilage: a template for tissue repair. Clin Orthop Relat Res. 2001 Oct;(391 Suppl):S26-33.

[33] I. Onyekwelu, MB. Goldring, and C.Hidaka. Chondrogenesis, Joint Formation, and Articular Cartilage Regeneration. Journal of Cellular Biochemistry 107(3):383–392 (2009)

[34] K A Staines, A S Pollard, I M McGonnell, C Farquharson and A A Pitsillides. Cartilage to bone transition in heathly and disease. Journal of endocrinology (2013) 219, R1–R12

[35] F. Guilak and VC Mow. The mechanical environment of the chondrocyte: a biphasic finite element model of cell-matrix interactions in articular cartilage. J Biomech. 2000 Dec;33(12):1663-73.

[36] VC. Mow and XE Guo. Mechano-Electrochemical Properties Of Articular Cartilage: Their Inhomogeneities and Anisotropies. Annu.Rev.Biomed.Eng.2002.4:175-209

[37] SM. McNary, KA Athanasiou AH. Reddi. Engineering Lubrification in Articular Cartilage - Tissue engineering part B Vol 18 Nb 2 2012

[38] GA. Ateshian. The Role of Interstitial Fluid Pressurization in Articular Cartilage Lubrication. J Biomech. 2009 Jun 19; 42(9): 1163–1176.

[39] LG Alexopoulos, GM Williams, ML Upton, LA Setton, F Guilak. Osteoarthritic changes in the biphasic mechanical properties of the chondrocyte pericellular matrix in articular cartilage. J Biomech. 2005 Mar;38(3):509-17.

[40] M. Wong and DR. Carter. Articular cartilage functional histomorphology and mechanobiology: a research perspective. Bone. 2003 Jul;33(1):1-13.

[41] J. Katta, Z. Jin, E. Ingham and J.Fisher. Biotribology of articular cartilage - A review of the recent advances - Medical Engineering & Physics Volume 30, Issue 10, December 2008, Pages 1349–1363

[42] C. Lee, S. Grad, M. Winner and M.Alini. The influence of mechanical stimuli on Articular Cartilage tissue Engineering - Chapiter 1. Topics in Tissue engineering , Vol 2, 2006

[43] J. Sanchez-Adams, HA. Leddy, AL. McNulty, CJ. O'Conor, F. Guilak. The mechanobiology of Articular Cartilage: bearing the burden of Osteoarthritis. Curr Rheumatol Rep. 2014 Oct;16(10):451

[44] PA Brama, JM TeKoppele, RA Bank, A Barneveld, PR van Weeren. Development of biochemical heterogeneity of articular cartilage: influences of age and exercise. Equine Vet.J. 2002;34:265 269.

[45] TJ Klein, M Chaudhry, WC Bae, RL Sah. Depth dependent biomechanical and biochemical properties of fetal, newborn, and tissue engineered articular cartilage. J.Biomech. 2007;40:182 190.

[46] P Julkunen, T Harjula, J Iivarinen, J Marjanen, K Seppänen, T Närhi, J Arokoski, MJ Lammi, PA Brama, JS Jurvelin, HJ Helminen. Biomechanical, biochemical and structural correlations in

immature and mature rabbit articular cartilage.Osteoarthritis Cartilage. 2009 Dec;17(12):1628-38

[47] EB Hunziker, E Kapfinger, J Geiss. The structural architecture of adult mammalian articular cartilage evolves by a synchronized process of tissue resorption and neoformation during postnatal development. Osteoarthritis Cartilage. 2007 Apr;15(4):403-13.

[48] J. Rieppo, MM Hyttinen, E Halmesmaki, H Ruotsalainen, A Vasara, I Kiviranta, JS Jurvelin, HJ Helminen. Changes in spatial collagen content and collagen network architecture in porcine articular cartilage during growth and maturation. Osteoarthritis Cartilage. 2009 Apr;17(4):448-55.

[49] HJ Helminen, MM Hyttinen, MJ Lammi, JP Arokoski, T Lapvetelainen, J Jurvelin, I Kiviranta, MI Tammi. Regular joint loading in youth assists in the establishment and strengthening of the collagen network of articular cartilage and contributes to the prevention of osteoarthrosis later in life: a hypothesis. J Bone Miner Metab. 2000;18(5):245-57.

[50] Stevens -Mowe. Histologies humaine. Chapitre 4

[51] M. Pacifici, E. Koyama, Y. Shibukawa, C. Wu, Y. Tamamura, M. Enomoto-Iwamoto, M. Iwamoto. Cellular and Molecular Mechanisms of Synovial Joint and Articular Cartilage Formation - Ann N Y Acad Sci. 2006 Apr;1068:74-86.

[52] AJ. Martin & JA. Buckwalter. Aging, articular cartilage chondrocyte senescence and osteoarthritis. Biogerontology. 2002;3(5):257-64.

[53] A. Woolf and B. Pfleger. Burden of major musculoskeletal conditions. Bull World Health Organ. 2003;81(9):646-56

[54] EV. Tchetina. Developmental Mechanisms in Articular Cartilage Degradation in Osteoarthritis. Arthritis Volume 2011 (2011), Article ID 683970, 16 pages

[55] N. Bomer, W. den Hollander, YF. Ramos, SD. Bos, R. van der Breggen, N. Lakenberg, BA. Pepers, AE. van Eeden, A. Darvishan, EW. Tobi, BJ. Duijnisveld, EB van den Akker, BT. Heijmans,WM van Roon-Mom , FJ Verbeek, GJ van Osch, RG Nelissen, PE Slagboom, I Meulenbelt. Underlying molecular mechanisms of DIO2 susceptibility in symptomatic osteoarthritis.Ann Rheum Dis. 2015 Aug;74(8):1571-9.annrheumdis-2013-204739

[56] S. Saarakkala, P. Julkunen, P. Kiviranta, J. Makitalo, JS. Jurvelin, RK. Korhonen. Depth wise progression of osteoarthritis in human articular cartilage: investigation of composition, structure and biomechanics. Osteoarthritis Cartilage. 2010 Jan;18(1):73-81.

[57] JA. Buckwalter and HJ. Mankin. Articular Cartilage. Part II: Degeneration and Osteoarthrosis, Repair, Regeneration, and Transplantation. J.Bone Joint Surg.Am. 1997;79:612 632 and Instr Course Lect. 1998;47:487-504.

[58] HE. Panula, MM. Hyttinen, JP. Arokoski, TK. Langsjo, A. Pelttari, I. Kiviranta, HJ. Helminen. Articular cartilage superficial zone collagen birefringence reduced and cartilage thickness increased before surface fibrillation in experimental osteoarthritis. Ann Rheum Dis. 1998 Apr;57(4):237-45.

[59] S. Saarakkala, MS. Laasanen, JS. Jurvelin, K. Torronen, MJ. Lammi, R. Lappalainen. Ultrasound indentation of normal and spontaneously degenerated bovine articular cartilage. Osteoarthritis Cartilage. 2003 Sep;11(9):697-705.

[60] CD. Thomson, "Selenium", in Encyclopedia of Human Nutrition 3rd Edition, LH. Allen, A. Prentice, B. Cabarellero, Eds. (Academic Press) 186-192 (2013). doi:10.1016/B978-0-12-375083-9.00248-8

[61] LH. Winkel, CA. Johnson, M. Lenz, T. Grundl, OX. Leupin, M. Amini, L. Charlet. Environmental selenium research: from microscopic processes to global understanding. Environ Sci Technol. 2012 Jan 17;46(2):571-9.

[62] A. Fernández-Martínez and L. Charlet. Selenium environmental cycling and bioavailability: a structural chemist point of view. Rev Environ Sci Biotechnol (2009) 8:81–110 DOI 10.1007/s11157-009-9145-3

[63] ZJ. Wang, YX. Gao Biogeochemical cycling of selenium in Chinese environments. Appl Geochem (2001) 16:1345–1351

[64] KS. Dhillon, SK. Dhillon Distribution and management of seleniferous soils. In: Sparks D (ed) Advances in agronomy, 1st edn. Elsevier, Amsterdam, (2003) pp 119–184

[65] F. Seby, MP. Gautier, G. Lespes, M. AstrucSelenium speciation in soils after alkaline extraction. Sci Total Environ (1997) 207:81–90

[66] Presser TS The Kesterson effect. Environ Manage (1994) 18:437–454

[67] M. Navarro-Alarcón, MC. López-Martínez. Essentiality of selenium in the human body: relationship with different diseases. Sci Total Environ. 2000 Apr 17;249(1-3):347-71.

[68] PM. Haygarth. Global importance and global cycling of selenium. In: FrankenbergerWT Jr, Benson S (eds) Selenium in the environment. Marcel Dekker, Inc.,HongKong, (1994) pp 1–28

[69] S.J. Fairweather-Tait, Y. Bao, MR. Broadley, R. Collings, D. Ford, JE. Hesketh, R. Hurst. Selenium in Human Health and Disease. Antioxid. Redox Signal. 14, 1337-1383 (2011). doi:10.1089/ars.2010.3275

[70] M.Iwaoka, R. Ooka, T. Nakazato, S. Yoshida, S. Oishi. Synthesis of selenocysteine and selenomethionine derivatives from sulfur-containing amino acids. Chem Biodivers. 2008 Mar;5(3):359-74. doi: 10.1002/cbdv.200890037.

[71] C. Jacob, GI. Giles, NM. Giles, H. Sies.Sulfur and selenium: the role of oxidation state in protein structure and function. Angew Chem Int Ed Engl. 2003 Oct 13;42(39):4742-58.

[72] EAH. Pilon-Smits and CF. Quinn. Selenium Metabolism in Plants. R. Hell and R. - R. Mendel (eds.), Cell Biology of Metals and Nutrients , Plant Cell Monographs 17, 2010.

[73] RA. Sunde. Ch38 Selenium 2006 - present knowledge 9thed. of bowman, BA and Russell, pp 480-497

[74] GF. Combs and SB. Combs. The nutritional biochemistry of selenium. Ann.Rev.Nutr.1984. 4:257-80

[75] B. Gammelgaard, L. Rasmussen, C. Gabel-Jensen and B. Steffansen. Estimating intestinal absorption of inorganic and organic selenium compounds by *in vitro* flux and biotransformation studies in Caco - 2 cells and I CP - MS detection. Biol. Trace Elem. Res., 2012, 145, 248–256.

[76] J. Pinsent. The need for selenite and molybdate in the formation of formic dehydrogenase by members of the coli - aerogenes group of bacteria. Biochem J. 1954 May; 57(1): 10–16.

[77] JE. Oldfield. The two faces of selenium. J Nutr. 1987 Dec;117(12):2002-8.

[78] L. Schomburg. Genetics and phenomics of selenoenzymes - how to identify an impaired biosynthesis? Mol Cell Endocrinol. 2010 Jun 30;322(1-2):114-24.

[79] VN. Gladyshev. Chapter9 - Selenoproteins and Selenoproteomes in Selenium: Its Molecular Biology and Role in Human Health- DL. Hatfield, MJ. Berry, N.Vadim. -Springer -3rd edition (2012)

[80] G. Feroci, A. Fini. Study of the antioxidant effect of several selenium and sulphur compounds. J Trace Elem Med Biol. 1998 Jul;12(2):96-100.

[81] L. Huang, Y. Shi, F. Lu, H. Zheng , X. Liu, B. Gong, J. Yang , Y. Lin, J. Cheng, S. Ma, H. Lin, Z. Yang. Association Study of Polymorphisms in Selenoprotein Genes and Kashin–Beck Disease and Serum Selenium/Iodine Concentration in a Tibetan Population. PLOS ONE, August 2013, Volume 8, Issue 8, e71411

[82] R. Ebert-Dümig R, J. Seufert, D. Schneider, J. Köhrle, N. Schütze, F. Jakob. Expression of selenoproteins in monocytes and macrophages - implications for the immune system. Med Klin (Munich). 1999 Oct 15;94 Suppl 3:29-34.

[83] H. Imai and Y. Nakagawa. Biological significance of phospholipid hydropero xide glutathione peroxidase (PHGPx, GPx4) in mammalian cells. Free Radic Biol Med. 2003 Jan 15;34(2):145-69.

[84] MS. Baker, J. Feigan, DA. Lowther. Chondrocyte antioxidant defences: the roles of catalase and glutathione peroxidase in protection against H2O2 dependent inhibition of proteoglycan biosynthesis. J Rheumatol. 1988 Apr;15(4):670-7.

[85] N. Pietschmann, E. Rijntjes, A. Hoeg, M. Stoedter, U. Schweizer, P. Seemann and L. Schomburg. Selenoprotein P is the essential selenium transporter for bones. Metallomics. 2014 May;6(5):1043-9.

[86] MP. Rayman. Food-chain selenium and human health: emphasis on intake. Br J Nutr. 2008 Aug;100(2):254-68.

[87] PN. Williams, E. Lombi, GX. Sun, K. Scheckel, YG. Zhu, X. Feng, J. Zhu, AM. Carey, E. Adomako, Y. Lawgali, C. Deacon and AA. Meharg. Selenium characterization in the global rice supply chain. Environ. Sci. Technol. 43, 6024–6030 (2009).

[88] MP. Rayman. Selenium and human health. Lancet. 2012 Mar 31;379(9822):1256-68.

[89] GF. Combs. Selenium in global food systems. Br. J. Nutr. 85, 517–547 (2001).

[90] A. Haug, RD. Graham, OA. Christophersen and GH. Lyons. How to use the world's scarce selenium resources efficiently to increase the selenium concentration in food. Microb Ecol Health Dis. 2007 Dec; 19(4): 209–228.

[91] GX. Sun, X. Liu, PN. Williams, YG Zhu. Distribution and translocation of selenium from soil to grain and its speciation in paddy rice (Oryza sativa L.). Environ. Sci. Technol. 44, 6706–6711 (2010).

[92] PD. Hodgson. An *in vitro* model to study cartilage metabolism in Kashin-Beck Disease. PhD Thesis, Carfiff University. 2012

[93] J. Tan, W. Zhu, W. Wang, R. Li, S. Hou, D. Wang, L. Yang. Selenium in soil and endemic diseases in China. Sci Total Environ. 2002 Feb 4;284(1-3):227-35.

[94] X.Chen, G. Yang, J.Chen, X.Chen, Z.Wen, K. Ge. Studies on the relations of selenium and Keshan disease. Biol. Trace Elem. Res. 2, 91–107 (1980).

[95] GA. Fleming. in Applied Soil Trace Elements. (ed Davies, B. E.) 199–234 (John Wiley & Sons, 1980)

[96] GX. Sun, AA. Meharg, G. Li, Z. Chen, L. Yang, S-C Chen,Y-G Zhu. Distribution of soil selenium in China is potentially controlled by deposition and volatilization? Nature Scientific Reports, 6:20953, DOI: 10.1038/srep20953

[97] T. Blazina, Y. Sun, A. Voegelin, M. Lenz, M. Berg, LHE. Winkel. Terrestrial selenium distribution in China is potentially linked to monsoonal climate Nature Communications,5:4717

[98] YG. Zhu, EA. Pilon-Smits, FJ. Zhao, PN. Williams, AA. Meharg. Selenium in higher plants: understanding mechanisms for biofortification and phytoremediation. Trends Plant Sci. 2009 Aug;14(8):436-42.

[99] MP. Rayman. Selenium and human health. Lancet. 2012 Mar 31;379(9822):1256-68.

[100] Y. Xia, K. E Hill, D. W Byrne, J. Xu, and RF Burk. Effectiveness of selenium supplements in a low-selenium area of China. Am J Clin Nutr. 2005 Apr;81(4):829-34. -

[101] DL. Hatfield, MJ. Berry, VN. Gladyshev, Eds., Selenium: its Molecular Biology and Role in Human Health (Springer, ed. 3, 2012). doi:10.1007/978-1-4614-1025-6

[102] Y. Wen, F. Zhang, C. Li, S. He, W. Tan, Y. Lei, Q.Zhang, H. Yu, J. Zheng, X.Guo. Gene Expression Analysis Suggests Bone Development-Related Genes GDF5 and DIO2 Are Involved in the Development of Kashin-Beck Disease in Children Rather than Adults. PLoS One. 2014 Jul 29;9(7):e103618

[103] Z. Zhang, J. Zhang, J. Xiaoa. Selenoproteins and selenium status in bone physiology and pathology. Biochim Biophys Acta. 2014 Nov;1840(11):3246-3256.

[104] H. Zeng, JJ. Cao and GF. Combs Jr. Selenium in Bone Health: Roles in Antioxidant Protection and Cell Proliferation. Nutrients. 2013 Jan 10;5(1):97-110.

[105] WB. Minich, C. Lenzner, A. Bergmann, NG. Morgenthaler. J. Clin. Endocrinol. Metab., 2004, 89, 352–356

[106] R. Moreno-Reyes, D. Egrise, M. Boelaert, S. Goldman, S. Meuris. Iodine deficiency mitigates growth retardation and osteopenia in selenium deficient rats. J Nutr. 2006 Mar;136(3):595-600.

[107] R. Moreno-Reyes, D. Egrise, J. Neve, JL. Pasteels, A. Schoutens. Selenium deficiency-induced growth retardation is associated with an impaired bone metabolism and osteopenia. J Bone Miner Res. 2001 Aug;16(8):1556-63.

[108] JJ. Cao, BR. Gregoire, H. Zeng. Selenium deficiency decreases antioxidative capacity and is detrimental to bone microarchitecture in mice. J Nutr. 2012 Aug;142(8):1526-31.

[109] H. Liu, W. Bian, S. Liu, K. Huang. Selenium protects bone marrow stromal cells against hydrogen peroxide- induced inhibition of osteoblastic differentiation by suppressing oxidative stress and ERK signaling pathway. Biol Trace Elem Res. 2012 Dec;150(1-3):441-50.

[110] CM. Beukhof, M. Medici, AW. van den Beld1, B.Hollenbach, A. Hoeg,WE. Visser, WW. de Herder, TJ. Visser, L. Schomburg, RP. Peeters. Selenium Status Is Positively Associated with Bone Mineral Density in Healthy Aging European Men. PLoS One. 2016 Apr 7;11(4):e0152748.

[111] RF. Burk and KE. Hill. Selenoprotein P: an extracellular protein with unique physical characteristics and a role in selenium homeostasis. Annu Rev Nutr. 2005;25:215-35.

[112] L. Schomburg, U. Schweizer, B. Holtmann, L. Flohe, M. Sendtner and J. Kohrle. Gene disruption discloses role of selenoprotein P in selenium delivery to target tissues. Biochem. J., 2003, 370, 397–402. 21

[113] RF. Burk, KE. Hill, A. Nakayama, V. Mostert, XA. Levander, AK. Motley, DA. Johnson, JA. Johnson, ML. Freeman, LM. Austin. Selenium deficiency activates mouse liver Nrf2-ARE but vitamin E deficiency does not. Free Radic Biol Med. 2008 Apr 15;44(8):1617-23.

[114] JH. Bassett, A. Boyde, PG. Howell, RH. Bassett, TM. Galliford, M. Archanco, H. Evans, MA. Lawson, P. Croucher, DL. St Germain, VA. Galton,GR. Williams. Optimal bone strength and

mineralization requires the type 2 iodothyronine deiodinase in osteoblasts. Proc Natl Acad Sci U S A. 2010 Apr 20;107(16):7604-9

[115] CM. Downey, CR. Horton, BA. Carlson, TE. Parsons, DL. Hatfield, B. Hallgrímsson, FR. Jirik. Osteo-chondroprogenitor-specific deletion of the selenocysteine tRNA gene, Trsp, leads to chondronecrosis and abnormal skeletal development: a putative model for Kashin–Beck disease. PLoS Genet. 2009 Aug; 5(8): e1000616.

[116] S. Wu, C. Duan, F. Zhang, RP. McKenzie, J. Zheng, U. Farooq, Y. Bai, X. Guo. Difference in apoptosis-associated genes expression profiling and immunohistology analysis between Kashin-Beck disease and primary osteoarthritis. Chinese Science Bulletin March 2014, Volume 59, Issue 9, pp 833–839

[117] K. Ge and G. Yang. The epidemiology of selenium deficiency in the etiological study of endemic diseases in China. Am J Clin Nutr. 1993 Feb;57(2 Suppl):259S-263S.

[118] WH. Zhang, J. Neve, JP. Xu, J. Vanderpas, ZL. Wang. Selenium, iodine and fungal contamination in Yulin District (People's Republic of China) endemic for Kashin - Beck disease. International Orthopaedics 2001;25(3):188-90.

[119] A. Peng, C. Yang, H. Rui, H. Li. Study on the pathogenic factors of Kashin - Beck disease. J Toxicol Environ Health. 1992 Feb;35(2):79-90.

[120] L. Sokoloff. Endemic forms of osteoarthritis. Clin Rheum Dis. 1985 Aug;11(2):187-202. & L. Sokoloff. Kashin - Beck disease: current status. Nutr Rev. 1988 Mar;46(3):113-9.

[121] K. Schepman, RHH. Engelbert, MM. Visser, C. Yu, Rien de Vos. Kashin Beck Disease: more than just osteoarthrosis. A cross-sectional study regarding the influence of body function-structures and activities on level of participation. Int Orthop. 2011 May; 35(5): 767–776.

[122] J. Cao, S. Li, Z. Shi, Y. Yue, J. Sun, J. Chen J, Q. Fu, CE. Hughes, B. Caterson. Articular cartilage metabolism in patients with Kashin - Beck Disease: an endemic osteoarthropathy in China. Osteoarthritis Cartilage. 2008 Jun;16(6):680-8. Epub 2007 Oct 22.

[123] RR Jr. Slater, MT. Bayliss, PF. Lachiewicz, DM. Visco, B. Caterson . Monoclonal antibodies that detect biochemical markers of arthritis in humans. Arthritis Rheum. 1995 May;38(5):655-9.

[124] S. Fuchs, B. Dankbar, G. Wildenau, W. Goetz, CH. Lohmann, CO. Tibesku. Expression of the CD44 variant isoform 5 in the human osteoarthritic knee joint: correlation with radiological, histomorphological, and biochemical parameters.J Orthop Res. 2004 Jul;22(4):774-80.

[125] H. Huang, Z.F. Li, J.Y.Deng, D.Y. Zhou, L. Zhang, Y.M. Zhao. Kashin-Beck disease survey analyses in Sichuan, 2006. End Dis Bull. 2007;22:56–57.

[126] G. Xiong. Diagnostic, clinical and radiological characteristics of Kashin - Beck disease in Shaanxi Province, PR China. International Int Orthop. 2001;25(3):147-50.

[127] RT. Ballock, RJ. O'Keefe. The biology o f the growth plate. J Bone Joint Surg Am, 2003 Apr; 85 (4): 715 -726

[128] JL. Pasteels, FD. Liu, M. Hinsenkamp, M. Rooze, F. Mathieu, N. Perlmutter. Histology of Kashin - Beck lesions. Int Orthop. 2001;25(3):151-3.

[129] R. Moreno-Reyes, C. Suetens, F. Mathieu, F. Begaux, D. Zhu, MT. Rivera, M. Boelaert, J. Nève, N. Perlmutter, J. Vanderpas. Kashin - Beck osteoarthropathy in rural Tibet in relation to selenium and iodine status. N Engl J Med. 1998 Oct 15;339(16):1112-20.

[130] Y. Yao, F. Pei, P. Kang. Selenium, iodine, and the relation with Kashin-Beck disease. Nutrition. 2011 Nov-Dec;27(11-12):1095-100.

[131] FL. Ren, X. Guo, RJ. Zhang, ShJ. Wang, H. Zuo, ZT. Zhang, D. Geng, Y. Yu, M. Su. Effects of selenium and iodine deficiency on bone, cartilage growth plate and chondrocyte differentiation in two generations of rats. Osteoarthritis Cartilage. 2007 Oct;15(10):1171-7.

[132] L. Huang, Y. Shi, F. Lu, H. Zheng, X. Liu, B. Gong, J. Yang, Y. Lin, J. Cheng, S. Ma, H. Lin, Z. Yang. Association Study of Polymorphisms in Selenoprotein Genes and Kashin–Beck Disease and Serum Selenium/ Iodine Concentration in a Tibetan Population. PLoS One. 2013 Aug 23;8(8):e71411

[132] FS. Li, YJ. Duan, SJ. Yan, JY. Guan, LM. Zou, FC. Wei, LY. Mong, L. Li, SY. Li. Presenile (early ageing) changes in tissues of Kaschin - Beck disease and its pa thogenetic significance. Mech Ageing Dev 54 (2): 103 - 120.

[133] J. Chen, Y. Chu, J. Cao, Z. Yang, X. Guo, Z. Wang. T-2 toxin induces apoptosis, and selenium

partly blocks, T-2 toxin induced apoptosis in chondrocytes through modulation of the Bax/Bcl-2 ratio. Food Chem Toxicol (2006)44:567–573

[134] C. Yang, E. Wolf, K. Röser, G. Delling, PK. Müller. Selenium deficiency and fulvic acid supplementation induces fibrosis of cartilage and disturbs subchondral ossification in knee joints of mice: an animal model study of Kashin - Beck disease. Virchows Arch A Pathol Anat Histopathol. 1993;423(6):483-91.

[135] JM. Jordan, F. Fang, J.B. Renner *et al.*, unpublished data, 2007

[136] JM. Jordan, LF Callahan. Community and Environmental Factors and Arthritis Outcomes. N C Med J. 2007 Nov-Dec;68(6):439-43.

[137] JM. Jordan. Low selenium levels associated with knee OA risk, severity. Orthopedics today 2005.

[138] I. Meulenbelt, JL. Min, S. Bos, N. Riyazi, JJ. Houwing-Duistermaat, HJ. van der Wijk, HM. Kroon, M. Nakajima, S. Ikegawa, AG. Uitterlinden, JB. van Meurs, WM. van der Deure, TJ. Visser, AB. Seymour, N. Lakenberg, R. van der Breggen, D. Kremer, CM. van Duijn, M. Kloppenburg, J. Loughlin, PE. Slagboom. Identification of DIO2 as a new susceptibility locus for symptomatic osteoarthritis. Hum Mol Genet. 2008 Jun 15;17(12):1867-75.

[139] M. Miura, K. Tanaka, Y. Komatsu, M. Suda, A. Yasoda, Y. Sakuma, A. Ozasa, K. Nakao. Thyroid hormones promote chondrocyte differentiation in mouse ATDC5 cells and stimulate endochondral ossification in fetal mouse tibias through iodothyronine deiodinases in the growth plate. J Bone Miner Res. 2002 Mar;17(3):443-54.

[140] H. Robson, T. Siebler, DA. Stevens, SM. Shalet, GR. Williams. Thyroid hormone acts directly on growth plate chondrocytes to promote hypertrophic differentiation and inhibit clonal expansion and cell proliferation. Endocrinology, 141, 3887–3897.

[141] AWM. Cheng, M. Bolognesi, V. Byers Kraus. DIO2 Modifies Inflammatory Responses in Chondrocytes. Osteoarthritis Cartilage. 2012 May;20(5):440-5.

[142] T. Aigner, J. Stove. Collagens-major component of the physiological cartilage matrix, major target of cartilage degeneration, major tool in cartilage repair. Adv Drug Deliv Rev. 2003 Nov 28;55(12):1569-93.

[143] AC. Bay-Jensen, E.Slagboom, P. Chen-An, P.Alexandersen, P. Qvist, C. Christiansen, I. Meulenbelt, MA. Karsdal. Role of hormones in cartilage and joint metabolism: understanding an unhealthy metabolic phenotype in osteoarthritis. Menopause: The Journal of The North American Menopause Society Vol. 20, No. 5, pp. 578-586

[144] N. Bömer , Y.F. Ramos , S.D. Bos , B.J. Duijnisveld , W. Koevoet , G.J. van Osch , R.G. Nelissen , P.E. Slagboom , I. Meulenbelt. Functional effect of DIO2 in an *in vitro* model for chondrogenesis Bomer Osteoarthritis and Cartilage 20 (2012) S54-S296

[145] H. Nagase, Y. Nagasawa, Y. Tachida, S. Sakakibara, J. Okutsu, N. Suematsu, S. Arita, K. Shimada. Deiodinase 2 upregulation demonstrated in osteoarthritis patients cartilage causes cartilage destruction in tissue-speci fi c transgenic rats. Osteoarthritis Cartilage. 2013 Mar;21(3):514-23.

[146] MB. Goldring. Insight into the function of DIO2, a susceptibility gene in human osteoarthritis, as an inducer of cartilage damage in a rat model: is there a role for chondrocyte hypertrophy? Osteoarthritis Cartilage. 2013 May;21(5):643-5.

[147] T. Vos, *et al.* A comparative risk assessment of burden of disease and injury attributable to 67 risk factors and risk factor clusters in 21 regions, 1990–2010: a systematic analysis for the Global Burden of Disease Study 2010. Lancet Volume 380, No. 9859, p2224–2260, 15 December 2012.

[148] CB. Little, P. Ghosh. Variation in proteoglycan metabolism by articular chondrocytes in different joint regions is determined by post-natal mechanical loading. Osteoarthritis Cartilage. 1997 Jan;5(1):49-62.

[149] EK. Moo, NAA. Osman, B. Pingguan-Murphy. The metabolic dynamics of cartilage explants over a long-term culture period. Clinics (Sao Paulo). 2011 Aug; 66(8): 1431–1436.

[150] AG. Clark, AL. Rohrbaugh, I. Otterness, VB. Kraus. The effects of ascorbic acid on cartilage metabolism in guinea pig articular cartilage explants. Matrix Biol. 2002 Mar;21(2):175-84. & AL. McNultya, TP. Vailb, VB. Krausa. Chondrocyte transport and concentration of ascorbic acid is mediated by SVCT2. Biochim Biophys Acta. 2005 Jun 30;1712(2):212-21.

[151] X. Lui, J. Liu, N. Kang, L. Yan, Q. Wang, X. Fu, Y. Zhang, R. Xiao, Y. Cao. Role of ITS in auricular chondrocyte proliferation and engineered cartilage formation *in vitro* - Int J Mol Sci. 2014 Jan 21;15(1):1525-37.

[152] N.Ashammakhi & P. Ferretti. Chapter 2 - Differentiation Factors and Articular Cartilage Regeneration MM French and KA Athanasiou Topics in Tissue Engineering 2003, EDS

[153] M. Stolz, R. Gottardi, R. Raiteri, S. Miot, I. Martin, R. Imer, R. Imer, U. Staufer, A. Raducanu, M. Düggelin, W. Baschong, AU. Daniels, NF. Friederich, A. Aszodi, U. Aeb. Early detection of aging cartilage and osteoarthritis in mice and patient samples using atomic force microscopy. Nat Nanotechnol 2009;4(3):186e92.

[156] Book review: Inductively Coupled Plasma Mass Spectrometry Edited by Akbar Montaser. Wiley-VCH: New York. 1998. 964 pages. ISBN 0-471-18620-1

[157] F. Fryer, K.Yamanaka. Measurement of Macro and Trace Elements in Plant Digests Using the 7500c ICP-MS System Application – Food – Agilent Technologies

[159] J. Retka, A.Maksymowicz, D.Karmasz, Determination of Cu, Ni, Zn, Pb, Cd by ICP-MS and Hg by AAS in Plant Samples, Accumalation in food and Crops, 15th ICHMET. 373-376

[160] H. Motz. Applications of the Radiation from Fast Electron Beams. J. Appl. Phys. 22 (1951), 527-535

[161] G. Margaritondo, Y. Hwu, G. Tromba. Synchrotron light: from basics to coherence and coherence-related applications.

[162] Goodman, J.W., Statistical Optics (John Wiley and Sons, New York, 1985). Chapter 5

[163] K.J. Kim. Nucl. Instr. Meth. Phys.Sect.A 246, 1-3, 1986, 71-76, proc. VII National Conference on Synchrotron Radiation. 1986

[164] Als-Nielsen, Jens, and Des McMorrow. Elements of modern X-ray physics. John Wiley & Sons, 2011.

[165] V. Baryshev, G. Kulipanov, A. Skrinsky. Handbook on Synchrotron Radiation, Vol. 3, chapter 16. Elsevier/North Holland (1991)

[166] B. Laforce, C. Carlier, B. Vekemans, J. Villanova, R. Tucoulou, W. Ceelen, L. Vincze "Assessment of ovarian cancer tumors treated with intraperitoneal cisplatin therapy by nanoscopic X-ray fluorescence imaging." Scientific Reports 6 29999 (2016)

[167] VA. Soléa, E. Papillon, M. Cotte, Ph. Walter, J. Susini. A multiplatform code for the analysis of energy-dispersive X-ray fluorescence spectra." Spectrochimica Acta Part B: Atomic Spectroscopy 62.1 (2007): 63-68.

[168] G. Sarret, L. Avoscan, M. Carrière, R. Collins, N. Geoffroy, F. Carrot, J. Covès, B. Gouget. Chemical forms of selenium in the metal-resistant bacterium Ralstonia metallidurans CH34 exposed to selenite and selenate. Appl Environ Microbiol. 2005 May;71(5):2331-7.

[169] T. Bacquart G. Devès A. Carmona, R. Tucoulou S. Bohic, R. Ortega. Subcellular speciation analysis of trace element oxidation states using synchrotron radiation micro-X-ray absorption near-edge structure. Anal. Chem. 79, 7353-7359 (2007).

[170] IJ. Pickering, GE. Brown, TK. Tokunaga. Quantitative speciation of selenium in soils using X-ray Absorption Spectroscopy. Environ. Sci. Technol. 29, 2456-2459 (1995).

[171] I. Llorens, E. Lahera, W. Delnet, O. Proux, A. Braillard, J.-L. Hazemann, A. Prat, D. Testemale, Q. Dermigny, F. Gelebart, M. Morand, A. Shukla, N. Bardou, O. Ulrich, S. Arnaud, J.-F. Berar, N. Boudet, B. Caillot, P. Chaurand, J. Rose, E. Doelsch, P. Martin, P. L. Solari. High energy resolution five-crystal spectrometer for high quality fluorescence and absorption measurements on an x-ray absorption spectroscopy beamline. Rev. Sci. Instrum. 83, 063104 (2012).

[172] SC. Lu. Glutathione synthesis. Biochimica et Biophysica Acta (BBA)-General Subjects 1830.5 (2013): 3143-3153.

[173] KH. Lee, D. Jeong. Bimodal actions of selenium essential for antioxidant and toxic pro-oxidant activities: the selenium paradox (Review). Mol Med Rep. 2012 Feb;5(2):299-304.

[174] U. Tinggi. Selenium: its role as antioxidant in human health. Environ. Health Prev. Med. 13, 102-108 (2008).

[175] JE. Penner-Hann. X-ray Absorption Spectroscopy. University of Michigan, Ann Arbor, MI, USA

[176] SP. Cramer, O. Tench, M. Yocum, GN. George. Nucl. Instrum. Methods Phys. Res. Sect. A-Accel. Spectrom. Dect. Assoc. Equip. 1988, 266, 586–591

[177] L.Jr. Que (ED.). Physical Methods in Bioinorganic Chemistry : spectroscopy and magnetism. Sausalito, Calif. : University Science Books, c2000)

[178] O. Proux, X. Biquard, E. Lahera, J.-J. Menthonnex, A. Prat, O. Ulrich, Y. Soldo, P. Trévisson, G. Kapoujvan, G. Perroux, P. Taunier, D. Grand, P. Jeantet, M. Deleglise, J.-P. Roux, J.-L. Hazemann, FAME: a new beamline for x-ray absorption investigations of very-diluted systems of environmental, material and biological interests. Physica Scripta T115, 970-973 (2005).

[179] O. Proux, V. Nassif, A. Prat, O. Ulrich, E. Lahera, X. Biquard, J.-J. Menthonnex, J.-L. Hazemann, Feedback system of a liquid-nitrogen-cooled double-crystal monochromator: design and performances. J. Synchrotron Radiat. 13, 59-68 (2006).

[180] G. Martinez-Criado, R. Steinmann, B. Alen, A. Labrador, D. Fuster, J.M. Ripalda, A. Homs, S. Laboure, J. Susini, New cryogenic environment for beamline ID22 at the European Synchrotron Radiation Facility. Rev. Sci. Instrum. 78, 025106 (2007). doi:10.1063/1.2536677

[181] I. Llorens, E. Lahera, W. Delnet, O. Proux, A. Braillard, J.-L. Hazemann, A. Prat, D. Testemale, Q. Dermigny, F. Gelebart, M. Morand, A. Shukla, N. Bardou, O. Ulrich, S. Arnaud, J.-F. Berar, N. Boudet, B. Caillot, P. Chaurand, J. Rose, E. Doelsch, P. Martin, P. L. Solari, High energy resolution five-crystal spectrometer for high quality fluorescence and absorption measurements on an x-ray absorption spectroscopy beamline. Rev. Sci. Instrum. 83, 063104 (2012).

[182] JL.Hazemann, O. Proux, V. Nassif, H. Palancher, E. Lahera, C. Da Silva, A. Braillard, D. Testemale, M.-A. Diot, I. Alliot, W. Delnet, A. Manceau, F. Gélébart, M. Morand, Q. Dermigny, A. Shukla, High-resolution spectroscopy on an X-ray absorption beamline. J. Synchrotron Radiat. 16, 283-292 (2009).

[183] F. De Groot, High-Resolution X-ray Emission and X-ray Absorption Spectroscopy. Chem. Rev. 101, 1779-1808 (2001).

[184] P. Glatzel, U. Bergmann, High resolution 1s core hole X-ray spectroscopy in 3d transition metal complexes—electronic and structural information. Coord. Chem. Rev. 249, 65–95 (2005).

[185] MO. Krause, JH. Oliver, Natural widths of atomic K and L levels, Kα X-Ray lines and several KLL Auger lines. J. Phys Chem. Ref. Data 8, 329-338 (1979).

[186] FK. Richtmyer, SW. Barnes, E. Ramberg, The widths of the L-series lines and of the energy levels of Au (79), Phys. Rev. 46, 843-860 (1934).

[187] B. Ravel and M. Newville, ATHENA, ARTEMIS, HEPHAESTUS: data analysis for X-ray absorption spectroscopy using IFEFFIT, J. Synchrotron Rad. 12, 537–541 (2005).

[188] TC. Stadtman, Selenocysteine. Annu Rev Biochem. 65, 83-100 (1996). doi:10.1146/annurev.bi.65.070196.0005

[189] N. Schmitz, S. Laverty, VB. Kraus, T. Aigner. Basic methods in histopathology of joint tissues. Osteoarthritis Cartilage. 2010 Oct;18 Suppl 3:S113-6.

[190] ED. Rodrigues, ER. Pimentel, PA. Mourão, L. Gomes. Distribution of small proteoglycans and glycosaminoglycans in humerus-related articular cartilage of chickens. Braz J Med Biol Res, March 2005, Volume 38(3) 381-390

[191] PJ. Roughley. The structure and function of cartilage proteoglycans. European Cells and Materials Vol. 12. 2006 pp 92-101

[192] N. Ballatori, SM. Krance, S. Notenboom, S. Shi, K. Tieu, CL. Hammond. Glutathione dysregulation and the etiology and progression of human diseases. Biological chemistry, 2009 Mar;390(3):191-214.

[193] M. Björnstedt, S. Kumar,A. Holmgren. 1992. Selenodiglutathione is a highly efficient oxidant of reduced thioredoxin and a substrate for mammalian thioredoxin reductase. Journal of Biological Chemistry, 267, pp.8030-8034. PMID:1569062

[194] J. Yan, J. Xu, Y. Fei, C. Jiang, W. Zhu, Y. Han, S. Lu. TrxR2 deficiencies promote chondrogenic differentiation and induce apoptosis of chondrocytes through mitochondrial reactive oxygen species. Experimental cell research, 344, 67-75 (2016).

[195] Y. Jirong, P. Huiyun, Y. Zhongzhe, D. Birong, L. Weimin, Y. Ming, S.Yi. Sodium selenite for treatment of Kashin-Beck disease in children: a systematic review of randomised controlled trials. Osteoarthritis and Cartilage, 20, pp.605-613. (2012)

[196] LA. Fortier, JU. Barker, EJ. Strauss, TM. McCarrel, BJ. Cole. The role of growth factors in cartilage repair. Clinical Orthopaedics and Related Research, 469, pp.2706-2715. (2011)

[197] X. Liu, H. Wu, M. Byrne, S. Krane, R. Jaenisch. Type III is crucial for collagen I fibrillogenesis and for normal cardiovascular development. PNAS (proc.Natl.Avcad.Sci).Usa, Vol 94, 1997

[198] JJ. Wu, MA. Weis, LS. Kim, DR. Eyre. Type III collagen, a fibril network modifier in articular cartilge. J Biol Chem. 2010 Jun 11;285(24):18537-44.

[199] SF. Wotton, VC. Duance, PR Fryer. Type IX collagen: a potential function in articular cartilage, FEBS letters vol 234, Issue 1, July 1988, P 79-82,

[200] TF. Linsenmayer, RD. Eavey, TM. Schmid. Type X Collagen: A Hypertrophic Cartilage-Specific Molecule. Pathol Immunopathol Res. 1988;7(1-2):14-9.

[201] CA. Poole, ZJ Zahnd, JM Ross. The differential distribution of acetylated and detyrosinated alpha-tubulin in the microtubular cytoskeleton and primary cilia of hyaline cartilage chondrocytes. J Anat. 2001 Oct; 199(Pt 4): 393–405.

[202] MJ. Mienaltowski, L. Huang, AJ. Stromberg, JN. MacLeod. Differential gene expression associated with postnatal equine articular cartilage maturation BMC Musculoskelet Disord. 2008 Nov 5;9:149.

[203] A. Boskey and N. Pleshko Camacho. FT-IR Imaging of Native and Tissue-Engineered Bone and Cartilage. Biomaterials. 2007 May; 28(15): 2465–2478

[204] V. Zohdi, DR. Whelan, BR. Wood, JT. Pearson, KR. Bambery, MJ. Black. Importance of tissue preparation methods in FTIR micro-spectroscopical analysis of biological tissues:'Traps for new users' . PLoS One. 2015 Feb 24;10(2):e0116491

[205] J. Rieppo, MM. Hyttinen, JS. Jurvelin, HJ. Helminen. Reference sample method reduces the error caused by variable cryosection thickness in Fourier transform infrared imaging. Appl Spectrosc. 2004 Jan;58(1):137-40.

[206] WD. Duncan, & GP. Williams. Infrared synchrotron radiation from electron storage rings. Appl Opt. 1983 Sep 15;22(18):2914.

[207] NP. Camacho, P. West, PA. Torzilli, R. Mendelsohn. FTIR microscopic imaging of collagen and proteoglycan in bovine cartilage. Copyright 2000 John Wiley & Sons, Inc. Biopolymers (Biospectroscopy) 62: 1-8, 2001

[208] L. Rieppo, S. Saarakkala, T. Närhi, HJ. Helminen, JS. Jurvelin, J. Rieppo. Application of second derivative spectroscopy for increasing molecular specificity of FTIR spectroscopic imaging of articular cartilage. Osteoarthritis Cartilage. 2012 May;20(5):451-9.

[209] NT. Khanarian, MK. Boushell, JP. Spalazzi, N. Pleshko, AL. Boskey , HH. Lu. FTIRI compositional mapping of the cartilage-to-bone interface as a function of tissue region and age. J Bone Miner Res. 2014 Dec;29(12):2643-52.

[210] PA. West, MP. Bostrom, PA. Torzilli, NP. Camacho. FTIR spectral analysis of degenerative cartilage: an infrared fiber optic probe and imaging study. Appl Spectrosc. 2004 Apr;58(4):376-81.

[211] B. de Campos Vidal, MLS. Mello. FTIR microscoscopy of rat ear cartilage. PLoS One. 2016; 11(3): e0151989.

[212] J. Yin, Y. Xia. Proteoglycan concentrations in healthy and diseased articular cartilage by fourier transform infrared imaging and principal component regression. Spectrochim Acta A Mol Biomol Spectrosc. 2014 Dec 10;133:825-30.

[213] J. Oinas, L. Rieppo, M. Finnilä, M. Valkealahti, P. Lehenkari, S. Saarakkala. Imaging of Osteoarthritic Human Articular Cartilage using Fourier Transform Infrared Microspectroscopy Combined with Multivariate and Univariate Analysis. Sci Rep. 2016 Jul 21;6:30008.

[214] L. Rieppo, J. Rieppo, JS. Jurvelin, S. Saarakkala. Fourier transform infrared spectroscopic imaging and multivariate regression for prediction of proteoglycan content of articular cartilage. PLoS One. 2012;7(2):e32344.

[215] Z.Movasaghi, S. Rehmann, I.Rehman. Fourier Transform Infrared (FTIR) Spectroscopy of Biological Tissue. Applied Spectroscopy reviews 43, 134-179,2008,

[216] J.Yin, Y. Xia. Macromolecular Concentrations in Bovine Nasal Cartilage by Fourier Transform Infrared Imaging and Principal Component Regression.Appl Spectrosc. 2010 Nov;64(11):1199-208

[217] F. Jamme, S. Kascakova, S. Villette, F. Allouche, S. Pallu, V. Rouam, M. Refregiers. Deep UV autofluorescence microscopy for cell biology and tissue histology. Biol. Cell (2013) 105, 277–288

[218] F. Jamme, S. Villette, A. Giuliani, V. Rouam, F. Wien, B. Lagarde, M. Réfrégiers. Synchrotron UV Fluorescence Microscopy Uncovers New Probes in Cells and Tissues. Microsc Microanal. 2010 Oct;16(5):507-14.

[219] S. Pallu, GY. Rochefort, C. Jaffre, M. Refregiers, DB. Maurel, D. Benaitreau, E. Lespessailles, F. Jamme, C. Chappard, CL Benhamou. Synchrotron Ultraviolet Microspectroscopy on Rat Cortical Bone: Involvement of Tyrosine and Tryptophan in the Osteocyte and Its Environment. August 2012, Volume 7, Issue 8, e43930- PLOSONE

[220] T. Rennert, KU. Totsche, K. Heister, M. Kersten, J. Thieme. Advanced spectroscopic, microscopic, and tomographic characterization techniques to study biogeochemical interfaces in soil. J Soils Sediments (2012) 12:3–23

[221] K. D. Jandt. Atomic force microscopy of biomaterials surfaces and interfaces. Surface Science, (2001) 491(3): 303-332.

[222] HJ. Butt, B. Cappella, M. Kappl. Force measurements with the atomic force microscope: Technique, interpretation and applications. Surface Science Reports 59 (2005) 1–152

[223] K.D. Jandt. Evolutions, Revolutions and Trends in Biomaterials Science – A Perspective.

Advanced engineering materials. Volume 9, Issue 12 December, 2007 Pages 1035–1050. Special Issue: Biomaterials.

[224] Y. Liu, TA. Camesano. Immobilizing Bacteria for Atomic Force Micro- scopy Imaging or Force Measurements in Liquids. ACS Symp. Ser. 2007.984 : 163–188

[225] Q. Zhong, D. Inniss, K. Kjoller, VB. Elings. Fractured polymer silica fiber surface studied by tapping mode atomic-force microscopy. Surface Science, (1993) 290(1-2): L688-L692.

[226] C.Möller, Allen, M., Elings, V., Engel, A. and Müller, D. J. (1999). Tapping-mode atomic force microscopy produces faithful high-resolution images of protein surfaces. Biophysical Journal, 77(2): 1150-1158.

[227] V. Dupres, C. Verbelen, and YF. Dufrêne. Probing molecular recognition sites on biosurfaces using AFM. Biomaterials, (2007) 28(15): 2393-2402.

[228] B. Gady, D. Schleef, R. Reifenberger, and DS. Rimai. The interaction between micrometer-size particles and flat substrates: A quantitative study of jump-to-contact. Journal of Adhesion, (1998) 67(1-4): 291-305.

[229] A. Alessandrini, P. Facci. AFM: a versatile tool in biophysics. Measurement Science & Technology, (2005).16(6): R65-R92.

[230] S. Moreno-Flores, R. Benitez, M. d. Vivanco, JL. Toca-Herrera. Stress relaxation and creep on living cells with the atomic force microscope: a means to calculate elastic moduli and viscosities of cell components. Nanotechnology, (2010).21(44).

[231] Y. F. Dufrêne. Application of atomic force microscopy to microbial surfaces: from reconstituted cell surface layers to living cells. Micron, (2001)32(2): 153-165.

[232] De Oliveira, D.A.C. Albuquerque, T.G.S. Cruz, F.M. Yamaji and F.L. Leite. Measurement of the Nanoscale Roughness by Atomic Force Microscopy: Basic Principles and Applications R.R.L.

[233] M. Loparic, D. Wirz, AU. Daniels, R. Raiteri, MR. Vanlandingham, G. Guex, I. Martin, U. Aebi, M. Stolz. Micro- and Nanomechanical Analysis of Articular Cartilage by Indentation-Type Atomic Force Microscopy: Validation with a Gel-Microfiber Composite. Biophys J. 2010 Jun 2;98(11):2731-40.

[234] M. Plodinec, M. Loparic, U. Aebi. Imaging Articular Cartilage Tissue Using Atomic Force Microscopy. Cold Spring Harb Protoc. 2010 Oct 1;2010(10):pdb.prot5499.

[235] AK. Williamson, K. Masuda, EJ. Thonar, RL. Sah. Growth of immature articular cartilage *in vitro*: correlated variation in tensile biomechanical and collagen network properties. Tissue Eng 2003;9(4):625-34.

[236] L. Keller, P. Schwinté, E. Gomez-Barrena, M. Arruebo, N. Benkirane-Jessel Smart Implants as a Novel Strategy to Regenerate Well-Founded Cartilage. Trends Biotechnol. (2016).

[237] P. Coan, F. Bamberg, PC. Diemoz, A. Bravin, K. Timpert, E. Mützel, JG. Raya, S. Adam-Neumair, MF. Reiser, C. Glaser. Characterization of osteearthritic and normal human patella cartilage by computed tomography X-ray phase-contrast imaging. Invest Radiol. 2010 Jul;45(7):437-44.

[238] A. Bravin, P. Coan, P. Suortti. X-ray phase-contrast imaging: from pre-clinical applications towards clinics. Phys Med Biol. 2013 Jan 7;58(1):R1-35

[239] A. Horng, E. Brun, A. Mittone, S. Gasilov, L. Weber, T. Geith, S. Adam-Neumair, SD. Auweter, A. Bravin, MF. Reiser, P. Coan. Cartilage and soft tissue imaging using X-rays: propagation-based phase-contrast computed tomography of the human knee in comparison with clinical imaging techniques and histology. Invest Radiol. 2014 Sep;49(9):627-34.

[240] M. Bech, O. Bunk, T. Donath, R. Feidenhans, C. David, F. Pfeiffer. Quantitative x-ray dark-field computed tomography. Phys Med Biol. 2010 Sep 21;55(18):5529-39.

[241] MJ. Nissi, F. Tóth, L. Wang, CS. Carlson, JM. Ellermann. Improved visualization of cartilage canals using quantitative susceptibility mapping. PLoS One. 2015 Jul 13;10(7):e0132167.

[242] AM. Lutfi. Mode of growth, fate and function of cartilage canals. J Anat. 1970 Jan; 106(Pt 1): 135–145.

[243] A. Chappard, R. Chol. Les canaux intrachondondraux: histogènese, anatomie et hisophysiologie de la vascularisation cartilagineuse du foetus humain. Lyon, Médical 1983,249,10,417-428.

[244] MJ. Blumer, S. Longato, E. Richter, MT. Perez, KZ. Konackci, H. Fritsch. The role of cartilage canals in endochondral and perichondral bone formation: are there similarities between these two processes. J Anat. 2005 Apr;206(4):359-72.-

[245] F. Zhang, X. Guo, C. Duan, S. Wu, H. Yu, M. Lammi. Identification of differentially expressed genes and pathways between primary osteoarthritis and endemic osteoarthritis (Kashin - Beck disease). Scand J Rheumatol. 2013;42(1):71-9.

[246] C. Duan, X. Guo, XD. Zhang, HJ. Yu, H. Yan, Y. Gao, WJ. Ma, ZQ. Gao, P. Xu P, M. Lammi. Comparative analysis of gene expression profiles between primary knee osteoarthritis and an osteoarthritis endemic to Northwestern China, Kashin-Beck disease. Arthritis Rheum. 2010 Mar;62(3):771-80.

[247] WS. Xiao, X. Guo, FL. Ren, J. Li, XM. Wu, .The Effect of Short Tandem Repeat Loci and Low Selenium Levels on Endemic Osteoarthritis in China. J Bone Joint Surg Am, 2010 Jan; 92 (1): 72 -80

[248] F. Guan, S. Li, Z. Wang, H. Yang, S. Xue, W. Wang, D. Song, X. Zhou, W. Zhou, J. Chen, B. Caterson, C. Hughes. Histopathology of chondronecrosis development in knee articular cartilage in a rat model of Kashin–Beck disease using T-2 toxin and selenium deficiency conditions. Rheumatol Int (2013) 33:157–166

[249] AK. Wann, N. Zuo, CJ. Haycraft, CG. Jensen, CA. Poole, SR. McGlashan, MM. Knight. Primary cilia mediate mechanotransduction through control of ATP-induced Ca^{2+} signaling in compressed chondrocytes. FASEB J. 2012 Apr;26(4):1663-71.

[250] SR. McGlashan, CG. Jensen, CA. Poole. Localization of Extracellular Matrix Receptors on the Chondrocyte Primary Cilium. J Histochem Cytochem September 2006 vol. 54 no. 9 1005-1014

[251] MK. Lotz, S. Otsuki, SP. Grogan, R. Sah, R. Terkeltaub, D. D'Lima. Cartilage Cell Clusters. Arthritis Rheum. 2010 Aug; 62(8): 2206–2218.

[252] P. Shah, V. Strezov, C. Stevanov, PF. Nelson. Speciation of Arsenic and Selenium in Coal Combustion Products. Energy & Fuels. 2007;21:506–512.

[253] CM. Weekley, JB. Aitken, PK. Witting, HH. Harris. XAS studies of Se speciation in selenite-fed rats. Metallomics. 2014 Dec;6(12):2193-203.

[254] CM. Weekley, A. Shanu, JB. Aitken, S. Vogt, PK. Witting, HH. Harris. XAS and XFM studies of selenium and copper speciation and distribution in the kidneys of selenite-supplemented rats. Metallomics. 2014 Sep;6(9):1602-15.

[255] V. Zubkovs, F. Jamme, S. Kascakova, F. Chiappini, F. Le Naour, M. Réfrégiers. Single vs. two-photon microscopy for label free intrinsic tissue studies in the UV light region. Analyst. 2014 Jun 7;139(11):2663-7.

[256] DR. Eyre, S. Apon, JJ. Wu, LH. Ericsson, KA. Walsh. Collagen type IX: Evidence for covalent linkages to type II collagen in cartilage Author links open the overlay panel. Numbers correspond to the affiliation list which can be exposed by using the show more link. FEBS Letters Volume 220, Issue 2, 17 August 1987, Pages 337-341

[257] J.J. Wu, D.R. Eyre. Identification of hydroxypyridinium crosslinking sites in type II collagen of bovine articular cartilage. Biochemistry,1984. 23(8), pp.1850-1857.

[258] TJ. Sims, NC. Avery, AJ. Bailey. Quantitative determination of collagen crosslinks. Extracellular Matrix Protocols,2000. pp.11-26.

[259] M. Saito, K. Marumo, K. Fujii, N. Ishioka. Single-column high-performance liquid chromatographic–fluorescence detection of immature, mature, and senescent cross-links of collagen. Analytical biochemistry, 1997. 253(1), pp.26-32.

[260] T.F. Cruz, G. Mills, KPH Pritzker, RA. Kandel. Inverse correlation between tyrosine phosphorylation and collagenase production in chondrocytes. Biochemical Journal, 1990.269(3), pp.717-721.

[261] D.R Eyre, J.J. Wu. Collagen cross-links. In Collagen. 2005. pp. 207-229. Springer Berlin Heidelberg.

[262] P. Hinterdorfer, HJ. Gruber, F. Kienberger, G. Kada, C. Riener, C. Borken, H. Schindler. Surface attachment of ligands and receptors for molecular recognition force microscopy. Colloids Surf. B Biointerfaces, 23 (2002), pp. 115–123

[263] DM. Ebenstein, LA. Pruitt. Nanoindentation of soft hydrated materials for application to vascular tissues. J. Biomed. Mater. Res. A. 2004;69:222–232.

[264] J. Mollenhauer, ME. Aurich, Z. Zhong. Diffraction-enhanced X-ray imaging of articular cartilage. Osteoarthritis and cartilage. 2002;10:163–171.

[265] E Brun, J Vicente, F Topin, R Occelli. IMorph: A 3D morphological tool to fully analyse all kind of cellular materials. Cellular Metals for Structural and Functional Applications, Conference Paper · January 2008

[266] K.M. Brown, J.R.Arthur. 2001. Selenium, selenoproteins and human health: a review. Public health nutrition, 4(2b), pp.593-599.

[267] L.A. Fortier, J.U. Barker , E.J. Strauss, T.M. McCarrel , B.J. Cole. The role of growth factors in cartilage repair. Clin Orthop Relat Res. 2011;469(10):2706–2715.

[268] LG. Alexopoulos, I.Youn, P. Bonaldo, F.Guilak. Developmental and osteoarthritic changes in Col6a1 knockout mice: the biomechanics of collagen VI in the cartilage pericellular matrix. Arthritis Rheum. 2009 Mar; 60(3): 771–779.

[269] O. Pullig, G. Weseloh, S. Gauer, Swoboda B. Osteopontin is expressed by adult human osteoarthritic chondrocytes: protein and mRNA analysis of normal and osteoarthritic cartilage. Matrix Biol. 2000;19:245–255.

[270] LG. Alexopoulos, MA. Haider, TP. Vail, F. Guilak. Alterations in the mechanical properties of the human chondrocyte pericellular matrix with osteoarthritis. J Biomech Eng. 2003;125(3):323_333

[271] P. Zhu, M. Fang. Nano-Morphology of Cartilage in Hydrated and Dehydrated Conditions Revealed by Atomic Force Microscopy. J Phys Chem Biophys (2012) 2:106.

[272] Y. Nomura. Structural change in decorin with skin aging. Connect Tissue Res 2006;47(5):249e55

[273] S. San Martin, TM. Zorn. The small proteoglycan biglycan is associated with thick collagen fibrils in the mouse decidua. Cell Mol Biol (Noisy-le-grand) 2003;49(4):673e8.

[274] M. Stolz, R. Raiteri, AU. Daniels, MR. VanLandingham, W. Baschong, U. Aebi. Dynamic elastic modulus of porcine articular cartilage determined at two di_erent levels of tissue organization by indentation-type atomic force microscopy. Biophys J 2004;86(5):3269e83.

[275] EM. Moshurchak, FN. Ghadially. A maturation change detected in the semilunar cartilages with the scanning electron microscope. J Anat 1978;126(Pt 3): 605e18.

[276] X. Bi, X. Yang, MPG. Bostrom, N.P. Camacho. Fourier transform infrared imaging spectroscopy investigations in the pathogenesis and repair of cartilage. Biochimica et Biophysica Acta 1758 (2006) 934-941

[277] UP. Palukuru, A. Hanifi, CM. McGoverin, S. Devlin, PI. Lelkes, N. Plesko. Near IR spectroscopy imaging assessment of cartilage composition validation with mid IR imaging spectroscopy. Anal Chim Acta. 2016 Jul 5;926:79-87.

[278] R. Gangadhar, K. Ahmed Jaleeli, A. Ahmad. A fourier transform infrared (FTIR) spectroscopic study on ovine scapular cartilage. International Journal of Science, Environment ISSN 2278-3687 (O) and Technology, Vol. 4, No 4, 2015, 1158 – 1162

[279] W. Feng, T. Zhao, Y. Zhou, F. Li, Y. Zou, S. Bai, W. Wang, L. Yang, X. Wu. Optimization of enzyme-assisted extraction and characterization of collagen from Chinese sturgeon (Acipenser sturio Linnaeus) skin. Pharmacogn Mag. 2013 Oct-Dec; 9(Suppl 1): S32–S37.

[280] K. Zou, G. Liu, T. Wu, L. Du. Selenium for preventing Kashin-Beck osteoarthropathy in children: a meta-analysis. Osteoarthritis Cartilage. 2009 Feb;17(2):144-51.

[281] O. Pullig, G. Weseloh, Swoboda B.. Expression of type VI collagen in normal and osteoarthritic human cartilage. Osteoarthritis Cartilage. 1999 Mar;7(2):191-202.

[282] S. Li, J. Cao, B. Caterson, CE. Hughes. Proteoglycan metabolism, cell death and Kashin-Beck Disease. Glycoconj J. 2012 Aug; 29(5-6): 241–248.

[283] In Lecture prepared by Connolly from "Introduction to X-ray Powder Diffraction", Spring, 2005, 2004.

[284] M. Jackson, LP. Choo, PH. Watson, WC. Halliday, HH. Mantsch. Beware of connective tissue proteins: assignment and implications of collagen absorptions in infrared spectra of human tissues. Biochim Biophys Acta. 1995 Jan 25;1270(1):1-6.

[285] D. Southern, G. Lutz, A. Bracilovic, P. West, M. Spevak, N.P. Camacho, S. Doty. Histological and Molecular structure characterization of annular collagen after intradiskal electrothermal annuloplasty. HSS J. 2006 Feb; 2(1): 49–54.

[286] S. Bohic, C. Rey, A. Legrand, H. Sfihi, R. Rohanizadeh, C. Martel, A. Barbier, G. Daculsi. Characterization of the trabecular rat bone mineral: effect of ovariectomy and bisphosphonate treatment. Bone April 2000 Volume 26, Issue 4, Pages 341–348

[287] M. Berggren, A. Gallegos, JR. Gasdaska, PY. Gasdaska, J. Warneke, G. Powis. Thioredoxin and thioredoxin reductase gene expression in human tumors and cell lines, and the effects of serum stimulation and hypoxia. Anticancer Res 16: 3459-3466, 1996

[288] JP. Arokoski, JS. Jurvelin, U. Vaatainen, HJ. Helminen. Normal and pathological adaptations of articular cartilage to joint loading. Scand.J.Med.Sci.Sports. 2000;10:186 198.

[289] F. Guilak, A. Ratcliffe, N. Lane, MP. Rosenwasser, VC. Mow. Mechanical and biochemical changes in the superficial zone of articular cartilage in canine experimental osteoarthritis. J.Orthop.Res. 1994;12:474 484.

[290] B. Laforce, C. Carlier, B. Vekemans, J. Villanova, R. Tucoulou, W. Ceelen, L. Vincze. Assessment of Ovarian Cancer Tumors Treated with Intraperitoneal Cisplatin Therapy by Nanoscopic X-ray Fluorescence Imaging. Sci Rep. 2016; 6: 29999. doi: 10.1038/srep29999

[291] H. Zhanga, X.Feng, C. Jiang, Q. Li, Y Liu, C. Gu, L.Shang, P. Li, Y. Lin, T. Larssen. Understanding the paradox of selenium contamination in mercury mining areas: High soil content and low accumulation in rice. Environmental Pollution 188:27–36,May 2014. DOI: 10.1016/j.envpol.2014.01.012.

[292] S. Li, W. Li, X. Hu, L. Yang, R. Xirao. Soil selenium concentration and Kashin-Beck disease prevalence in Tibet, China. Front Envir Sci Eng Chin 2009, Vol. 3 Issue (1) : 68 DOI: 10.1007/s11783-009-0009-4

Part XI
Communication, Publications and Awards

Poster Session:

December 2014 – Berlin (Germany): Poster entitled « Selenium GeoHealth Interest in Articular Cartilage Maturation and Metabolism » presented in Architectured Biomaterials - Medical and Tissue Engineering Symposium.

Talk:

October 2015 – Sao Paulo (Brazil): « Role of the selenium in articular cartilage metabolism, growth, and maturation » presented in the 4th International Conference on Selenium in the Environment and Human Health.

Publications:

Published:

« Role of the selenium in articular cartilage metabolism, growth, and maturation » Abstract Chapiter 36, p77-78, published in "Global Advances in Selenium Research from Theory to Application", Gary S. Banuelos, Zhi-Qing Lin, Milton Ferreira Moraes, Luiz Roberto Guimarães Guilherme, Andre Rodrigues dos Reis, CRC Press, 5 oct. 2015 DOI: 10.1201/b19240-40

Submitted Publications:

C. Bissardon, O. Proux, S. Bureau, E. Suess, L.H.E. Winkel, R.S. Conlan, L.W. Francis, I.L. Khan, L. Charlet, S. Bohic, J.L. Hazemann. High resolution X-ray spectroscopy of selenium in articular cartilage at 400 ppb level.

Abstract: The speciation of highly-diluted elements by X-ray absorption spectroscopy in a diverse range of materials is extremely challenging, especially in biological matrices such as cartilage. Here we present an innovative synchrotron spectroscopy analysis, namely high energy resolution fluorescence detected X-ray absorption spectroscopy (HERFD-XAS) coupled to an array of crystal analyzers, which provides, for the first time, a clear demonstration of selenium speciation at concentrations of few hundreds of ppb (μg/kg) within articular cartilage. This is a major advance in the speciation of highly-diluted elements through X-ray absorption spectroscopy and opens new possibilities to study the metabolic role of selenium and other elements in mammalian cells and tissues.

Publications in Preparation:

« Characterization of biochemical and biomechanical variation between different maturation treatments influenced by the selenium status of cultured bovine articular cartilage » is in progress.

« Geohealth Implication of Selenium: Cells, Tissues and Environment », literature review in progress. It will be submitted to "Environmental Health Perspectives" Journal.

Two further papers are in preparation promoting the interest of the Synchrotron X-ray Phase Contrast Imaging Technique as complemental technique for morphological studies in 3D (3D Histomorphometry) of articular cartilage.

Awards:

For Women in Science

FONDATION L'ORÉAL

POUR LES FEMMES ET LA SCIENCE
EN PARTENARIAT AVEC

ATTESTATION D'OBTENTION DE LA BOURSE FRANCE
L'OREAL-UNESCO *POUR LES FEMMES ET LA SCIENCE*

David MacDonald, directeur général adjoint de la Fondation L'Oréal, et **Sonia Bahri**, Conseillère pour les affaires scientifiques et le développement durable, Commission nationale française pour l'UNESCO, attestent que :

Madame Caroline BISSARDON,
née le 21/11/1990 à Lyon 3ème (069),

a été retenue le 22 Juin 2016 par le Jury du programme, présidé par le Professeur Meunier, Président de l'Académie des Sciences, pour bénéficier de la bourse L'Oréal-UNESCO 2016.

Madame Caroline Bissardon se verra décerner la Bourse le 12 Octobre 2016 à l'Institut Pasteur lors de la cérémonie française *Pour les Femmes et la Science*.

Fait à Clichy, le 13 septembre 2016

David Macdonald
Directeur général adjoint
de la Fondation L'Oréal

Sonia Bahri
Conseillère pour les affaires scientifiques
et le développement durable
Commission nationale française pour
l'UNESCO

Résumé: Le Rôle du Sélenium dans le Métabolisme, la Croissance et la Maturation du Cartilage Articulaire.

En Chine, une grave maladie musculo-squelettique appelée la maladie de Kashin-Beck (KBD) se retrouve distribué sur une large zone géographique. Cette maladie touche plus de deux millions d'individus, notamment dans le centre de la Chine, et il est admis que plus de 30 millions d'individus seraient à risque. Des études géologiques et épidémiologiques ont montré une forte corrélation entre les zones de déficience en Se dans les sols et de KBD. KBD est une ostéoarthropathie, caractérisée par la destruction des chondrocytes du cartilage, très douloureuse et invalidantes, pouvant conduire à des déformations articulaires importantes. Le sélénium (Se) est présent partout dans l'environnement (eau, air, sols) et nos besoins physiologiques en Se sont couverts par notre alimentation quotidienne (eau, céréales). Bien que cet élément trace soit un nutriment essentiel pour la fonction cellulaire normale, ses mécanismes d'action ainsi que les transformations métaboliques de ses composés dans le corps humain ne sont toujours pas bien déterminés. Toutefois, à une dose un peu supérieure à la dose recommandée, il peut, selon la forme chimique ingéré, devenir toxique. Par conséquent, on retrouve le Se en très faible quantité (μg/L) dans l'organisme, ce qui rend difficile sa localisation et l'analyse de son rôle dans le métabolisme. Le Se fait partie de sites biologiquement actifs de protéines impliquées dans les mécanismes antioxydants de défense et le contrôle rédox des réactions intracellulaires. En outre, plusieurs études ont mis en évidence le rôle que joue de Se dans le développement des tissus tels que le cartilage articulaire. Cette action semble être médiée par l'intermédiaire de sélénoprotéines et seraient indirectement impliqués dans la croissance du cartilage normal et l'homéostasie. Aux Etats-Unis, une étude clinique a montré des preuves solides de l'influences d'un déficit en Se dans le métabolisme du cartilage conduisant un environnement favorable à l'apparition et la progression de l'arthrose. Même si le Se n'est pas le seul facteur dans le développement de maladies, il est fort probable que son absence impacte la croissance et le développement du cartilage articulaire. Un modèle *in vitro* de maturation accélérée du cartilage articulaire (explants) nous a permis d'analyser l'impact du sélénium dans la croissance et le développement de ce tissu. Des expériences biologiques, biophysiques et chimiques ont été réalisées pour comprendre comment la présence de Se affecte l'organisation des tissus. Un schéma récurrent de la distribution du Se dans le tissu a été découvert. Il semble être localisé au niveau des interfaces cellule-matrice, offrant des hypothèses intéressantes pour de futures études sur le rôle potentiel du Se dans la signalisation cellulaire ou transduction mécanique. Des analyses biomécaniques, structurelles et moléculaires ont été faites pour caractériser la matrice extracellulaire du cartilage articulaire traités avec différentes concentrations de Se. Il semble être localisé au niveau des interfaces cellule-matrice, ce qui suggère que le Se joue un rôle dans la signalisation cellulaire ou transduction mécanique. Des analyses biomécaniques, structurelles et moléculaires ont été faites pour caractériser la matrice du cartilage articulaire traités avec différentes concentrations de Se. Nous avons découvert qu'un déficit en Se peut induire à une morphologie proche de celle de l'arthrose lors de la maturation du cartilage immature. Cependant, le rôle exact de ce déficit en Se induisant ce type de phénotype reste inconnu. Ce projet contribue à une meilleure compréhension du Se dans le cartilage tout en montrant les difficultés d'étude du Se dans les milieux biologiques et les techniques permettant d'y répondre, mais aussi souligne l'importance de prendre en compte le Se comme élément important de traitements régénérateurs ou préventifs pour ce types de maladies.

Abstract: Role of Selenium in Articular Cartilage Metabolism, Growth and Maturation

In China, a severe musculoskeletal disease called Kashin-Beck disease (KBD) is largely endemic over a large geographical area. It has been reported that more than 2.5 million people in China suffer from KBD and about 30 million people are at risk. Geological and epidemiological investigations have shown that a strong correlation exists between the location of selenium (Se) deficient soils and the distribution of KBD in the population. The disease is manifested as degradation of the matrix, cell necrosis mainly in the articular and growth plate cartilage, which can result in growth retardation, secondary osteoarthrosis, and disability in daily life. The worst forms of this disease tend to start in childhood, which may lead to dwarfism. Selenium is present everywhere in the environment (water, air, soils) and it is mainly incorporated to the human organism through the daily diet (water, cereals). Although this trace nutriment element is essential for normal cellular function. Most of the selenium-related -functions and pathways remain incompletely understood. Whilst vital for normal function, it is toxic at concentration slightly higher than that required by the body. Consequently, it is present within the organism in parts per billion (μg/L) making it difficult to localize and analyze its role in metabolism. Despite being a trace element it is an essential component of antioxidant and anti-inflammatory-related proteins that protect cells against oxidative attack. Furthermore, several studies have exposed the role selenium plays in tissue development such as in articular cartilage. This action seems to be mediated via selenoproteins that are indirectly involved in normal cartilage growth and homeostasis. In the USA, a clinical study has shown strong evidence that Se-deficiency influences cartilage metabolism inducing a favorable environment for the onset and the progression of osteoarthritis. Even if the selenium is not the only factor in the development of degenerative joint disease, it is highly likely that its absence impacts its growth and development of articular cartilage. The main focus of this study was then to understand better the role of Se in the normal metabolic processes of articular cartilage. Cultures of articular cartilage explants were used on a previously validated *in vitro* model of tissue maturation to analyze the role of selenium in growth and development. Physical and chemical experiments were preformed to understand how the presence of selenium affects tissue organization. It has been possible to determine a fundamental recurrent pattern of Se-distribution in the tissue. It appears to be localized at cell-matrix interfaces and it can be hypothesized that Se plays role in cell signaling or mechanotransduction. Biomechanical, structural and molecular analyses have been made to characterize the extracellular matrix of articular cartilage treated with different concentrations of Se-level. We discovered that Se-deficiency induces morphological changes in the cartilage matrix during the fast maturation-like process, which could be related to degenerative-like morphology of the cartilage. This could potentially be associated with degenerative changes that occur in KBD patient during childhood. This project is a prospective work for a potential future enhancement of the regenerative or preventive treatments for specific musculoskeletal diseases with a metabolic component.